Computational Models of Intracellular Signalling in Cerebellar Purkinje Cells

Volker Steuber

PhD
The University of Edinburgh

1998

Declaration

I have composed this thesis myself and it reports original research that has been conducted by myself unless otherwise indicated.

Edinburgh, 12 December 1998

Volker Steuber

Acknowledgements

I would like to thank David Willshaw for all his encouragement, his support, his patience, and for giving me both the time and the freedom to find out and pursue exactly what I wanted to study. Most of all, I would like to thank David for making me feel that I could ask his advice about anything at any time, and for creating the atmosphere that made the Centre for Neural Systems an environment that could not be improved in any way.

It is not just David who made the Centre for Neural Systems such a special place. Everybody else in the group made me feel at home here, and almost everybody contributed in some way to my thesis.

Alastair Reid and Sam Joseph were not only good office mates, but also good friends. I will miss our serious and less serious discussions and our common basketball, squash and other social activities. Al supplied me with English sentences while I was writing this thesis, he was always happy to listen to my problems and he helped me with his dynamical systems knowledge. Sam was an unlimited source of neural network advice, and we had great fun developing a model of synapse elimination at the neuromuscular junction.

Arjen van Ooyen first introduced me to linear stability theory. We had many stimulating discussions, and I am looking forward to simplifying models and analysing phase planes together with him in the future. Bruce Graham gave me an excellent idea that resulted in the improvement of the adaptive leaky integrator model, and he was always there to answer my practical and theoretical questions about different aspects of computational neuroscience. Without Andrew Gillies, I would still fiddle with one of my numerous computing problems. I admire both Andrew's knowledge and his patience. David Sterratt helped me with my maths problems and pointed out that $k_1^2\,k_3^2/k_2^2 + k_2^2 + k_4^2 - 2\,k_1\,k_3\,k_4/k_2 + 2\,k_1\,k_3 - 2\,k_2\,k_4$ is the same as $(-k_2 - k_1\,k_3/k_2 + k_4)^2$. Tim Hely interrupted my talks with interesting questions and taught me how to present my work in a more positive way. Dina Kronhaus-Peled lent me her power book and introduced me to the world of Adobe Acrobat. Gert Westermann showed me how to get LaTex to behave in the way I wanted it to behave. I will miss our Friday lunches and talk & tea meetings. Stephen Eglen helped me with a grant application and taught me a few very good squash techniques, for example not to get upset about losing (against him). I would like to thank all of them, and also Rosanna, Cati, Martin, Sarah, Mark and everybody else in the Centre for Neural Systems who contributed to the good time I had in Edinburgh.

Outside the Centre for Neural Systems, I would like to thank Frank Keller for his patience and his computational and non-computational advice, Saturnino Luz for helping me to install a Lisp-based simulator that sadly failed to produce any positive results, Mike Spratling for his Genetic Algorithm help, and everybody in the university and the AI department who was involved in awarding me a Premier Scholarship that provided my financial support. Finally, I would like to thank Christina and my mother who really made this thesis possible (a special thanks goes to Christina for putting up with my idiosyncratic working hours).

Abstract

In spite of the regular and well-characterised anatomy of the cerebellum, its function is still not clear. To understand the function of the cerebellum, it is necessary to understand the behaviour of a single cerebellar Purkinje cell. The behaviour of Purkinje cells is determined by their intracellular calcium dynamics, and by the network of intracellular signalling molecules that control the calcium dynamics. The aim of this thesis is to contribute to an understanding of the intracellular signalling network that is linked to the activation of metabotropic glutamate receptors (mGluRs) in a cerebellar Purkinje cell. In the thesis, ten different computational models of the mGluR signalling network are mathematically analysed and numerically integrated.

The main result of this thesis is that the mGluR signalling network can implement an *adaptive time delay* between the activation of the mGluRs by glutamate and the release of calcium from intracellular stores. The adaptation of the time delay has at least three different computational functions. Based on the delay adjustment, a single Purkinje cell can learn the adaptive timing of the classically conditioned eye-blink response. A more general function of the adaptive time delay is that it enables a Purkinje cell to learn a radial basis function (RBF)-like response to temporal parallel fibre input patterns. Furthermore, different Purkinje cells in a group can discover different clusters in a temporal parallel fibre input space.

The adaptation of a synaptic delay as opposed to a synaptic weight is a novel *non-Hebbian* learning mechanism. By systematically simplifying the original model, it is shown that the delay learning can be produced by a very limited set of intracellular processes. Two antagonistic phosphorylations can adjust the concentration of available mGluRs and implement the *adaptation* of the time delay. A *delayed* as opposed to an *immediate* response can be generated by the combination of calcium dependent negative feedback and autocatalytic release of calcium from intracellular stores.

Apart from producing a delayed calcium response, the combination of negative feedback and autocatalysis can lead to the generation of *damped calcium oscillations* in the mGluR network. The mGluR network belongs to a general class of *excitable systems* where a small deviation from the steady state results in a large excursion of the system through the state space. The excursion through the state space can either lead to a single calcium spike or to a series of oscillatory calcium spikes. The presence of calcium spikes makes the mGluR network noise resistant and enables it to use either a *temporal code* or a *rate code* to represent information. The computations that can be performed by the mGluR network and by other intracellular signalling networks are a promising subject for future research.

Contents

Chapter 1

Introduction

1.1 Motivation

In many respects, the cerebellum is a very unique part of the brain. It contains the majority of the neurons in the brain, but there is no apparent spatial variability, and the neurons are organised in an extremely regular and repetitive way. Because of its crystalline structure, it is one of the few parts of the brain where the neuronal connectivity pattern is almost entirely understood.

Only five different types of neurons make up the circuitry of the cerebellar cortex. The structure of the cerebellar cortex is determined by the morphology of the *parallel fibre* axons of one these types of neurons. All parallel fibres run in transverse direction, and the whole cerebellar cortex consists of transverse folia that are continuous across the midline. The dendritic trees of three of the five cortical neurons are spread in a plane perpendicular to the parallel fibres.

The largest of the three neurons with planar dendritic trees, the *Purkinje cell*, is particularly remarkable. Purkinje cells receive excitation from approximately 150,000 different parallel fibres. The massive convergence of the parallel fibre inputs is in contrast

with the other input to the Purkinje cell, the *climbing fibre*. During development, a competitive process guarantees that each Purkinje cell receives input from *only a single climbing fibre*. Nevertheless, the climbing fibre input excites the whole cell, and results in a large calcium spike and potentially two different forms of synaptic plasticity. The Purkinje cells are inhibitory neurons, and they represent the only output from the cerebellar cortex. Through the parallel fibres, the Purkinje cells receive direct excitation from the input neurons of the cerebellar cortex, and there is no significant inhibitory feedback connection that controls the Purkinje cell firing pattern.

Because of these remarkable features, cerebellar research is one of the major fields of neuroscience, and between 1700 and 1900 new papers appear each year (Ito, 1998). In spite of the continuing experimental and theoretical work, it is still not clear what exactly the cerebellum does or how it does it. The crystalline structure of the cerebellum has inpired a large number of theories of cerebellar function. For example, Braitenberg and Atwood (1958) suggested that the cerebellar cortex is a *timing device*, and Eccles et al. (1967) described the cerebellum as a computer-like structure and proposed the *beam theory* of parallel fibre effects.

A major focus of cerebellar research is the involvement of the cerebellum in *motor learning*. The two most influential theories of motor learning in the cerebellar cortex were formulated by Marr (1969) and Albus (1971) almost thirty years ago. Most other theories of cerebellar learning are developments of Marr's and Albus' ideas (for example, Gilbert, 1974, 1975; Ito, 1984). However, all of these theories are based on assumptions on synaptic integration and synaptic plasticity in cerebellar Purkinje cell which are very controversial (see for example De Schutter, 1995; Ito, 1996). Whether or not the cerebellum contributes to motor learning is an unresolved question.

To formulate a computational theory of the cerebellum which is more than speculation, we have to acquire a better understanding of the computations that are performed by a *single cerebellar Purkinje cell*. The behaviour of Purkinje cells is highly dependent on their intracellular *calcium dynamics*. Calcium is critically important for the regulation of the dendritic spike pattern, the spatial and temporal integration of

synaptic inputs, and the modification of the excitatory and inhibitory synaptic efficacies (for review, see Eilers et al., 1996).

Both the *dynamics* and the *effects* of calcium are controlled by a complex network of intracellular signalling molecules in the Purkinje cell cytoplasm. Understanding the interactions between the components of the intracellular signalling network is a prerequisite for a complete understanding of both the behaviour of a single Purkinje cell and the computations that are performed by the cerebellar circuitry.

1.2 Aims of the Thesis

The aim of the thesis is to contribute to an understanding of the intracellular signalling network in a cerebellar Purkinje cell.

The intracellular signalling network in the Purkinje cell cytoplasm is under the control of at least four different neurotransmitters that are released by five different types of presynaptic neurons. Three of the neurotransmitters, *noradrenaline*, *dopamine* and *serotonin*, have a modulatory role. The fourth neurotransmitter, *glutamate*, is released by the two major excitatory inputs of the Purkinje cells, the parallel fibres and the climbing fibres. Glutamate exerts its effect on the Purkinje cell by stimulating two different receptors, *ionotropic* (AMPA) receptors and *metabotropic* receptors.

The stimulation of the *AMPA receptors* is responsible for the short-term behaviour of the Purkinje cell. The influx of sodium through the AMPA receptors depolarises the Purkinje cell membrane and results in a local excitatory postsynaptic potential (EPSP). The spatial and temporal summation of a large number of EPSPs leads to the activation of fast sodium channels in the soma, the axon hillock and the initial segment of the Purkinje cell axon, and to the generation of an action potential.

The activation of the *metabotropic glutamate receptors (mGluRs)* has slower and longer lasting effects. Activated mGluRs trigger an intracellular signalling cascade leading

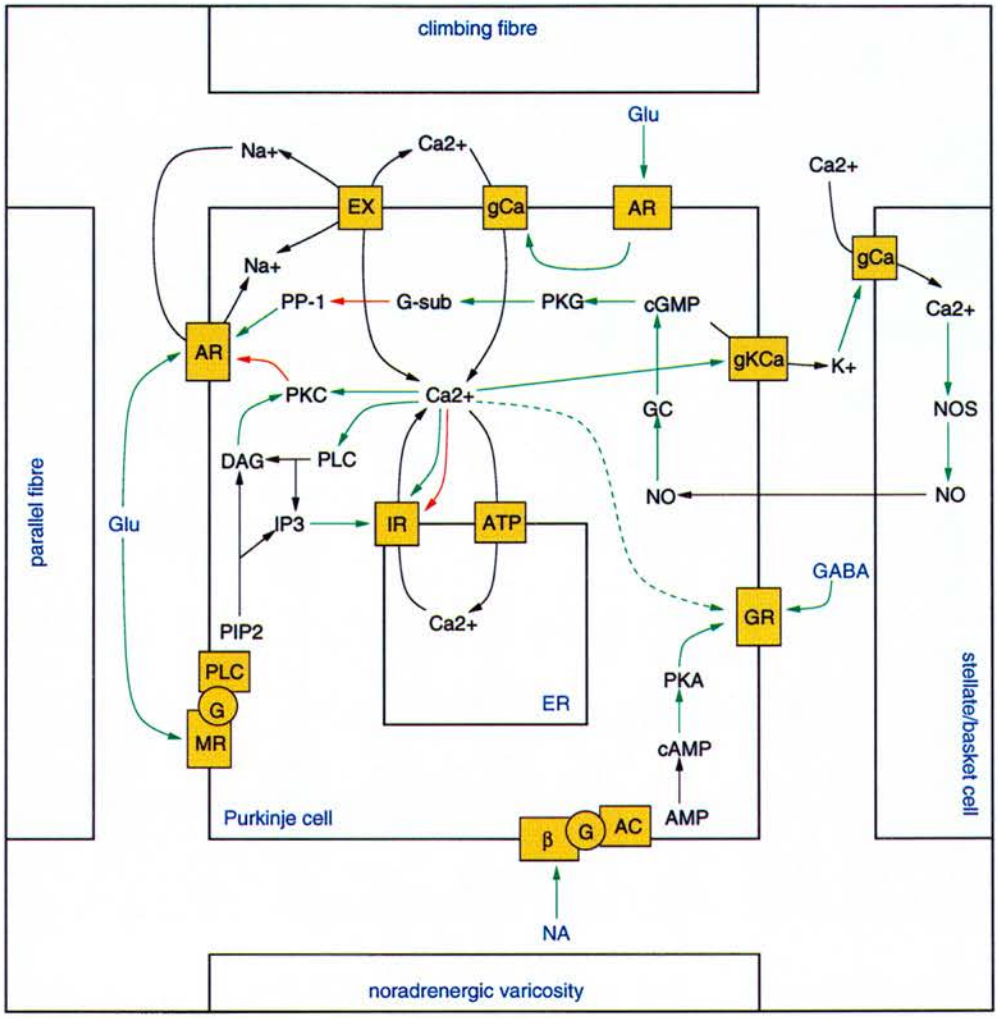

Figure 1.1: Simplified diagram of the intracellular signalling network in a cerebellar Purkinje cell. Black arrows indicate chemical reactions, transport or diffusion, green arrows represent the activation of a component by another, and red arrows are inhibitory connections. The red arrow and green arrow that point to the AMPA receptor (AR) represent the phosphorylation and dephosphorylation of the receptor, respectively. The green arrows pointing to the voltage dependent calcium channels (gCa) indicate the opening of the channels in response to depolarisation of the Purkinje cell. The red and green arrow between Ca^{2+} and the IP_3 receptor (IR) represent the Ca^{2+} dependent activation and inactivation of the receptor that result in a bell shaped dependence of the receptor opening on the cytoplasmic Ca^{2+} concentration. The dashed green arrow between Ca^{2+} and the $GABA_A$ receptor (GR) indicates the potentiation of the inhibitory synapses after an increase in the Ca^{2+} concentration in the Purkinje cell. The components are: Glu glutamate, GABA gamma-aminobutyric acid, NA noradrenaline, MR metabotropic glutamate receptors, AR AMPA receptors, GR $GABA_A$ receptors, β adrenergic β-receptors, G G-proteins, PLC phospholipase C, PIP2 phosphatidylinositol 4,5-bisphosphate, IP3 inositol 1,4,5-trisphosphate, DAG diacylglycerol, PKC protein kinase C, IR IP3 receptors, EX Na^+/Ca^{2+} exchanger, ATP calcium ATPase, gCa voltage dependent Ca^{2+} channels, gKCa calcium dependent potassium channels, NO nitric oxide, NOS NO synthase, GC guanylate cyclase, cGMP cyclic guanosine monophosphate, PKG protein kinase G, G-sub G-substrate, PP-1 protein phosphatase-1, AC adenylate cyclase, AMP adenosine monophosphate, cAMP cyclic adenosine monophosphate, PKS protein kinase A, ER endoplasmic reticulum.

to the release of calcium from intracellular stores, the activation of protein kinase C (PKC), and the phosphorylation of several types of neurotransmitter receptors. One of the effects of the mGluR activation is the phosphorylation of AMPA receptors that is reponsible for long-term depression (LTD) of the parallel fibre synapses.

To understand the mechanisms of synaptic plasticity and synaptic integration in cerebellar Purkinje cells, it is crucial to understand the intracellular signalling network that is linked to the activation of the mGluRs. The aim of this thesis is to investigate the computational capabilities of the mGluR signalling network. The following two questions will be addressed:

1. *What can the mGluR signalling network compute?*
2. *How exactly does it perform the computations?*

To address the two questions, ten different computational models of the mGluR signalling network were constructed. The ten differents models, the techniques that were used to study them and the results of the thesis will be summarised briefly in the following section.

1.3 Overview of the Thesis

The ten models of the mGluR signalling network that were developed in the thesis differ considerably in their complexity. Four of the ten models represent the mGluR signalling network with five ordinary differential equations (ODEs) or more, and their behaviour is investigated by *numerically integrating* them. In four other models, the interactions between the cytoplasmic calcium and the active receptors are described by two ODEs, and they can be analysed using *linear stability theory* and *phase plane methods*. The remaining two models are even further simplified and use a single ODE to represent the behaviour of a Purkinje cell in response to mGluR stimulation. Like the complex models, they are numerically integrated.

The thesis is organised as follows. In **chapter 2**, the anatomy and biochemistry of the cerebellum will be summarised. The cerebellum is one of the few structures in the brain where the pattern of neuronal connections is known in considerable detail. In the first half of chapter 2, the anatomical and functional subdivisions of the cerebellum, their efferents and afferents, the five types of neurons in the cerebellar cortex and the microcircuitry of the cerebellum will be described. In the second half of the chapter, four different forms of plasticity in the cerebellar cortex will be discussed. By far the most thoroughly studied form of cerebellar plasticity is long-term depression (LTD) of the synapses between parallel fibres and Purkinje cells, and the final section of the chapter will present two possible biochemical mechanism for the induction of parallel fibre LTD.

One of the most contentious issues in cerebellar research is whether or not the cerebellum is involved in motor learning. The contribution of the cerebellum to motor learning has been studied extensively for classical conditioning of the eye-blink response. In **chapter 3**, some of the features of eye-blink conditioning will be described, a number of experimental results will be discussed, and it will be argued that most of the experimental evidence indicates that the eye-blink memory is formed and stored in the cerebellar cortex and the interpositus nucleus. In the cerebellar cortex, a form of synaptic plasticity that could implement the eye-blink learning is LTD of the parallel fibre – Purkinje cell synapses. In the final section of the chapter, the arguments for and against parallel fibre LTD as substrate for the eye-blink conditioning will be discussed.

Although the existence of cerebellar LTD can explain the formation of the associative memory during eye-blink conditioning, it is unable to explain why the eye-blink response is *timed adaptively* and peaks at the time of the unconditioned stimulus during training. Recently, Fiala et al. (1996) have published a model of intracellular signalling in a cerebellar Purkinje cell that provides an explanation for the adaptive timing of the eye-blink response. Fiala and collaborators propose that the adaptively timed eye-blink response is learnt by a group of Purkinje cells with a *spectrum of time delays* between mGluR activation and intracellular calcium release. Fiala et al.'s *Spectral Timing*

Model will be discussed in detail in **chapter 4**. The chapter will also describe a few minor corrections that were necessary to implement the model, and present numerical simulation results.

The *Spectral Timing Model* assumes that the eye-blink conditioning is implemented by a *group* of Purkinje cells, and that the time delays between mGluR activation and intracellular calcium release in the different Purkinje cells in the group are *appropriately prespecified* and cover the spectrum of conditionable intervals between conditioned stimulus and response. In **chapter 5**, it will be shown that the adaptive timing of the eye-blink response can be explained *without* a spectrum of appropriately prespecified time delays. The chapter describes the *Adaptive Timing Model*, an extension of the Spectral Timing Model that demonstrates how a *single Purkinje cell* can learn an adaptively timed reponse. In the Adaptive Timing Model, the phosphorylation of the mGluRs implements an *adaptive time delay* between receptor stimulation and intracellular calcium release. Simulation results will be presented, and it will be shown that the model can learn adaptively timed responses in simulations of both delay and trace conditioning experiments.

The activity-dependent adaptation of the time delay between receptor activation and intracellular response represents a new learning mechanism, and chapters 6 and 7 will investigate the computational capabilities of the delay adaptation in more detail. In **chapter 6**, an extension of the the Adaptive Timing Model to a multi-compartmental model of a cerebellar Purkinje cell will be described. It will be shown that the multi-compartmental Purkinje cell model can learn to respond to temporal parallel fibre input pattern in a radial basis function (RBF)-like way, and implement the *temporal decoding mechanism* that was postulated by Hopfield (1995).

Chapter 7 will present a phenomenological simplification of the multi-compartmental Purkinje cell model. The simplified model uses a *leaky integrator* formalism, and describes the response of the Purkinje cell to mGluR stimulation with a single ODE. The chapter will demonstrate that a *single* leaky integrator Purkinje cell model can reproduce the behaviour of the multi-dimensional version of the Adaptive Timing Model

and learn an RBF-like response to temporal patterns, and that a *group* of leaky integrators can discover different clusters in a temporal parallel fibre input space. In the final section of the chapter, it will be shown that the *desensitisation* of the mGluRs can improve the clustering performance and guarantee that each of the integrators in the group specialises on a *different subset* of parallel fibre patterns.

In **chapter 8**, the *mechanism* of the adaptive time delay will be studied. The *phosphorylation of the mGluRs* is responsible for the *adaptation* of the time delay. To identify the interactions between the components of the mGluR signalling network that implement a *delayed* as opposed to an *immediate* response, the Adaptive Timing Model will be systematically simplified. The thirteen components of the Adaptive Timing Model will be divided into different categories and, based on the categorisation of the components, two simplified models with *five* and *two* ordinary differential equations (ODEs) will be developed. The two-ODE model will be analysed with phase plane methods, and it will be shown that the combination of calcium dependent *negative feedback* and *autocatalysis* is sufficient to generate the delayed response, given that the calcium dependent processes exhibit a sigmoidal calcium dependence.

Finally, recent experiments have shown that another possible behaviour of the mGluR signalling network is the generation of damped calcium oscillations in response to a glutamate pulse. In **chapter 9**, it will be demonstrated that a complex mGluR signalling model that contains a negative feedback connection between the cytoplasmic calcium concentration and the concentration of active mGluRs can implement a damped oscillatory calcium response. Three simplified *two-ODE* versions of the model will be analysed, and it will be shown that the presence of *negative feedback* is sufficient to generate the calcium oscillations, and that the presence of *autocatalytic calcium release* results in a decrease of the damping and enables the system to oscillate for a larger range of parameter values. Thus, the conditions that can implement the damped oscillations are very similar to the conditions that are responsible for the delayed response.

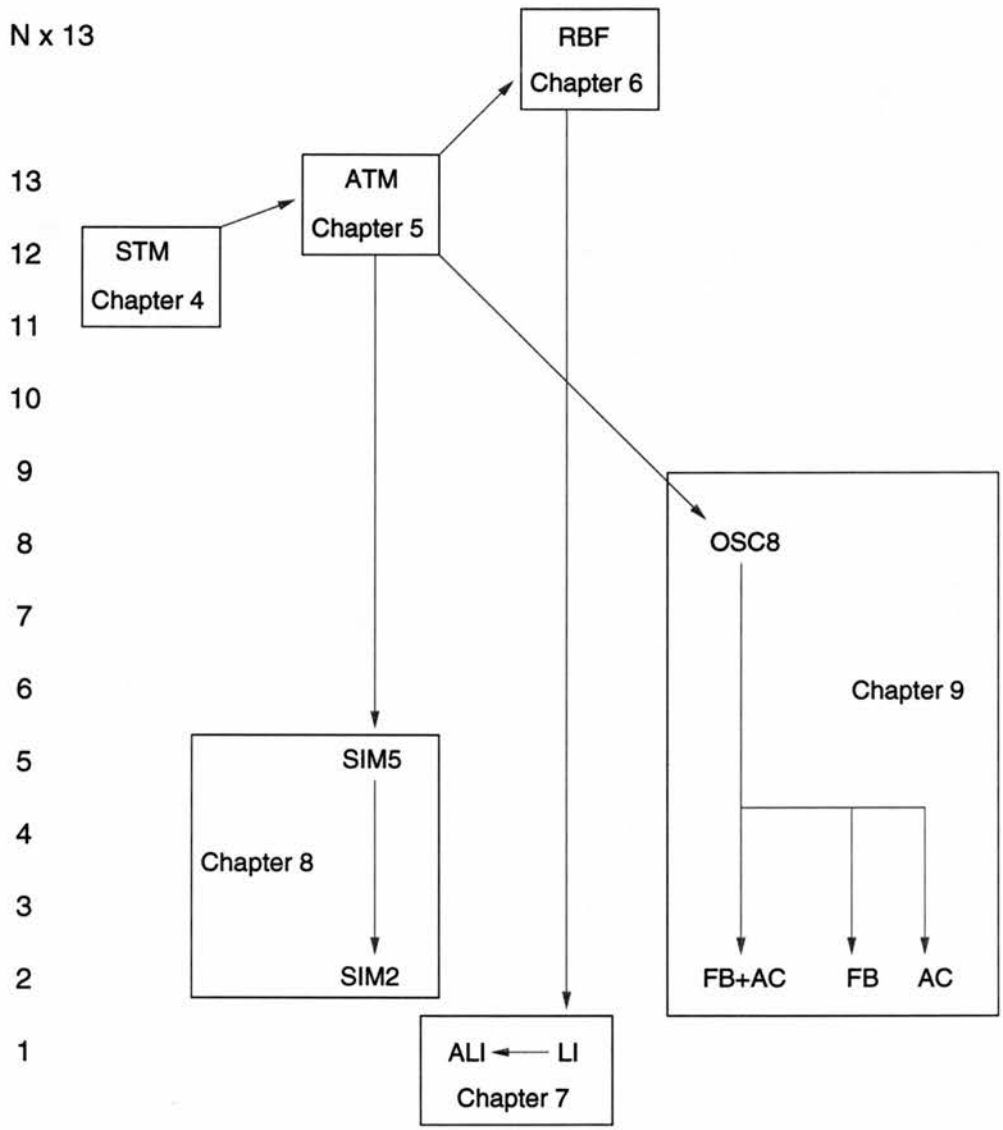

Figure 1.2: Relationship between the ten models that are developed in the thesis. All of the models are derived from Fiala et al.'s Spectral Timing Model (STM). The number of ODEs in each of the models is indicated on the left. N is the number of dendrites in the multi-compartmental model. ATM Adaptive Timing Model, SIM5 five-ODE simplification of the ATM, SIM2 two-ODE simplification of the ATM, RBF multi-compartmental Purkinje cell model, LI leaky integrator model, ALI adaptive leaky integrator model, OSC8 complex eight-ODE Ca^{2+} oscillations model, FB+AC two-ODE Ca^{2+} oscillation model with negative feedback and autocatalysis, FB two-ODE model without autocatalysis, AC two-ODE model without feedback.

Chapter 2

The Cerebellum

2.1 Introduction

The cerebellum is one of the most regular and repetitive structures in the brain. Because of its crystalline anatomical organisation, it is one of the few parts of the brain where the pattern of neuronal connections is almost entirely understood.

In the first half of this chapter, the anatomy of the cerebellum will be summarised. The gross structure of the cerebellum, its anatomical and functional subdivisions, the different afferent and efferent connections of the subdivisions, the five types of neurons in the cerebellar cortex, and the canonical microcircuit of the cerebellum will be described in detail. Unless stated otherwise, the sources of the anatomical data are Eccles et al. (1967), Palay and Chan-Palay (1982), Nauta and Feirtag (1986), Kandel et al. (1991), and Voogd and Glickstein (1998).

In spite of the regular and well-characterised anatomy of the cerebellum, its function remains unclear. One of the most contentious issues in cerebellar research is whether or not the cerebellum contributes to motor learning, and what the role of the synaptic plasticity in the cerebellar cortex is.

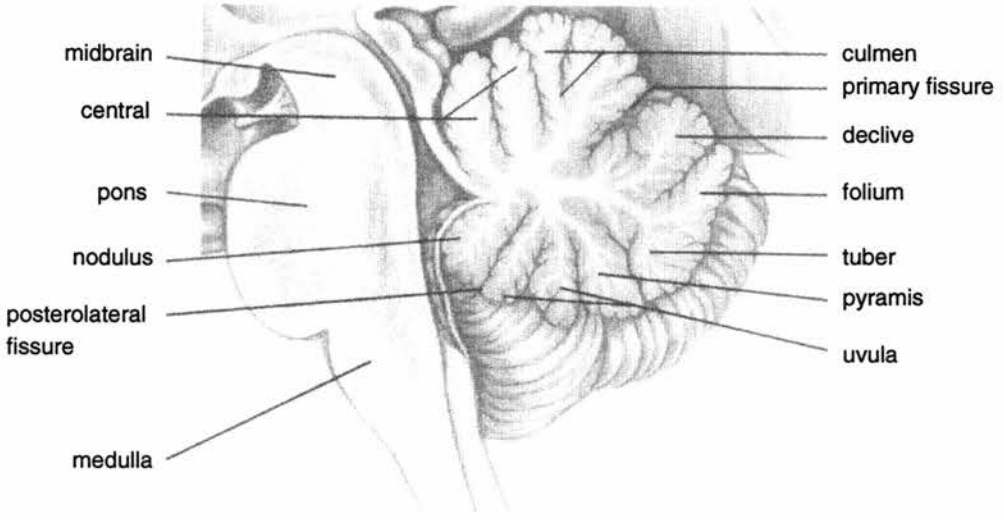

Figure 2.1: Midsagittal section through brain stem and cerebellum, showing the division of the cerebellum into lobes, lobules and folia, the tree shaped white matter and the surrounding grey matter of the cerebellar cortex. From Kandel et al. (1991).

In the second half of the chapter, four different forms of synaptic plasticity in the cerebellar cortex will be described, and two possible biochemical mechanisms for the long-term depression of the synapses between parallel fibres and Purkinje cells will be discussed.

2.2 Structure of the Cerebellum

In many respects, the basic structure of the cerebellum is governed by the same principles that underly the structure of the telencephalon. As in the telencephalon, the afferent and efferent fibres form a tree-shaped *white matter*. Based on the tree-like appearance, the structure has been called *arbor vitae*, tree of life. The white matter is surrounded by an outer mantle of cell bodies: the *grey matter* of the *cerebellar cortex*. Other groups of cell bodies are hidden inside the white matter. Three pairs of *deep cerebellar nuclei* project out of the cerebellum, to other parts of the brain. The three pairs of deep nuclei are the *dentate*, the *fastigial* and the *interpositus* nuclei. Each of the three nuclei has a different function and sends projections to different areas of the brain.

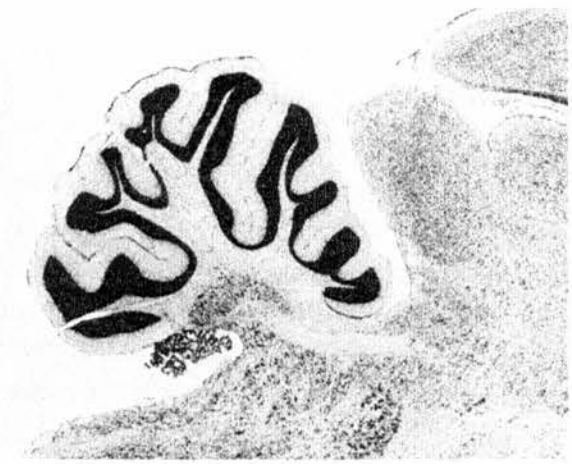

Figure 2.2: Midsagittal section through the cerebellum of a rat. The section is *Nissl-stained* to indicate the location of the cell bodies and shows the large number of neurons in the granular layer of the cerebellar cortex. From Nauta and Feirtag (1986).

All of the efferent fibres leave, and all of the afferent fibre enter the cerebellum through the *cerebellar peduncles*: three pairs of fibre tracts that connect the cerebellum to the brain stem. The most prominent of the afferent projections to the cerebellum comes from the *pontine nucleus* in the brain stem. Together, the cerebellum and the pontine nucleus make up the *metencephalon* or *hindbrain*.

The common structural principles of the cerebellum and the telencephalon result in a similar external appearance. Both the cerebellar and the cerebral cortex are highly convoluted sheets, divided by *fissures* into larger *lobes* and smaller *lobules*. However, there are significant differences. In the *telencephalon*, the fissures are curved, and the cerebral cortex is divided into a number of convoluted *gyri*. Furthermore, the cerebral cortex is discontinous across the midline. The *central sulcus* splits the telencephalon into two symmetrical hemispheres.

In contrast, the cerebellar cortex only has *transverse* fissures. The cerebellum is divided into three major transverse lobes, each of which is subdivided into several transverse lobules and a large number of transverse *folia*. Thus, the cerebellar cortex is one of the few structures in the brain that are continuous across the midline.

2.3 The Basic Cerebellar Circuit

In the *cerebral cortex*, the basic circuit of interconnections is still not know, and it is not even know if a canonical circuit exists (Nauta & Feirtag, 1986, K. Martin, personal communication). In contrast, the basic circuit of the cerebellum is relatively well established. The afferents fibres form synapses with neurons in both the cerebellar cortex and the deep cerebellar nuclei. In the cerebellar cortex, all of the incoming information is collected by a single group of output neurons: the cerebellar *Purkinje cells*. The Purkinje cells project to the three pairs of deep nuclei which in turn send projections to various other parts of the brain. In the following sections, the cerebellar afferents and efferents, and the neurons of the cerebellar cortex and their connectivity will be discussed in detail.

2.4 Cerebellar Afferents and Efferents

2.4.1 Afferents

The cerebellum receives input from two major *excitatory* and a variety of *modulatory* afferent systems. The two major excitatory afferents, the *mossy fibres* and the *climbing fibres*, form localised glutamatergic synapses. The diffusely organised modulatory afferents release noradrenaline, dopamine, serotonin and acetylcholine into the extracellular space of the cerebellar cortex (see e.g. Freund & Palmer, 1997; Barik & deBeaurepaire, 1996; Maura et al., 1995; Bickford, 1995). In the following, the mossy fibre and climbing fibre input will be described in more detail.

Mossy fibres. The mossy fibre system carries the major input to the cerebellum. Mossy fibres arise from neurons in the spinal cord and in various brain stem nuclei, and project to the neurons in the deep cerebellar nuclei, and to the *granule cells* and *Golgi cells* in the cerebellar cortex. On entering the cerebellar cortex, each mossy fibre

branches and gives rise to a number of *rosettes* that activate a local cluster of granule cells. The synapses between mossy fibres and granule cells are located in the *cerebellar glomeruli*, isolated structures that also contain two other types of synapses: excitatory synapses between mossy fibres and Golgi cells, and inhibitory synapses between Golgi cells and granule cells.

Climbing fibres. The second major excitatory system is very different from the mossy fibres and one of the features that distinguish the cerebellum from other parts of the brain. All of the climbing fibres originate in the *inferior olivary nucleus* in the medulla. Like the mossy fibres, they send collaterals to the neurons in the deep cerebellar nuclei. In the cerebellar cortex, the climbing fibres contact the *Purkinje cells*, with a ratio of $1 - 10$ Purkinje cells per climbing fibre and, in the adult animal, only a *single climbing fibre per Purkinje cell.*

The name of the *climbing* fibres stems from the morphology of their contacts with Purkinje cells. The climbing fibre is attached to the Purkinje cell dendritic tree in an "ivy-like fashion" (Eccles et al., 1967), and forms a large number of excitatory synapses, predominantly with the proximal dendrites. The connection between the climbing fibre and the Purkinje cell is very powerful, and a single action potential in the climbing fibre results in a burst of spikes in the Purkinje cell. The climbing fibre induced depolarisarion is associated with a large influx of Ca^{2+} into the Purkinje cell and called a *complex spike.*

2.4.2 Efferents

Compared to the different types of cerebellar input, the organisation of the output is very simple. The cerebellar cortex contains only a single type of output neuron: the Purkinje cell. The Purkinje cell axons form inhibitory synapses with neurons in the deep cerebellar nuclei. The deep cerebellar nuclei project to other parts of the brain, including the inferior olivary nucleus and various motor systems. As a consequence, the firing of the Purkinje cells has an indirect influence on the execution of movements.

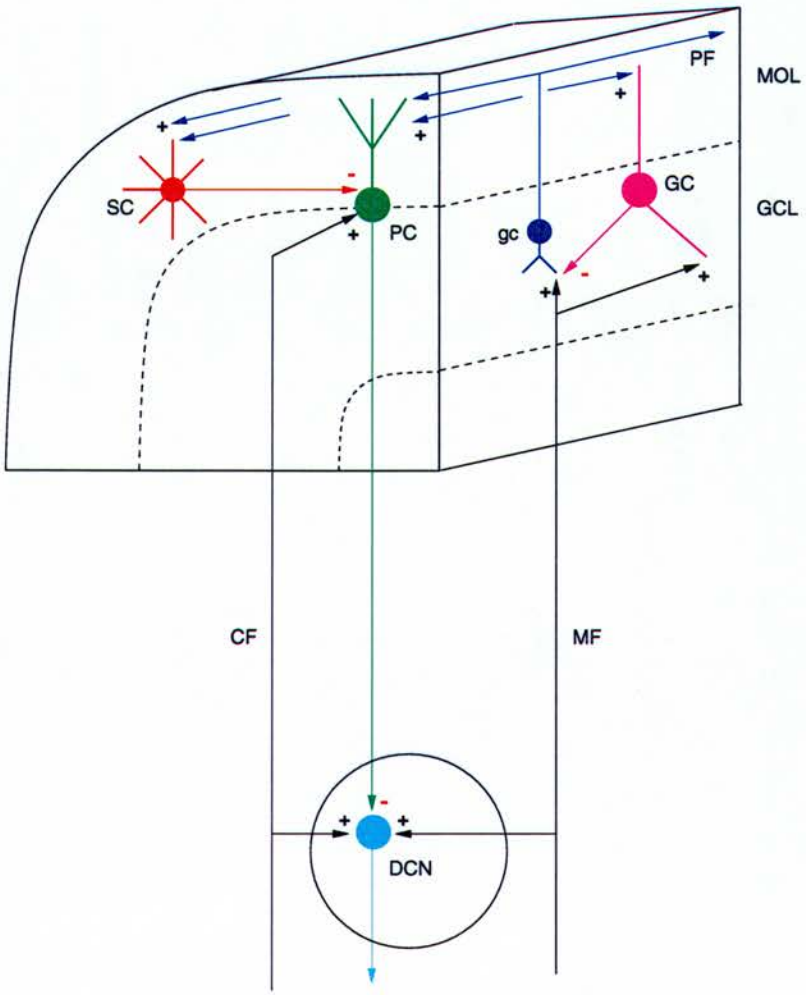

Figure 2.3: The basic circuit of the cerebellum. Excitatory and inhibitory synapses are indicated by (+) and (−), respectively. MOL molecular layer of the cerebellar cortex, GCL granular layer, DCN deep cerebellar nucleus, MF mossy fibre, CF climbing fibre, PF parallel fibre, PC Purkinje cell, GC Golgi cell, gc granule cell. SC summarises stellate and basket cells.

In addition to the inhibitory input from the Purkinje cells, the neurons in the deep cerebellar nuclei receive excitation through the mossy fibre and the climbing fibre collaterals. The loop that is formed by these collaterals is sometimes called the *primary cerebellar circuit*. It is only through modulation of the primary circuit that the Purkinje cell inhibition of the neurons in the deep nuclei exerts its effect.

2.4.3 The Three Cerebella

Based on the origin of the afferents, and the destination of the efferents, the cerebellum can be divided into three functional divisions: the *vestibulocerebellum*, the *spinocerebellum* and the *cerebrocerebellum*. Each of the three divisions consists of a region of the cerebellar cortex and an associated nucleus or group of nuclei.

Vestibulocerebellum. The vestibulocerebellum is the smallest of the three regions. It includes only one of the 10 cerebellar lobules, called *flocculonodular lobe*. As an exception to the rule that all of the Purkinje cells project to the deep cerebellar nuclei, the Purkinje cells in the *flocculonodular lobe* inhibit neurons in the *vestibular nuclei* in the medulla. Through the vestibular nuclei, the vestibulocerebellum influences axial muscles that are involved in the control of balance. Accordingly, the input to the vestibulocerebellum comes mainly from the semicircular channels and the otolith organs. In addition, visual input reaches the vestibulocerebellum from the visual cortex, superior colliculus and lateral geniculate nucleus.

Spinocerebellum. The spinocerebellum comprises the central 30 percent of the cerebellar cortex, together with the fastigial and the interpositus nuclei. The major inputs to the spinocerebellum are auditory, visual, vestibular and somatosensory, but it also receives information from the motor and sensory cortices of the telencephalon. The output from the spinocerebellum is equally diverse. Neurons in the fastigial nuclei project via the vestibular nuclei and the reticular formation in the hindbrain to motor neurons in the spinal cord, and via the thalamus to the primary motor cortex in the telencephalon. Neurons in the interpositus nuclei send axons to the red nucleus in the midbrain, and collaterals to the ventral lateral nucleus of the thalamus which projects to the limb area of the primary motor cortex. Through the rubrospinal and corticospinal tracts, the red nucleus and the motor cortex activate motor neurons in the spinal cord.

Cerebrocerebellum. The cerebrocerebellum consists of the dentate nucleus and the lateral 70 percent of the cerebellar cortex. It is the largest part of the cerebellum, and

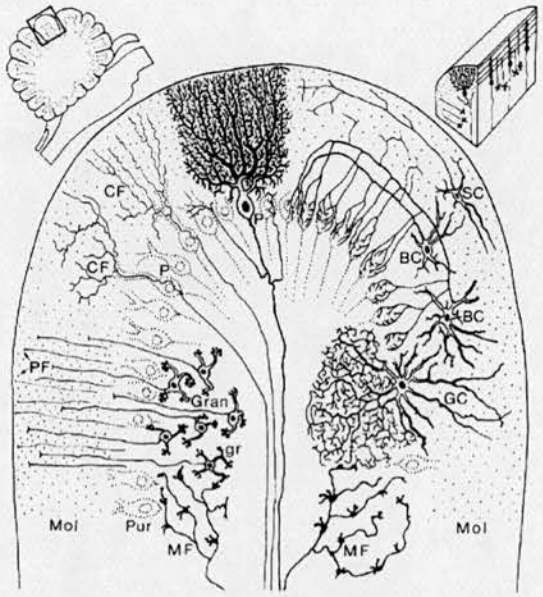

Figure 2.4: Neurons of the cerebellar cortex. The drawing represents a sagittal section through a single cerebellar folium. Mol molecular layer, Pur Purkinje cell layer, Gran granular layer, MF mossy fibre, CF climbing fibre, gr granule cell, P Purkinje cell, BC basket cell, SC stellate cell, GC Golgi cell. From Jacobson (1991).

the last part that appeared during the evolution of the vertebrates. The input to the cerebrocerebellum comes from the cerebral cortex via the corticopontine tract, and the neurons of the dentate nucleus project back through the thalamus to the motor and premotor cortices. In addition, there is a feedback circuit through the red nucleus and the inferior olive back to the cerebellum.

2.5 The Cerebellar Cortex

2.5.1 Structure of the Cerebellar Cortex

The cerebellar cortex is a very regular structure with only five different types of neurons: *granule cells*, *Purkinje cells*, *basket cells*, *stellate cells* and *Golgi cells*. As indicated in figure 2.3, the granule cells and the Purkinje cells form a direct excitatory route

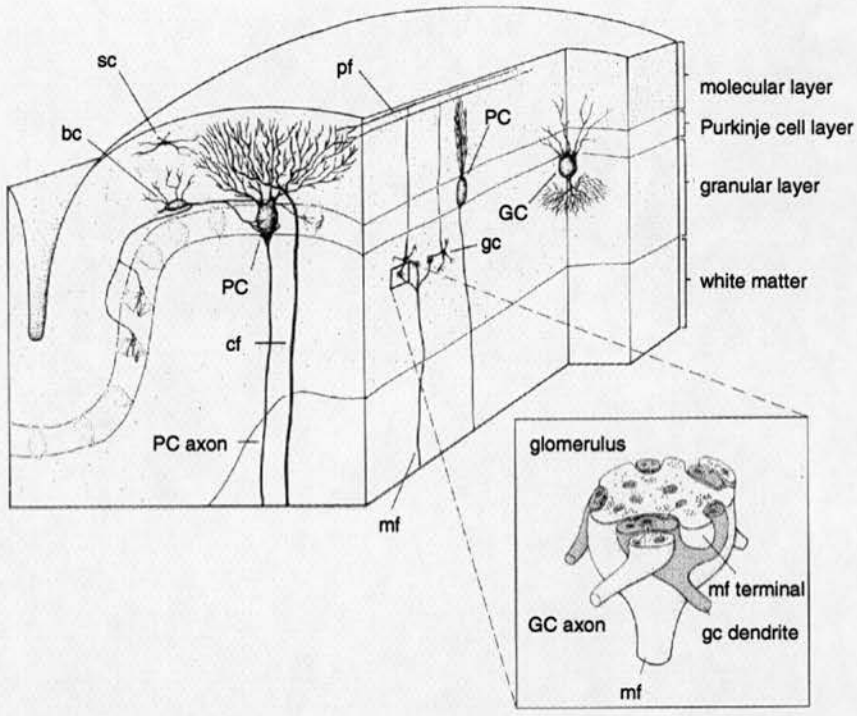

Figure 2.5: Organisation of the cerebellar cortex. The magnification shows the structure of a cerebellar glomerulus. PC Purkinje cell, GC Golgi cell, gc granule cell, bc basket cell, sc stellate cell, mf mossy fibre, cf climbing fibre. From Kandel et al. (1991).

through the cortex. The granule cells receive excitation from the mossy fibres and activate the Purkinje cells which in turn project to the neurons in the deep cerebellar nuclei. The excitatory connection through granule and Purkinje cells is modulated by inhibition from the basket, stellate and Golgi cells.

The five types of neurons are distributed over three different layers. The outer layer, called *molecular layer*, contains mainly the granule cell axons, the Purkinje cell dendrites, and scattered stellate and basket cells. Based on their uniform orientation along the axis of the folium, the axons of the granule cells are called *parallel fibres*. Directly below the molecular layer, a single layer of Purkinje cell somata makes up the *Purkinje cell layer*. Finally, the innermost or *granular layer* is composed of a large number of small granule cells, together with a few Golgi cells near the border with the Purkinje cell layer. In the following sections, the five different types of neurons will be described in detail.

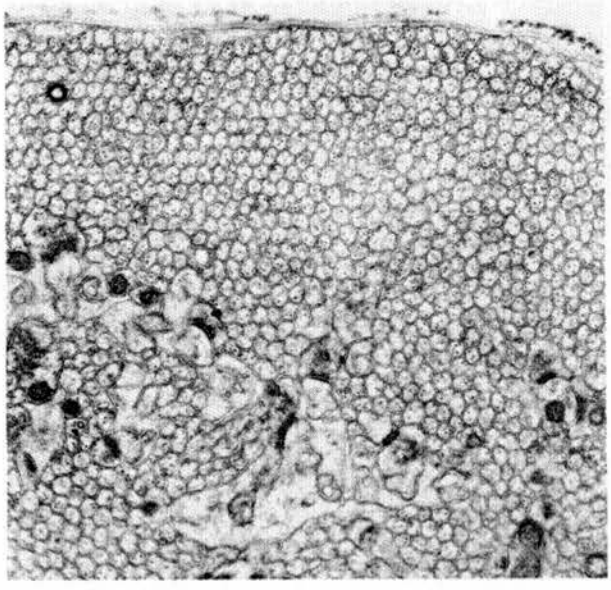

Figure 2.6: Electron micrograph (30,000 x) showing the densely packed parallel fibres in the molecular layer of the cerebellar cortex. From Nauta and Feirtag (1986).

2.5.2 Granule Cells

The granule cell is the most numerous neuronal cell type in the whole central nervous system. The number of granule cells in the cerebellum is estimated to be in the order of 10^{11}, more than the total number of neurons in the whole cerebral cortex.

Each of the small granule cells sends an average number of 10 dendrites down towards the incoming mossy fibres. The granule cell dendrites, called *granule cell claws*, receive mossy fibre excitation and Golgi cell inhibition in the cerebellar glomeruli. The axons of the granule cells ascend into the molecular layer, bifurcate and give rise to the *parallel fibres*. Each of the parallel fibres extends for several millimeters along the axis of the cerebellar folium, making connections with all of the four other types of cortical neurons on its way. All of these synapses are excitatory and glutamatergic.

Figure 2.7: Golgi staining of a cerebellar Purkinje cell, showing the extensive dendritic tree and the large number of spines. From Nauta and Feirtag (1986).

2.5.3 Purkinje Cells

The Purkinje cells are large neurons with an extensive dendritic tree that extends upwards through the molecular layer. In contrast to most other types of neurons, the Purkinje cell dendritic tree is nearly two-dimensional and spreads in a plane perpendicular to the axis of the folium. Purkinje cells receive at least six different types of synaptic input:

1. Excitation from approximately 150,000 different parallel fibres.
2. Excitatory input from a single climbing fibre.
3. Excitatory input from the ascending portion of the granule cell axons.
4. Inhibitory input from stellate cells.
5. Inhibitory input from basket cells.
6. Inhibitory input from recurrent collaterals of the Purkinje cell axons.

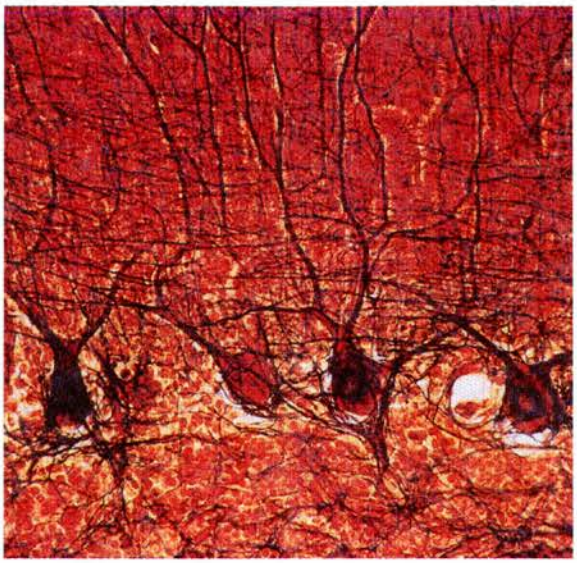

Figure 2.8: Cajal staining of cerebellar Purkinje cells. From Nauta and Feirtag (1986).

The relative importance of the input from the ascending granule cell axons and the parallel fibre input is an unresolved issue. According to the classical view of cerebellar function, the main excitatory input to the Purkinje cells comes from the parallel fibres (see for example Eccles et al., 1967; Kandel et al., 1991). However, it has been reported that the activation of peripheral nerves results in Purkinje cell activity in very restricted areas of the cerebellar cortex, and that the area of Purkinje cell activity does not exceed the area of granule cell activity (summarised in Llinas, 1982). Based on these observations, it has been suggested that the *ascending portion of the granule cell axon* mediates the major excitatory input to the Purkinje cell (Llinas, 1982), and that the function of the parallel fibres is to provide the Purkinje cell with information about the *context* of this main input (J. Bower, personal communication). Recent experimental results seem to confirm this suggestion (I. Segev, personal communication).

The Purkinje cell axons descend through the granular layer and form inhibitory GABAergic synapses with the neurons in the deep cerebellar nuclei. The Purkinje cell axons send recurrent inhibitory collaterals to other Purkinje cells and stellate and basket cells in both the same and in other folia of the cerebellar cortex. However, the inhibitory effect of the collaterals seems to be very weak (Eccles et al., 1967), and their functional significance is not known.

The behaviour of the Purkinje cell in response to parallel fibre and climbing fibre input is very different. A single climbing fibre spike results in a characteristic burst of action potentials in the Purkinje cell. The burst is called *complex spike* and associated with a large influx of Ca^{2+} into the Purkinje cell cytoplasm. In contrast, a single action potential in a parallel fibre triggers only a small excitatory postsynaptic potential (EPSP) in the Purkinje cell, and the spatial and temporal integration of several parallel fibre evoked EPSPs is necessary before the Purkinje cell fires a single action potential, called a *simple spike*.

In vivo, both the inferior olivary neurons that are the source of the climbing fibres, and the granule cells that are the source of the parallel fibres, are spontaneously active. As a consequence, Purkinje cells are also spontaneously active and fire simple spikes with a frequency between 30 and 100 Hz (Murphy & Sabah, 1970; Armstrong & Rawson, 1979), and complex spikes with a much lower frequency of about $1-2$ Hz (Eccles et al., 1967).

2.5.4 Stellate and Basket Cells

Stellate and basket cells are two similar types of inhibitory interneurons. Both cell types are situated in the molecular layer, receive excitation from parallel fibres and inhibit Purkinje cells. Like the Purkinje cell dendritic trees, the stellate and basket cell dendritic trees extend in a plane perpendicular to the parallel fibres.

Based on the length and morphology of their axons, stellate cells can be classified as *type A* or *type B* cells. Type A stellate cells have a *short* axon and inhibit Purkinje cells that receive excitation from the *same* set of parallel fibres (*on-beam* inhibition, see Eccles et al., 1967). Type B stellate cells have *longer* axons and inhibit Purkinje cells that are activated by a *neighbouring* set of parallel fibres (*off-beam* inhibition). The axons of basket cells are even longer. Eccles et al. (1967) have estimated that each basket cell axon provides *off-beam* inhibition for approximately 50 Purkinje cell bodies in a 7×10 Purkinje cell rectangle.

The functional role of the stellate and basket cells is still unresolved. In his theory of motor learning in the cerebellar cortex, Marr (1969) has proposed that they implement a thresholding mechanism for the recall of stored parallel fibre patterns from Purkinje cells. More recently, De Schutter and Bower (1994b) have suggested that the inhibitory input to the Purkinje cells is necessary to prevent the generation of dendritic Ca^{2+} spikes, and to enable the Purkinje cell to detect small fluctuations in the excitatory input. However, neither of these suggestions takes the *off-beam* inhibition into account, and further experiments and modelling studies will be necessary before the issue can be resolved.

2.5.5 Golgi Cells

The Golgi cell is the third type of inhibitory interneuron, and the one with the most complex structure. The Golgi cell dendritic trees are three times larger than the Purkinje cell dendritic trees, and expand equally far in all directions in the cerebellar cortical plane. Most of the dendrites ascend into the molecular layer and receive synaptic input from the parallel fibres. In addition, a few of the dendrites descend into the granular layer and contact the mossy fibre terminals in the cerebellar glomeruli.

Again, the functional role of the Golgi cells is not clear. According to Marr (1969), the combined parallel fibre and mossy fibre excitation of the Golgi cells, together with the Golgi cell inhibition of the granule cells, is a mechanism to decrease the average parallel fibre activity below the level of the average mossy fibre activity. In Marr's *Theory of Cerebellar Cortex*, the decreased parallel fibre activity leads to an increased number of parallel fibre patterns that can be stored by a Purkinje cell. However, experimental evidence for Marr's suggestion still needs to be found. Recent experiments and modelling studies indicate that another function of the Golgi cell inhibition could be the *synchronisation* of the granule cell activity (Maex & De Schutter, 1998).

2.6 Cerebellar Plasticity

2.6.1 Cerebellar Plasticity and Motor Learning

A major focus of cerebellar research is the involvement of the cerebellum in motor learning. The most influential theory of motor learning in the cerebellum was formulated by David Marr (1969) almost thirty years ago. In Marr's *Theory of Cerebellar Cortex*, the synapses between the parallel fibres and the Purkinje cells are *binary*, and they are *switched on* if a parallel fibre (PF) pattern is presented together with a climbing fibre (CF) signal. Thus, David Marr's theory can be viewed as an implementation of an associative network by a group of cerebellar Purkinje cells (Willshaw et al., 1969; Tyrrell & Willshaw, 1992). Marr suggested functional roles for the different types of cerebellar cortical neurons, and he predicted that each Purkinje cell should be able to learn the recognition of approximately 200 different mossy fibre patterns.

Two years later, a similar theory of the cerebellum was published by Albus (1971). Like Marr, Albus assumed that the cerebellar cortex operates as a pattern associator, but his suggested learning mechanism was slightly different, and he postulated that the parallel fibre synapses are *depressed* rather than *potentiated*. The hypothesis that the modification of the synapses between parallel fibres and Purkinje cells implements motor learning in the cerebellum has become known as the *Marr-Albus theory* (Ito, 1984).

In 1982, the hypothetical plasticity of the PF synapses that was postulated by the *Marr-Albus theory* was observed in experiments (Ito et al., 1982). Ito and collaborators found that the coactivation of climbing fibres and parallel fibres *in vivo* resulted in *long-term depression (LTD)* of the synaptic efficacy between the stimulated parallel fibres and the Purkinje cell. The parallel fibre LTD is input specific (Ekerot & Kano, 1985), lasts up to several hours (Linden, 1994), and can also be induced in cerebellar slices (e.g. Sakurai, 1987) and in cultures of Purkinje cells (Hirano, 1990; Linden et al., 1991).

Whether or not the Marr-Albus theory is correct and parallel fibre LTD is involved in motor learning is an unresolved issue (see for example Ekerot & Kano, 1989; Konnerth et al., 1992; Schreurs & Alkon, 1993; Karachot et al., 1994; Ito, 1996; Hartell, 1996; De Schutter, 1995, 1996, 1997). One of the arguments *against* the involvement of LTD in motor learning is the relative timing of the CF and PF inputs that is required. The discrepancy between the temporal requirements for LTD induction and motor learning will be discussed in detail in section 3.3.7.

Recently, it has been shown that LTD can also be induced by stimulation of the parallel fibres alone, *without* conjunctive activation of the climbing fibre input (Hartell, 1996). Based on these results, Erik De Schutter (1995, 1997) has suggested that the function of LTD is not motor learning, but a slow *negative feedback* mechanism that establishes an adequate balance between excitatory and inhibitory inputs, and prevents the overstimulation of the Purkinje cell.

To summarise, the *function* of parallel fibre LTD is still not clear. Another unresolved question is the exact *mechanism* of the LTD induction. Two different mechanisms that could be reponsible for the induction of LTD will be described in the next section.

2.6.2 The Biochemistry of Cerebellar LTD

Since parallel fibre LTD was first described by Masao Ito in 1982, the biochemical machinery of cerebellar Purkinje cells that implements the induction of LTD has been studied extensively (see e.g. Ito et al., 1982; Ekerot & Kano, 1985; Sakurai, 1987; Crépel & Krupa, 1988; Ekerot & Kano, 1989; Ito & Karachot, 1990; Crépel & Jaillard, 1991; Linden et al., 1991; Linden & Connor, 1992; Konnerth et al., 1992; Daniel et al., 1993; Karachot et al., 1994; Hartell, 1996; Freeman et al., 1998). In spite of all these experimental results, the exact mechanism of the LTD induction is still not known.

A detailed evalution of the experimental evidence is beyond the scope of the thesis (for review, see Ito, 1989; Linden, 1994; Plant et al., 1996; Daniel et al., 1998). Here, two

possible LTD induction scenarios will be described. Both scenarios assume that, under physiological conditions, LTD is only induced if the Purkinje cell receives conjunctive parallel fibre and climbing fibre input.

The classic LTD induction mechanism

The release of glutamate by the *climbing fibre* terminals results in the activation of AMPA receptors and a strong depolarisation of the Purkinje cell membrane potential. A consequence of the strong depolarisation is the influx of a large amount of Ca^{2+} through voltage-gated Ca^{2+} channels on the membrane of the Purkinje cell dendritic shafts. According to the classic view, the climbing fibre effect is mediated by the increase in the cytoplasmic Ca^{2+} concentration (summarised in figure 2.9 A).

The glutamate that is released by the *parallel fibres* activates two types of receptors: AMPA receptors, and metabotropic receptors (mGluRs). The activated mGluRs bind the G-protein-GDP complex, which stimulates the exchange of GTP for GDP and the dissociation of the G-protein complex into the $G_{\beta\gamma}$ and $G_{PLC\alpha}$-GTP subunits. The $G_{PLC\alpha}$-GTP subunit activates phospholipase C (PLC), and active PLC catalyses the hydrolysis of phosphatidylinositol 4,5-bisphosphate (PIP_2) into the diffusible second messenger molecules inositol 1,4,5-trisphosphate (IP_3) and diacylglycerol (DAG). The classic theory of LTD induction assumes that the major contribution of the parallel fibre input is the formation of cytoplasmic DAG.

The combined increase in the Ca^{2+} concentration and the concentration of DAG results in activation of protein kinase C (PKC). Thus, the PKC protein is a *coincidence detector* for climbing fibre and parallel fibre input, and calculates an *AND* function for the two inputs. Active PKC phosphorylates the postsynaptic AMPA receptors at the parallel fibre synapse. The consequence of the AMPA receptor phosphorylation is a decrease in the *number* of receptors, or a reduced *sensitivity* of the receptors to glutamate, both of which result in LTD of the parallel fibre evoked EPSPs.

In addition to the parallel fibre induced activation of the *mGluRs*, the *AMPA receptors* at the parallel fibre synapse must also be activated (Linden & Connor, 1992). A possible explanation for the required activation of the AMPA receptors by parallel fibre input is that the AMPA receptor evoked increase in the cytoplasmic Na^+ concentration reduces the efflux of Ca^{2+} through the Na^+/Ca^{2+} exchanger (Linden, 1994).

A nitric oxide mediated LTD induction mechanism

A problem with the classic LTD induction mechanism is that it takes neither the involvement of nitric oxide (NO) nor the release of Ca^{2+} from intracellular stores into account. Several experimental results indicate that the production of NO and the NO-induced production of cGMP are necessary for LTD induction (e.g. Crépel & Jaillard, 1990; Ito & Karachot, 1990; Daniel et al., 1993; Lev-Ram et al., 1995). However, NO synthase does not seem to exist in Purkinje cells, and the NO would have to be produced by another cell in the cerebellar cortex (for review, see Schumann & Madison, 1994). To complicate things even further, the release of Ca^{2+} from intracellular stores seems to be involved in LTD (for review, see Daniel et al., 1998).

Based on these results, an alternative mechanism for LTD induction has been suggested (Fiala et al., 1996, summarised in figure 2.9 B). In the alternative scenario, the *climbing fibre* induced complex spike results in efflux of a large amount of K^+ through Ca^{2+} dependent K^+ channels on the Purkinje cell membrane and depolarises the neighbouring stellate and basket cells in the cerebellar cortex. The depolarisation of the stellate and basket cells leads to Ca^{2+} influx through voltage gated channels , the binding of Ca^{2+} to calmodulin (CaM), and the binding of the Ca^{2+}-CaM complex to NO synthase in the stellate and basket cell cytoplasm. The binding of Ca^{2+}-CaM results in the activation of NO synthase and the production of the small and diffusible messenger molecule NO from the amino acid arginine.

NO diffuses back into the Purkinje cell dendrites and activates an NO-dependent form of guanylate cyclase (GC). Activated GC catalyses the formation of cGMP in the Purkinje cell cytoplasm. The elevated cGMP level leads to the activation of protein kinase

G (PKG) and enables PKG to phosphorylate a small protein called G-substrate. The phosphorylated form of G-substrate is an inhibitor of protein phosphatase-1 (PP-1). Given that PP-1 dephosphorylates the AMPA receptors, the effect of the climbing fibre input is to *prevent the dephosphorylation of AMPA receptors at the parallel fibre synapse.*

As in the classic scenario, the *parallel fibre* input leads to the activation of mGluRs, to the G-protein mediated activation of PLC, and to the formation of IP_3 and DAG from PIP_2. In contrast to the classic scenario, the binding of IP_3 to the IP_3 receptor Ca^{2+} channels on the membrane of intracellular stores results in the release of Ca^{2+} from the stores, and in a significant rise of the Ca^{2+} concentration in the Purkinje cell dendritic spines. The increase in the Ca^{2+} and DAG concentrations leads to the activation of PKC and to the PKC phosphorylation of the AMPA receptors. Thus, in the alternative scenario the parallel fibre effect is the *phosphorylation of the AMPA receptors by PKC.*

Conjunctive parallel fibre and climbing fibre input results in PKC *phosphorylation* of the AMPA receptors at the parallel fibre synapse, and at the same time in inhibition of the AMPA receptor *dephosphorylation*. Thus, the effect of the combined PF and CF input is the *persistent* phosphorylation of the AMPA receptors. Again, this leads to a decreased number or sensitivity of the AMPA receptors, and to a long-lasting depression of the parallel fibre evoked response.

That the parallel fibre induced Ca^{2+} release from intracellular stores is necessary for the induction of LTD can only be explained if the climbing fibre input does not provide enough Ca^{2+} to activate PKC. It is a well-documented fact that the climbing fibre input triggers a large Ca^{2+} spike in the Purkinje cell dendrites (see e.g. Knöpfel et al., 1991). Thus, it must be assumed that the CF evoked Ca^{2+} rise in the *dendritic shafts* is insulated from the PF evoked Ca^{2+} rise in the *spine heads*. Fiala et al. (1996) have suggested that a functional separation of the Ca^{2+} pools in the shafts and the spine heads can be achieved by the inhibitory input to the Purkinje cells.

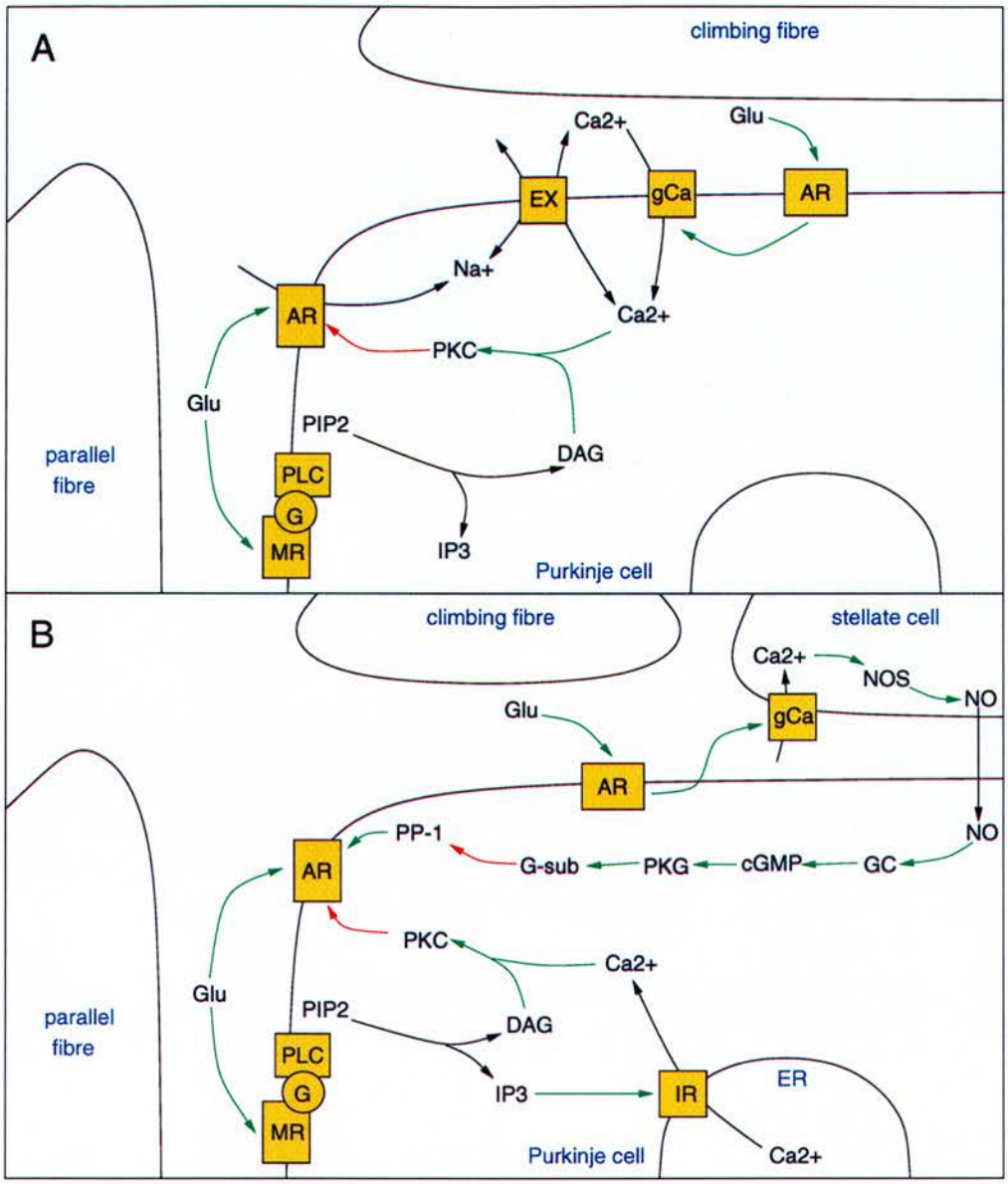

Figure 2.9: Two possible mechanism for the induction of parallel fibre LTD. (A) summarises the classic LTD induction mechanism, and (B) outlines an alternative mechanism that takes the requirement for NO and intracellular calcium release into account. Black arrows indicate chemical reactions, transport or diffusion, green arrows represent the activation of a component by another, and red arrows are inhibitory connections. The red arrow and green arrow that point to the AMPA receptor (AR) represent the phosphorylation and dephosphorylation of the receptor, respectively. The green arrows pointing to the voltage dependent calcium channels (gCa) indicate the opening of the channels in response to depolarisation of the Purkinje cell. The components are: Glu glutamate, MR metabotropic glutamate receptors, AR AMPA receptors, G G-protein, PLC phospholipase C, PIP2 phosphatidylinositol 4,5-bisphosphate, IP3 inositol 1,4,5-trisphosphate, DAG diacylglycerol, PKC protein kinase C, IR IP3 receptors, EX Na^+/Ca^{2+} exchanger, gCa voltage dependent Ca^{2+} channels, NO nitric oxide, NOS NO synthase, GC guanylate cyclase, cGMP cyclic guanosine monophosphate, PKG protein kinase G, G-sub G-substrate, PP-1 protein phosphatase-1, ER endoplasmic reticulum.

2.6.3 Other Forms of Cerebellar Plasticity

The long-term depression of the parallel fibre synapses is not the only form of synaptic plasticity in cerebellar Purkinje cells. Three other modifications of the excitatory and inhibitory synapses on Purkinje cells have been observed:

- A short-term potentiation (STP) of the parallel fibre synapses (Sakurai, 1987; Hirano, 1990; Crépel & Jaillard, 1991; Schreurs & Alkon, 1993). The parallel fibre STP can be induced by low-frequency (4 Hz) stimulation of the parallel fibres without conjunctive climbing fibre input, and disappears completely after about 20 minutes (Sakurai, 1987). The mechanism of the STP induction is not known.

- A Ca^{2+} mediated potentiation of the inhibitory synapses (Llano et al., 1991; Kano et al., 1992; Vincent et al., 1992). The Ca^{2+} mediated plasticity has been called *rebound potentiation* (Kano et al., 1992), can be induced by climbing fibre stimulation and decays in less than 60 minutes. An elevated cytoplasmic Ca^{2+} concentration is the *only* requirement for the potentiation of the inhibitory currents, the simultaneous activation of the inhibitory inputs is not necessary. Thus, the rebound potentation is *non-specific* and very likely a negative feedback mechanism that prevents overstimulation of the Purkinje cells (see e.g De Schutter, 1995, 1997).

- A *cAMP* mediated potentiation of the inhibitory synapses. Cheun and Yeh (1996) have reported that the activation of β-adrenergic receptors by noradrenaline results in the potentiation of GABA mediated inhibitory postsynaptic currents (IPSCs) in Purkinje cells. The intracellular application of cAMP derivatives and the adenylate cyclase (AC) activator forskolin have the same effect, and the probable mechanism of the IPSC potentiation is the activation of AC by the β-adrenergic receptors which leads to the production of cAMP, the activation of protein kinase A (PKA) and the PKA phosphorylation of the $GABA_A$ receptors. Consequence of the $GABA_A$ receptor phosphorylation is an increase in the GABA dependent Cl^- conductance.

2.7 Chapter Conclusions

In this chapter, the anatomy of the cerebellum was briefly summarised. The cerebellum is one of the few structures in the brain where the pattern of neuronal connections is almost entirely understood. This knowledge has inspired a large number of theories of cerebellar function. However, apart from the vague concept that the cerebellum contributes to motor control and, based on more recent data, also to cognition, there is still no general agreement about its functional role.

One of the most contentious issues in cerebellar research is whether or not the cerebellum is involved in *motor learning*. The most influential theory of cerebellar learning was formulated by David Marr almost thirty years ago. Marr suggested that the cerebellar cortex is a pattern associator, and that patterns are stored by adjusting the synaptic efficacies betwen parallel fibres and Purkinje cells.

In the early eighties, Masao Ito and his collaborators presented experimental results showing that the synapses between the parallel fibres and the Purkinje cell are indeed modifiable. Ito and colleagues found that the repeated conjunctive stimulation of parallel and climbing fibres results in long-term depression (LTD) of the parallel fibre induced response in the Purkinje cell. Often, the existence of parallel fibre LTD is presented as evidence for the involvement of the cerebellum in motor learning. However, several experimental results cast some doubt on this assumption, and the function of parallel fibre LTD is still an unresolved issue.

One of the paradigms that has been used extensively to study the involvement of the cerebellum in motor learning is classical conditioning of the eye-blink response. In the next chapter, the contribution of the cerebellum to eye-blink conditioning will be discussed in detail.

Chapter 3

Classical Conditioning of the Eye-Blink Response

3.1 Introduction

In the previous chapter, the anatomy of the cerebellum was summarised. It was mentioned that the cerebellum is a highly regular structure, and that its neuronal circuitry is almost entirely understood. In spite of this detailed anatomical knowledge, the exact function of the cerebellum is still an unresolved question. It is generally agreed that the cerebellum contributes to *motor control*, but it is not clear what its exact contribution to motor control is, or what the underlying computations are.

Another open question is whether or not the cerebellum is involved in *motor learning*. The contribution of the cerebellum to motor learning, and the synaptic plasticity in the cerebellum that could implement the motor learning, are two of the major foci in cerebellar research. The involvement of the cerebellum in motor learning has been investigated extensively in the contex of classical conditioning of simple motor responses, such as the vestibulo-ocular reflex (VOR) and the nictitating membrane or eye-blink reflex.

This chapter focusses on the involvement of the cerebellum in the associative learning that occurs during *classical conditioning of the eye-blink response*. In the following sections, the characteristics of eye-blink conditioning will be described, some of the experimental evidence for and against the contribution of the cerebellar cortex and the deep cerebellar nuclei will be summarised, and it will be discussed if the adaptation of synaptic efficacies in the cerebellum can implement the eye-blink learning.

3.2 The Classically Conditioned Eye-Blink Response

3.2.1 Classical Conditioning

Classical conditioning is one of the simplest and most thoroughly investigated examples of associative learning. The concept was introduced more than 70 years ago by Ivan Pavlov (1927) who combined Aristotle's suggestion that learning involves the association of ideas with knowledge about simple reflex acts. In classical conditioning, an association is learnt between two *stimuli*: the *conditioned stimulus* (CS) and the *unconditioned stimulus* (US). Originally, only the US elicits an observable response (called *unconditioned response* or UR) and the CS is ineffective. After repeated pairing of CS and US, both stimuli become associated and the CS is now also effective in eliciting a response (called *conditioned response* or CR). The CS has come to signal the likely occurrence of a US and the CR prepares the animal for this event. Thus, CR and UR are usually (but not always) quite similar.

3.2.2 Eye-Blink Conditioning

The most commonly studied form of classical conditioning is eye-blink conditioning, more specifically, conditioning of the nictitating membrane response (NMR) in rabbits. In NMR conditioning, a light, tone or vibrotactile CS is associated with a noxious US like a periorbital electric shock or an airpuff to the cornea. Both UR and CR protect

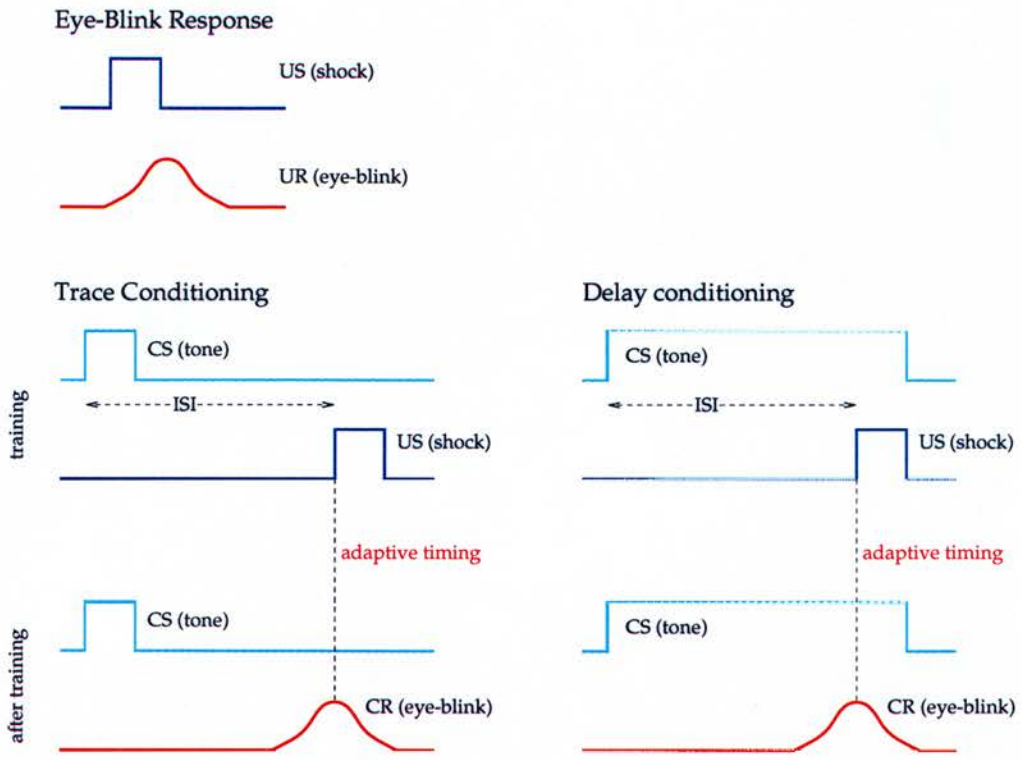

Figure 3.1: The eye-blink response and two different protocols for classical conditioning. In trace conditioning, the unconditioned stimulus (US) terminates before onset of the conditioned stimulus (CS), in delay conditioning, both stimuli overlap. UR unconditioned response, CR conditioned response, ISI interstimulus interval. The CR is *timed adaptively* and peaks at the time of the US onset during training.

the animal against damage to the eye and involve a complex behaviour consisting of nictitating membrane extension, eyelid closure, eyeball retraction and some contraction of face and neck muscles (Gormezano et al., 1962; McCormick et al., 1982b). With the exception of the nictitating membrane extension which is specific to rabbits, the phenomenon is very similar in all mammals, including humans, and the more general terms *eye-blink response* and *eye-blink conditioning* are used in the thesis.

3.2.3 Temporal Specificity

A general feature of associative learning which is also shared by classical conditioning is *temporal specificity* (e.g. Rescorla, 1988; Hawkins et al., 1986). Learning is optimal if the CS precedes the US by some period of time, depending on the response which is

being conditioned. For eye-blink conditioning, the optimal interstimulus interval (ISI) between CS (e.g. tone) and US (e.g. shock) onset is 200–400 ms (Smith et al., 1969; Steinmetz, 1990a). Shorter or longer CS-US ISIs lead to a decrease in both amplitude and probability of occurrence of eye-blink CRs. The window of effective ISIs which result in association of CS and US depends on the conditioning protocol. If the CS terminates before US onset (a protocol which is called *trace* conditioning, see figure 3.1), the ISI must not be longer than 2 s (Solomon et al., 1986). With overlapping stimuli (*delay* conditioning), conditioning is easier to achieve and the CS onset can precede the US onset by up to 4 s (Gormezano, 1966). Both in trace and delay conditioning, no learning occurs if the ISI is shorter than 50–100 ms or if the US precedes the CS (Smith et al., 1969; Steinmetz et al., 1989; Steinmetz, 1990a). The restrictions on relative timing of CS and US have implications for possible synaptic learning mechanisms and give rise to much debate (discussed for example in Thompson & Krupa, 1994; De Schutter, 1995, 1997, and section 3.3.7).

3.2.4 Extinction

Conditioning enables the animal to predict relationships between events in the environment. During eye-blink conditioning, the animal learns that the occurrence of, for example, a tone CS predicts that a shock US is likely to follow. If the tone CS is presented repeatedly without a shock US, it comes to predict the opposite. The animal now learns that a tone is probably *not* followed by a shock. The amplitude and frequency of eye-blink CRs in response to a tone CS decrease, a phenomenon which is known as *extinction*.

3.2.5 Adaptive Timing

Although the unconditioned eye-blink response to a shock US and the conditioned eye-blink response to a tone CS are similar, there are also significant differences indicating that they are at least partly mediated by different efferent neural systems (for

review, see Thompson & Krupa, 1994). One obvious difference concerns the latency of the responses: the minimum time delay between CS and CR is more than three times longer than the delay between US and UR. More importantly, the conditioned eye-blink response is *timed adaptively* and peaks at about the time of US onset during learning, thus providing optimal protection against the expected noxious effects of the US (Coleman & Gormezano, 1971; Millenson et al., 1977; Steinmetz, 1990a, see figure 3.1). The adaptive timing phenomenon is interesting in a wider than just the classical conditioning context and raises the fundamental question how a network of neurons can learn a time delay between input and output.

3.3 Eye-Blink Conditioning and the Cerebellum

3.3.1 Experimental Results are Inconclusive

Identifying the memory storage sites for eye-blink conditioning has turned out to be a much more difficult task that one might expect for this relatively simple and well-defined behaviour. Experimental results are contradictory and there is an ongoing controversial debate (e.g. Bloedel, 1992; Thompson & Krupa, 1994; De Schutter, 1997; Bloedel et al., 1997; Kim & Thompson, 1997). Some of the controversies have arisen over the interpretation of lesion and inactivation studies, partly because of ill documented variations in placement and extent of the lesions and partly because of difficulties distinguishing learning deficits from performance deficits (De Schutter, 1997; Bloedel et al., 1997). Another cause of confusion is the disagreement about the use of controls in some experiments (Welsh & Harvey, 1989; Thompson & Krupa, 1994; Bloedel et al., 1997).

A summary of the available experimental data can be found in tables 3.1 and 3.2. Most experiments fall into one of four categories: permanent lesions, electrophysiological recordings, electrical microstimulation and reversible inactivation studies. Microstimulation and reversible inactivation are particularly interesting: substituting electrical

Experiment	Result	Reference
IN recordings	firing pattern of cells models CR	Berthier and Moore (1990), McCormick and Thompson (1984b)
IN lesions after training	CR abolished, no effect on UR	McCormick et al. (1981), Yeo et al. (1985a), Steinmetz et al. (1992)
	effect on CR *and* UR (*)	Welsh and Harvey (1989)
IN lesions before training	no learning	Lincoln et al. (1982)
SCP lesions after training	CR abolished, no effect on UR	McCormick et al. (1982a)
IN stimulation	eye-blink response, abolished by SCP lesions	McCormick and Thompson (1984a)
RN recordings	firing pattern of cells models CR	Chapman et al. (1990)
RN stimulation	eye-blink response	Chapman et al. (1988)
RN lesions after training	CR abolished, no effect on UR	Rosenfield and Moore (1983), Chapman et al. (1988)
PN recordings	cells respond to tone CS	Steinmetz et al. (1987)
PN lesions after training	CR abolished (CS modality specific)	Steinmetz et al. (1987)
MCP lesions after training	CR abolished	Lewis et al. (1987)
PN and MCP stimulation	effective as CS	Steinmetz et al. (1986)
IO recordings	cells respond to airpuff US	Sears and Steinmetz (1991)
IO lesions before training	no learning	McCormick et al. (1985)
IO lesions after training	extinction with continued training	McCormick et al. (1985)
IO stimulation	effective as US	Mauk et al. (1986)

Table 3.1: Experiments aimed at identifying the site of memory storage for eye-blink conditioning. IN dorsal anterior interpositus nucleus, SCP superior cerebellar peduncle, RN magnocellular red nucleus, PN pontine nucleus, MCP middle cerebellar peduncle, IO dorsal accessory inferior olive. All experiments apart from the ones marked with (*) indicate that the memory storage sites for eye-blink conditioning are in the cerebellar cortex and/or the interpositus nucleus.

Experiment	Result	Reference
Purkinje cell recordings before training	CS results in increased simple spike frequency	Foy and Thompson (1986)
	US results in complex spikes	
Purkinje cell recordings after training	CS results in decreased simple spike frequency	Foy et al. (1992), Berthier and Moore (1986)
	no US evoked complex spikes in CS-US trials	Foy and Thompson (1986)
cerebellar cortical lesions after training	impaired adaptive CR timing	Perrett et al. (1993)
decerebrate, decerebellate rabbits	able to learn CRs (*)	Kelly et al. (1990)
	*un*able to learn CRs	Nordholm et al. (1991)
pcd mutant mice (no Purkinje cells)	learning is reduced but not completely abolished, impaired adaptive CR timing	Chen et al. (1996), Kim and Thompson (1997)
reversible inactivation of MN during training	CR and UR abolished, normal learning	Thompson et al. (1993), Zhang and Lavond (1991)
reversible inactivation of RN during training	CR abolished, no effect on UR, normal learning	Krupa et al. (1993)
	effect on CR and UR (*)	Bracha et al. (1993)
reversible inactivation of IN and overlying cortex during training	CR abolished, no effect on UR, no learning	Clark et al. (1992), Nordholm et al. (1993), Krupa et al. (1993)
reversible inactivation of IN during training	CR abolished, normal learning (*)	Welsh and Harvey (1991)
	effect on CR and UR (*)	Bracha et al. (1994)
reversible inactivation of white matter ventral to IN during training	CR abolished, no effect on UR, normal learning	Nordholm et al. (1993)
reversible inactivation of SCP during training	CR abolished, no effect on UR, normal learning	Krupa and Thompson (1995)
inhibition of protein synthesis in IN	no learning, no effect on CR execution	Bracha et al. (1995)

Table 3.2: More experiments aimed at identifying the site of memory storage for eye-blink conditioning. MN 7th and accessory 6th motor nuclei, RN magnocellular red nucleus, IN dorsal anterior interpositus nucleus, SCP superior cerebellar peduncle. All experiments apart from the ones marked with (*) indicate that the memory storage sites for eye-blink conditioning are in the cerebellar cortex and/or the interpositus nucleus.

stimulation for peripheral stimuli can serve to identify the sites which are *sufficient* for memory storage, and reversible inactivation during training can help to distinguish the *memory storage* sites from its *efferent effector* sites, something which is quite difficult with other techniques. In the following, some of the evidence will be discussed in more detail.

3.3.2 Pontine Nucleus Stimulation as Conditioned Stimulus

Different regions of the pontine nuclei (PN) respond to auditory, visual and somatosensory stimuli (Steinmetz et al., 1987). Animals can be classically conditoned with PN stimulation as CS and a corneal airpuff as US, resulting in faster learning than a tone or light CS (Steinmetz et al., 1986). CRs obtained in this way are abolished by lesions of the middle cerebellar peduncle (MCP) which carries mossy fibre projections from the PN to granule cells in the cerebellar cortex, and MCP stimulation is also effective as CS. Interpositus nucleus (IN) lesions abolish the conditioned response (Steinmetz et al., 1986), and some of the animals trained with a PN stimulation CS react with eye-blink CRs to a tone CS (Steinmetz, 1990b). Altogether, these results indicate that the PN–mossy fibre–cerebellar cortex–IN system is part of the pathway which links CS and CR.

3.3.3 Inferior Olive Stimulation as Unconditioned Stimulus

Before training, a corneal airpuff US results in increased neuronal activity in a region of the dorsal accessory inferior olive (IO). During training, the IO response to the airpuff US decreases for paired CS-US trials, but remains constant for US alone trials, consistent with increased IN activity after CS presentation and an inhibitory connection between IN and IO (this might also indicate that the IO provides an *error signal*, see Sears & Steinmetz, 1991). IO stimulation can elicit eye-blinks and, depending on electrode location, a variety of other responses. If an IO stimulation US is paired with a tone CS, the response caused by IO stimulation is learnt as CR to the tone CS (Mauk

et al., 1986; Steinmetz et al., 1989). Both the CR to the tone and the UR to IO stimulation are abolished by IN lesions, indicating that the US is transmitted through climbing fibres from the IO to the cerebellum (Thompson, 1989).

3.3.4 Reversible Inactivation

Permanent lesion studies can be used to identify a *pathway* in the brain which is necessary for learning. Once the essential pathway is known, *reversible* inactivation can help to identify the *exact site* of memory storage within the pathway. If a site is reversibly inhibited (by cooling or injection of GABA agonists) during training, and the animal shows no sign of having learnt after training, when the effect of the inactivation has stopped, the site in question must be the memory storage site or a necessary afferent. In contrast, if the animals have learnt during inactivation training, the reversibly inactivated site must be *efferent* to the site of memory storage. In the cerebellar system, Thompson and co-workers found that inhibiting different structures can lead to three different patterns of results (see table 3.2). Reversible inactivation of the seventh and accessory sixth motor nuclei (MN) prevents expression of both CR and UR during training, and the animals learn as well as the uninhibited controls (Thompson et al., 1993; Zhang & Lavond, 1991, locus of inhibition is indicated by (1) in figure 3.2). Inactivation of the magnocellular red nucleus (RN) abolishes the CR without affecting the UR and has no effect on learning (Krupa et al., 1993, (2) in figure 3.2). The same result is found for inhibiting the white matter ventral to the interpositus nucleus (IN) which contains the efferent projections from the IN to RN and other brain regions (Nordholm et al., 1993, (3) in figure 3.2). Finally, Thompson, Lavond and colleagues report that inactivation of the dorsal anterior IN and the overlying cerebellar cortex prevents both learning and expression of the CR without any effect on the UR (Clark et al., 1992; Nordholm et al., 1993; Krupa et al., 1993, (4) in figure 3.2).

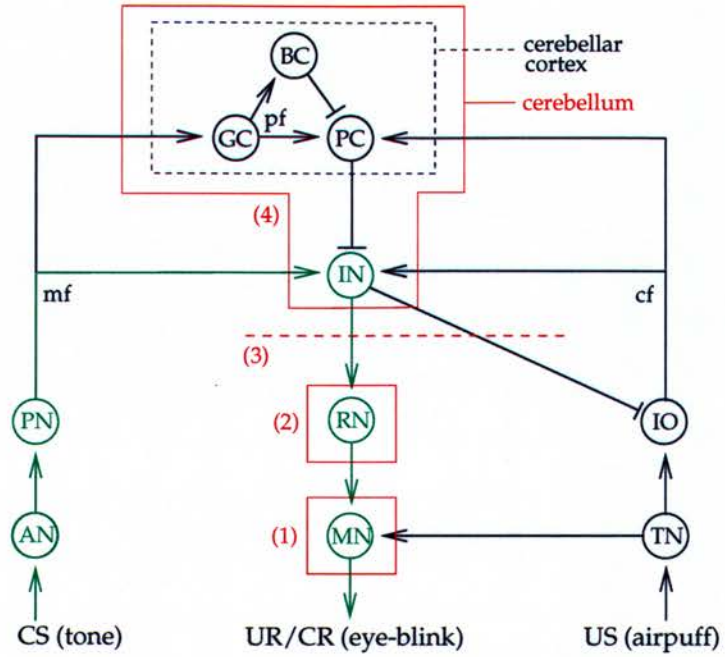

Figure 3.2: Some of the neural circuitry which could be the substrate for eye-blink conditioning. AN auditory nuclei, PN pontine nuclei, GC granule cell, BC basket cell, PC Purkinje cell, IN interpositus nucleus, RN red nucleus, MN cranial motor nuclei, IO inferior olive, TN trigeminal nucleus, mf mossy fibres, pf parallel fibres, cf climbing fibres. ↓ represents an excitatory, ⊥ an inhibitory connection. The potential link between CS and CR is indicated in green, different sites for reversible inactivation experiments are shown in red (1-4).

3.3.5 Cerebellar Plasticity as Substrate for Eye-Blink Conditioning?

Figure 3.2 shows the simplest explanation for these results. Eye-blink conditioning is based on plasticity in the cerebellum (cerebellar cortex and/or interpositus nucleus, indicated by (4) in the figure). The CS reaches the cerebellum through mossy fibres and pontine nuclei PN (and in the case of a tone CS, auditory nuclei AN). The US pathway to the cerebellum leads through trigeminal nucleus TN and inferior olive IO. The inhibitory connection from IN to IO accounts for the decrease of US-evoked IO activity during training, indicating that the IO conveys an error signal. A CS which results in the correct CR leads to IN activity just before the US reaches the IO. Thus, the IO is inhibited and unnecessary climbing fibre input to the cerebellum is switched off. Finally, the US triggers a UR through a connection between TN and cranial motor nuclei MN, both directly and indirectly via the reticular formation (not shown in the figure).

Although this scenario seems to provide a very straightforward explanation for the results summarised in sections 3.3.2 – 3.3.4, there are a few problems and several open questions. One of the open questions is where exactly in the cerebellum the synaptic efficacy changes which implement the conditioning take place. As both the cerebellar cortex and the IN receive information about the CS through mossy fibres and about the US through climbing fibres, they are both potential sites for the formation of CS-US associations. Unfortunately, it is very difficult to lesion the cerebellar cortex selectively without damaging the IN (Kim & Thompson, 1997). Furthermore, the cerebellar circuitry is not purely feedforward and contains recurrent connections from the IN back to the cortex (Batini et al., 1989), making the interpretation of inactivation studies difficult even if they are selective for either cortex or IN. Excluding either cortex or IN as memory storage site would only be possible after selective inhibition of both structures *with different results*, something which has not been achieved yet.

Recently, eye-blink conditioning has been investigated in *Purkinje cell degeneration (pcd)* mutant mice which are devoid of Purkinje cells after the fourth postnatal week (Chen et al., 1996; Kim & Thompson, 1997). The *pcd* mice exhibit reduced but existing eye-blink conditioning and impaired adaptive CR timing, similar to rabbits with cerebellar cortical lesions (Yeo et al., 1985b; Perrett et al., 1993). Thus, eye-blink conditioning memory might be distributed over *both* cerebellar cortex and IN, and the cortex seems to play a special role in learning the *time delay* between CS and CR.

A further complication is that several groups have consistently failed to reproduce Thompson et al.'s results (experiments marked by (*) in tables 3.1 and 3.2). In contrast to Thompson, Yeo and colleagues (section 3.3.4), Welsh and Harvey (1989) claim that IN lesions impair *both CR and UR*, and Bracha et al. (1994) have published the same result for reversible inactivation of the IN. Similarly, Bracha et al. (1993) and Clark and Lavond (1993) report reduced UR performance during inhibition of the RN. According to Thompson and Krupa (1994), Welsh and Harvey's results might be due to individual differences between animals; they only compared the UR performance in lesioned and unlesioned animals and not before and after lesioning in the *same* animal. However, this criticism does not apply to Bracha et al.'s experiments. In an attempt to

distinguish learning and performance, Bracha et al. (1995) have shown that injection of the protein synthesis inhibitor anisomycin into the IN inhibits acquisition but not execution of eye-blink CRs (for review, see Bloedel et al., 1997). A potential interpretation of all these results can be summarised as:

- Both cerebellar cortex and interpositus nucleus are memory storage sites for eye-blink conditioning.
- The cerebellar cortex is necessary for the adaptive timing of the conditioned response.
- The formation of long-term eye-blink memory is based on protein synthesis in the interpositus nucleus.
- Output from the cerebellum via the red nucleus is necessary for *perfect* execution of *both* the conditioned and unconditioned eye-blink response.

In conflict with this interpretation is a study by Welsh and Harvey (1991) who report unimpaired eye-blink learning during reversible inactivation of the IN. Interestingly, Nordholm et al. (1993) find normal learning during inactivation of the white matter ventral to the IN. Thus, an explanation for Welsh and Harvey's results might be the exact placement of their inhibition. To summarise, although there are some discrepancies which need to be resolved, the majority of experiments support the hypothesis that eye-blink conditioning is based on memory formation in the cerebellar cortex and the IN.

3.3.6 Purkinje Cell LTD as Substrate for Eye-Blink Conditioning?

If the cerebellum is the memory storage site for eye-blink conditioning, what are the exact cellular and subcellular changes that implement the memory formation? Given that the modifiable synapses must be to postsynaptic neurons that receive information about both CS and US, there are four possible changes of synaptic efficacy which could establish the effective link between CS and CR in the cerebellum (compare figure 3.2):

1. An *increase* in mossy fibre → interpositus neuron synaptic efficacy.
2. A *decrease* in Purkinje cell → interpositus neuron synaptic efficacy.
3. A *decrease* in parallel fibre → Purkinje cell synaptic efficacy.
4. An *increase* in inhibitory interneuron → Purkinje cell synaptic efficacy.

Not much is known about synaptic plasticity in the interpositus nucleus. Long-term potentiation (LTP) of mossy fibre → IN synapses has been described (Racine et al., 1986), but it is unclear if it depends on US input through the climbing fibres, making the connection to eye-blink conditioning doubtful. However, the results from Thompson's and Bloedel's groups (section 3.3.5) indicate that plasticity in the IN does play a role and further experiments are needed to clarify the situation.

The plasticity of the inhibitory and excitatory synapses on Purkinje cells has been studied extensively (see section 2.6). It was found that the synapses between inhibitory interneurons and Purkinje cells are potentiated after repetitive climbing fibre input (Llano et al., 1991; Kano et al., 1992; Vincent et al., 1992). However, the potentiation is non-specific, only requiring Purkinje cell depolarisation or an increased intradendritic Ca^{2+} concentration and not the concurrent activation of the respective inhibitory inputs (Llano et al., 1991). This lack of input-specificity rules it out as a potential mechanism for eye-blink learning.

By far the most thoroughly studied form of cerebellar plasticity is long-term depression (LTD) of the parallel fibre → Purkinje cell synapses (discussed in detail in section 2.6.2). According to the standard paradigm, LTD is induced by concurrent activation of parallel fibres and climbing fibres (e.g. Ito et al., 1982; Ito, 1989). Furthermore, a *potentiation* of the same synapses has been observed after stimulation of parallel fibres alone (Sakurai, 1987; Hirano, 1990; Crépel & Jaillard, 1991; Schreurs & Alkon, 1993). Thus, the following processes have been suggested to underlie memory formation and extinction during eye-blink conditioning (e.g. Ito, 1989; Thompson & Krupa, 1994, compare figure 3.2):

1. Before training, the connection between CS and CR through PN, IN, RN and MN (indicated in green in figure 3.2) is inhibited by Purkinje cell input to the IN neurons, and a CS (e.g. a tone) is unable to elicit an eye-blink CR.

2. Repeated paired presentation of CS (e.g. tone) plus US (e.g. airpuff) results in repeated coinciding parallel and climbing fibre input to Purkinje cells and in LTD of the parallel fibre → Purkinje cell synapses.

3. Because of the depressed parallel fibre synapses after training, the CS leads to decreased Purkinje cell activation and to disinhibition of the IN neurons. The connection between CS and CR is now open and the animal has learnt to respond to the CS with an eye-blink CR.

4. If the CS is presented several times without a US, the parallel fibre input without a coinciding climbing fibre signal results in potentiation of the parallel fibre → Purkinje cell synapses.

5. As a consequence, the situation is back to what it was before training (stage 1): the IN neurons are inhibited and the CS-CR connection is closed (*extinction* of the eye-blink response, see section 3.2.4).

This scenario is currently the simplest and therefore the most attractive neuronal explanation for eye-blink conditioning. However, as it fails to take IN plasticity, adaptive CR timing and the effect of cerebellar output on performance into account, it must be *too* simplified. More importantly, a serious problem is that the temporal properties of eye-blink conditioning and LTD induction seem to differ. The timing requirements for LTD induction are yet another contentious issue in cerebellar research (e.g. Schreurs & Alkon, 1993; Thompson & Krupa, 1994; Chen & Thompson, 1995; De Schutter, 1995, 1997) and will be discussed in the following section.

3.3.7 Different Temporal Properties of Conditioning and LTD?

The temporal requirements for classical conditioning of the eye-blink response are fairly well established (section 3.2.3). For successful conditioning, the CS must precede the US by 50-100 ms, whether external stimuli or direct stimulation of mossy/parallel and climbing fibres are used (Smith et al., 1969; Steinmetz et al., 1989; Steinmetz, 1990a). From the animal's point of view, this is sensible: it is only worth reacting to a CS which predicts and therefore precedes the US.

In contrast, the temporal properties of LTD induction are still very controversial. In most experiments, the climbing fibre (CF) stimulation has been applied simultaneously with or about 10 ms *before* the parallel fibre (PF) or mossy fibre (MF) stimulation (Ito, 1989; Thompson & Krupa, 1994). According to the hypothetical classical conditioning scenario in the previous section, this order of stimuli should be ineffective and the reverse order (CF input *after* PF input) should be maximally effective for LTD induction. Several attempts to systematically investigate the parameter dependence of LTD induction have produced different results.

- Ekerot and Kano (1985, 1989) studied simple spike peristimulus time histograms (PSTHs) as indication for the Purkinje cell (PC) responsiveness *in vivo* in decerebrated rabbits. In their experiments, 8 minutes of 2 Hz stimulation applied to PFs and CFs resulted in a maximal decrease of PC responsiveness if the CF stimuli preceded the PF stimuli by an interstimulus interval (ISI) of 20 ms. A CF - PF ISI of 125 ms was less effective, and ISIs of 250 ms and 375 ms were only weakly effective (Ekerot & Kano, 1985) or completely ineffective (Ekerot & Kano, 1989). Interestingly, reduced PC responsiveness was also observed after stimulation with ISIs between -5 ms and -20 ms (i.e. PF stimulus first), but only in 4 out of 7 cells. Inhibitory input to the PCs caused by conjunctive stimulation of *off-beam* PFs (see section 2.5.4) prevented the long-term responsiveness change.
- Using intradendritic PC recordings in rabbit cerebellar slice, Schreurs and Alkon (1993) found that 30 s of conjunctive 4 Hz CF and PF stimulation resulted in LTD

of the PF evoked EPSP amplitudes if a CF - PF ISI of 50 ms was used and the $GABA_A$ antagonist bicuculline was present, but *not* if the PF stimulus came first (ISI -20 ms or -50 ms) or if the $GABA_A$ antagonist was absent. Paired stimulation with CF and PF stimulus trains in a delay conditioning-like protocol (400 ms of 100 Hz PF stimulation co-terminating with 100 ms of 10 Hz CF stimulation, repeated 20 times with an intertrial interval of 30-60 s, compare figure 3.1) produced LTD in the absence of $GABA_A$ blockers. However, unpaired stimulation of PF and CF pulse trains was equally effective and the depression might be due to an unphysiological depletion of glutamate and irrelevant for classical conditioning.

- In a similar experiment with intradendritic PC recordings in rat cerebellar slice, Karachot et al. (1994) applied 280 ms of 50 Hz stimulation to PFs, immediately followed by 40 ms of 50 Hz stimulation (i.e. 3 pulses) to CFs, and repeated the combined stimulation every 20 s for 10 minutes. In contrast to what might be expected after Schreurs et al.'s results, this trace conditioning-like protocol (see figure 3.1) did *not* result in LTD. Similar to Ekerot, Schreurs and colleagues, Karachot et al. (1994) also investigated the LTD induction capability of paired single stimuli to PFs and CFs. Using 300 pulses of conjunctive PF and CF stimulation with frequencies between 0.5 and 4 Hz, LTD could be induced for a wide range of CF - PF ISIs between 0 and 1750 ms. The reverse order of stimulation (PF before CF, ISIs between 0 and -100 ms) was also effective, but to a lesser degree. All of Karachot et al.'s experiments were performed in the presence of the $GABA_A$ blocker picrotoxin.

- Chen and Thompson (1992, 1995) used extracellular field-potential recordings in rat cerebellar slice to investigate the influence of $GABA_A$ inhibition, number of stimuli and ISI on the formation of LTD. In the absence of $GABA_A$ blockers, 600 s of 1 Hz conjunctive stimulation induced LTD for all CF - PF ISIs tested (250 ms, 0 ms, -125ms and -250 ms), but 100 s of stimulation were only effective for an ISI of -250 ms (PF *before* CF) and to a much lesser extent for -125 ms. However, if $GABA_A$ receptor-mediated inhibition was blocked by bicuculline, simultaneous stimulation (0 ms ISI) became also effective in inducing LTD.

The variation in stimulation protocols and the different ways of measuring LTD make these results difficult to interprete. Chen's and Thompson's results seem to indicate that Purkinje cell LTD *could* be the basis of eye-blink conditioning. However, field-potential recordings in cerebellar preparations can be contaminated by contributions from the large number of inhibitory interneurons (Ito, 1984, 1989), and because of the influence of $GABA_A$ inhibition on LTD induction it is not easy to control for this effect.

A general problem of all experiments with repeated presentation of single stimulus pairs is that every positive ISI Δt corresponds to a negative ISI given by Δt minus the period of the repetitive stimulation. For example, in Karachot et al.'s experiments, the ability of a 750 ms CF - PF ISI to induce LTD during conjunctive stimulation with a frequency of 1 Hz could also be interpreted as the effect of a -250 ms ISI with a CF pulse *after* the PF pulse, consistent with LTD as mechanism for eye-blink conditioning. Furthermore, the result that ISIs between 0 ms and -100 ms are less effective is in agreement with the observation that the CS must precede the US by 50-100 ms for successful conditioning. In any case, the low-frequency conjunctive stimulation is quite different from the actual PF and CF firing during conditioning and the results should not be overrated.

The most serious argument *against* LTD as substrate for conditioning is Karachot et al.'s failure to induce LTD with PF and CF trains in a trace conditioning protocol. However, Schreurs and Alkon *did* induce LTD using higher stimulation frequencies and a delay conditioning-like protocol. Even though the mechanism for this form of LTD is likely to be neurotransmitter depletion or an unphysiologically high Ca^{2+} concentration caused by the PF input, the experiments should be repeated with varying stimulation frequencies of PFs and CFs and in the presence and absence of $GABA_A$ inhibition before they can be used to rule out the LTD/conditioning hypothesis.

The only consistent observation in all experiments is that block of $GABA_A$ inhibition makes it easier to induce LTD. The origin of the inhibition is unclear, potential candidates are stellate and basket cells, Purkinje cell recurrent collaterals or autapses. Even Golgi cells could influence Purkinje cell LTD indirectly by inhibiting granule cells. One

of the reasons for the $GABA_A$ mediated reduction of LTD could be that the inhibitory inputs suppress the CF evoked plateau potentials in Purkinje cells (Ekerot & Oscarsson, 1981; Ekerot & Kano, 1985, 1989). The CF plateau potentials are at least partly based on an increased Ca^{2+} conductance (Llinas & Sugimori, 1980) and result in an elevated intracellular Ca^{2+} concentration. Temporal conjunction of the CF evoked Ca^{2+} rise and an accumulation of the second messenger DAG triggered by the PF input might be responsible for the induction of LTD by PKC phosphorylation of AMPA receptors (see section 2.6.2). Thus, the GABAergic modulation of the intradendritic Ca^{2+} dynamics in the Purkinje cell could determine if and when PF LTD can be induced.

To summarise, more detailed knowledge about the time course of Ca^{2+} in Purkinje cells and its modification by inhibitory inputs will be necessary to understand the temporal properties of LTD induction. At the moment, it is still too early to say if LTD of the parallel fibre $\rightarrow$ Purkinje cell synapses is one of the mechanisms of eye-blink conditioning, and more experiments and modelling studies are needed before the issue can be resolved.

3.4 Chapter Conclusions

One of the most contentious issues in cerebellar research is whether or not the cerebellum contributes to motor learning. Over the past thirty years, the involvement of the cerebellum in motor learning has been studied extensively in the context of classical conditioning of the vestibulo-ocular and the eye-blink response.

In this chapter, the involvement of the cerebellum in classical conditioning of the eye-blink response was discussed. In spite of the extensive knowledge about the cerebellar anatomy and physiology, and the simple and well-defined eye-blink conditioning paradigm, the experimental evidence is inconclusive and there is an ongoing controversial debate. Many experimental results are based on lesion studies, and many

controversies have arisen over the exact location or extent of the lesions, the use of the correct controls, and the differences between learning deficits and performance deficits.

Although additional experiments are needed to resolve the issue, most of the existing evidence supports the hypothesis that the eye-blink memory is formed and stored in the cerebellar cortex and the interpositus nucleus, and that the conditioned stimulus (CS) and the unconditioned stimulus (US) reach the cerebellum through the mossy fibres and the climbing fibres, respectively. According to this hypothesis, the conditioned eye-blink response (CR) is triggered by an increased firing rate of the neurons in the interpositus nucleus.

In the cerebellar cortex, a form of synaptic plasticity that could implement the eye-blink conditioning is long-term depression (LTD) of the synapses between parallel fibres and Purkinje cells. Given that parallel fibre LTD can be induced by conjunctive mossy fibre and climbing fibre input, the paired presentation of CS and US could result in the depression of the parallel fibre synapses and in the disinhibiton of the interpositus neurons. After several paired presentations of CS and US, the CS alone will be able to elicit an eye-blink CR. The repeated presentation of the CS alone will result in potentiation of the parallel fibre synapses and extinction of the eye-blink CR.

Thus, parallel fibre LTD could implement the association between CS and CR that is formed during eye-blink conditioning. However, based on parallel fibre LTD alone, it is not possible to explain why the eye-blink CR is *timed adaptively* and peaks at the time of the US onset during training. Recently, Fiala and collaborators have formulated a model of intracellular signalling in cerebellar Purkinje cells that suggests an explanation for the adaptive timing of the classically conditoned eye-blink response. Fiala et al.'s model will be discussed in detail in the next chapter.

Chapter 4

The Spectral Timing Model

4.1 Introduction

In the previous chapter, experiments aimed at identifying the memory storage sites for classical conditioning of the eye-blink response were summarised, and it was argued that most of the evidence indicates that eye-blink conditioning is based on plasticity in the cerebellar cortex and in the interpositus nucleus. In the cerebellar cortex, a potential mechanism for eye-blink conditioning is long-term depression (LTD) of the synapses between parallel fibres and Purkinje cells. Parallel fibre LTD could result in a decreased Purkinje cell response after presentation of the conditioned stimulus (CS), leading to disinhibition of neurons in the interpositus nucleus (IN) and an open connection between the CS and the eye-blink conditioned response (CR).

Although the existence of LTD could explain the *formation* of the CS-CR association, it is unable to explain why the CRs are *timed adaptively* and peak at the time of the unconditioned stimulus (US) onset during training. Recently, Fiala, Grossberg and Bullock (1996) have developed a computational model of intracellular signalling in Purkinje cells which provides a potential explanation for the adaptive CR timing. All of the models that will be discussed in the following chapters are derived from Fiala

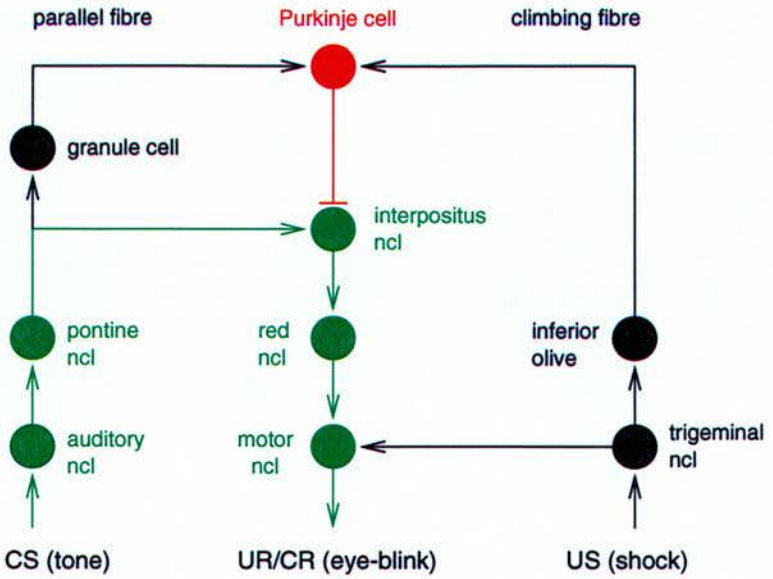

Figure 4.1: The neural circuitry which implements eye-blink conditioning in the *Spectral Timing Model*. Before training, the connection between CS and CR (green) is inhibited by Purkinje cell input (red). Repeated paired presentation of CS and US results in decreased responsiveness of Purkinje cells, disinhibition of interpositus neurons and an open connection between CS and CR. In contrast, repeated presentation of a CS alone leads to increased Purkinje cell responsiveness, inhibition of the interpositus neurons and extinction of the CR. Single circles in the diagram represent groups of neurons in the brain.

et al.'s *Spectral Timing Model*. In this chapter, the biochemical foundations and mathematical formulation of the Spectral Timing Model will be summarised, a few minor improvements will be suggested and numerical simulation results will be presented.

4.2 Biology and Biochemistry of the Model

In the Spectral Timing Model, the eye-blink conditioning is implemented by a group of Purkinje cells which inhibit a common target neuron or group of neurons in the interpositus nucleus (IN). As shown in figure 4.1, output from the IN triggers execution of the eye-blink CR. Information about CS and US reaches the Purkinje cells via parallel fibres and climbing fibres, respectively. All Purkinje cells in the group receive parallel fibre input at the same time and, after the interstimulus interval (ISI), climbing fibre input at the same time.

During conditioning, paired presentation of CS and US results in concurrent parallel fibre (PF) and climbing fibre (CF) input to the Purkinje cells (PC) and in depression of the PC response to PF input, similar to the conditioning scenario in section 3.3.6. However, in contrast to the previously described scenario, the PC responsiveness decrease in the Spectral Timing Model is *not* based on parallel fibre LTD but on phosphorylation and activation of calcium dependent potassium (K_{Ca}) channels. The postulated mechanism for the K_{Ca} channel phosphorylation is analogous to the nitric oxide mediated mechanism for the induction of AMPA receptor LTD that was discussed in detail in section 2.6.2.

To summarise, PF input activates postsynaptic metabotropic glutamate receptors (mGluRs) on the Purkinje cell membrane. Activation of mGluRs triggers a second messenger cascade in the Purkinje cell cytoplasm leading to the formation of diacylglycerol (DAG) and the release of Ca^{2+} from intracellular stores. Ca^{2+} and DAG activate protein kinase C (PKC) which phosphorylates and activates the K_{Ca} channels.

If the PF evoked PKC activation does *not* coincide with CF input, instantaneous dephosphorylation of the K_{Ca} channels by protein phosphatase-1 (PP-1) prevents their persistent activation. At the same time, the PF evoked Ca^{2+} rise leads to activation of the protein phosphatase calcineurin, dephosphorylation and inhibition of the PP-1 inhibitor G-substrate, re-activation of previously inhibited PP-1, dephosphorylation of already phoshorylated K_{Ca} channels and extinction of a previously learnt eye-blink response.

However, if the Purkinje cell *does* receive CF input at the time of the PKC activation, PP-1 is inhibited and the K_{Ca} channels are persistently phosphorylated and activated. As suggested in section 2.6.2, a potential mechanism for the inhibition of PP-1 by CF input could be that the CF evoked complex spikes in the Purkinje cell trigger depolarisation of neighbouring stellate and basket cells. Ca^{2+} influx into the stellate and basket cells leads to activation of NO synthase and production of nitric oxide (NO). NO diffuses back into the Purkinje cell and stimulates production of cGMP by guanylate cyclase (GC). The cGMP rise in the PC cytoplasm activates protein kinase G (PKG) which phosphorylates and activates the PP-1 inhibitor G-substrate.

An important assumption in the Spectral Timing Model is that the CF input triggers an almost instantaneous PKG activation in the Purkinje cell. In contrast, the second messenger cascade between PF input and PKC activation implements a *time delay* of several tens or hundreds of milliseconds. Simultaneous PKC and PKG activation is a necessary prerequisite for persistent K_{Ca} channel phosphorylation and successful eye-blink conditioning. Thus, eye-blink learning can only take place if the latency of the PF evoked PKC activation is sufficiently similar to the ISI between CS/PF input and US/CF input[1].

Another important assumption is that the Purkinje cell firing is significantly influenced by the intracellular Ca^{2+} increase which follows the PF activation of the mGluRs. Normally, the main effect of the PF inputs on the Purkinje cell membrane potential is assumed to be mediated by *ionotropic* AMPA receptors. However, *mGluR* mediated depolarising responses have also been observed several hundreds of milliseconds after a brief repetitive PF stimulation (Batchelor & Garthwaite, 1993; Batchelor et al., 1994). In Fiala et al.'s model, the mGluR coupled Ca^{2+} rise triggers two electric currents in opposite directions across the Purkinje cell membrane:

1. An *inward* current through the Na^+/Ca^{2+} exchanger, leading to *depolarisation* of the Purkinje cell membrane. The inward direction of this current is due to the fact that the exchanger carries 3 Na^+ ions into the cell for every Ca^{2+} ion which is transported out of the cell.

2. An *outward* current through the Ca^{2+} activated K^+ channels, leading to *hyperpolarisation* of the Purkinje cell membrane.

The overall effect of the mGluR stimulation depends on the phosphorylation state of the K_{Ca} channels. *Before* training, the K_{Ca} channels are unphosphorylated and inactive. Thus, the electrogenic effect of the Na^+/Ca^{2+} exchanger dominates and the

[1]The afferent delays between CS and PF input and between US and CF input are assumed to be similar enough to cancel out (see section 5.5.2).

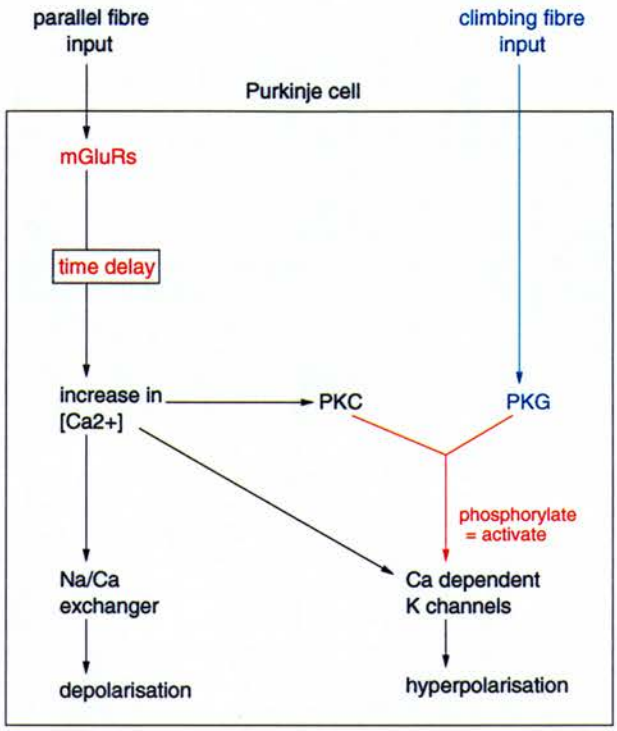

Figure 4.2: Simplified diagram showing the interactions of the mGluR signalling components in the Spectral Timing Model.

mGluR evoked Ca^{2+} increase results in a net *inward* current. *After* successful training, coinciding PKC and PKG peaks have led to persistently phosphorylated and activated K_{Ca} channels and the Ca^{2+} rise triggers a net *outward* current.

Both currents affect the Purkinje cell firing pattern. Purkinje cells *in vivo* receive a continuous background level of PF activity leading to continuous simple spike firing with an average frequency between 30 and 100 Hz (Murphy & Sabah, 1970; Armstrong & Rawson, 1979). In the model, the Ca^{2+} induced outward current after training leads to a decreased simple spike firing rate, disinhibition of the interpositus neurons and execution of the eye-blink response. Similarly, the Ca^{2+} induced inward current before training results in an increased simple spike frequency, continued inhibition of the interpositus neurons and failure to execute the eye-blink response.

Two additional modelling assumptions are needed to implement the *adaptive timing* of the eye-blink response. The first assumption is that the PKC activation happens

almost simultaneously with the Ca^{2+} rise. As a consequence, the latencies of the Ca^{2+} induced voltage response and the PKC phosphorylation of the K_{Ca} channels differ by less than a few tens of milliseconds.

The second assumption which is crucial for the adaptive timing is that the population response of a *group of Purkinje cells* determines if and when the interpositus neurons are disinhibited and an eye-blink CR occurs, and that the Ca^{2+}/PKC latencies of the Purkinje cells in the group *span the range of conditionable CS-US ISIs*. This assumption is what makes the model a *Spectral Timing Model*: out of a spectrum of potential response latencies, conditioning selects the latencies which are closest to the CS-US ISI.

The temporal coincidence of the CS evoked PKC peak and the US evoked PKG peak is a necessary prerequisite for persistent activation of the K_{Ca} channels. Thus, only the K_{Ca} channels of the Purkinje cells with PKC latencies which match the CS-US ISI are activated, and only these Purkinje cells respond to CS presentations with a decreased simple spike firing rate. Given that the PKC activation coincides with the Ca^{2+} rise which is responsible for the change in the simple spike firing rate, the maximum decrease of the simple spike frequency in the affected Purkinje cells after training happens at the time of the US presentation during training. Thus, the maximum disinhibition of the interpositus neurons after training also coincides with the time of the US presentation during training and the eye-blink response is *timed adaptively*.

The remaining part of this chapter summarises the mathematical formulation of the Spectral Timing Model and describes numerical simulation results.

4.3 Mathematical Model

4.3.1 Calcium and Voltage Response

In Fiala et al.'s model, the conditioned stimulus results in simultaneous parallel fibre input to all Purkinje cells in the group. Active parallel fibre terminals release the

neurotransmitter glutamate into the synaptic cleft. Glutamate binds to and activates metabotropic receptors (mGluRs) located at the periphery of the Purkinje cell post-synaptic membrane (Nusser et al., 1994). The active receptors B can be inactivated by dissociation of glutamate or by phosphorylation by PKC (C) which gives rise to phosphorylated receptors A (Herrero et al., 1994; Nishizuka, 1988). The concentration of native receptors which can activated by glutamate (Glu) is given by the total concentration of available receptors B_a minus the sum of activated and phosphorylated receptors ($B + A$). Thus, the change of the concentrations of activated (B) and phosphorylated (A) mGluRs is modelled by:

$$\frac{dB}{dt} = k_1 \, (B_a - B - A) \, [Glu] - k_{-1} \, B - k_2 \, B \, C \tag{4.1}$$

$$\frac{dA}{dt} = k_2 \, B \, C - k_3 \, A \tag{4.2}$$

The k_i represent biochemical rate constants; a convention which is used throughout the whole thesis.

The activated mGluRs trigger the dissociation of the phospholipase C (PLC) specific G-protein into a regulatory subunit $G_{\beta\gamma}$ and a catalytic subunit $G_{PLC\alpha}$. Fiala et al. assume that $G_{PLC\alpha}$ can be inactivated by PKC phosphorylation and describe the change of its concentration (G) by:

$$\frac{dG}{dt} = k_4 \, (G_{max} - G) \, B - k_5 \, G - k_6 \, G \, C \tag{4.3}$$

The next step in the intracellular signalling cascade is the activation of phospholipase C (PLC) by $G_{PLC\alpha}$. Active PLC catalyses the formation of the diffusible second

messengers inositol (1,4,5)-trisphosphate (IP_3) and diacylglycerol (DAG) from phosphatidylinositol (4,5)-bisphosphate (PIP_2). As there is also a Ca^{2+} dependent form of PLC (Mignery et al., 1992), the production of IP_3 (I) and DAG (D) is modelled as:

$$\frac{dI}{dt} = (I_{max} - I)\,(k_7\,G + k_8\,PLC([Ca^{2+}])) - k_9\,I \tag{4.4}$$

$$\frac{dD}{dt} = (D_{max} - D)\,(k_7\,G + k_8\,PLC([Ca^{2+}])) - k_9\,D \tag{4.5}$$

The Ca^{2+} dependent phospholipase C activity is given by a Hill function with a Hill coefficient of 2:

$$PLC([Ca^{2+}]) = \frac{[Ca^{2+}]^2}{[Ca^{2+}]^2 + K_{PLC}} \tag{4.6}$$

IP_3 activates IP_3 receptor Ca^{2+} channels on the membrane of the endoplasmic reticulum (ER) leading to release of Ca^{2+} into the cytoplasm. In addition to the dependence on IP_3, Ca^{2+} release through the IP_3 receptors (IP_3Rs) also shows a bell-shaped dependence on cytoplasmic Ca^{2+} (Bezprozvanny et al., 1991). In the model, the bell shaped Ca^{2+} dependence is based on the interaction of Ca^{2+} with two antagonistic binding sites, one with a stimulating effect on IP_3R opening and one which inhibits it. The inhibitory site binds Ca^{2+} with a cooperativity of $n = 1.65$ (Meissner et al., 1986).

The binding and dissociation of IP_3 is assumed to be much faster than all other reactions in the model. Thus, the IP_3 binding is in equilibrium with respect to the Ca^{2+} binding and the concentration of open IP_3R channels R_o is given by

$$R_o = \frac{I}{I + K_I}\,R_a \tag{4.7}$$

where R_a is the concentration of IP_3R channels with Ca^{2+} bound to the stimulating, but not to the inhibitory site, and $\frac{I}{I+K_I}$ is the fraction of channels with bound IP_3. Because of the fast IP_3 binding, the concentrations of Ca^{2+} activated receptors R_a and inhibited receptors R_i can be modelled with two differential equations:

$$\frac{dR_a}{dt} = k_{12}\,(R_{max} - R_a - R_i)\,[Ca^{2+}] - k_{13}\,R_a - k_{14}\,R_a\,[Ca^{2+}]^n + k_{15}\,R_i \tag{4.8}$$

$$\frac{dR_i}{dt} = k_{14}\,R_a\,[Ca^{2+}]^n - k_{15}\,R_i \tag{4.9}$$

The Ca^{2+} which enters the cytoplasm through the IP_3Rs is removed by the Na^+/Ca^{2+} exchanger in the plasma membrane and the Ca^{2+} ATPase in the ER membrane. Thus, the change of the cytoplasmic Ca^{2+} concentration is given by the sum of three terms:

$$\frac{d[Ca^{2+}]}{dt} = \frac{d[Ca^{2+}]}{dt}(IP_3) - \frac{d[Ca^{2+}]}{dt}(ATPase) - \frac{d[Ca^{2+}]}{dt}(NaCa) \tag{4.10}$$

The IP_3 induced Ca^{2+} release increases linearly with the concentration of open IP_3Rs R_o and the Ca^{2+} concentration difference between ER and cytoplasm:

$$\frac{d[Ca^{2+}]}{dt}(IP_3) = k_{16}\,R_o\,([Ca^{2+}]_{ER} - [Ca^{2+}]) \tag{4.11}$$

The activity of the ER ATPase is modelled by a Hill function with a coefficient of 2 (Lytton et al., 1992):

$$\frac{d[Ca^{2+}]}{dt}(ATPase) = k_{17}\,\frac{[Ca^{2+}]^2}{[Ca^{2+}]^2 + K_{ATPase}} \tag{4.12}$$

The Na^+/Ca^{2+} exchanger carries Na^+ and Ca^{2+} ions with a stoichometry of 3:1 in opposite directions across the plasma membrane. The Ca^{2+} flux is *outward* if the cytoplasmic concentration is larger than the equilibrium concentration $[Ca^{2+}]_{eq}$ (Carafoli, 1987):

$$[Ca^{2+}]_{eq} = [Ca^{2+}]_{ext} \frac{[Na^+]^3_{cyt}}{[Na^+]^3_{ext}} exp(\frac{V\,F}{R\,T}) \tag{4.13}$$

where $[Ca^{2+}]_{ext}$ and $[Na^+]_{ext}$ are extracellular calcium and sodium concentrations, $[Na^+]_{cyt}$ is the sodium concentration in the cytoplasm, V represents the membrane voltage, T the thermodynamic temperature, R the gas constant and F the Faraday constant. The Ca^{2+} flux through the exchanger is modelled by (Hodgkin & Nunn, 1987):

$$\frac{d[Ca^{2+}]}{dt}(NaCa) = k_{18} \frac{[Ca^{2+}] - [Ca^{2+}]_{eq}}{[Ca^{2+}] - [Ca^{2+}]_{eq} + K_{NaCa}} \tag{4.14}$$

The rise in the cytoplasmic Ca^{2+} concentration triggers the activation of protein kinase C (PKC). PKC is transformed into its active form (C) by binding one Ca^{2+} ion and one molecule of DAG (D):

$$\frac{dC}{dt} = k_{10}\,(C_{max} - C)\,D\,[Ca^{2+}] - k_{11}\,C \tag{4.15}$$

Furthermore, the Ca^{2+} rise affects the Purkinje cell firing pattern (see section 4.2). Changes of the simple spike firing rate are represented by deviations from an elevated *in vivo* baseline potential $V_{base} = -50\,mV$. The Ca^{2+} effect on the membrane potential is mediated by two currents: a, for sufficiently elevated Ca^{2+} concentrations, *inward* current through the Na^+/Ca^{2+} exchanger, and an *outward* current through Ca^{2+} activated K^+ channels. In addition, a leakage current $I_L = -k_{20}\,(V - V_{base})$ drives the

potential back to the baseline. Thus, the total change of the membrane potential is given by:

$$\frac{dV}{dt} = k_{19}\frac{d[Ca^{2+}]}{dt}(NaCa) - \bar{g}_{KCa}\, m_{KCa}([Ca^{2+}], V)\,(V - V_K) - k_{20}\,(V - V_{base}) \tag{4.16}$$

with a constant k_{19} which converts the Ca^{2+} concentration change through the exchanger (equation 4.14) into an electric current[2].

The outward current through the K_{Ca} channels is modelled as the product of three terms: a driving force given by the difference between membrane potential V and potassium equilibrium potential $V_K = -85\,mV$, a maximum conductance $\bar{g}_{KCa}$, and a Ca^{2+} and voltage dependent activation variable $m_{KCa}([Ca^{2+}], V)$. The activation of the channels by Ca^{2+} rise and membrane depolarisation is assumed to be instantaneous:

$$m_{KCa}([Ca^{2+}], V) = m_{KCa,\infty}([Ca^{2+}], V) = \frac{[Ca^{2+}]^{2.6}\, s{-}1S^{-1}}{[Ca^{2+}]^{2.6} + exp(\frac{11-V/mV}{22.5})\,\mu M^{2.6}} \tag{4.17}$$

As discussed in detail in section 4.2, the maximum conductance of the K_{Ca} channels $\bar{g}_{KCa}$ is increased by appropriately timed conjunctive parallel and climbing fibre input, and decreased by parallel fibre input alone. In the following section, the mathematical formulation of the $\bar{g}_{KCa}$ modification will be described.

[2]For clarity, the definition of k_{19} has been slightly changed compared to Fiala et al.'s original model (see appendix A).

4.3.2 Learning

In the Spectral Timing Model, the unconditioned stimulus (US) results in climbing fibre input and a sharp cGMP peak in the Purkinje cell cytoplasm. The time course of the cGMP concentration after US presentation at t_{US} is described explicitly by:

$$[cGMP] = \begin{cases} [cGMP]_{max}\,[\,exp(\,\frac{t_{US}-t}{\tau_1}) - exp(\,\frac{t_{US}-t}{\tau_2})\,] & \text{for } t > t_{US} \\ 0 & \text{for } t \leq t_{US} \end{cases} \tag{4.18}$$

where $[cGMP]_{max}$ is the maximum concentration of cGMP and τ_1 and τ_2 are the decay and rise time constants. The cGMP peak triggers activation of protein kinase G (PKG) and enables simultaneously active PKC (C) to persistently phosphorylate and activate the K_{Ca} channels (section 4.2). The K_{Ca} channel activation or inactivation is represented by an increase or decrease in $\bar{g}_{KCa}$ according to:

$$\frac{d\bar{g}_{KCa}}{dt} = k_{23}\,(\bar{g}_{KCa,max} - \bar{g}_{KCa})\,C\,[cGMP] - k_{24}\,\bar{g}_{KCa}\,N \tag{4.19}$$

The second term in equation 4.19 describes the K_{Ca} channel dephosphorylation caused indirectly via PP-1 activation and G-substrate inhibition by the protein phosphatase calcineurin (N). Calcineurin is activated by Ca^{2+}/calmodulin with a cooperativity of approximately 3 (Stemmer & Klee, 1994). Thus, the concentration change of active calcineurin N is given by:

$$\frac{dN}{dt} = k_{21}\,(N_{max} - N)\,[Ca^{2+}]^3 - k_{22}\,N \tag{4.20}$$

The activation of calcineurin by conditioned stimulus (CS), parallel fibre (PF) input and Ca^{2+} rise is responsible for the extinction of the eye-blink response after repeated presentations of the CS alone.

In the model, each of the Purkinje cells in the group is represented by a set of equations 4.1–4.20. The next section summarises the formalisation of the collective properties of the Purkinje cell group which form the basis of the adaptive CR timing.

4.3.3 Population Response and the Spectrum of Time Delays

As described in section 4.2, one of the fundamental assumptions in the Spectral Timing Model is that the population response of a *group of Purkinje cells* determines if and when an eye-blink CR occurs. Fiala et al. calculate the population response as:

$$P(t) = V_{base} + \alpha \sum_{i=1}^{N} \Delta V_i(t) \tag{4.21}$$

where $V_{base} = -50\,mV$ is the *in vivo* baseline potential, $\Delta V_i(t) = V_i(t) - V_{base}$ is the CS evoked membrane potential change in Purkinje cell i, N is the number of Purkinje cells in the group and α is a constant scaling factor. In the model, the CR is executed a few tens of milliseconds after a negative peak in $P(t)$, and with an amplitude which is proportional to the height of the negative peak.

Another important modelling assumption is that the time delays between CS presentation and Ca^{2+}/PKC/voltage response in the Purkinje cells in the group cover the range of conditionable CS-US ISIs. In Fiala et al.'s model, the Ca^{2+} latency variations between different Purkinje cells are implemented by variations in the concentration of available mGluRs B_a (equation 4.1). A smaller B_a results in slower activation of the mGluRs by glutamate and a longer time delay between CS and Purkinje cell response. Thus, the adaptive timing is based on the assumption that the B_a values of the Purkinje cells in the group are appropriately prespecified to span the range of conditionable CS-CR time delays.

4.4 Simulation Results

4.4.1 Modelling Assumptions and Parameters

Most current computational models of single neurons consist of a multitude of isoelectric compartments (e.g. 1600 in De Schutter & Bower, 1994a, 1994b, 1994c), and in models attempting to account for the effects of Ca^{2+} or other second messengers, the individual compartments are often subdivided into a set of radial diffusion shells (e.g. De Schutter & Smolen, 1998). However, this high degree of compartmentalisation is only necessary if a model tries to reproduce neuronal behaviours in the single millisecond range like the formation of action potentials or ionotropic receptor mediated EPSPs. In the Spectral Timing Model, the behaviour which is being investigated is in the range of several hundreds of milliseconds, and electrical conduction or chemical diffusion delays can be ignored. Thus, Fiala et al. apply a *well-stirred assumption* (U. Bhalla, personal communication) and consider only three biochemically distinct compartments: the cytoplasm, the ER lumen and the extracellular space. The extracellular and reticular Ca^{2+} concentrations and the extracellular and cytoplasmic Na^{+} concentrations are assumed to be constant and the only ion concentration which changes in the model is $[Ca^{2+}]$ in the cytoplasm.

Because of the large number of equations (4.1–4.20), the model contains a large number of parameters like rate constants k_i and maximum concentrations X_{max}. A list of all the published parameters can be found in appendix A. Fiala et al. (1996) claim that the "results are not particularly sensitive to any given parameter value". Numerical simulations of the model were unable to confirm this statement. The model was implemented in C++, using a fifth order Runge-Kutta algorithm with adaptive stepsize control, and it was found that (a) the qualitative behaviour of the simulation changed with small parameter variations and (b) it was impossible to reproduce Fiala et al.'s results with the originally published parameter values. The numerical simulation results and the necessary changes to the parameters will be discussed in the following three sections.

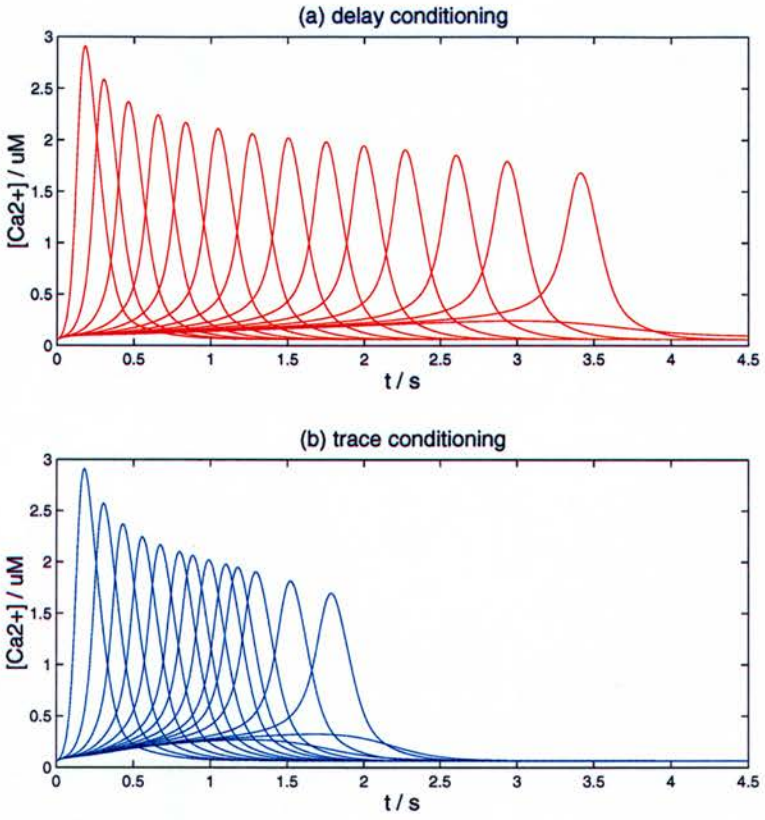

Figure 4.3: The spectrum of calcium responses produced by variations in the total concentration of available mGluRs B_a in a group of 15 Purkinje cells. (a) Calcium responses to a sustained 10 μM glutamate pulse similar to a *delay* conditioning experiment. B_a values are 360, 21, 4.7, 1.73, 0.97, 0.625, 0.458, 0.368, 0.315, 0.283, 0.261, 0.245, 0.236, 0.23 and 0.226 μM. (b) Calcium responses to a 200 ms 10 μM glutamate pulse as in a *trace* conditioning experiment, with B_a values of 360, 20, 6.0, 3.0, 2.0, 1.5, 1.3, 1.15, 1.05, 1.0, 0.95, 0.90, 0.88, 0.87 and 0.86 μM.

4.4.2 The Spectrum of Purkinje Cell Responses

A parameter which is missing in the original Spectral Timing paper (Fiala et al., 1996) is the total concentration of available IP_3 receptors R_{max}. In the simulations, the exact value of R_{max} proved to be critical both for the Ca^{2+}/voltage response latency for a given B_a and for the spectrum of latencies which could be produced by a range of B_a values and a glutamate pulse of a particular duration. For $R_{max} = 1.105\,\mu M$, the simulation of a *sustained* glutamate application resulted in a spectrum of Ca^{2+} latencies between 0 and 3.5 ms (figure 4.3 (a)), corresponding to the conditionable range of CS-US ISIs up to $\sim$ 4 s in *delay* conditioning experiments (Gormezano, 1966, see section 3.2.3).

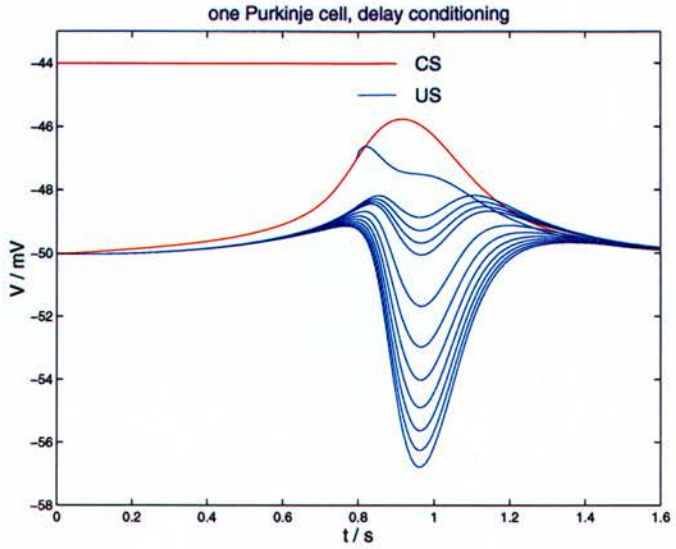

Figure 4.4: Voltage response of a single Purkinje cell with $B_a = 0.97\,\mu M$ to repeated presentations of a 900 ms CS (red bar) co-terminating with a 100 ms US (blue bar). The response is shown before training (red) and for CS+US trial number 1, 2, 3, 4, 5, 10, 15, 20, 25, 30, 35 and 40.

Using the same value of R_{max}, a *200 ms* glutamate pulse produced a Ca^{2+} latency spectrum of approximately 2 s (figure 4.3 (b)), in accordance to what is found in *trace* conditioning experiments (Solomon et al., 1986). Apart from R_{max}, the simulation used Fiala et al.'s original parameter values (appendix A).

4.4.3 Learning in a Single Purkinje Cell

In the original Spectral Timing Model, the dephosphorylation of the mGluRs which converts them back into the native state is assumed to be slow enough to ignore, and the rate constant k_3 in equation 4.2 is set to zero. Without this assumption, repetitive receptor inhibition and activation can generate damped Ca^{2+} oscillations. However, if the assumption is included in the model, repeated parallel fibre input transforms all mGluRs into the phosphorylated and inactivated state and all Ca^{2+} and voltage responses and the ability to learn are completely abolished. Thus, to simulate learning k_3 had to be changed to a non-zero value.

Simulation results for a single Purkinje cell with $k_3 = 0.5\,\mu M s^{-1}$ are shown in figure 4.4. In the single cell simulation, the total concentration of available mGluRs B_a is set to $0.97\,\mu M$ to implement a Ca^{2+}/PKC/voltage response latency in the vicinity of the 800 ms ISI between CS and US. As a consequence, repeated presentation of a 900 ms glutamate pulse CS co-terminating with a 100 ms US results in K_{Ca} channel phosphorylation and a gradual shift from the depolarising response before training (red trace) to a hyperpolarising response after training. The hyperpolarising response after training corresponds to a decreased simple spike firing rate, disihibition of the interpositus neurons and execution of the eye-blink CR. To demonstrate the gradual increase of the hyperpolarisation peak during learning and to create a learning rate which is more similar to *in vivo* values, the original K_{Ca} channel phosphorylation and dephosphorylation rate constants were set to slightly smaller values (appendix A).

4.4.4 Learning and the Purkinje Cell Spectrum

In the Spectral Timing Model, the adaptive timing of the eye-blink CR is implemented by a group of Purkinje cells with varying concentrations of available mGluRs B_a. Results of a delay conditioning simulation with a group of 15 Purkinje cells are shown in figure 4.5. The spectrum of B_a values is the same as in figure 4.3 (a), resulting in a 3.5 s range of conditionable ISIs.

In the simulation, repeated presentation of a 900 ms CS co-terminating with a 100 ms US results in a shift of the population response (equation 4.21) from a broad depolarisation plateau before training to a hyperpolarisation peak between 750 and 800 ms after training, corresponding to disinhibition of the interpositus neurons at the US time and an adaptively timed CR. Fluctuations in the population response are due to the small number of Purkinje cells in the simulation, a smooth response which is more similar to experimental data (Batchelor & Garthwaite, 1993; Batchelor et al., 1994) can be simulated with a larger number of Purkinje cells with adequate B_a values (see Fiala et al., 1996).

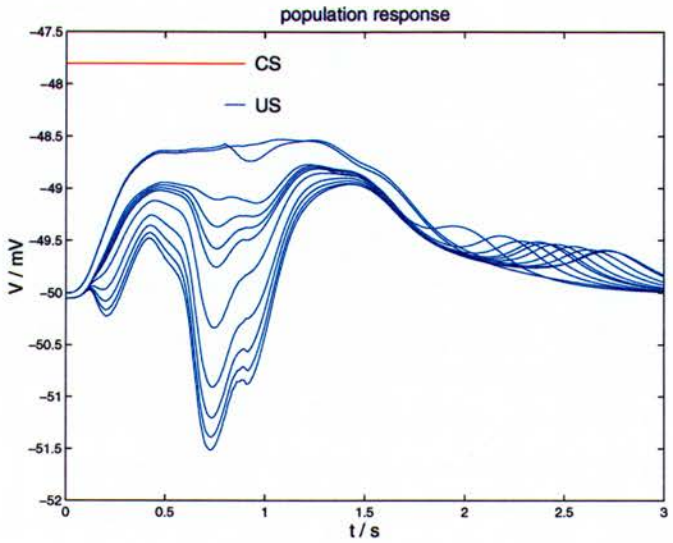

Figure 4.5: Population response ($\alpha = 0.1$, see equation 4.21) of a group of 15 Purkinje cells to repeated presentations of a 900 ms CS (red bar) co-terminating with a 100 ms US (blue bar). The response is shown before training and for CS+US trial number 1, 2, 3, 4, 5, 10, 20, 30, 40 and 50. The B_a values are the same as in figure 4.3 (a).

Other features of eye-blink conditioning which can be reproduced by the Spectral Timing Model include the extinction of the CR by repeated presentations of the CS alone and the experimentally observed maximum of the CR strength for ISIs between 200 and 400 ms (section 3.2.3).

4.5 Chapter Conclusions

Experimental evidence indicates that the cerebellum is involved in the adaptive timing of the classically conditioned eye-blink reponse. Recently, Fiala et al. (1996) have suggested that the adaptive timing of the eye-blink CR is implemented by a spectrum of metabotropic glutamate receptor (mGluR) responses in a group of cerebellar Purkinje cells. In this chapter, the biological concepts and mathematical formulation of Fiala et al.'s *Spectral Timing Model* were discussed, a few minor corrections to the model were described and numerical simulation results were presented.

In the Spectral Timing Model, the presentation of the *conditioned stimulus (CS)* results in parallel fibre input to the Purkinje cells, in activation of mGluRs and, after a *time delay*, in release of Ca^{2+} from intracellular stores and an increase or decrease of the simple spike firing rate. The presentation of the *unconditioned stimulus (US)* leads to climbing fibre input and an immediate increase in cGMP. The *temporal coincidence* of the CS evoked Ca^{2+} rise and the US evoked cGMP rise triggers persistent phosphorylation and activation of K_{Ca} channels. Thus, the repeated paired presentation of CS and US results in K_{Ca} channel activation *only* in the Purkinje cells in the group which have a Ca^{2+} latency similar to the CS-US ISI. Fiala et al. assume (a) that the Ca^{2+} latencies of the Purkinje cells in the group span the range of conditionable ISIs and (b) that the population response of the group determines if and when the interpositus neurons are disinhibited and an eye-blink CR occurs. As a consequence, CS plus US training with a conditionable ISI results in CRs which are timed adaptively and follow the CS by the ISI after training.

In the next chapter, improvements to the Spectral Timing Model will be suggested and it will be demonstrated how a *single Purkinje cell* could learn the adaptive timing of the eye-blink reponse.

Chapter 5

The Adaptive Timing Model

5.1 Introduction

Several experimental results indicate an involvement of the cerebellum in the adaptive timing of the classically conditioned eye-blink response. In their *Spectral Timing Model*, Fiala et al. (1996) suggested that the adaptive timing of the eye-blink response is implemented by a temporal spectrum of delayed voltage responses after stimulation of metabotropic glutamate receptors (mGluRs) in a group of cerebellar Purkinje cells. In the previous chapter, the biological concepts and mathematical formulation of the *Spectral Timing Model* were summarised, some minor improvements were suggested and numerical simulation results were described.

Two fundamental assumptions of the *Spectral Timing Model* are (a) that the eye-blink response is learnt by a *group of Purkinje cells*, and (b) that the mGluR mediated voltage response latencies of the Purkinje cells in the group are *appropriately prespecified* and cover the range of conditionable interstimulus intervals (ISIs) between conditioned stimulus (CS) and unconditioned stimulus (US). In this chapter, the *Adaptive Timing Model* will be described, an extension of the Spectral Timing Model which manages to explain the adaptive timing of the eye-blink response without having to rely on

either of the assumptions (a) or (b). In the *Adaptive Timing Model*, adaptively timed eye-blinks are based on plasticity of the mGluR signalling network in a *single Purkinje cell*. This chapter will examine the assumptions of the Spectral Timing Model in more detail, describe the biochemistry and mathematical formulation of the Adaptive Timing Model and present numerical simulation results.

5.2 Spectral Timing Assumptions

As described in detail in the previous chapter, the adaptive timing of the eye-blink response in Fiala et al.'s Spectral Timing Model is based on the following assumptions:

1. The population response of a group of Purkinje cells determines if and when an eye-blink response occurs. More specifically, eye-blinks are executed a few tens of milliseconds after a hyperpolarisation peak in the population response and only if a sufficiently negative hyperpolarisation peak exists.

2. All Purkinje cells in the group receive information about the CS through parallel fibre input at the same time and, after the ISI, information about the US through climbing fibre input at the same time.

3. The concentrations of available mGluRs in the Purkinje cells in the group are appropriately specified to generate a spectrum of Ca^{2+}/PKC/voltage response latencies which covers the range of conditionable CS-US ISIs.

It is not easy to see how the second assumption could be implemented in the cerebellar cortex, given that a single parallel fibre activates its target Purkinje cells in sequence and not simultaneously. The Spectral Timing Model could easily be modified to take the parallel fibre conduction delays into account. However, a more elegant solution which makes all three assumptions unnecessary is an *adaptive* time delay between parallel fibre input and Ca^{2+}/PKC/voltage response that is adjusted to match the particular ISI between CS and US. The remaining part of this chapter describes how the mGluR signalling network in a single Purkinje cell can implement such an adaptive time delay.

5.3 Adaptive Timing by a Single Purkinje Cell

One of the factors determining the latency of the intracellular Ca^{2+} release and therefore also the latencies of the PKC activation and the voltage response is the concentration of mGluRs which are available for activation by glutamate. As a consequence, an adaptive time delay can be implemented by an adaptive concentration of available mGluRs. In the Adaptive Timing Model, the initial concentration of available mGluRs is assumed to be sufficiently high to generate a time delay which is shorter than the shortest possible ISI between CS and US. Thus, for successful delay learning, the conjunctive presentation of CS and US during training should result in a *decrease* of the available receptor concentration until an equilibrium is reached where the CS evoked Ca^{2+}/PKC/voltage response coincides with the US. Given that the CS triggers parallel fibre input and activation of PKC, and the US triggers climbing fibre input and activation of PKG, there are two possible scenarios which could implement the CS plus US induced reduction of the available mGluRs and stabilise at the desired equilibrium.

In the **first scenario**, the concentration of available mGluRs is *decreased* by PKC phosphorylation of the receptors at an *inhibitory site* I_C which is insensitive to dephosphorylation by protein phosphatase-1 (PP-1), and *increased* by PKC phosphorylation at an *activation site* A_C which is a substrate for immediate PP-1 dephosphorylation. Persistent PKC phosphorylation of the PP-1 sensitive site A_C requires simultaneous inhibition of PP-1 through phosphorylation and activation of the PP-1 inhibitor G-substrate by PKG, similar to the PKC phosphorylation of the Ca^{2+} dependent K^+ channels described in section 4.2. Thus, the excitatory phosphorylation at A_C is *gated by both PKC and PKG* and the change in the concentration of available mGluRs B_a by the two antagonistic PKC (C) phosphorylations is modelled by:

$$\frac{dB_a}{dt} = k_f\,(B_{max} - B_a)\,[cGMP]\,C - k_b\,B_a\,C \tag{5.1}$$

where active PKG is represented by the concentration of its activator [cGMP]. The concentration of receptors which are *inhibited and not available* for activation of glutamate is given by the total mGluR concentration B_{max} minus the concentration of available mGluRs B_a, and k_f and k_b are the two phosphorylation rate constants.

The **second scenario** is based on the assumption that the decrease in the concentration of available receptors is achieved through US evoked *PKG phosphorylation at an inhibitory site* I_G. As in the first scenario, PKC phosphorylation of a PP-1 sensitive site A_C leads to an increase in the available mGluRs and makes it possible to reach an equilibrium with a stable concentration of available receptors. In the second scenario, the concentration change of available mGluRs B_a is given by:

$$\frac{dB_a}{dt} = k_f\,(B_{max} - B_a)\,[cGMP]\,C - k_b\,B_a\,[cGMP] \tag{5.2}$$

In both scenarios, repeated conjunctive CS and US presentations during conditioning should lead to a decrease of the concentration of available mGluRs and an increase of the time delay between CS and PKC activation peak until the CS evoked PKC peak and the US evoked PKG peak overlap. Once the PKC and the PKG activation peaks have a sufficiently large overlap, the PKG independent PKC phosphorylation (in scenario 1) or the PKG phosphorylation (in scenario 2) can be compensated by the PKG *dependent* PKC phosphorylation and an equilibrium can be reached with a stable concentration of available receptors.

As in the Spectral Timing Model, it is assumed that the PKG activation peak follows US and climbing fibre input by less than ten milliseconds[1]. Thus, the equilibrium concentration of available mGluRs after conditioning should implement a time delay between CS and PKC peak which approximates the interstimulus interval between

[1] As in the Spectral Timing Model, the conduction delays between CS and parallel fibre input and between US and climbing fibre input are assumed to be similar enough to be ignored (discussed in detail in section 5.5.2).

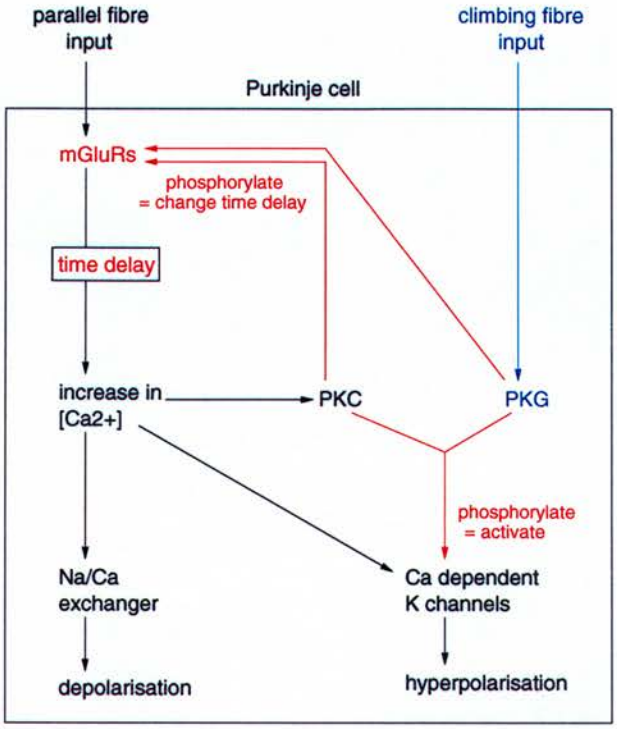

Figure 5.1: Simplified diagram showing the interactions of the mGluR signalling components in the Adaptive Timing Model.

CS and US. Given that the timing of PKC activation, Ca^{2+} peak and voltage response also differs by less than a few milliseconds, the Purkinje cell should be able to learn a conditioned voltage response at the time of the US presentation during training, and the resulting eye-blink response should also be timed adaptively.

Although both versions of the Adaptive Timing Model should be able to learn adaptively timed eye-blink conditioned responses (CRs), a problem of the *first* version of the model is its behaviour if the Purkinje cell receives parallel fibre input *without* climbing fibre input in CS alone trials. In the first scenario, the activation of PKC after presentation of a CS *with or without a US* leads to a decrease in the concentration of available mGluRs. As a consequence, repeated CS alone presentations should result not only in extinction of a previously learnt CR, but also in a shift to longer time delays. A time delay shift by parallel fibre input alone is not biologically plausible, and only the behaviour of the second version of the Adaptive Timing Model (equation 5.2) will be discussed in the remaining parts of the thesis.

5.4 Simulation Results

5.4.1 Simulation Architecture and Parameters

The complete Adaptive Timing Model consists of a set of equations 4.1-4.20 plus the adaptive timing equation 5.2 which describes the change of available mGluRs. The model was implemented in C++, using a fifth order Runge-Kutta algorithm with adaptive stepsize control. Most of the parameter values in the simulation were identical to the original Spectral Timing values (appendix A.1.1). Changes to the original parameters and the Adaptive Timing specific parameters are listed in appendix A.2.

In the following sections, numerical simulation results for *delay* and *trace* conditioning experiments will be summarised (see section 3.2.3). The behaviour of the model during CS plus US training and CS alone trials will be described, and the dependence of the performance on conditioning paradigm and CS-US ISI will be investigated.

5.4.2 Delay Learning and Weight Learning

In both delay and trace conditioning simulations, the learning process can be divided into two overlapping phases: a *delay learning phase* and a *weight learning phase* (see figure 5.2). During the *delay learning phase*, presentation of the US leads to formation of cGMP in the Purkinje cell, PKG phosphorylation of the mGluRs and a decrease in the concentration of available receptors B_a. A consequence of the B_a decrease is a slower accumulation of glutamate-activated receptors and an *increase* in the time delay between CS and Ca^{2+}/PKC/voltage latency until the CS evoked PKC and US evoked cGMP/PKG peaks overlap. Overlapping PKC and cGMP/PKG peaks result in an equilibrium between PKG induced B_a decrease and PKC plus PKG gated B_a increase and a stable Ca^{2+}/PKC/voltage latency which matches the CS-US ISI. A constant latency signals the end of the delay learning phase.

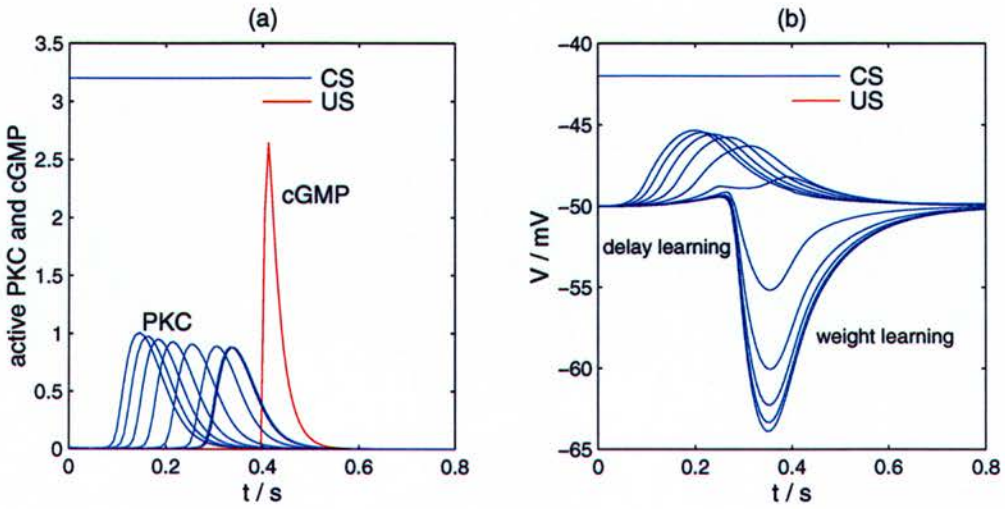

Figure 5.2: Simulation results for delay conditioning with 75 presentations of a $10\mu M$ glutamate pulse CS from $t = 0$ until $t = 0.5s$ (blue bar) and a cGMP peak US starting from $t_{US} = 0.4s$ (red). Conditioning results in a shift of the CS induced PKC peak (a, blue) towards the US induced cGMP peak (red) and in a shift of the voltage response from a depolarisation at $t = 0.15s$ towards a hyperpolarisation around $t = 0.36s$ (b). Results are shown for every fifth CS plus US trial.

A few CS plus US trials before the end of the delay learning phase, the overlap of the PKC and PKG peaks triggers the beginning of the *weight learning phase*. During the weight learning phase, coinciding PKC and PKG activation results in persistent phosphorylation and activation of Ca^{2+} dependent K^+ (K_{Ca}) channels. As a consequence of the K_{Ca} channel activation, the CS evoked depolarisation reponse (corresponding to a *positive synaptic weight*) is gradually transformed into a hyperpolarisation response (a *negative synaptic weight*). At the end of the weight learning phase, the dephosphorylation of the K_{Ca} channels caused indirectly by Ca^{2+}/calmodulin activation of calcineurin (see section 4.2) compensates for the phosphorylation by PKC and the Purkinje cell model reaches a state where all concentrations are constant.

After both learning phases, presentation of the CS leads to hyperpolarisation of the Purkinje cell at the time of the US presentation during training. Consequence of the adaptively timed hyperpolarisation is an adaptively timed disinhibition of the Purkinje cell target neurons in the interpositus nucleus and the execution of an adaptively timed eye-blink CR. Thus, in the Adaptive Timing Model, a *single Purkinje cell* is able to learn the adaptive timing of the classically conditioned eye-blink response.

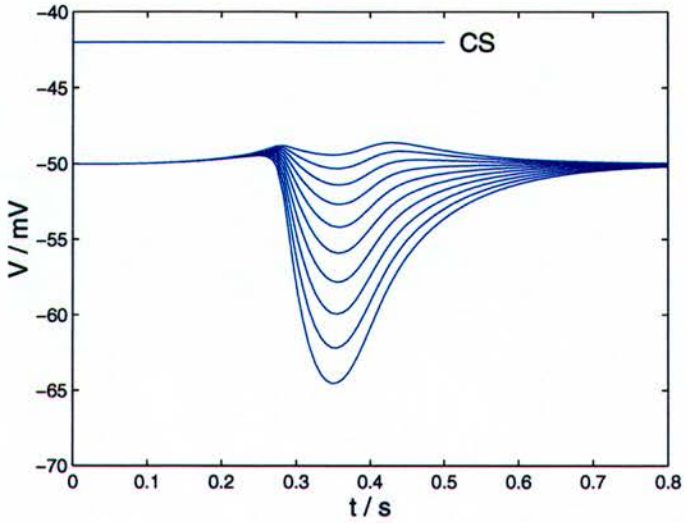

Figure 5.3: Simulation results for 20 presentations of a $10\mu M$ glutamate pulse CS from $t = 0$ until $t = 0.5s$ (blue bar) to a Purkinje cell which has previously learnt an adaptively timed eye-blink CR around $t_{US} = 0.4s$. Repeated CS alone trials result in gradual reduction of the hyperpolarisation response and *extinction* of the eye-blink CR. Results are shown for every second CS alone trial.

If the CS is presented repeatedly *without* an accompanying US, the CS induced Ca^{2+} activation of the protein phosphatase calcineurin leads to dephosphorylation of the PP-1 inhibitor G-substrate, activation of PP-1 and dephosphorylation and inactivation of the K_{Ca} channels. Thus, repeated CS alone trials result in reduction of the hyperpolarisation response and *extinction* of the eye-blink CR (figure 5.3).

5.4.3 Interstimulus Interval Dependence

In experiments, delay conditioning is easier to achieve than trace conditioning (see section 3.2.3). The range of *delay conditionable* interstimulus intervals lies between 100 ms and 4 s, compared to an effective ISI range of 100 ms – 2 s if a *trace conditioning* protocol is used (Gormezano, 1966; Smith et al., 1969; Solomon et al., 1986; Steinmetz et al., 1989; Steinmetz, 1990a). In both delay and trace conditioning experiments, ISIs between 200 and 400 ms are maximally effective and the CR amplitude and frequency decreases with increasing ISIs (Smith et al., 1969; Steinmetz, 1990a).

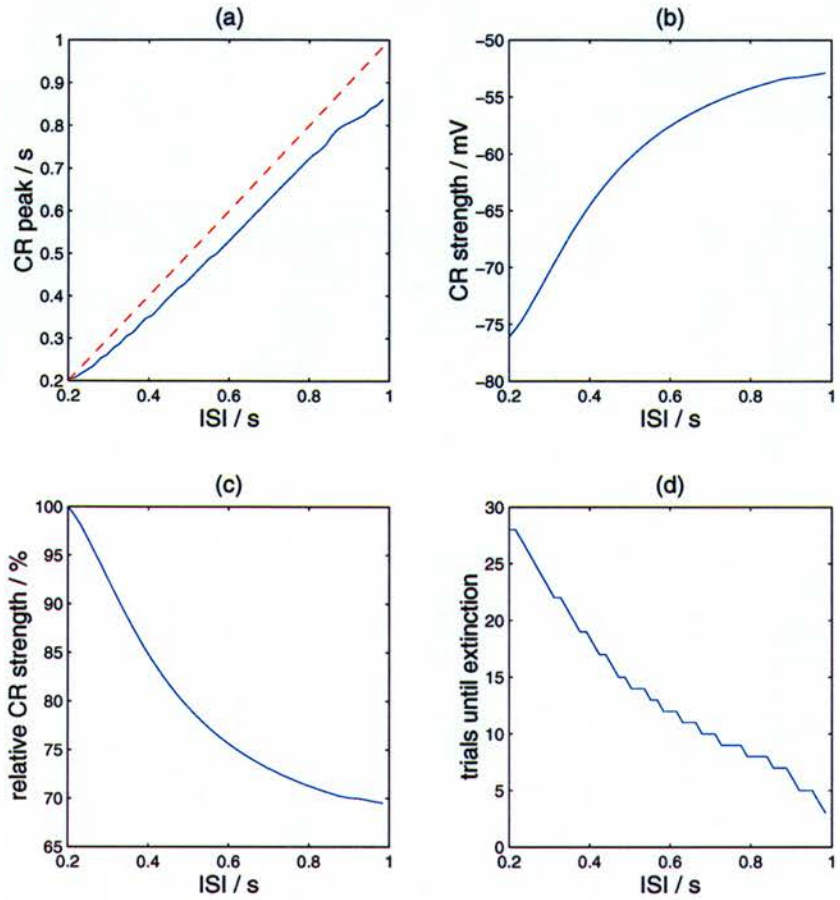

Figure 5.4: Simulation results for delay conditioning with a 10 μM glutamate pulse CS from $t = 0$ until $t = t_{US} + 100ms$ and a cGMP peak US at varying times t_{US}. The ISI is given by t_{US}. (a) The CR (the hyperpolarisation peak, shown in blue) occurs shortly before the US onset (given by the ISI, broken red line: y=x). (b) CR strength given as the extent of the hyperpolarisation peak in mV. (c) relative CR strength compared to the maximum for a 200 ms ISI. (d) number of CS alone presentations necessary for extinction of the CR.

Simulations of the Adaptive Timing Model exhibit the same *qualitative* behaviour, but not the same *quantitative* relation between ISI length and CR strength. In *delay conditioning* simulations, the Purkinje cell model is able to learn adaptively timed CRs for ISIs between 200 ms and 1 s (figure 5.4). In *trace conditioning* simulations, conditioning is more difficult to achieve and the range of effective ISIs spans 200 – 600 ms (figure 5.5). Simulation with both protocols reproduce the experimentally observed decrease in CR strength, measured as the extent of the hyperpolarisation, for increasing ISI durations $\leq$ 200 ms. A prediction of the model is faster extinction of the eye-blink CR after conditioning with longer ISIs (figures 5.4 and 5.5 d).

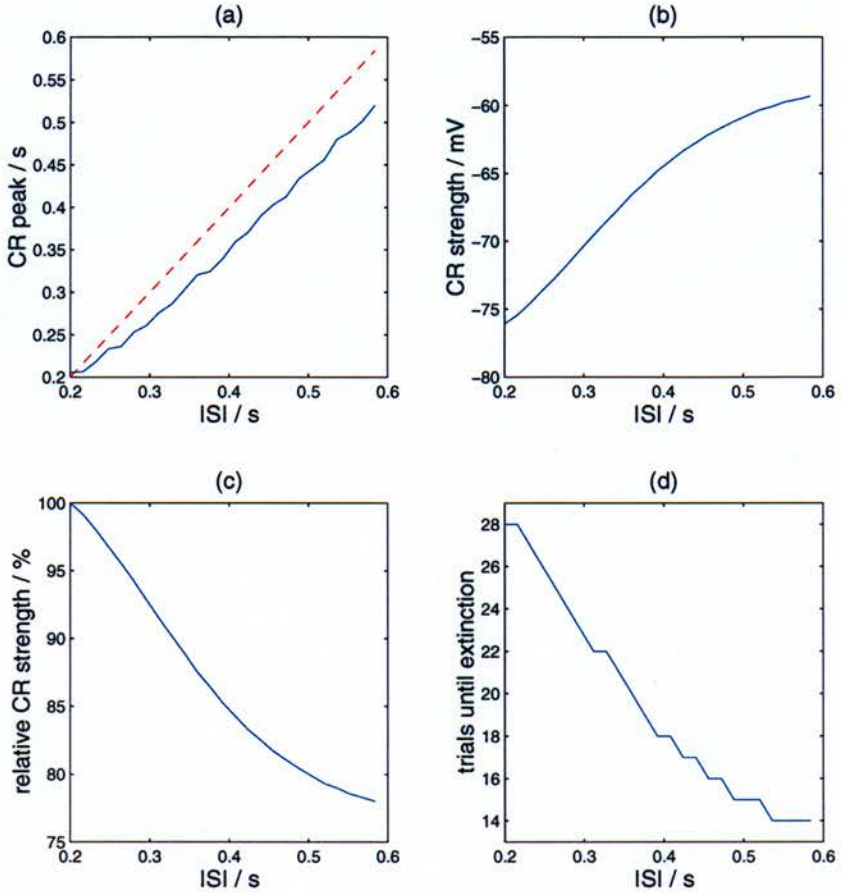

Figure 5.5: Simulation results for trace conditioning with a 10 μM glutamate pulse CS from $t = 0$ until $t = 200ms$ and a cGMP peak US at varying times t_{US}. The ISI is given by t_{US}. (a) The CR (the hyperpolarisation peak, shown in blue) occurs shortly before the US onset (given by the ISI, broken red line: y=x). (b) CR strength given as the extent of the hyperpolarisation peak in mV. (c) relative CR strength compared to the maximum for a 200 ms ISI. (d) number of CS alone presentations necessary for extinction of the CR.

5.5 Plausibility of the Adaptive Timing Assumptions

5.5.1 PKC and PKG Phosphorylation of the mGluRs

Vital for the functioning of the Adaptive Timing Model is the assumption that PKC phosphorylation increases and PKG phosphorylation decreases the number of mGluRs which are available for activation by glutamate. The simplest mechanism that could implement this assumption is *direct* phosphorylation of the mGluRs by PKC and

PKG. In general, a protein kinase is able to phosphorylate a target protein if it contains a kinase-specific amino acid recognition sequence as part of its intracellular domain.

The recognition sequences of most PKC isoforms consist of a serine or threonine residue in the vicinity of the basic amino acids arginine or lysine (Marais et al., 1990). In Purkinje cell dendrites, the predominant PKC isoform is PKC-γ (Nishizuka et al., 1991; Huang et al., 1991) which has been shown to preferentially phosphorylate serines and threonines in sequences with an R/KXXS/T motif, where R/K represents arginine or lysine, X an arbitrary amino acid and S/T the phosphorylated serine or threonine, respectively. However, this requirement is not very strict and SXRR (in peptides), RRS (in $pp60^{c-src}$) and RKT (in the epidermal growth factor receptor) can also be phosphorylated by PKC-γ (Marais et al., 1990). The metabotropic receptor subtype mGluR1 in Purkinje cells contains several potential PKC-γ phosphorylation sites, including RXXT (residues 868-871), KXXS (residues 891-894), KXXTK (residues 931-935) and KXXT (residues 942-945) (Masu et al., 1991). Thus, in accordance with the Adaptive Timing assumption, mGluRs in Purkinje cells are a potential substrate for phosphorylation by PKC.

In contrast, no evidence for PKG phosphorylation of the mGluRs is known to date. However, the relatively low activity of PKG compared with a high background level of other protein kinases makes PKG phosphorylation difficult to investigate, and several PKG substrates in the brain have yet to be identified (Wang & Robinson, 1995). Another problem is that the recognition sequence for PKG phosphorylation appears to be less well defined (see e.g. Butt et al., 1994). In one study, the sequence KRKKSL (where L is leucine) was identified as a PKG consensus (Tegge et al., 1995). The closest match between this consensus and the amino acid sequence of the mGluR1 subtype in Purkinje cells are two KSL fragments in positions 942-944 and 1035-1037. However, several of the identified PKG substrates like histone H2B and the protein kinase inhibitor (PKI) peptide also fail to match the consensus (Tegge et al., 1995), and further experiments will be necessary to determine if the mGluRs are a substrate for phosphorylation by PKG.

To summarise, experimental evidence indicates that the mGluRs in cerebellar Purkinje cells can be phosphorylated by PKC, but it is not known yet if they can also be phosphorylated by PKG. Furthermore, the *effects* of the PKC and the hypothetical PKG phosphorylation still need to be determined to clarify if the postulated adaptive timing mechanism is biologically plausible. And even if it can be shown that PKC does *not* phosphorylate the GluRs, or if the predicted effects of the phosphorylations are wrong, the adaptive timing mechanism could still be implemented by the interaction of PKC and PKG with other elements of the mGluR signalling network.

5.5.2 No Afferent Delays

Finally, a simplification which has been applied in this and the previous chapter is the interchangeable use of the terms *CS time* and *parallel fibre input time*, and *US time* and *climbing fibre input time*. There are two reasons why the afferent delays between peripheral stimuli and inputs to the Purkinje cell can be ignored. Firstly, both conduction delays from the periphery to the cerebellum are in the range of a few tens of milliseconds (see e.g. Thompson & Krupa, 1994) which is only a small fraction of the overall response time. Secondly, the conduction delays between CS and parallel fibre input, and between US and climbing fibre input are very similar. Thus, the *difference* between the afferent delays for both CS and US is expected to be less than a few milliseconds, and for modelling purposes, the times of the CS presentation and the parallel fibre input, and the times of the US presentation and the climbing fibre input can be assumed to be identical.

5.6 Chapter Conclusions

In the previous chapter, Fiala, Grossberg and Bullock's *Spectral Timing Model* was summarised. In the Spectral Timing Model, a *spectrum* of cerebellar Purkinje cells with *appropriately prespecified* time delays between parallel fibre input and voltage response is responsible for the adaptive timing of the classically conditioned eye-blink response.

In this chapter, the *Adaptive Timing Model* was presented, an extension of the Spectral Timing Model which enables a *single Purkinje cell* to learn an adaptively timed eye-blink response. In the Adaptive Timing Model, the time delay between parallel fibre input and voltage response in the Purkinje cell is adjusted until it matches the inter-stimulus interval (ISI) between conditioned and unconditioned stimulus (CS and US). Substrate for the adaptive timing are modifications of the metabotropic glutamate receptor (mGluR) activated intracellular signalling network in the Purkinje cell.

The central assumption in the model is that the concentration of mGluRs which are available for activation by glutamate is *increased* by CS induced protein kinase C (PKC) phosphorylation and *decreased* by US induced protein kinase G (PKG) phosphorylation. PKC phosphorylation of mGluRs has been described. However, no evidence for phosphorylation of the receptors by PKG is known to date, and further experiments will be necessary to clarify the biological plausibility of the model.

Numerical simulations show that the learning process can be divided into two overlapping phases, a *delay learning* phase and a *weight learning* phase. During the *delay learning* phase, phosphorylation of the mGluRs adjusts the latency of the calcium and voltage response. During the *weight learning* phase, phosphorylation of calcium dependent potassium channels transforms the initial depolarisation reponse into a hyperpolarisation response which leads to disinhibition of interpositus neurons and execution of an adaptively timed eye-blink response. In the simulations, adaptively timed responses can be learnt for ISIs between 200 ms and 1 s if a delay conditioning paradigm is used, and for ISIs between 200 and 600 ms if a trace conditioning paradigm is used.

The modification of postsynaptic delays represents a new learning mechanism with other potential applications apart from the adaptive timing of the classically conditioned eye-blink response. In the next chapter, the integration of the adaptive timing mechanism in a *multi-compartmental* model of a Purkinje cell will be described, and it will be shown how a higher-dimensional version of the Adaptive Timing Model can learn a radial basis function (RBF)-like response to temporal input patterns.

Chapter 6

Radial Basis Function Learning in Purkinje Cells

6.1 Introduction

In the previous chapter, the *Adaptive Timing Model* was introduced and it was described how the metabotropic glutamate receptor (mGluR) signalling network in a cerebellar Purkinje cell can implement the adaptive timing of the classically conditioned eye-blink response. In the Adaptive Timing Model, the phosphorylation of the mGluRs by protein kinase C (PKC) and protein kinase G (PKG) provides the basis for an *adaptive time delay* between parallel fibre input and voltage response. The adaptively timed response is established through a learning process which can be divided into two overlapping phases. During a *delay learning phase*, the latency of the voltage reponse is adjusted, and during the following *weight learning phase*, the initial depolarisation response is transformed into a hyperpolarisation response.

The adaptive timing of the classically conditioned eye-blink response is not the only computation that can be performed with adaptive synaptic delays, and certainly not the only computational function of cerebellar Purkinje cells. In this chapter, it will be

shown that a more general function of synaptic delay adaptation in Purkinje cells is to provide a mechanism to *learn the recognition of temporal parallel fibre input patterns.*

It is widely accepted that neuronal firing *times* as well as neuronal firing *rates* are important for the representation of information in the brain (for examples, see Bialek et al., 1991; Hopfield, 1995; Gerstner et al., 1996; Thorpe et al., 1996; Laurent, 1996; Wehr & Laurent, 1996). If this is the case and patterns of firing times are used for biological information processing, neurons in the brain must have a mechanism to *learn* to respond to a specific temporal input. Recently, J.J. Hopfield has suggested that temporal patterns are recognised by *radial basis function* (RBF) neurons using a combination of time delays and coincidence detection (Hopfield, 1995, see figure 6.1). If Hopfield's suggestion is correct, the *time delays* for the recognition of a particular temporal input pattern have to be learnt.

In the following section, Hopfield's temporal coding model will be briefly summarised. The remaining sections of the chapter will describe an extension of the *one-compartmental* Adaptive Timing Model (chapter 5) to a *multi-compartmental* model of a cerebellar Purkinje cell and present simulation results which show that the multi-compartmental version of the Adaptive Timing Model can learn to respond to temporal parallel fibre input patterns in an RBF-like way, similar to the form of temporal RBF learning which was postulated by Hopfield.

6.2 Temporal Encoding and Hopfield's RBF Neurons

Many sensory patterns can be represented by analogue vectors with constant direction and variable length. For example, a smell $\mathbf{c}$ which consists of a number of chemical components with concentrations c_j is still recognised as the same smell if all of the concentrations are multiplied by the same factor λ. Thus, the brain performs a *stimulus quality specific* and *scale-invariant* classification of a set of sensory input vectors $\lambda\mathbf{c}$.

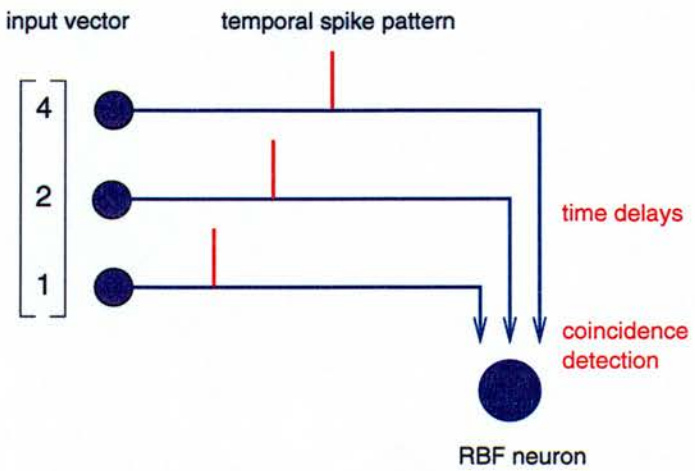

Figure 6.1: The encoding and decoding of temporal patterns suggested by Hopfield (1995). In Hopfield's model, analogue input vectors are *encoded* by the timing of spikes relative to the phase of collective subthreshold membrane potential oscillations. The temporal spike pattern is *decoded* by a radial basis function (RBF) neuron using a combination of time delays and coincidence detection.

Hopfield's model provides a mechanism for the temporal encoding of analogue vectors in a scale-invariant form. In the model, the analogue input vectors are encoded by a group of *encoding neurons* which exhibit synchronous subthreshold oscillations of the membrane potential. The encoding neuron j fires when the input current I_j corresponding to the jth component of the input vector $\mathbf{c}$ drives the membrane potential over the threshold. Thus, a *large input component* c_j results in an early action potential and a *large time advance* τ_j relative to the phase of the collective subthreshold oscillations (figure 6.2). Hopfield assumes that the preprocessing of the sensory stimulus leads to a logarithmic relation between stimulus strength c_j and time advance of the spikes τ_j:

$$\tau_j = \alpha \ln(c_j/\delta) \tag{6.1}$$

where α and δ are constant factors. As a consequence of the logarithmic encoding, the *relative* time advance $\tau_j - \min(\tau_k)$ of the spikes representing the different components c_j stays the same if all c_j are multiplied by the same factor λ, and the encoding is stimulus quality specific and scale invariant.

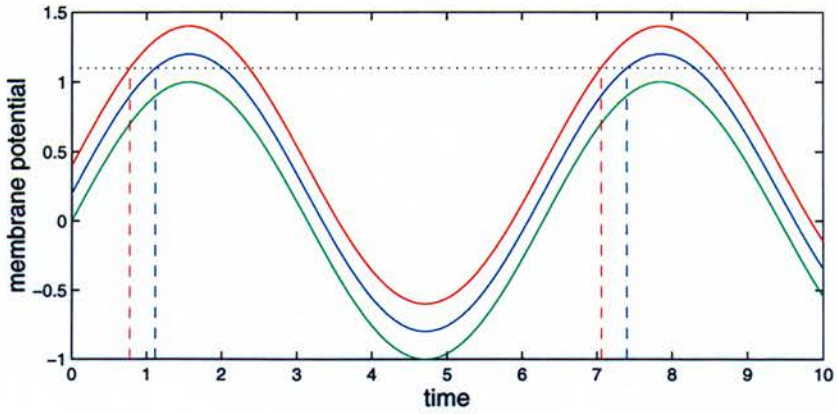

Figure 6.2: Hopfield's encoding mechanism. Each of the *encoding neurons* exhibits subthreshold membrane potential oscillations (green). Input currents drive the potential over the threshold (dotted black line) and trigger action potentials. A large input current (red) leads to earlier firing (red dashed line) than a small input current (blue dashed line).

The resulting temporal spike patterns are recognised by *decoding neurons* using a combination of time delays and coincidence detection. A decoding neuron responds to a particular temporal spike pattern if the set of its afferent or synaptic delays evens out the differences between the input spike times (compare figure 6.1). The integration time constant of the encoding neuron determines the range of temporal patterns that can be recognised with a particular set of delays: a smaller integration time constant implements a stricter coincidence detection and a smaller receptive field size. The response of each encoding neuron is maximal for one specific *template* input pattern and decreases with increasing distance of the inputs from the template pattern. This is a property which is shared with radial basis function (RBF) units in artificial neural networks, and Hopfield's decoding neurons are often referred to as *RBF neurons* (e.g. Natschläger & Ruf, 1998).

If this kind of temporal encoding and decoding takes place in the brain, the encoding neurons must have a mechanism to *learn* the time delays for the recognition of a new temporal pattern. A potential learning mechanism which was first suggested by Gerstner et al. (1996) and further elaborated by Natschläger and Ruf (1998) is that the correct delays are chosen from a predefined spectrum of existing delays. However, it would be more elegant and efficient if the individual delays could be adapted, and the remaining sections of the chapter will describe how a multi-dimensional version of

the Adaptive Timing Model can provide the necessary delay adaptation mechanism, and how a multi-compartmental Purkinje cell model can learn an RBF-like response to temporal parallel fibre input patterns.

6.3 Adaptive Timing in More Than One Dimension

The multi-compartmental version of the Adaptive Timing Model consists of a soma compartment connected via axial resistances R_a to several dendrite compartments (figure 6.3). According to Kirchhoff's law, the net outward current $I_{m,s}$ through the membrane of the soma compartment equals the sum of the currents $I_{dj \to s}$ that enter the soma compartment from the N dendrite compartments j:

$$I_{m,s} = \sum_{j=1}^{N} I_{dj \to s} \tag{6.2}$$

The current $I_{dj \to s}$ from each of the dendrites into the soma can be described by the voltage gradient between dendrite and soma $V_{dj} - V_s$ divided by the axial resistance $R_{a,j \to s}$:

$$I_{dj \to s} = \frac{V_{dj} - V_s}{R_{a,j \to s}} \tag{6.3}$$

As indicated in figure 6.3, the net current through the soma membrane $I_{m,s}$ is given by the sum of the capacitative current and the net ionic current $I_{ion,s}$:

$$I_{m,s} = C_m \frac{dV_s}{dt} + I_{ion,s} \tag{6.4}$$

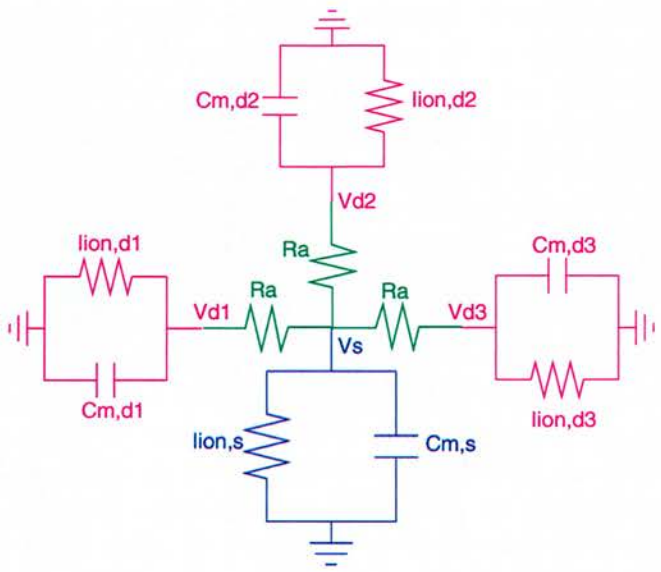

Figure 6.3: Simplified circuit diagram of the multi-compartmental Purkinje cell model. Several dendrite compartments (magenta, for clarity, only three are shown) are connected through axial resistances R_a to a soma compartment (blue). V_s and V_{dj} represent the somatic and dendritic membrane potential, $C_{m,s}$ and $C_{m,dj}$ are the respective capacitances and $I_{ion,s}$ and $I_{ion,dj}$ the ionic currents.

Similar to the Spectral Timing Model (Fiala et al., 1996) and the one-compartmental version of the Adaptive Timing Model described in the previous chapter, the membrane potential in the soma is assumed to correspond to the simple spike firing rate of the Purkinje cell caused by the background of parallel fibre inputs. As a consequence, the soma contains no explicit representation of voltage dependent channels, and the net ionic current across the soma membrane equals the leakage current:

$$I_{ion,s} = I_l = k_{20} (V_s - V_{base}) \tag{6.5}$$

with an elevated *in vivo* baseline potential of $V_{base} = -50mV$ (see section 4.3.1). By summarising equations 6.2 – 6.5, the change of the membrane potential in the soma is given as:

$$\frac{dV_s}{dt} = k_{25} \sum_{j=1}^{N} (V_{dj} - V_s) - k_{20} (V_s - V_{base}) \tag{6.6}$$

The axial resistances $R_{a,j\to s}$ between all the dendrites and the soma are assumed to be equal and can be summarised by the constant k_{25}:

$$k_{25} = \frac{1}{C_m R_{a,j\to s}} = \frac{1}{C_m R_a} \tag{6.7}$$

As in the one-compartmental model, the ionic current in the dendrites is given by the sum of three terms: an inward current through the Na^+ / Ca^{2+} exchanger, an outward current through Ca^{2+} dependent K^+ (K_{Ca}) channels and a leakage current:

$$\begin{aligned} I_{ion,dj} = \; & k_{19} \frac{d[Ca^{2+}]}{dt}(NaCa) - \bar{g}_{KCa}\, m_{KCa}([Ca^{2+}], V_{dj})\,(V_{dj} - V_K) \\ & -k_{20}\,(V_{dj} - V_{base}) \end{aligned} \tag{6.8}$$

with an exchanger current $d[Ca^{2+}]/dt$ and a K_{Ca} channel activation variable m_{KCa} which are described by equations 4.14 and 4.17 (section 4.3.1).

Again, Kirchhoff's law states that the sum of the ionic and capacitative currents in each dendrite compartment equals the current entering the dendrite from the soma (see figure 6.3):

$$I_{ion,dj} + C_m \frac{dV_{dj}}{dt} = I_{s\to dj} = -I_{dj\to s} = \frac{V_s - V_{dj}}{R_{a,j\to s}} \tag{6.9}$$

Thus, the change of the dendritic membrane potential is given by:

$$\begin{aligned} \frac{dV_{dj}}{dt} = \; & k_{19} \frac{d[Ca^{2+}]}{dt}(NaCa) - \bar{g}_{KCa}\, m_{KCa}([Ca^{2+}], V_{dj})\,(V_{dj} - V_K) \\ & -k_{20}\,(V_{dj} - V_{base}) + k_{25}\,(V_s - V_{dj}) \end{aligned} \tag{6.10}$$

In addition, each of the dendrite compartments is represented by a set of equations 4.1-4.20 (chapter 4) and 5.2 (chapter 5). The soma compartment receives no synaptic inputs and is simply described by equation 6.6.

In the next section, numerical simulation results will be presented and it will be shown how the Purkinje cell model can learn to recognise temporal parallel fibre input patterns in an RBF-like way.

6.4 Simulation Results

6.4.1 Delay Learning in a Single Dendritic Compartment

The model was implemented in C++ and numerical simulations were performed using a 5th order Runge-Kutta algorithm with adaptive stepsize control. All parameter values in the simulation were identical to the original Adaptive Timing parameters (appendix A.2), with the exception of k_{25} which was set to $25s^{-1}$.

In each of the dendrite compartments, the repeated presentation of parallel fibre (PF) input followed by climbing fibre (CF) input leads to the same course of events as in the one-compartmental Adaptive Timing Model (figure 6.4, compare section 5.4.2):

1. Before training, the concentration of available mGluRs B_a in all dendrites is assumed to be large, and most of the K_{Ca} channels are dephosphorylated and inactive. As a consequence, PF input, represented as mGluR activation by a $10\mu M$ glutamate pulse from t_j to $t_j + 200ms$, leads to Ca^{2+} increase, protein kinase C (PKC) activation and dendritic depolarisation shortly after t_j. CF input results in a cGMP peak and protein kinase G (PKG) activation at t_{CF}.

2. During training, the PKG phosphorylation of the mGluRs leads to a decrease in the concentration of available receptors B_a and to an increase in the time delay between PF input and Ca^{2+}, PKC and depolarisation response. The PF evoked Ca^{2+}/PKC/depolarisation peak moves towards the CF evoked cGMP/PKG peak until the PKC and cGMP peaks overlap. Overlapping PKC and cGMP peaks result in an equilibrium between cGMP/PKG induced B_a decrease and PKC induced B_a increase, and in a stable time delay between PF input and Ca^{2+}, PKC and depolarisation response.

3. Coinciding PKC and PKG activation also leads to persistent phosphorylation and activation of the K_{Ca} channels, and the dendritic response to PF input changes from depolarisation to hyperpolarisation.

4. After training, the $200ms$ PF input starting at t_j triggers a dendritic hyperpolarisation response at approximately the CF input time t_{CF}, and the dendrite has *learnt the time delay between* t_j *and* t_{CF} (figure 6.4).

6.4.2 Learning to Recognise a Temporal Parallel Fibre Pattern

In the previous section, it was shown that the jth dendrite of the Purkinje cell model can learn a time delay between a specific parallel fibre (PF) input at t_j and a climbing fibre (CF) input at t_{CF}. In the multi-compartmental model, all dendrite compartments communicate with the soma compartment through axial currents $I_{dj\to s}$ (equation 6.3), and the membrane potential in the soma is influenced by the sum of all of the N dendritic voltages.

As a consequence, the repeated presentation of a temporal parallel fibre pattern $\mathbf{t}$, consisting of PF input at different times t_j to the different dendrites j, together with a climbing fibre input at t_{CF} to the whole cell results in a change of the dendritic time delays until *all dendrites and the soma* respond to the PF pattern $\mathbf{t}$ with a hyperpolarisation peak at t_{CF} (figure 6.5). Thus, the multi-compartmental Purkinje cell model has *learnt to recognise a particular temporal parallel fibre input pattern.*

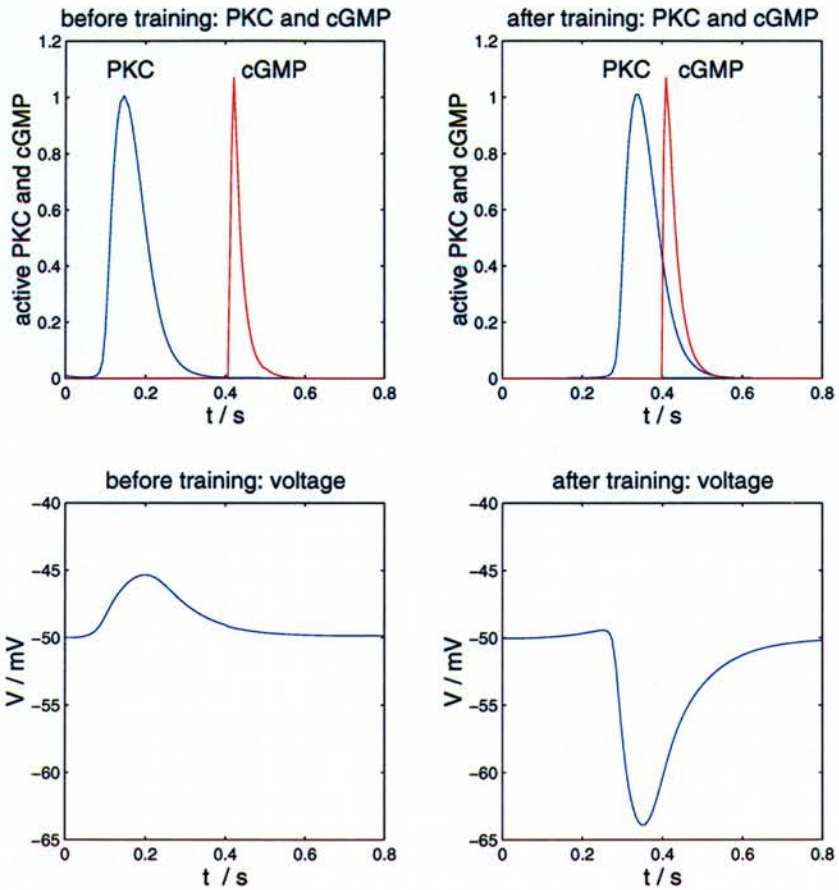

Figure 6.4: Simulation results for a single dendritic compartment in the multi-compartmental Purkinje cell model. Before training, parallel fibre (PF) input, represented by a $10\mu M$ glutamate pulse from $t = 0$ to $t = 0.2s$, results in a PKC peak and a *depolarisation* response around $t = 0.2s$. After 75 training cycles with PF input from $t = 0$ to $t = 0.2s$ and climbing fibre (CF) input at $t = 0.4s$, the PF input leads to a PKC peak which overlaps with the CF evoked cGMP peak, and to a *hyperpolarisation* response around $t = 0.4s$.

In the simulation, the parallel fibre input times t_j for the different dendrites are random values between 0 and $t_{CF} - 100ms$. Thus, the different Purkinje cell dendrites have to learn very different time delays between t_j and t_{CF} which results in very different equilibrium concentrations of available mGluRs B_a. The relation between the parallel fibre input times t_j and the final mGluR concentrations B_a in the 10 dendrites of an 11-compartmental Purkinje cell model is shown in figure 6.6.

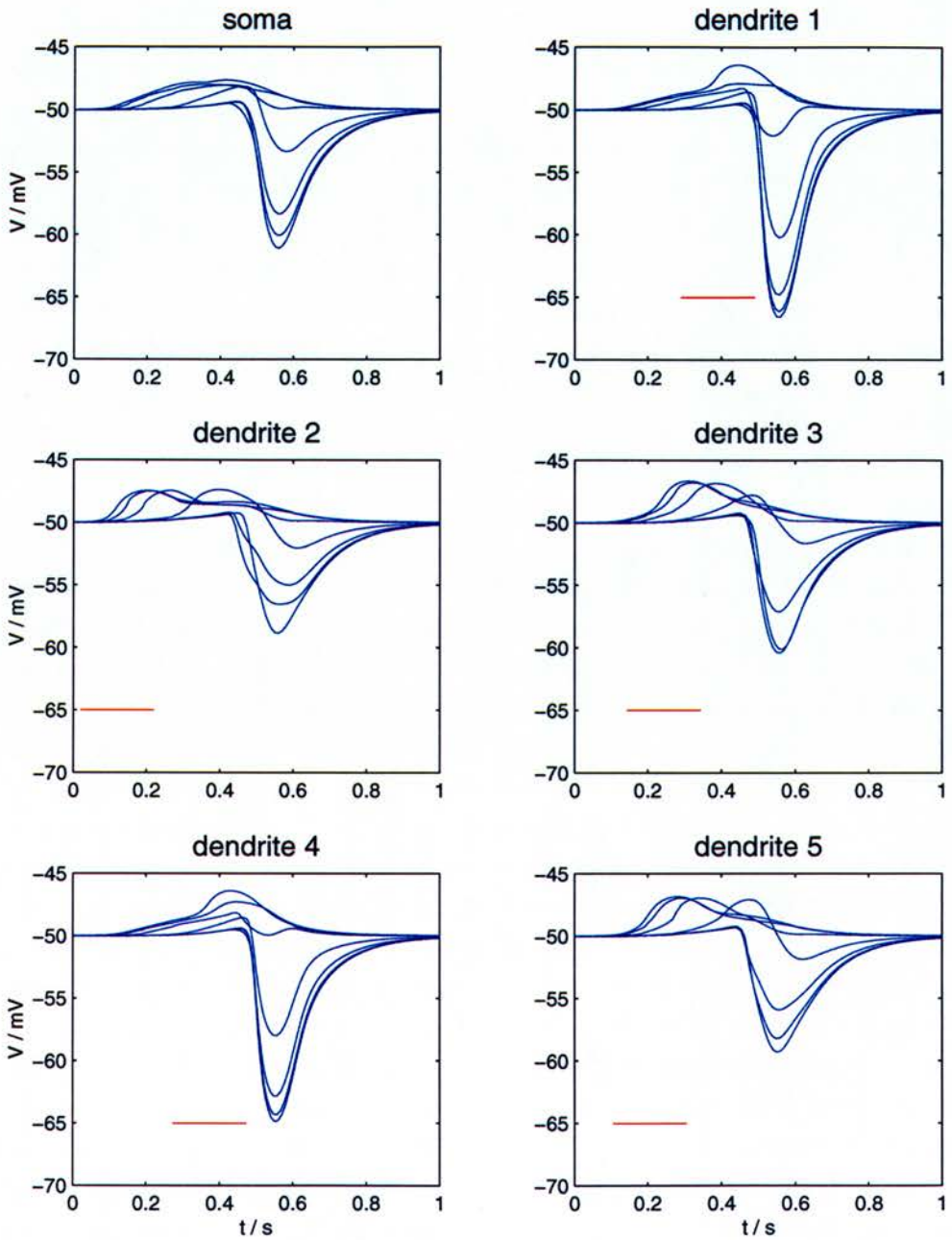

Figure 6.5: Simulation results for 75 presentations of a parallel fibre (PF) pattern $\mathbf{t}$, consisting of PF input from t_j to $t_j + 200ms$ (red bars), and a climbing fibre (CF) input at $t_{CF} = 0.6s$ to each of the 10 dendrites of an 11-compartmental Purkinje cell model. In all of the dendrites, the response to the PF input at t_j changes from an initial *depolarisation* shortly after t_j to a *hyperpolarisation* around t_{CF}. Voltage traces are shown for the soma and 5 of the 10 dendrites, and for every 5th learning cycle.

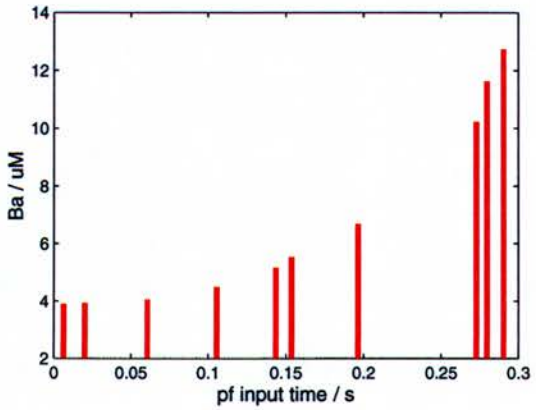

Figure 6.6: Relation between the parallel fibre (PF) input times t_j and the final concentrations of available mGluRs B_a in the 10 dendrites of an 11-compartmental Purkinje cell model which has been trained by 75 presentations of a PF pattern $\mathbf{t}$ and a climbing fibre input at t_{CF}.

6.4.3 RBF Response to Random Inputs

After training with a temporal parallel fibre pattern $\mathbf{t}$ and a climbing fibre signal at t_{CF}, the Purkinje cell has encoded the PF pattern $\mathbf{t}$ in its dendritic time delays and reponds to it in a radial basis function (RBF)-like way. The similarity with Hopfield's RBF neurons (section 6.2) can be demonstrated by representing the Purkinje cell as an RBF centre vector $\mathbf{c}$ whose components c_j are given by the difference between the CF input time t_{CF} and the dendritic time delays d_j between the PF input at t_j and the hyperpolarisation peak at $t_{v_{min}}$:

$$c_j = t_{CF} - d_j = t_{CF} - (t_{v_{min}} - t_j) \tag{6.11}$$

Thus, the distance between the Purkinje cell centre vector $\mathbf{c}$ and the PF input vector $\mathbf{t}$ depends on the difference between the CF time t_{CF} and the time of the hyperpolarisation peak $t_{v_{min}}$:

$$\| \mathbf{c} - \mathbf{t} \| = \sqrt{N} \, (t_{CF} - t_{v_{min}}) \tag{6.12}$$

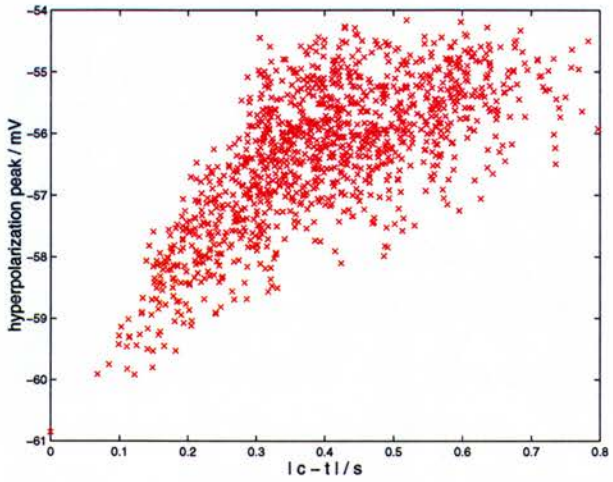

Figure 6.7: Maximum of the hyperpolarisation response of a Purkinje cell model with an RBF centre vector $\mathbf{c}$ to random PF input patterns $\mathbf{t}$. The hyperpolarisation peak decreases with an increasing distance $\| \mathbf{c} - \mathbf{t} \|$, similar to RBF units in artificial neural networks.

where N is the dimension of the PF input vector which is given by the number of dendrites in the Purkinje cell model. Repeated presentations of a parallel fibre pattern $\mathbf{t}$ and a climbing fibre signal at t_{CF} move the the RBF centre vector $\mathbf{c}$ towards the PF input vector $\mathbf{t}$ until the distance between the vectors $\| \mathbf{c} - \mathbf{t} \|$ becomes very small, with an exact equilibrium value of $\| \mathbf{c} - \mathbf{t} \|$ which depends on the rate constants for the receptor phosphorylation k_f and k_b (equation 5.2).

To illustrate the analogy with Hopfield's RBF-like decoding neurons and RBF units in artificial neural networks, a Purkinje cell model with a centre $\mathbf{c}$ was presented with random parallel fibre input patterns $\mathbf{t}$, and the maximum of the hyperpolarisation response was measured as a function of the distance between the two vectors $\| \mathbf{c} - \mathbf{t} \|$. As shown in figure 6.7, temporal PF input patterns $\mathbf{t}$ which are closer to the Purkinje cell centre vector $\mathbf{c}$ result in a stronger hyperpolarisation response. Thus, the Purkinje cell model is able to implement the decoding of temporal inputs and learn an RBF-like response as postulated by Hopfield.

6.5 Chapter Conclusions

It is widely accepted that the temporal encoding of input patterns is important for the processing of information in the brain (e.g. Bialek et al., 1991; Gerstner et al., 1996; Thorpe et al., 1996; Laurent, 1996; Wehr & Laurent, 1996). Recently, Hopfield (1995) has suggested a form of temporal encoding where analogue input vectors are represented by the timing of action potential relative to the phase of collective subthreshold membrane potential oscillations. In Hopfield's model, the resulting temporal spike patterns are decoded by *radial basis function (RBF) neurons* using a combination of *time delays* and *coincidence detection*.

If this kind of encoding is used in the brain, the decoding RBF neurons must have a mechanism to *learn* the time delays for the recognition of a new temporal pattern. In the previous chapter, the Adaptive Timing Model was presented and it was shown that the metabotropic glutamate receptor (mGluR) signalling network in a cerebellar Purkinje cell can implement synaptic delay learning. In this chapter, an extension of the one-compartmental Adaptive Timing Model to a *multi-compartmental Purkinje cell model* was described.

The multi-compartmental Purkinje cell model consists of a soma compartment which provides the output of the cell, and a number of dendrite compartments which receive synaptic inputs through parallel fibres (PFs) and climbing fibres (CFs). As in the one-compartmental version of the Adaptive Timing Model, the mGluR signalling network in each of the dendrites is respresented by 13 ordinary differential equations (ODEs). In the dendrites, the presentation of PF plus CF input during training triggers the phosphorylation of the mGluRs by protein kinase C (PKC) and protein kinase G (PKG), changes the concentration of receptors which are available for activation by glutamate and adjusts the time delay between mGluR activation and voltage response. Through axial currents, the dendritic voltage responses are transmitted to the soma.

As a consequence, *all of the dendrites and the soma* can learn to respond to a PF input with a hyperpolarisation peak at the time of the CF input during training, and the whole Purkinje cell model can learn to recognise a particular temporal parallel fibre pattern $\mathbf{t}$. The Purkinje cell can be represented by a radial basis function (RBF) centre vector $\mathbf{c}$, and it can be shown that the maximum of the hyperpolarisation response decreases with an increasing distance between RBF centre vector and PF input vector $\| \mathbf{c} - \mathbf{t} \|$. Thus, the multi-compartmental version of the Adaptive Timing Model implements the temporal pattern decoding mechanism and the RBF learning postulated by Hopfield.

One of the conclusions from the detailed mGluR signalling model is that a temporal RBF learning mechanism based on adaptive synaptic delays might be biologically plausible. As a result, it is now possible to simplify the model to investigate its computational capabilities in more detail. In the next chapter, a simplified, *leaky integrator* version of the Purkinje cell model will be presented, and it will be described how different leaky integrator Purkinje cells in a group can discover different clusters of temporal parallel fibre input patterns, and how the clustering performance can be improved by use-dependent desensitisation of the response.

Chapter 7

The Adaptive Leaky Integrator

7.1 Introduction

Ever since Donald Hebb published *The Organization of Behavior* in 1949, it has been widely accepted that learning in biological and artificial neural networks involves the *adaptation of synaptic efficacies* between pre- and postsynaptic neurons. According to Hebb's influential postulate, the efficacy of a connection between two neurons is increased if the pre- and postsynaptic neurons are simultaneously active, more precisely (Hebb, 1949):

> *When an axon of cell A is near enough to excite cell B or repeatedly or consistently takes part in firing it, some growth process or metabolic change takes place in one or both cells such that A's efficiency, as one of the cells firing B, is increased.*

Since 1949, the concept of a *Hebbian synapse* has evolved, due to a large number of new experimental findings (for review, see e.g. Linden, 1994; Artola & Singer, 1993) and theoretical considerations (e.g. Brown et al., 1990; Bear et al., 1987). However, there is still a general consensus that the formation of memories in the brain is based on different forms of potentiation or depression of *synaptic weights* with a Hebbian flavour.

In the previous two chapters, a detailed biochemical model of the metabotropic glutamate receptor (mGluR) signalling network in a cerebellar Purkinje cell was presented, and it was shown that the phosphorylation of the mGluRs can implement an *adaptive postsynaptic time delay* between receptor activation and voltage response. In chapter 5, it was demonstrated how the synaptic delay adjustment can enable a single Purkinje cell to learn the adaptive timing of the classically conditioned eye-blink response, and in chapter 6, it was shown that a multi-compartmental Purkinje cell model can use the delay adaptation mechanism to learn a radial basis function (RBF)-like response to temporal parallel fibre input patterns.

The adaptation of synaptic *delays* as opposed to synaptic *weights* represents a new *non-Hebbian* learning mechanism, and in the following chapters of the thesis, two simplifications of the model will be used to study (a) the *computational capabilities* and (b) the underlying *biochemical mechanism* of the synaptic delay learning in more detail. In chapter 8, an *analytical simplification* of the complex mGluR signalling model will be described and the essential biochemical ingredients of the delay adaptation will be characterised. This chapter presents the *leaky integrator*, a *phenomenological simplification* of the Purkinje cell model, and investigates the behaviour of a group of leaky integrators in a temporal pattern clustering task.

Recently, Natschläger and Ruf (1998) have shown that a group of integrate-and-fire neurons can learn the clustering of temporal patterns by selecting the appropriate time delays from a predefined spectrum of existing delays. Natschläger and Ruf's model will be briefly summarised in the following section. The remaining sections of the chapter will introduce the leaky integrator version of the Purkinje cell model, present numerical simulation results for the clustering of temporal patterns by a group of leaky integrators and describe an extension of the leaky integrator model with adaptive input currents which demonstrates an improved performance in clustering tasks.

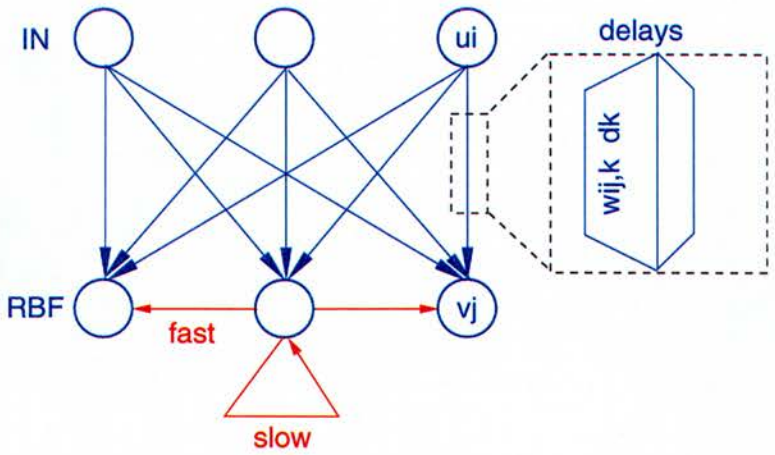

Figure 7.1: Architecture of Natschläger & Ruf's RBF network. Initially, each input neuron u_i is connected to each RBF neuron v_j through a set of connections with different delays d^k and weights w_{ij}^k (indicated in the box on the right). Each RBF neuron forms fast inhibitory connections to all other RBF neurons and a slow inhibitory connection to itself (red). Adapted from Natschläger and Ruf (1998).

7.2 Learning RBFs with Multiple Delay Lines

In Natschläger and Ruf's model, an array of input neurons $u_1, ..., u_n$ is connected to an array of *RBF neurons* $v_1, ..., v_n$ (figure 7.1). The RBF neurons are modelled as integrate-and-fire neurons (see e.g. Maass, 1996; Gerstner et al., 1996) and generate a spike if the sum of the excitatory inputs is large enough to push the membrane potential over the threshold.

The network starts off with a *spectrum of connections* with different delays d^k and weights w_{ij}^k between each input neuron u_i and each RBF neuron v_j (see figure 7.1). Initially, the weights w_{ij}^k are set to random values out of a prespecified range so that each RBF neuron v_j has to receive at least one spike from every input neuron u_i before it fires. Once the RBF neuron fires, the spike is transmitted back to all of its synapses, and the synaptic weights are increased or decreased, depending on the time difference between the arrival of the pre- and postsynaptic spikes at the synapse. More precisely, synapses which receive a presynaptic input spike shortly before the backpropagated spike arrives at the postsynaptic side are strengthened, and synapses where the presynaptic spike arrives much earlier or later are weakened. For a synapse between an

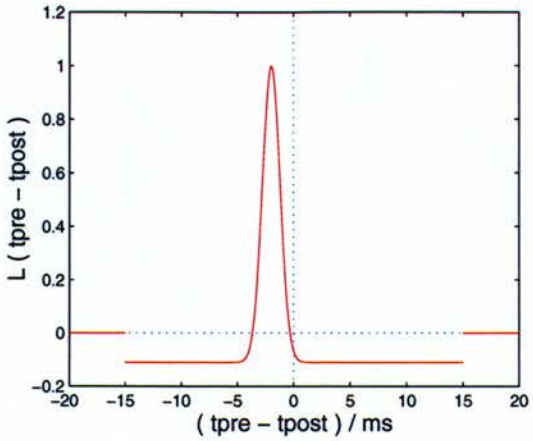

Figure 7.2: Natschläger & Ruf's learning function $L(t_{pre} - t_{post})$ that describes how the the synaptic weight change Δw_{ij}^k varies with the difference between pre- and postsynaptic spike arrival times $t_{pre} - t_{post}$ (see equation 7.1). Adapted from Natschläger and Ruf (1998).

input neuron u_i which fires at t_i and an RBF neuron v_j which fires at t_j, the change of the weight w_{ij}^k is given by:

$$\Delta w_{ij}^k = \eta\, L(\,(t_i + d^k) - (t_j + d^{back})\,) \tag{7.1}$$

where d^k is the delay between the input firing time t_i and the arrival time of the presynaptic spike t_{pre}, d^{back} is the delay between the RBF firing time t_j and the postsynaptic arrival time t_{post}, $\eta > 0$ is the constant learning rate and $L(\,t_{pre} - t_{post}\,)$ the learning function shown in figure 7.2.

The application of the learning rule results in the selective *strengthening* of the connections whose delays even out the difference between the firing times of the input neurons, and the *weakening* and eventually pruning of all other connections. To represent the *relative* rather than the *absolute* input firing times t_i, Natschläger and Ruf define an *input vector* $\mathbf{x}$ with components x_i:

$$x_i = max\{\, t_i \,|\, 1 \leq i \leq n \,\} - t_i \tag{7.2}$$

Each RBF neuron v_j is represented by an *RBF centre vector* $\mathbf{c}_j$ with components c_{ji}:

$$c_{ji} = \tilde{d_{ji}} - min\{\, \tilde{d_{ji}} \,|\, 1 \leq i \leq m \,\} \tag{7.3}$$

where $\tilde{d_{ji}}$ is the weighted average of the set of the l delays between input neuron u_i and RBF neuron v_j:

$$\tilde{d_{ji}} = \frac{\sum_{k=1}^{l} w_{ij}^k \, d^k}{\sum_{k=1}^{l} w_{ij}^k} \tag{7.4}$$

An RBF neuron v_j fires if it receives an input $\mathbf{x}$ which is sufficiently close to its centre $\mathbf{c}_j$. The firing *time* of the RBF neuron is a measure of the distance between the two vectors $\| \mathbf{c}_j - \mathbf{x} \|$, with small distances leading to earlier spikes. As a consequence, fast lateral inhibition between the RBF neurons can implement a winner-take-all mechanism so that only the RBF neuron v_j with the smallest distance $\| \mathbf{c}_j - \mathbf{x} \|$ to the input vector fires.

Given that the firing of an RBF neuron is a necessary condition for the adjustment of its weights (equation 7.1), only the weights of the *winning* RBF neuron whose centre $\mathbf{c}_j$ is the closest to the input vector $\mathbf{x}$ are modified. Thus, if several RBF neurons are presented with input patterns $\mathbf{x}$ from a number of clusters C_μ, different RBF neurons converge to the centres of different input clusters, and the RBF network can learn the clustering of temporal patterns.

A common problem in clustering tasks which also occurs in the model is that it is very likely for some of the neurons not to be used while others specialise on more than one cluster. To solve this problem and decrease the frequency of unused RBF neurons, Natschläger and Ruf use a "conscience" mechanism (Grossberg, 1976) and add a slow self-inhibitory connection to each of the RBF neurons (figure 7.1).

To summarise, Natschläger and Ruf have demonstrated that a network of spiking neurons can discover clusters in a temporal input space, by using a Hebbian weight update rule which selects the correct delays from a predefined spectrum of initial delays. More elegant than a prespecified set of delays would be the adaptation of the individual delays, and in the previous two chapters, it was described how the metabotropic glutamate receptor (mGluR) signalling network in a cerebellar Purkinje cell can implement an appropriate delay adaptation mechanism. In the following sections of this chapter, a simplified leaky integrator version of the Purkinje cell model will be presented, and the behaviour of a group of leaky integrators will be investigated in a temporal pattern clustering task.

7.3 The Leaky Integrator

7.3.1 The Basic Model

In the basic version of the leaky integrator Purkinje cell model, the membrane potential V is described as in a standard integrate-and-fire neuron (e.g. Gerstner et al., 1996):

$$\frac{dV}{dt} = -\frac{V}{\tau_m} + \sum_{j=1}^{N} I_j(t) \tag{7.5}$$

where $I_j(t)$ is the current induced by mGluR activation in synapse j, and τ_m is the apparent membrane time constant which determines how fast the membrane potential returns to the arbitrarily chosen baseline $V_{base} = 0$.

In contrast to an integrate-and-fire neuron and similar to the complex version of the Purkinje cell model described in the previous chapters, there is no explicit representation of spikes in the leaky integrator model. Instead, the membrane potential V corresponds directly to the simple spike frequency caused by the contineous background

of parallel fibre inputs (Murphy & Sabah, 1970; Armstrong & Rawson, 1979, compare section 4.2). A decrease in V represents a slower Purkinje cell firing rate, disinhibition of neurons in the interpositus nucleus and an increased output from the cerebellum. Thus, different from a normal *excitatory* neuron, the magnitude of the effective response of the *inhibitory* Purkinje cell is given by the extent of voltage minimum, i.e. the *hyperpolarisation* peak.

As described in detail in section 4.2, parallel fibre input stimulates metabotropic glutamate receptors (mGluRs) on the Purkinje cell membrane and triggers a second messenger cascade leading to release of Ca^{2+} from intracellular stores. The increase in the cytoplasmic Ca^{2+} concentration affects the Purkinje cell membrane potential by activating the Na^{+}/Ca^{2+} exchanger and Ca^{2+} dependent K^{+} (K_{Ca}) channels.

In the complex Purkinje cell model, the K_{Ca} channels are initially unphosphorylated and inactive, and parallel fibre input before training leads to a net *inward* current through the Na^{+}/Ca^{2+} exchanger. In each synapse of the complex model, the learning process can be divided into two phases: during the *delay learning phase*, phosphorylation of the mGluRs adjusts the time delay between receptor stimulation and voltage response, and during the *weight learning phase*, phosphorylation and activation of the K_{Ca} channels reverses the direction of the mGluR evoked current from *inward* to *outward*.

The leaky integrator is a phenomenological simplification of the complex Purkinje cell model designed to study the *computational capabilities of synaptic delay learning*. As a consequence, in the leaky integrator model it is unnecessary to represent the K_{Ca} channel phosphorylation which implements the weight learning, and the stimulation of the mGluRs results in an *outward current at all times*. For a synapse with a postsynaptic delay d_j, the outward current in response to a parallel fibre input at t_j is given by:

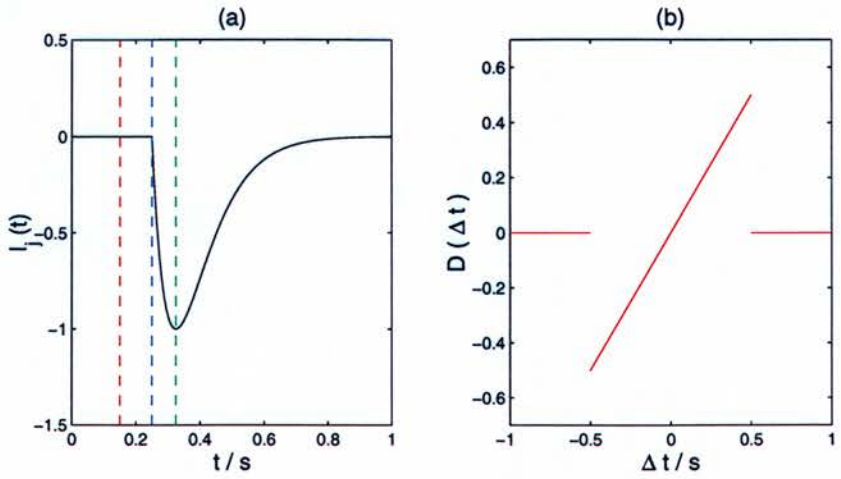

Figure 7.3: Input current and delay learning function in the leaky integrator model. (a) Time course of the outward current $I_j(t)$ after mGluR stimulation by parallel fibre (PF) input at t_j (red dashed line). The onset of the current is given by the PF input time plus the synaptic delay $t_j + d_j$ (blue dashed line), and the current peaks at $t_j + d_j + \tau_s$ (green dashed line) where τ_s is the apparent synaptic time constant. The values used in the example are $t_j = 0.15s$, $d_j = 0.1s$ and $\tau_s = 0.075s$ (compare equation 7.6). (b) Delay learning function $D(t_{CF} - (t_j + d_j))$ that describes how the change of synaptic delays d_j is influenced by the difference between the climbing fibre input time t_{CF} and the time of the onset of the PF evoked current $t_j + d_j$ (with $\delta = 0.5s$, compare equations 7.7 and 7.8).

$$I_j(t) = \begin{cases} \frac{(t_j+d_j)-t}{\tau_s} \, exp(\, 1 - \frac{t-(t_j+d_j)}{\tau_s}) & \text{for } t > t_j + d_j \\ 0 & \text{for } t \leq t_j + d_j \end{cases} \tag{7.6}$$

with an apparent synaptic time constant τ_s which equals the time delay between parallel fibre input plus synaptic delay $(t_j + d_j)$ and the peak of the outward current (see figure 7.3 (a)).

When the model is presented with a temporal parallel fibre pattern $\mathbf{t} = \langle t_1, ..., t_j, ..., t_N \rangle$ and a climbing fibre input at t_{CF}, the change in the concentration of available mGluRs in the different synapses leads to an adjustment of the vector of postsynaptic delays $\mathbf{d} = \langle d_1, ..., d_j, ..., d_N \rangle$ which is modelled by:

$$\Delta d_j = \eta \, D(\, t_{CF} - (t_j + d_j)\,) \tag{7.7}$$

where $\eta > 0$ is a constant learning rate and $D(\Delta t)$ is a simple delay learning function (see figure 7.3 (b)). To restrict the change of delays to pairs of climbing fibre and parallel fibre inputs *within the same trial*, $D(\Delta t)$ has to be set to zero for $\| \Delta t \| > \delta$:

$$D(\Delta t) = \begin{cases} \Delta t & \text{for } -\delta \leq \Delta t \leq \delta \\ 0 & \text{otherwise} \end{cases} \tag{7.8}$$

with an effective time window for the delay learning 2δ which is smaller than the intertrial interval (ITI) between two successive climbing fibre inputs.

The leaky integrator model was implemented in C++ and numerically integrated, using a 5th order Runge-Kutta algorithm with adaptive step size control and the parameters listed in appendix A.3. In the following sections of the chapter, numerical simulation results will be presented that show how a *single* leaky integrator Purkinje cell model can learn a radial basis function (RBF)-like response to temporal parallel fibre input pattern, and how a *group* of leaky integrators can discover different clusters in a temporal parallel fibre input space.

7.3.2 RBF Learning by a Single Integrator

If a leaky integrator Purkinje cell model with random initial delays d_j is presented repeatedly with a single temporal parallel fibre pattern $\mathbf{t} = \langle t_1, ..., t_j, ..., t_N \rangle$ and a climbing fibre input at t_{CF}, the vector of synaptic delays $\mathbf{d} = \langle d_1, ..., d_j, ..., d_N \rangle$ is changed according to equation 7.7 until a stable state is reached where the different delays d_j even out the differences between the parallel fibre input times t_j. In the stable state, all of the N sums $t_j + d_j$ equal the climbing fibre time t_{CF} and, as a consequence, all of the input currents $I_j(t)$ peak at $t_{CF} + \tau_s$ (compare equation 7.6 and figure 7.3 (a)). Thus, the training transforms the broad hyperpolarisation response which is caused by the random initial delays into a narrow hyperpolarisation peak shortly after $t_{CF} + \tau_s$ (figure 7.4 (a)).

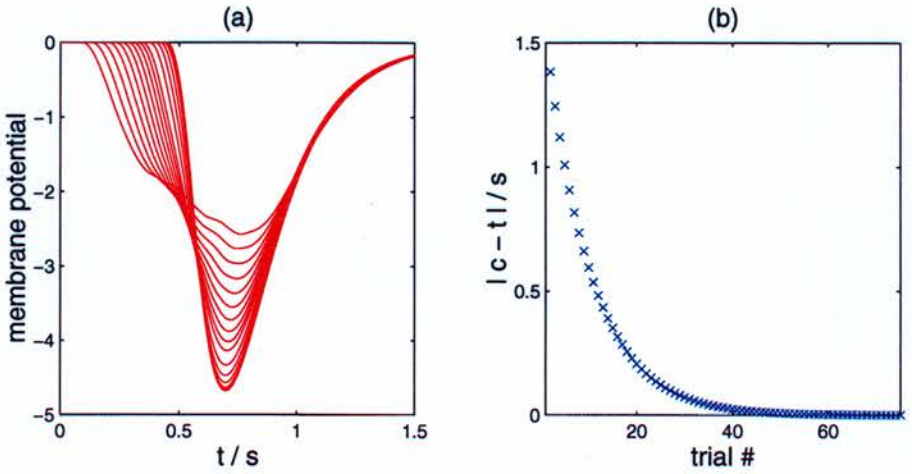

Figure 7.4: Simulation results for repeated presentations of a 50-dimensional temporal parallel fibre input $\mathbf{t}$ and a climbing fibre input at $t_{CF} = 0.5s$ to a leaky integrator Purkinje cell model with random initial delays $d_j \in [0, 0.5s]$. (a) The application of the delay learning rule (equation 7.7) transforms the broad hyperpolarisation reponse which is caused by the random initial delays into a narrow peak around $t = 0.7s$. Voltage traces are shown for trials number 1-20. (b) During training, the RBF centre vector of the leaky integrator $\mathbf{c}$ (equation 7.9) moves towards the parallel fibre input vector $\mathbf{t}$ until both vectors are identical.

Similar to the complex Purkinje cell model (section 6.4.3), the leaky integrator model can be represented by a radial basis function (RBF) centre vector $\mathbf{c} = \langle c_1, ..., c_j, ..., c_N \rangle$ with components c_j which are given by the difference between the climbing fibre input time t_{CF} and the individual synaptic delays d_j:

$$c_j = t_{CF} - d_j \tag{7.9}$$

If a *single* leaky integrator with an RBF centre $\mathbf{c}$ is trained with a climbing fibre signal and a *single* parallel fibre pattern $\mathbf{t}$, the centre vector $\mathbf{c}$ moves towards the input vector $\mathbf{t}$ until both vectors are identical (figure 7.4 (b)).

To demonstrate the analogy with radial basis functions, the leaky integrator was presented with random temporal parallel fibre inputs, and the extent of the hyperpolarisation response was measured as a function of the distance between the centre of the leaky integrator $\mathbf{c}$ and the parallel fibre input vector $\mathbf{t}$.

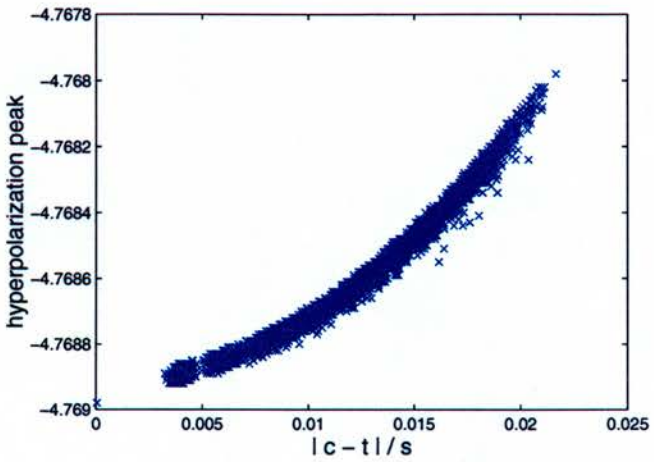

Figure 7.5: Simulation results for the presentation of random parallel fibre input patterns $\mathbf{t}$ to a leaky integrator with a centre $\mathbf{c}$. Similar to the radial basis function neurons which were postulated by Hopfield (1995), the extent of the hyperpolarisation response of the leaky integrator decreases with an increasing distance between the centre vector and the input vector $\| \mathbf{c} - \mathbf{t} \|$.

As shown in figure 7.5, the hyperpolarisation response is maximal for a template input pattern $\mathbf{t}$ and decreases with an increasing distance between the two vectors $\| \mathbf{c} - \mathbf{t} \|$. Thus, like the multi-compartmental Purkinje cell model that was described in the previous chapter, a single leaky integrator can learn a response which is very similar to RBF units in artificial neural networks and to the RBF-like decoding neurons postulated by Hopfield (1995).

7.3.3 Temporal Pattern Clustering by a Group of Integrators

As a consequence of the RBF-like response of a *single* leaky integrator Purkinje cell model to temporal input patterns, it is possible to use a *group* of leaky integrators for a temporal pattern clustering task. By assuming that the leaky integrator Purkinje cell with the strongest hyperpolarisation response inhibits the delay adaptation in all the other cells in the group, a winner-take-all situation can be created so that the modification of synaptic delays is restricted to the Purkinje cell whose centre $\mathbf{c}_k$ is the closest match to the current input vector $\mathbf{t}$.

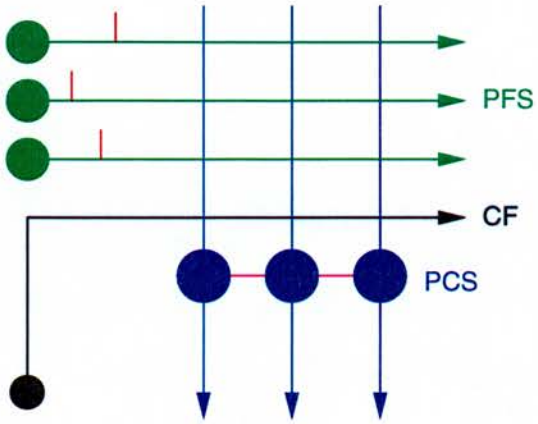

Figure 7.6: Connectivity of the group of leaky integrator (LI) Purkinje cells (PCs, indicated in blue) in the simplified model of the cerebellar cortex. Each of the LI Purkinje cells receives a temporal pattern of parallel fibre inputs $\mathbf{t}$ (PFS, green) and a climbing fibre input at t_{CF} (CF, black). The effect of recurrent connections (e.g. Purkinje cell axon collaterals or multi-synaptic connections via the deep cerebellar nuclei) limits the modification of synaptic delays to the Purkinje cell LI with the strongest response and implements a winner-take-all mechanism (indicated in magenta).

Thus, if a group of leaky integrator Purkinje cell models is presented with temporal parallel fibre patterns $\mathbf{t}$ from a number of input clusters, the RBF centre vectors $\mathbf{c}_k$ of the different integrators move towards the centres of different clusters, and each Purkinje cell specialises on the recognition of a different subset of temporal parallel fibre input patterns (figure 7.7).

Similar to Natschläger and Ruf's results for their network of spiking neurons (section 7.2), it was found that the clustering performance of a group of leaky integrators varies depending on the initial RBF centres and the positions of the input clusters. For equal numbers of integrators and clusters, it is quite common that some of the integrators are not used at all, while others are activated by two clusters and oscillate between them.

Simulation results for the presentation of 3-dimensional parallel fibre input patterns $\mathbf{t} = \langle t_1, t_2, t_3 \rangle$ from four clusters C_μ to a group of four leaky integrators $\mathbf{c}_k = \langle c_{k1}, c_{k2}, c_{k3} \rangle$ are shown in figure 7.7. In the typical example which is shown in the figure, only the integrators number 1 and 4 find their way to the centres of two dif-

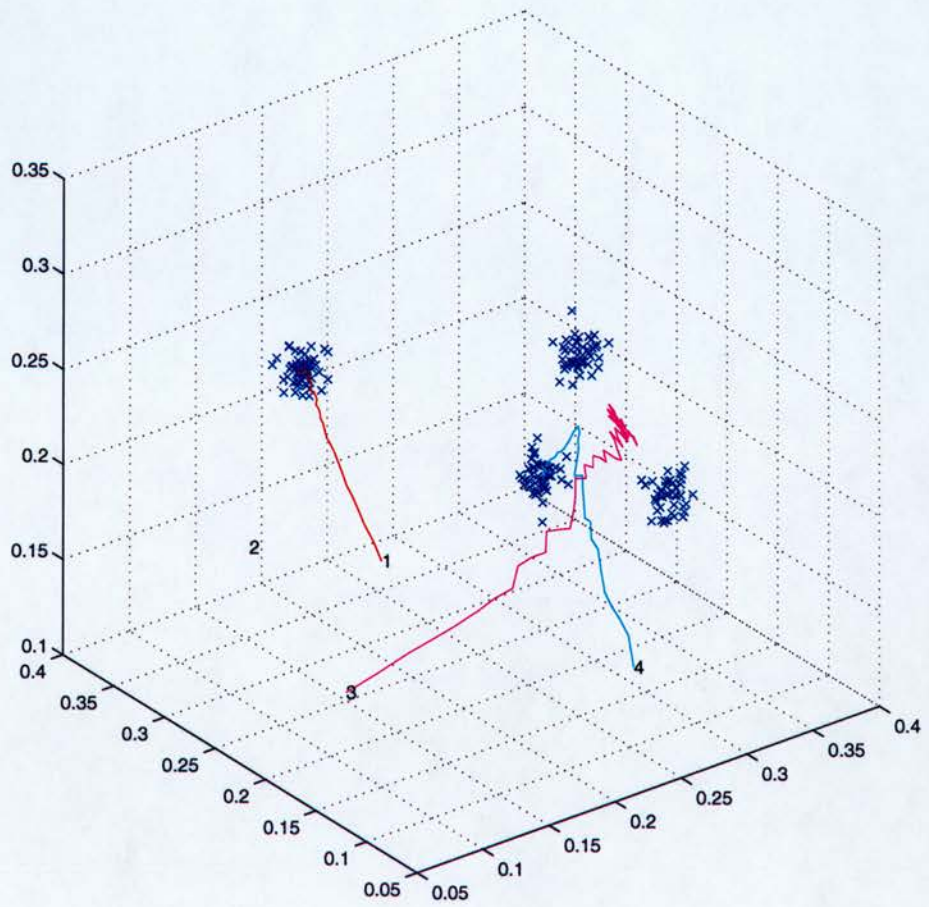

Figure 7.7: Simulation results for four *non-adaptive* leaky integrators and four clusters in a 3-dimensional temporal parallel fibre input space. Integrators 1 and 4 move to the centres of two separate clusters, integrator 3 averages between two clusters and integrator 2 is not used at all. The three axes indicate the three coordinates of both the parallel fibre input patterns t_j and the RBF centres of the integrators c_{kj} in seconds.

ferent clusters. Integrator 3 responds to two clusters and calculates their average, and integrator 2 is not activated by any of the inputs and stays in its initial position.

One possibility to decrease the frequency of leaky integrators which oscillate between two or more clusters, and to make sure that the input space is properly partitioned and all of the clusters are discovered, is to use a larger number of integrators than clusters. However, this results in a number of integrators which are not used and is therefore not as efficient as possible. A more elegant solution which will be discussed in the next section is to assume that the input currents of the leaky integrator undergo a form of use-dependent desensitisation.

7.3.4 Adaptive Input Currents

It has been known for a while that the repeated activation of neurotransmitter receptors can lead to a decrease in their responsiveness. The process is called *desensitisation*, can occur over different time scales and involve the formation of various inactivated receptor states (see e.g. Hille, 1992; Kandel et al., 1991). Often, the transformation of the receptors into a *desensitised* state is a consequence of multiple different phosphorylations. For example, the response of β-adrenergic receptors is gradually downregulated through repeated phosphorylation by a specific β-adrenergic receptor kinase (βARK, Lefkowitz & Caron, 1988), and nicotinic acetylcholine receptors can be desensitised through phosphorylation by protein kinase A, protein kinase C and a tyrosine kinase at seven different sites (Huganir & Greengard, 1990).

In the *adaptive leaky integrator* version of the Purkinje cell model, the metabotropic glutamate receptor (mGluR) mediated response is assumed to undergo a similar form of desensitisation. As a result of the mGluR desensitisation, the mGluR evoked outward currents are downregulated every time a parallel fibre input triggers a response which is strong enough to result in modification of the synaptic delays, and the change of the membrane potential V is given by:

$$\frac{dV}{dt} = -\frac{V}{\tau_m} + \alpha^W \sum_{j=1}^{N} I_j(t) \tag{7.10}$$

where α is an adaptation factor between zero and one, and W is the number of past delay updates or "wins" of the adaptive integrator.

Simulation results for four adaptive leaky integrators $\mathbf{c}_k$ and four clusters of 3-dimensional parallel fibre patterns $\mathbf{t}$ are shown in figures 7.8 - 7.10. In all of the 150 examples that were tested in the simulations, the four integrators managed to specialise on their personal clusters in the parallel fibre input space, taking a route through the

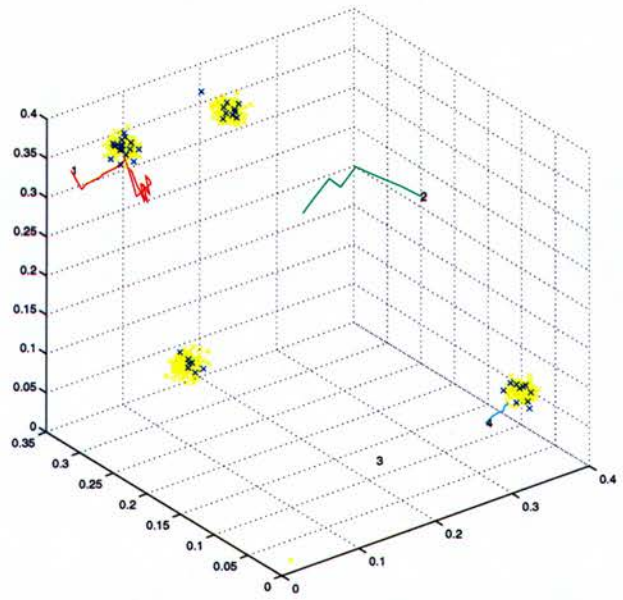

Figure 7.8: Simulation results for four *adaptive* ($\alpha = 0.995$) leaky integrators and four clusters in a 3-dimensional temporal parallel fibre input space. After presentation of 50 input patterns, integrator 1 has started to oscillate in the space between three clusters, resulting in the desensitisation of its response and the activation of integrator 2. Already presented inputs are indicated in blue, inputs that are still to be presented in yellow.

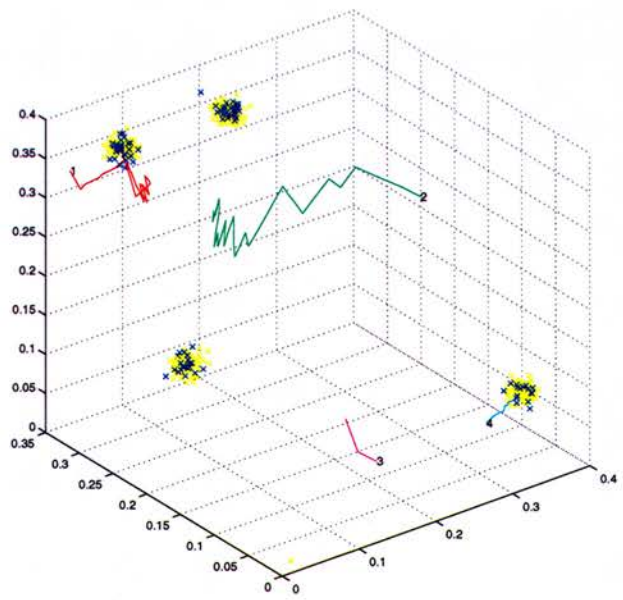

Figure 7.9: Simulation results for four *adaptive* ($\alpha = 0.995$) leaky integrators and four clusters in a 3-dimensional temporal parallel fibre input space. After presentation of 100 input patterns, integrators 1 and 2 have become adapted, leading to the recruitment of integrator 3.

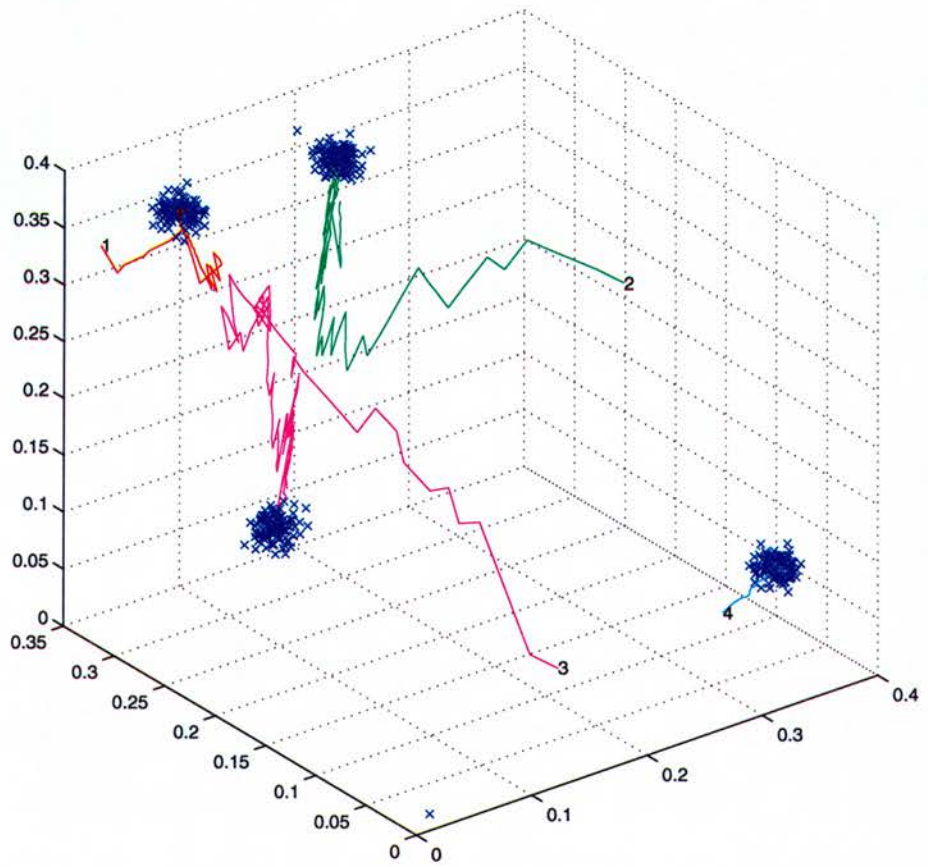

Figure 7.10: Simulation results for four *adaptive* ($\alpha = 0.995$) leaky integrators and four clusters in a 3-dimensional temporal parallel fibre input space. After presentation of 500 input patterns, each of the adaptive integrators 1-4 has moved to the centre of a different input cluster.

input space which can be quite convoluted depending on the initial centres and the cluster positions. In the example in figures 7.8 - 7.10, the initial centre of integrator 1 is the closest match to parallel fibre patterns from three out of the four input clusters. Thus, integrator 1 moves towards and oscillates between the three clusters until the use-dependent adaptation of its input currents (equation 7.10) leads to a desensitised response which is weaker than the response of integrator 2. As a consequence, it is now integrator 2 that moves towards the three clusters (figure 7.8), oscillates between them and becomes desensitised, which in turn results in activation of integrator 3 (figure 7.9). After presentation of a sufficient number of input patterns, each of the four integrators has moved to the centre of a different cluster and specialises on a different subset of temporal parallel fibre patterns (figure 7.10).

7.4 Chapter Conclusions

Inspired by Donald Hebb's famous postulate that the formation of memories in the brain can be implemented by selectively increasing the connection strengths between two simultaneously active neurons (Hebb, 1949), most previous studies of learning in biological and artificial neural networks have focussed on various algorithms and mechanisms for the modification of *synaptic efficacies*. In contrast, this chapter investigated a *non-Hebbian* form of learning which is based on *adaptive synaptic time delays*.

In the two previous chapters, it was shown that the metabotropic glutamate receptor (mGluR) signalling network in a cerebellar Purkinje cell can implement a form of synaptic delay adaptation, and that a multi-compartmental model of a Purkinje cell can use the adaptive synaptic delays to learn a radial basis function (RBF)-like response to temporal parallel fibre input patterns. In this chapter, a simplified *leaky integrator* version of the Purkinje cell model was presented, and the behaviour of a group of leaky integrators was studied in a temporal pattern clustering task.

In contrast to the complex Purkinje cell model, which uses a set of 13 ordinary differential equations (ODEs) to represent the mGluR signalling cascade in each of the dendritic compartments, the basic leaky integrator model consists of a single ODE for the change of the membrane potential, and a simple delta-like rule for the change of synaptic delays. Using numerical simulations, it was shown that a single leaky integrator can learn the decoding of temporal parallel fibre pattern in an RBF-like way, and that a group of leaky integrators can discover different clusters in a temporal parallel fibre input space.

A problem of the basic leaky integrator model is that the performance in clustering tasks varies depending on the initial synaptic delays and the particular structure of the temporal input space. For equal numbers of integrators and input clusters, it is very common that some of the integrators are not used at all while others specialise on the recognition of more than one cluster. A possibility to decrease the frequency

of idle integrators and to make sure that the input space is properly partitioned is to assume that the mGluR mediated response is downregulated depending on the number of previous activations of the cell. In the *adaptive* version of the leaky integrator Purkinje cell model, the mGluR evoked currents undergo a form of use-dependent desensitisation. As a consequence, all of the different *adaptive leaky integrators* in a group are able to specialise on their personal subset of parallel fibre input patterns.

The leaky integrator model was developed based on the knowledge how the complex Purkinje cell model behaves, and to find out more about the computational capabilities of synaptic delay learning. Thus, the leaky integrator is a *phenomenological simplification* of the complex Purkinje cell model, analogous to the phenomenological thermodynamics branch of physical chemistry whose aim is to *predict* rather than *understand* the behaviour of a chemical system.

To get a better understanding of the *mechanism* of synaptic delay learning, a different, *analytical*, simplification of the complex mGluR signalling model was developed which will be discussed in detail in the following chapter.

Chapter 8

Isolating the Mechanism of Synaptic Delay Adaptation

8.1 Introduction

In the previous three chapters of the thesis, two mathematical models of intracellular signalling in cerebellar Purkinje cells were presented. The two models were developed to address different questions and, as a consequence, differ considerably in their complexity.

The *Adaptive Timing Model*, described in chapters 5 and 6, is a complex biophysically realistic model of the signalling cascade that links mGluR stimulation, intracellular Ca^{2+} release and activation of Ca^{2+} dependent K^+ channels in a Purkinje cell. In the basic one-compartmental version of the Adaptive Timing Model, 13 different components of the mGluR signalling network, including active mGluRs, G-protein $G_{PLC\alpha}$, IP_3, Ca^{2+} and the membrane potential, are represented by variables, and their interactions are modelled by 13 ordinary differential equations (ODEs).

As described in chapter 5, the one-compartmental Adaptive Timing Model attempts to answer a straightforward *yes-or-no* question: *can the mGluR signalling network in a single cerebellar Purkinje cell provide the basis for the adaptive timing of the classically conditioned eye-blink response?* The model is not only a biophysically realistic model, it is also a *theory demonstration model* (see e.g. Bower, 1994), which means it was developed to demonstrate that the answer to this question is *yes*. Numerical simulations of the model show that this is indeed the case. Thus, a result of the Adaptive Timing Model is that the mGluR signalling network in a Purkinje cell *can* implement the adaptive timing of the classically conditioned eye-blink response, *given* that all of the parameters are chosen appropriately *and* that all of the biochemistry and connectivity assumptions in chapters 4 and 5 are correct.

In the Adaptive Timing Model, the Purkinje cell learns the timing of the eye-blink response by adjusting the time delay between activation of the mGluRs by glutamate and release of Ca^{2+} from intracellular stores. The adjustment of a postsynaptic *time delay* as opposed to a postsynaptic *conductance* represents a novel *non-Hebbian* form of learning, and eye-blink conditioning is just one of the potential computational applications. More generally, the adaptation of synaptic delays can enable a cell to learn a specific response to a particular subset of temporal input patterns. Synaptic delay adaptation as an unsupervised learning mechanism for temporal pattern recognition was the subject of the previous two chapters.

In chapter 6, the recognition of temporal patterns by a *single* Purkinje cell was studied with a multi-compartmental version of the Adaptive Timing Model, and in chapter 7, the clustering of temporal patterns by a *group* of Purkinje cells was investigated using a *leaky integrator* version of the model. In the *leaky integrator* model, a Purkinje cell is represented by three equations: a single ODE for the change of the somatic membrane potential, an alpha function for the delayed outward current through Ca^{2+} dependent K^+ (K_{Ca}) channels, and a delta rule for the adjustment of the postsynaptic delays. Like the Adaptive Timing Model, the leaky integrator is a theory demonstration model, and numerical simulations of the model demonstrate that different Purkinje cells in

a group can discover different clusters in a temporal parallel fibre input space. To summarise, the four main results of chapters 5 - 7 are:

1. The mGluR signalling network in a cerebellar Purkinje cell can implement an adaptive postsynaptic delay.
2. Based on the synaptic delay adjustment, a single Purkinje cell can learn the adaptive timing of the classically conditioned eye-blink response.
3. A Purkinje cell can use the synaptic delay adaptation to learn an RBF-like response to temporal parallel fibre input patterns.
4. Different Purkinje cells can learn to recognise different subsets of temporal parallel fibre input patterns and partition the parallel fibre input space.

Thus, so far it has been shown that synaptic delay learning is possible, and several computational applications have been described. Basis of the synaptic delay learning are interactions between components of the mGluR signalling network. However, the exact nature of the mGluR signalling interactions that implement the delay adaptation still needs to be characterised. To characterise the exact mechanism of the delay learning, two different questions have to be answered:

1. Which process is responsible for the *adaptation* of the postsynaptic delays?
2. What is the mechanism that implements a *delayed* rather than an *immediate* response?

The first of these two questions has already been answered in chapter 5. The *adaptation* of the synaptic time delay represents the difference between the *Adaptive* Timing Model and the *Spectral* Timing Model (Fiala et al., 1996, see chapter 4). In the Adaptive Timing Model, but not in the Spectral Timing Model, the concentration of available

mGluRs is adjusted by protein kinase C (PKC) and protein kinase G (PKG) phosphorylation after parallel and climbing fibre input. Given that the synaptic delay between mGluR stimulation and intracellular Ca^{2+} release, K_{Ca} channel activation and voltage response varies with the concentration of available receptors, the phosphorylation of the mGluRs by PKC and PKG is what makes the synaptic delay *adaptive*.

An answer to the second question still needs to be found. In the Adaptive Timing Model, the synaptic delay is not only a function of the concentration of available mGluRs, it also depends on many other parameters, including the concentrations of available G-proteins and IP_3 receptors and most of the biochemical rate constants. A possible explanation for the delayed response could be that the delay is simply caused by the sum of the time delays that are introduced by the successive signalling steps between mGluR stimulation and intracellular Ca^{2+} release. A similar kind of additive mechanism has been used by Goldbeter (1995) to generate a time delay between mRNA production and negative feedback in a model of circadian oscillations in the *Drosophila* PER protein.

Alternatively, the delayed response could be based on a set of specific interactions between a few components of the mGluR signalling cascade. The Adaptive Timing Model is too complex to be able to exclude either of these two alternatives (for a diagram of the complex interactions between the components of the Adaptive Timing Model, see figure 8.1). A possible strategy for identifying the components and interactions which form the basis of the time delay is to simplify the original model by successively removing the components and interactions which are not essential. The model that is left at the end of the simplification process is the *minimal model* that generates a delay between mGluR stimulation and intracellular Ca^{2+} release.

The following sections of the chapter describe the systematic simplification of the mGluR signalling model. In the next section, the behaviour of the thirteen components of the Adaptive Timing Model will be analysed and, depending on their behaviour, the components will be categorised into different groups. In the remaining sections, a simplification of the model down to five ODEs will be presented, followed by the 2-ODE minimal model.

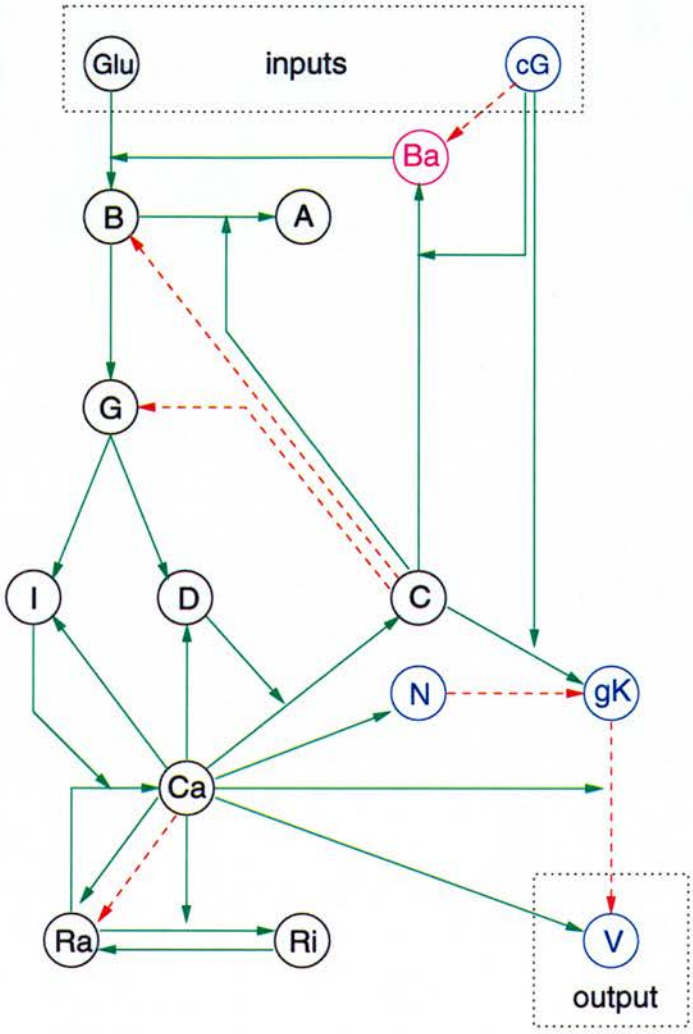

Figure 8.1: A simplified diagram of the interactions between the components of the Adaptive Timing Model. A green arrow between two components indicates that an increase in the value of the first component results in an *increase* in the value of the second component, a dashed red arrow symbolises that the first component *decreases* the value of the second component, and a green arrow that points to another arrow represents a *multiplicative* effect. In addition to affecting the values of other components, all components apart from glutamate (Glu) and cGMP (cG) exhibit a negative *decay* effect on their own values (not shown). Components that are only involved in learning, but not in the generation of the time delay, are indicated in blue, and the concentration of available mGluRs (B_a) which is only involved in the *adaptation* of the time delay is indicated in magenta. The individual components are: Glu glutamate, cG cGMP, B active mGluRs, A inactive mGluRs, G G-protein $G_{PLC\alpha}$, I IP_3, D DAG, C protein kinase C, Ca calcium, R_a Ca activated IP_3 receptors, R_i Ca inactivated IP_3 receptors, N calcineurin, g_K maximum K_{Ca} channel conductance, V voltage and B_a available mGluRs.

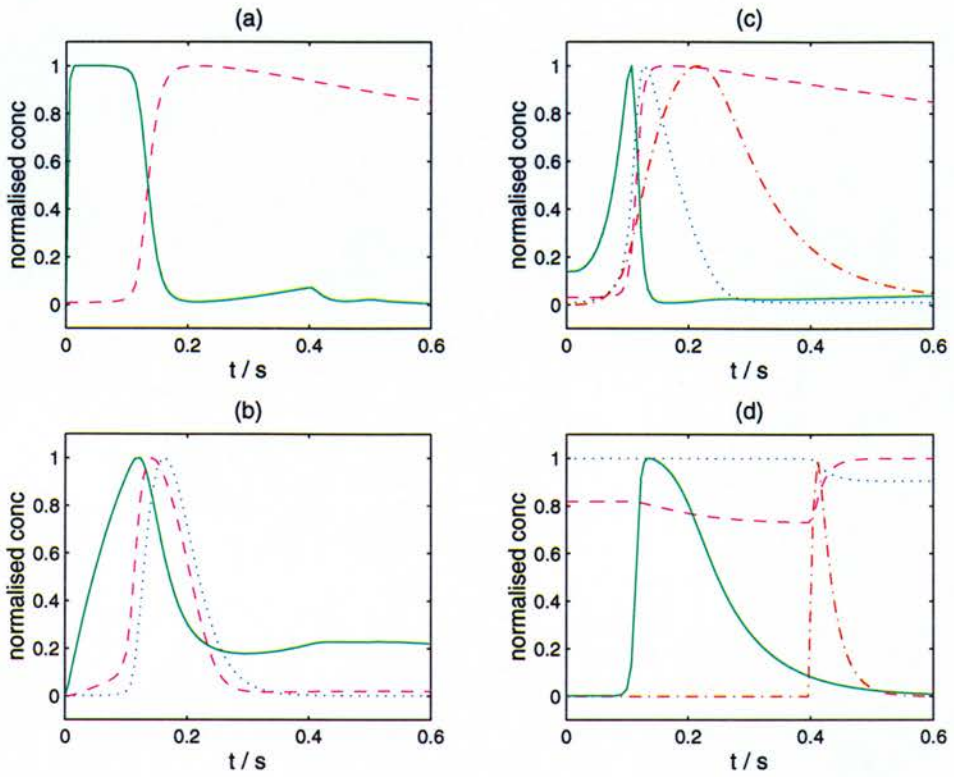

Figure 8.2: Behaviour of the Adaptive Timing Model in response to the 5th paired presentation of a $10\mu M$ glutamate pulse from $t = 0$ to $t = 0.5s$ and a cGMP peak at $t = 0.4s$. For easier comparison, all concentrations and the voltage are normalised by plotting $X/max(X)$ for a concentration X and $(V - min(V))/(max(V) - min(V))$ for the voltage V. (a) active mGluRs (B, solid green) and PKC-inactivated mGluRs (A, dashed magenta). (b) $G_{PLC\alpha}$ (G, solid green), IP_3 (I, dashed magenta) and PKC (C, dotted blue). (c) active IP_3 receptors (R_a, solid green), inactive IP_3 receptors (R_i, dashed magenta), Ca^{2+} (dotted blue) and the membrane voltage (V, dashdot red). (d) calcineurin (N, solid green), $\overline{g}_{KCa}$ (dashed magenta), available mGluRs (B_a, dotted blue) and cGMP (dashdot red). The extreme values of the different variables are: $max(B) = 64.044\mu M$, $max(A) = 65.624\mu M$, $max(G) = 0.478\mu M$, $max(I) = 0.259\mu M$, $max(C) = 0.972\mu M$, $max(R_a) = 0.521\mu M$, $max(R_i) = 0.995\mu M$, $max([Ca^{2+}]) = 6.765\mu M$, $max(V) = -45.46mV$, $min(V) = -50.03mV$, $max(N) = 1.918\mu M$, $max(\overline{g}_{KCa}) = 0.076S$, $max(B_a) = 66.498\mu M$, $max([cGMP]) = 2.646\mu M$.

8.2 Thirteen Equations: Different Categories of Components

The network of interactions between the components of the Adaptive Timing Model is shown in figure 8.1. In spite of the complexity of the network, there are several ways of introducing a structure by categorising the components into different groups. Characterising the structure of the model is a first step towards simplifying it.

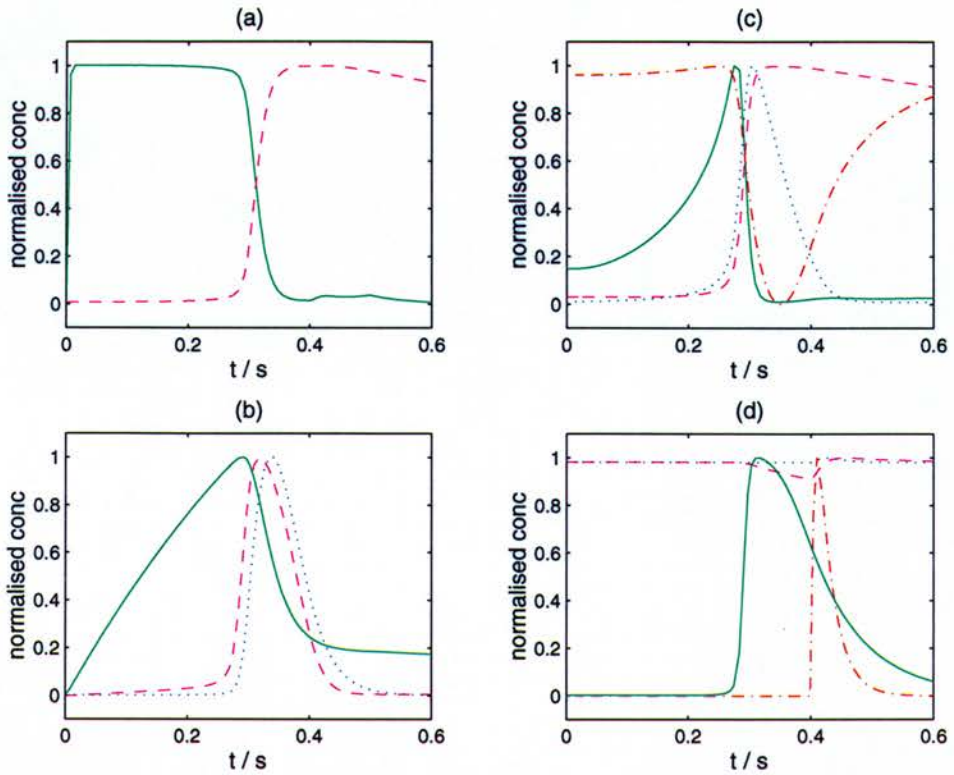

Figure 8.3: Behaviour of the Adaptive Timing Model in response to the 70th paired presentation of a $10\mu M$ glutamate pulse from $t = 0$ to $t = 0.5s$ and a cGMP peak at $t = 0.4s$. For easier comparison, all concentrations and the voltage are normalised by plotting $C/max(C)$ for a concentration C and $(V - min(V))/(max(V) - min(V))$ for the voltage V. (a) active mGluRs (B, solid green) and PKC-inactivated mGluRs (A, dashed magenta). (b) $G_{PLC\alpha}$ (G, solid green), IP_3 (I, dashed magenta) and PKC (C, dotted blue). (c) active IP_3 receptors (R_a, solid green), inactive IP_3 receptors (R_i, dashed magenta), Ca^{2+} (dotted blue) and the membrane voltage (V, dashdot red). (d) calcineurin (N, solid green), $\overline{g}_{KCa}$ (dashed magenta), available mGluRs (B_a, dotted blue) and cGMP (dashdot red). The extreme values of the different variables are: $max(B) = 7.451\mu M$, $max(A) = 7.621\mu M$, $max(G) = 0.163\mu M$, $max(I) = 0.243\mu M$, $max(C) = 0.878\mu M$, $max(R_a) = 0.491\mu M$, $max(R_i) = 0.994\mu M$, $max([Ca^{2+}]) = 6.355\mu M$, $max(V) = -49.46mV$, $min(V) = -64.48mV$, $max(N) = 1.897\mu M$, $max(\overline{g}_{KCa}) = 20.691S$, $max(B_a) = 7.894\mu M$, $max([cGMP]) = 2.646\mu M$.

It has been observed before that similarities exist between networks of intracellular signalling molecules and artificial neural networks (Bray, 1990, 1995; Arkin & Ross, 1994). Similar to the computational elements of artificial neural networks, the components of an intracellular signalling network can be divided into *input*, *output* and *hidden* units. In the Adaptive Timing Model, the *inputs* are the glutamate (Glu) that is released by the parallel fibres, and the cGMP (cG) which is produced in response to a climbing fibre pulse. As indicated in figure 8.1, the most obvious *output* of the

system is the membrane voltage V, but this is really only a question of definition and all of the other components could also be regarded as outputs. More importantly, the *inputs* are the only components whose time course is modelled explicitely by dynamically clamping them to time-dependent values, and the temporal evolution of all other components is described by 13 ODEs (equations 4.1 - 4.20 and 5.2).

Another criterion that can be used to classify the components is their qualitative temporal behaviour in response to parallel fibre input. Figures 8.2 and 8.3 summarise the response of all components of the Adaptive Timing Model during the 5th and during the 70th learning cycle with a parallel fibre evoked glutamate pulse and a climbing fibre induced cGMP peak. As shown in figure 8.2, the 5th presentation of glutamate pulse plus cGMP signal triggers an early cytoplasmic Ca^{2+} peak and an early *depolarisation* reponse at $t \approx 0.2s$. After 70 trials, the decrease in the concentration of available mGluRs has resulted in a shift of the Ca^{2+} and voltage peaks towards the cGMP signal at $t \approx 0.4s$, and the K_{Ca} channel phosphorylation has transformed the *depolarisation* into a *hyperpolarisation* response (figure 8.3). Although the time delay between the onset of the glutamate pulse and the Ca^{2+} and voltage response has almost doubled, and the relative voltage response has undergone a sign inversion, the *qualitative temporal behaviour* of all components has remained the same, and the components can be divided into five different categories (compare figures 8.2 and 8.3):

1. Components that rise very quickly up to a plateau, stay constant for a while and decrease rapidly back to the baseline: active mGluRs and glutamate.

2. Components that increase slowly and, after reaching a peak, decrease quickly: G-protein $G_{PLC\alpha}$ and Ca^{2+}-activated IP_3 receptors.

3. Components that, *after a time delay*, rise quickly, reach a peak and decay quickly: Ca^{2+}, IP_3, DAG, PKC, the membrane voltage[1], and calcineurin.

4. Components that, *after a time delay*, rise very quickly, reach a plateau and decay very slowly: PKC-inactivated mGluRs and Ca^{2+}-inactivated IP_3 receptors.

[1] After training, the voltage response is a negative rather than a positive peak.

5. *Memory* components that, during each learning cycle, change by a small amount and keep their new values: the maximum K_{Ca} channel conductance and the concentration of available mGluRs.

Finally, it is possible to divide the components according to their position in the mGluR signalling network. The earliest of the *delayed* components in categories three and four is Ca^{2+}. As a consequence, only components which are *upstream* from Ca^{2+} can be involved in the generation of the delayed response. Components without any direct or indirect influence on Ca^{2+} are unable to contribute to the time delay. Furthermore, both the Spectral Timing Model and the Adaptive Timing Model after training show delayed responses in the presence of a constant concentration of available mGluRs B_a. Thus, in addition to the glutamate input, only nine components remain whose dynamics can be responsible for the production of the synaptic delay (indicated in black in figure 8.1):

1. Active mGluRs (B).
2. PKC-inactivated mGluRs (A).
3. G-protein $G_{PLC\alpha}$ (G).
4. IP3 (I).
5. DAG (D).
6. Calcium (Ca).
7. Ca^{2+}-activated IP_3 receptors (R_a).
8. Ca^{2+}-inactivated IP_3 receptors (R_i).
9. PKC (C).

In the next section, the knowledge about the different categories of components will be used to develop a simpler version of the model with five ODEs.

8.3 Five Equations: The Thresholding Effect

In the previous section, the behaviour of all components of the Adaptive Timing Model was analysed, and the components were divided into different categories. Based on connectivity and categorisation of the components, the following simplifications can be introduced:

- Ca^{2+} and PKC are both *category three* components (see section 8.2) with a very similar time course, and Ca^{2+} directly precedes PKC in the intracellular signalling network (figure 8.1). Thus, PKC can be omitted from the model and, in the simplified equations, the effects of PKC can be represented as Ca^{2+} effects.
- Similarly, IP_3 and DAG are both *category three* components and, because of the choice of parameters in the Adaptive Timing Model, they follow an identical time course. As a consequence, only IP_3 needs to be represented in the simpler version of the model.
- Both glutamate input and glutamate-activated mGluRs are *category one* components. As shown in figures 8.2 and 8.3, the mGluR plateau results in a slow increase of the *category two* component $G_{PLC\alpha}$. As the temporal evolution of active mGluRs in the cell is not known, a possible simplification of the model is to leave out $G_{PLC\alpha}$, reduce the rate constant for mGluR activation so that the active mGluRs turn from a *category one* component into a slowly increasing *category two* component, and replace all $G_{PLC\alpha}$-effects by mGluR effects.
- Finally, numerical simulations show that it is possible to generate a time delay without representing the PKC-inactivated mGluRs as a variable in the model.

In the previous section, it was argued that only the components which are *upstream* from Ca^{2+} in the intracellular signalling network can be involved in the generation of the delayed response. Thus, cGMP, calcineurin, the maximum K_{Ca} channel conductance and the membrane voltage can all be omitted from the model. In the simplified model, five ODEs describe the temporal evolution of the following five variables:

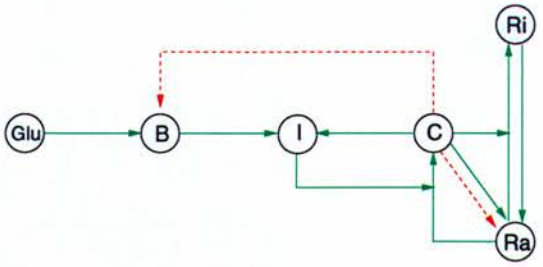

Figure 8.4: Interactions between the components of the 5-ODE model. A green arrow between two components indicates that an increase in the value of the first component results in an *increase* in the value of the second component, a dashed red arrow symbolises that the first component *decreases* the value of the second component, and a green arrow that points to another arrow represents a *multiplicative* effect. The components are: Glu glutamate, B active mGluRs, I IP_3, C calcium, R_a calcium-activated IP_3 receptors and R_i calcium-inactivated IP_3 receptors.

---

1. Active mGluRs (B).
2. IP_3 (I).
3. Ca^{2+}-activated IP_3 receptors (R_a).
4. Ca^{2+}-inactivated IP_3 receptors (R_i).
5. Calcium (C).

Similar to the 13-ODE Adaptive Timing Model, in the 5-ODE model the change of the concentration of active mGluRs is given by:

$$\frac{dB}{dt} = k_1 \, (B_a - B) \, [Glu] - k_{-1} \, B - k_2 \, B \, C \tag{8.1}$$

where $[Glu]$ and B_a are the concentrations of glutamate and available mGluRs. Different from the original model, C is the cytoplasmic concentration of Ca^{2+}, and the third term in equation 8.1 represents the inactivation of the receptors by Ca^{2+} dependent PKC phosphorylation.

The activation of the mGluRs leads to an increase in the concentration of IP_3 which is modelled by:

$$\frac{dI}{dt} = (I_{max} - I)\,(k_7\,B + k_8\,\frac{C^2}{C^2 + K_C}) - k_9\,I \tag{8.2}$$

As in the Adaptive Timing Model, the term $k_8\,C^2/(C^2 + K_C)$ describes the IP_3 production by a Ca^{2+} dependent form of phospholipase C.

IP_3 binds to IP_3 receptor Ca^{2+} channels on the membrane of the endoplasmic reticulum. Condition for the opening of the IP_3 receptors is the binding of IP_3 *and* the binding of Ca^{2+} to an activation site. In the model, the change in the concentration of Ca^{2+}-activated IP_3 receptors R_a is given by:

$$\frac{dR_a}{dt} = k_{12}\,(R_{max} - R_a - R_i)\,C - k_{13}\,R_a - k_{14}\,R_a\,C^n + k_{15}\,R_i \tag{8.3}$$

Activated IP_3 receptors can be inactivated by the binding of Ca^{2+} to an inhibitory site. The Ca^{2+} inactivation of the receptors exhibits a cooperativity of $n = 1.65$, and the change of inactivated receptors R_i is described by:

$$\frac{dR_i}{dt} = k_{14}\,R_a\,C^n - k_{15}\,R_i \tag{8.4}$$

As mentioned in section 4.3.1, the binding of IP_3 is assumed to be in equilibrium with respect to the binding and dissociation of Ca^{2+}, and the concentration of open IP_3 receptor channels R_o is given by:

$$R_o = \frac{I}{I + K_I}\,R_a \tag{8.5}$$

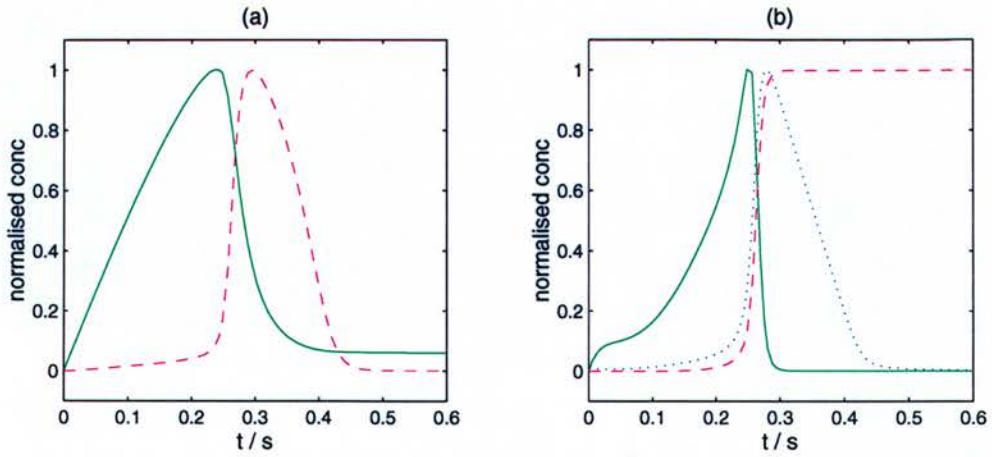

Figure 8.5: Behaviour of the 5 ODE model in response to a $10\mu M$ glutamate pulse from $t = 0$ to $t = 0.25s$. A constant concentration of available mGluRs $B_a = 20\mu M$ implements a time delay of $\Delta t \approx 0.3s$. (a) active mGluRs (B, solid green) and IP_3 (I, dashed magenta). (b) active IP_3 receptors (R_a, solid green), inactive IP_3 receptors (R_i, dashed magenta) and Ca^{2+} (C, dotted blue). For easier comparison, all concentrations X are normalised by plotting $X/max(X)$. The maximum values of the variables are: $max(B) = 3.657\mu M$, $max(I) = 0.255\mu M, max(R_a) = 0.507\mu M, max(R_i) = 1.00\mu M, max(C) = 6.931\mu M$.

The release of Ca^{2+} through the open IP_3 receptor channels R_o leads to an increase in the cytoplasmic Ca^{2+} concentration C:

$$\frac{dC}{dt} = k_{16}\, R_o\, (C_{ER} - C) - k_{17}\, \frac{C^2}{C^2 + K_{ATPase}} \tag{8.6}$$

where C_{ER} is the Ca^{2+} concentration in the endoplasmic reticulum. The second term in equation 8.6 describes the removal of Ca^{2+} by the endoplasmic Ca^{2+} ATPase. As opposed to the 13 ODE model, the 5 ODE model is not concerned with the electrogenic effects of the Ca^{2+} currents, and the Na^+/Ca^{2+} exchanger flux is not modelled.

As the original Adaptive Timing Model, the 5 ODE model was implemented in C++ and numerically integrated, using a 5th order Runge-Kutta algorithm with adaptive step size control and the parameters that are listed in appendix A.4. Simulation results for the application of a $250ms$ glutamate pulse to a model with a constant concentration of available mGluRs $B_a = 20\mu M$ are shown in figure 8.5. The glutamate pulse

results in a slow increase in the concentration of active mGluRs which in turn leads to a *very slow* increase in the concentrations of IP_3 and Ca^{2+}. After a time delay of approximately 0.25 seconds, the IP_3 and Ca^{2+} concentrations begin to rise very quickly, and the model "fires" an IP_3 peak and a Ca^{2+} peak, both of which reach their maxima at $t \approx 0.3s$. Consequence of the Ca^{2+} rise is a fast decrease in the concentrations of active mGluRs and IP_3 receptors.

To understand the mechanism of the delayed response, it is crucial to understand the transition between the *slow* rise of IP_3 and Ca^{2+} during the first several hundred milliseconds of glutamate application, and the *fast* rise during the upstrokes of the peaks. A possible reason for this transition could be that the concentrations of IP_3 or Ca^{2+} reach a threshold where one or several *regenerative processes* lead to a large increase in the IP_3 production and the Ca^{2+} release rates. In general, such a regenerative process could be a *direct autocatalytic* effect of a single component on its own formation, or an *indirect autocatalytic* or *cross catalytic* effect between two components, meaning that the first component has a positive influence on the formation of the second component *and vice versa* (see figure 8.6).

Figure 8.6: *Direct* autocatalysis (left) versus *indirect* autocatalysis or *cross* catalysis (right). Green arrows represent positive connections, possibly via other components.

Two examples for *indirect autocatalysis* can be found in the model (compare figure 8.4):

1. Ca^{2+} has a positive effect on the formation of IP_3,
   and IP_3 stimulates release of Ca^{2+} into the cytoplasm.

2. Ca^{2+} binds to and activates IP_3 receptors which leads to
   release of Ca^{2+} into the cytoplasm.

Although the existence of autocatalysis might be able to explain the *upstrokes* of the peaks, another mechanism is needed to generate the *downstrokes* which reset the IP_3 and Ca^{2+} concentrations back to their baseline values. A possible reset mechanism could be the Ca^{2+} dependent negative feedback through PKC phosphorylation of the active mGluRs (see equation 8.1 and figure 8.4). To investigate if the combination of autocatalysis and negative feedback is sufficient for the generation of the delayed response, the 5 ODE model was further simplified down to a minimal model with 2 ODEs. The 2 ODE model will be presented in the next section of the chapter.

8.4 Two Equations: The Minimal Model

In the minimal model of the delayed intracellular Ca^{2+} response, the dynamics of the glutamate-activated mGluRs B and the cytoplasmic calcium C are described by two equations:

$$\frac{dB}{dt} = k_1 (B_a - B) [Glu] - k_2 B - k_3 B f_1(C) \tag{8.7}$$

$$\frac{dC}{dt} = k_4 B f_2(C) - k_5 f_3(C) \tag{8.8}$$

where B_a is the total concentration of available mGluRs. The five terms in equations 8.7 and 8.8 represent the following five processes:

1. The activation of inactive mGluRs $(B_a - B)$ by glutamate.
2. The inactivation of active mGluRs by dissociation of glutamate.
3. The inactivation of active mGluRs by Ca^{2+} dependent PKC phosphorylation.
4. The mGluR and Ca^{2+} dependent release of Ca^{2+} into the cytoplasm.
5. The removal of Ca^{2+} from the cytoplasm.

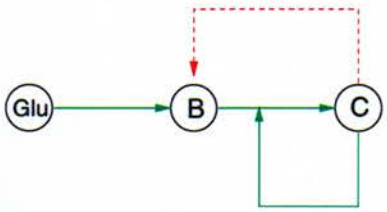

Figure 8.7: Interactions between the glutamate-activated mGluRs (B) and the cytoplasmic calcium (C) in the minimal model of the delayed response. Green arrows represent positive, dashed red arrows negative and arrows which point to other arrows multiplicative effects.

In the previous section, it was suggested that the time delay between receptor stimulation and Ca^{2+} response might be based on the combined action of negative feedback and autocatalysis. The following scenario could be responsible for the delayed Ca^{2+} peak:

1. Initially, the glutamate pulse leads to a slow increase in the concentration of active receptors B and a very slow increase in the Ca^{2+} concentration C. As long as C is smaller than a threshold concentration Θ_a, neither autocatalysis nor negative feedback have a significant effect, and the rate of Ca^{2+} uptake back into the stores is very low.

2. When C reaches Θ_a, the autocatalysis is switched on which leads to a large increase in the Ca^{2+} *release* rate and the onset of the Ca^{2+} peak.

3. On the way to the top of the peak, C passes a second threshold concentration Θ_b which results in a large increase in the Ca^{2+} *uptake* rate.

4. After reaching a third threshold Θ_c, the negative feedback is activated and the concentration of active receptors B is beginning to fall.

5. Consequence of the decrease in B is a decrease in the Ca^{2+} release rate until Ca^{2+} release and uptake compensate each other and the maximum of the peak is reached.

6. The continued decrease in the Ca^{2+} release rate leads to the downstroke of the peak and the return of the Ca^{2+} concentration to the baseline.

A similar kind of regenerative mechanism is reponsible for the generation of action potentials in neurons with fast sodium (NaF) and delayed rectifier potassium (Kdr) channels. The classical formalism that can be used to describe a neuron with NaF and Kdr channels is the Hodgkin-Huxley model (Hodgkin & Huxley, 1952). In the Hodgkin-Huxley model, both the firing threshold for an action potential and the recovery of the voltage back to the resting potential are based on the sigmoidal voltage dependence of the steady-state activation and inactivation parameters. Similarly, in the simplified model of the mGluR response, the Ca^{2+} peak can be generated by assuming that the three functions $f_i(C)$ which describe the negative feedback, the autocatalysis and the Ca^{2+} removal in equations 8.7 and 8.8 exhibit a sigmoidal dependence on the Ca^{2+} concentration C. The sigmoidal Ca^{2+} dependence can be described with a modified version of the *logistic* or *Glauber* function (Hertz et al., 1991; Glauber, 1963) that is commonly used in artificial neural networks:

$$f_i(C) = \frac{1}{1 + exp(-\beta_i (C - \theta_i))} \tag{8.9}$$

where the three constants β_i determine the steepness of the curves, and the three constants θ_i correspond to the three threshold concentrations Θ_a, Θ_b and Θ_c for Ca^{2+} dependent negative feedback, autocatalysis and removal that were postulated above.

Alternatively, the Ca^{2+} effects can be represented by three Hill functions:

$$f_i(C) = \frac{C^n}{C^n + K_i^n} \tag{8.10}$$

If the *cooperativity* n is larger than one, a Hill function describes a sigmoid with a steepness which is given by n and a half-maximal value for $C = K_i$. Thus, in the model with three Hill functions, the three constants K_i correspond to the threshold concentrations Θ_a, Θ_b and Θ_c for the three Ca^{2+} dependent processes. Hill functions are widely used in biochemical kinetics, and in the following the 2 ODE model will be analysed and simulated for equation 8.10 rather than equation 8.9.

Compared to the 13 ODE and the 5 ODE model, the two-dimensional model can be much more easily analysed, and it is possible to display the temporal evolution of the complete system in the phase plane. A first step towards analysing the behaviour of the system is to determine the *nullclines* where the temporal derivative of one of the variables is zero, and the *fixed points* where the temporal derivatives of *both* variables are zero. In the 2 ODE model, the set of $\langle B, C \rangle$ loci that satisfy $\dot{B} = 0$ defines a single B-nullcline:

$$B = \frac{k_1 \, [Glu] \, B_a \, (C^n + K_1^n)}{k_1 \, [Glu] \, (C^n + K_1^n) + k_2 \, (C^n + K_1^n) + k_3 \, C^n} \tag{8.11}$$

The model has two C-nullclines that describe the $\langle B, C \rangle$ loci which are given by $\dot{C} = 0$. The first of the C-nullclines is the B-axis $C = 0$, and the second C-nullcline is described by:

$$B = \frac{k_5 \, (C^n + K_2^n)}{k_4 \, (C^n + K_3^n)} \tag{8.12}$$

The intersections of the B-nullcline with the two C-nullclines are the *fixed points* of the system. For all possible combinations of parameter values, the B-nullcline intersects the B-axis exactly once. At this intersection, the system has a fixed point $\langle \overline{B}_1, \overline{C}_1 \rangle$ with coordinates:

$$\overline{B}_1 = \frac{k_1 \, [Glu] \, B_a}{k_1 \, [Glu] + k_2} \tag{8.13}$$

and

$$\overline{C}_1 = 0 \tag{8.14}$$

Depending on the choice of parameters in the model, the B-nullcline can also intersect the *second* C-nullcline (equation 8.12) at a single location. Thus, the model can have a second fixed point $\langle \overline{B}_2, \overline{C}_2 \rangle$ whose coordinates are:

$$\overline{B}_2 = \frac{k_5 \left(2K_2^n \overline{S} - \overline{R} + \sqrt{\overline{R}^2 - 4\overline{S}\,\overline{T}} \right)}{k_4 \left(2K_3^n \overline{S} - \overline{R} + \sqrt{\overline{R}^2 - 4\overline{S}\,\overline{T}} \right)} \tag{8.15}$$

and

$$\overline{C}_2 = \left(\frac{-\overline{R} + \sqrt{\overline{R}^2 - 4\overline{S}\,\overline{T}}}{2\overline{S}} \right)^{1/n} \tag{8.16}$$

where $\overline{S}$, $\overline{T}$ and $\overline{R}$ are given by:

$$\begin{aligned} \overline{R} \;=\; & k_1 k_5 K_2^n [Glu] + k_1 k_5 K_1^n [Glu] + k_2 k_5 K_2^n + k_2 k_5 K_1^n \\ & + k_3 k_5 K_2^n - k_1 k_4 K_3^n - k_1 k_4 K_1^n [Glu] B_a \end{aligned} \tag{8.17}$$

$$\overline{S} = k_1 k_5 [Glu] + k_2 k_5 + k_3 k_5 - k_1 k_4 [Glu] B_a \tag{8.18}$$

$$\overline{T} = k_1 k_5 K_1^n K_2^n [Glu] + k_2 k_5 K_1^n K_2^n - k_1 k_4 K_1^n K_3^n [Glu] B_a \tag{8.19}$$

Using the *GRIND* integration package (De Boer, 1983), the behaviour of the model was investigated for different combinations of parameter values. It was found that only parameter sets which result in the intersection of the B-nullcline (equation 8.11) with the second C-nullcline (equation 8.12), and therefore the existence of the second fixed point $\langle \overline{B}_2, \overline{C}_2 \rangle$, are able to implement a time delay between the onset of the mGluR activation and the intracellular Ca^{2+} response. Furthermore, the delayed response could only be generated for Hill coefficients $n \geq 4$. Apparently, the three Hill functions $f_i(C)$ that represent the Ca^{2+} dependent processes have to be sufficiently steep to implement the thresholding behaviour which is responsible for the delayed Ca^{2+} peak.

Figure 8.8 summarises the behaviour of the model for a cooperativity $n = 4$ and the parameter values that are given in appendix A.5. As shown in figure 8.8 (a), the B-nullcline and the second C-nullcline divide the biologically meaningful area of the phase plane with concentrations of active mGluRs B and Ca^{2+} C which are larger than or equal to zero into four different regions:

1. A region between B-axis, B-nullcline and second C-nullcline where both temporal derivatives $\dot{B}$ and $\dot{C}$ are positive (represented by $(++)$ in the figure).
2. A region above the B-nullcline and the second C-nullcline where $\dot{B}$ is negative and $\dot{C}$ is positive $(-+)$.
3. A region between the B-nullcline and the second C-nullcline where both $\dot{B}$ and $\dot{C}$ are negative $(--)$.
4. A region below the B-nullcline and the second C-nullcline where $\dot{B}$ is positive and $\dot{C}$ is negative $(+-)$.

In figure 8.8 (a), the location of the two fixed points is indicated by (x) and (o). The fixed point $\langle \overline{B}_2, \overline{C}_2 \rangle$ at the intersection of the B-nullcline and the second C-nullcline (o) is *stable*, and the fixed point $\langle \overline{B}_1, \overline{C}_1 \rangle$ at the intersection of the B-nullcline with the

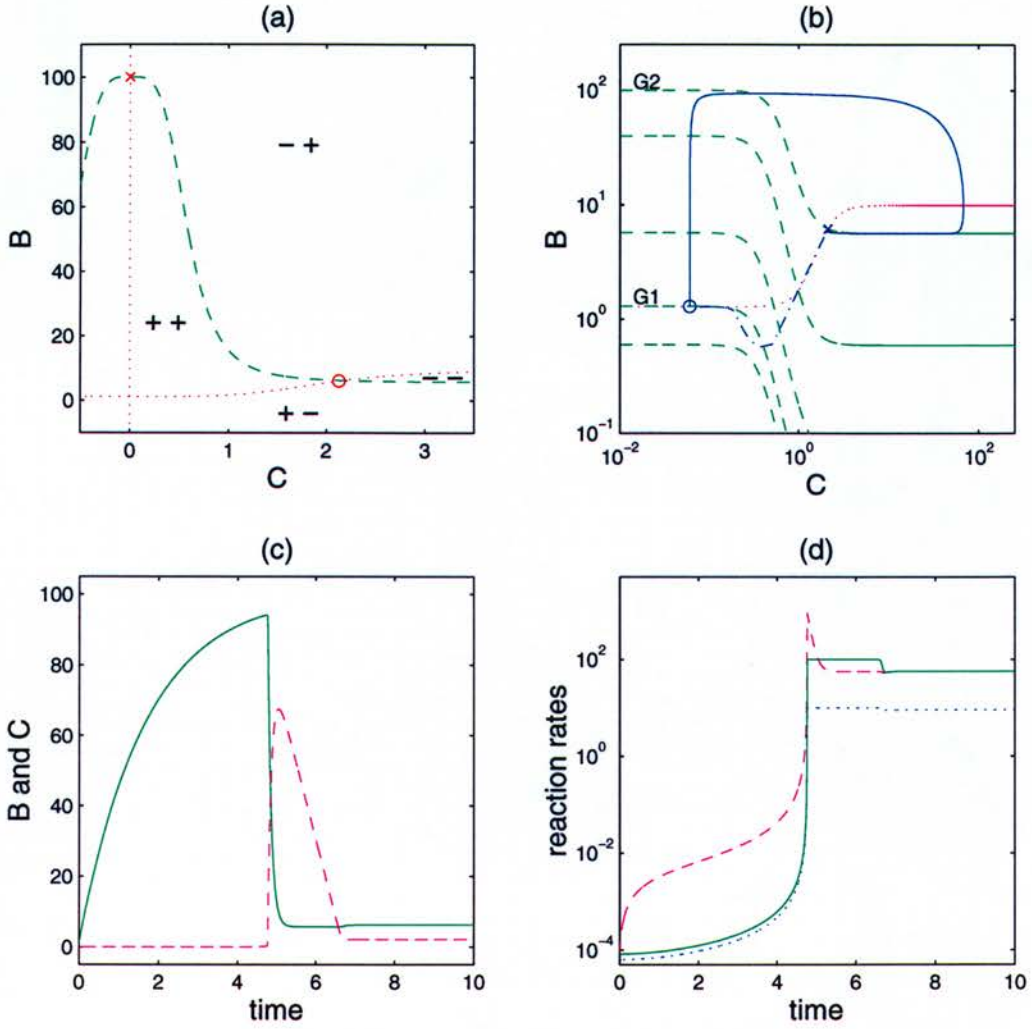

Figure 8.8: Generation of the delayed Ca^{2+} response in the minimal model with two ODEs which represent the temporal evolution of the concentrations of active mGluRs B and Ca^{2+} C. (a) B-nullcline (dashed green) and C-nullclines (dotted magenta) of the model for a glutamate concentration $G_2 = 10.0$ and the parameter values in appendix A.5. The system has a saddle point at the intersection of the B-nullcline with the B-axis (x), and a stable fixed point at the intersection of the B-nullcline with the second C-nullcline (o). The nullclines divide the phase plane into four regions with different orientations of the direction vector $\langle \dot{B}, \dot{C} \rangle$: $(++)$ indicates $\dot{B} > 0$ and $\dot{C} > 0$, $(-+)$ $\dot{B} < 0$ and $\dot{C} > 0$, $(--)$ $\dot{B} < 0$ and $\dot{C} < 0$ and $(+-)$ $\dot{B} > 0$ and $\dot{C} < 0$. (b) Response of the model to a transient increase of the glutamate concentration [Glu] from $G_1 = 0.02185$ to $G_2 = 10.0$. The B-nullclines for [Glu] = $\{0.01, 0.02185, 0.1, 1.0, 10.0\}$ are shown as dashed green lines. (o) and (x) mark the location of the stable fixed points $\mathbf{S}^0$ for $[Glu] = G_1$ and $\mathbf{S}^*$ for $[Glu] = G_2$, respectively. In response to the $G_1 \rightarrow G_2$ step, the state vector $\mathbf{S} = \langle B, C \rangle$ travels from $\mathbf{S}^0$ (o) to $\mathbf{S}^*$ (x) through the phase plane (solid blue line). When the glutamate concentration is stepped back to G_1, $\mathbf{S}$ travels back to $\mathbf{S}^0$ (dashdot blue line). (c) Temporal evolution of B (solid green) and C (dashed magenta) in response to the $G_1 \rightarrow G_2$ step at $t = 0$. (d) Temporal evolution of the rates of the three Ca^{2+} dependent processes: auotcatalytic release (dashed magenta), reuptake (green) and negative feedback (dotted blue).

B-axis (x) is a *saddle point*. Thus, if the initial Ca^{2+} concentration $C(0)$ is equal to zero, the system will travel along the B-axis and end up at $\langle \overline{B}_1, \overline{C}_1 \rangle$, and if $C(0)$ is different from zero, the system will move through the phase plane and come to rest at $\langle \overline{B}_2, \overline{C}_2 \rangle$.

The behaviour of the model in response to synaptic input is shown in figure 8.8 (b). Without any input to the cell, the glutamate concentration in the synaptic cleft is assumed to be at a very low level G_1, and the system rests in the stable state $\mathbf{S}^0 = \langle \overline{B}_2, \overline{C}_2 \rangle$ at the intersection of the B-nullcline and the second C-nullcline (represented by (o) in the figure). When the cell receives an input, the glutamate concentration is temporarily stepped up to a much higher value $G_2 \gg G_1$. As a result of the glutamate step, the B-nullcline (equation 8.11) is shifted in the phase plane, and the stable fixed point moves to a new location at $\mathbf{S}^* = \langle \overline{B}_2^*, \overline{C}_2^* \rangle$. Thus, the current state of the system $\mathbf{S}^0$ is no longer a fixed point, and the state vector $\mathbf{S} = \langle \overline{B}, \overline{C} \rangle$ travels through the phase plane until it settles into the new stable state at $\mathbf{S}^*$ (indicated by (x) in figure 8.8 (b)).

On its way from the old fixed point $\mathbf{S}^0$ to the new fixed point $\mathbf{S}^*$, the state vector $\mathbf{S}$ crosses all of the four regions of the phase plane that were outlined above. The temporal evolution of the system in response to the $G_1 \rightarrow G_2$ step can be divided into the following five phases:

1. A slow increase in B and a very slow increase in C while the state vector $\mathbf{S}$ crosses the $(++)$ region (see figure 8.8 (a)).
2. A fast decrease in B and a fast increase in C while crossing the $(-+)$ region.
3. A slow and very small decrease in B and a fast decrease in C on the way through the $(--)$ region.
4. A very small increase in B and a very small decrease in C while traversing the $(+-)$ region.
5. Finally, a very small increase in B and C while $\mathbf{S}$ crosses the $(++)$ region for a second time before the system settles into the new stable state $\mathbf{S}^*$.

Thus, although the high-glutamate fixed point $\mathbf{S}^*$ is very close to the low-glutamate fixed point $\mathbf{S}^0$, the state vector makes a large excursion through the phase plane (indicated by the solid blue line in figure 8.8 (b)), a phenomenon which is called *excitability* (Edelstein-Keshet, 1987). The long trajectory in the phase diagram corresponds to the large transient increase in the concentrations of active mGluRs and Ca^{2+} that is shown in figure 8.8 (c).

If the input to the cell is switched off, the glutamate concentration is reset to the rest value G_1, and the B-nullcline moves back to its original location. As a consequence, the stable fixed point shifts back to $\mathbf{S}^0$ and the current state $\mathbf{S} = \mathbf{S}^*$ is destabilised. Thus, the state vector $\mathbf{S}$ travels back to $\mathbf{S}^0$, this time without a large detour from the direct route through the phase plane (indicated by the dashdot blue line in figure 8.8 (b), note the double logarithmic scale).

To summarise, the 2 ODE model can implement the time delay between receptor activation and intracellular Ca^{2+} release. The basis of the delayed Ca^{2+} peak is the combination of Ca^{2+} dependent negative feedback, autocatalysis and reuptake, and all three processes have to exhibit a sigmoidal Ca^{2+} dependence.

8.5 Chapter Conclusions

So far, the thesis has addressed the following three questions about intracellular signalling in cerebellar Purkinje cells:

1. Can the intracellular signalling network in a cerebellar Purkinje cell implement an adaptive time delay between the stimulation of metabotropic glutamate receptors (mGluRs) and the release of Ca^{2+} from intracellular stores?
2. If an adaptive time delay between the mGluR stimulation and the Ca^{2+} response is possible, what are its potential functions?

3. What is the mechanism that generates the adaptive delay?

The first of the three question was addressed in chapter 5, the second question was studied extensively in chapters 5, 6 and 7, and the third question was the subject of the current chapter.

In chapter 5, the Adaptive Timing Model was presented. The Adaptive Timing Model is a complex biophysically realistic model of the mGluR signalling network in a Purkinje cell that uses 13 ordinary differential equations (ODEs) to represent the temporal evolution of 13 different signalling components. By numerically simulating the model, it was shown that the mGluR signalling network *can* implement an adaptive delay between mGluR activation and Ca^{2+} release, given that all of the modelling and parameter assumptions are correct.

In chapter 5, it was also demonstrated that a possible application of the time delay adjustment is the adaptive timing of the classically conditioned eye-blink response. In chapters 6 and 7, two other potential functions of the delay adaptation were described: a form of temporal radial basis function learning by a single Purkinje cell, and the clustering of temporal patterns by a group of Purkinje cells.

In the previous sections of the current chapter, the mechanism of the delay adaptation was investigated. To understand the mechanism of the delay adaptation, it was necessary to answer two different questions:

1. Why is the time delay *adaptive*?
2. Why is the response *delayed* rather than *immediate*?

The first of the two questions has already been answered in chapter 5: the delay *adaptation* is based on the adjustment of the concentration of available mGluRs by protein kinase C and protein kinase G phosphorylation.

To answer the second question and identify the basis for the *delayed* response, the Adaptive Timing Model was systematically simplified. The following step-by-step simplification procedure was used:

1. The behaviour of the 13 components of the Adaptive Timing Model was analysed, and the components were divided into five different categories: plateau components, slow components, delayed fast components, delayed inhibited components and memory components.
2. Depending on their categories, several pairs of components could be replaced by single components, and a 5 ODE simplification of the model was developed.
3. The behaviour of the 5 ODE model was analysed, and the combination of Ca^{2+} dependent negative feedback and autocatalysis was identified as a possible mechanism for the delayed reponse.
4. Based on this idea, a minimal model with 2 ODEs was developed. The behaviour of the 2 ODE model was analysed using phase plane techniques.

In the minimal model, two ODEs represent the dynamics of the active mGluRs and the cytoplasmic Ca^{2+}. A delayed intracellular Ca^{2+} response could be generated by the interaction of five different processes:

1. Activation of the mGluRs by glutamate.
2. Inactivation of the mGluRs by dissociation of glutamate.
3. Ca^{2+} dependent inactivation of the mGluRs.
4. mGluR and Ca^{2+} dependent (autocatalytic) Ca^{2+} release into the cytoplasm.
5. Ca^{2+} dependent removal of Ca^{2+} from the cytoplasm.

To create a delayed Ca^{2+} peak, the three Ca^{2+} activated processes have to exhibit a sigmoidal Ca^{2+} dependence. The sigmoidal Ca^{2+} dependence of the Ca^{2+} dependent processes in the Ca^{2+} response model is reminiscent of the sigmoidal voltage dependence of the steady state activation and inactivation variables in the Hodgkin-Huxley model that describes the generation of action potentials. Thus, a sigmoidal relation between a variable and its temporal derivative might be a general feature of a subset[2] of excitable systems.

The generation of an adaptive time delay between receptor stimulation and intracellular Ca^{2+} response is only one of the possible computational functions of the mGluR signalling network. This chapter concludes the main part of the thesis that is concerned with the adaptation of synaptic delays. In the next chapter, it will be shown how the mGluR signalling network can implement another kind of behaviour: damped Ca^{2+} oscillations.

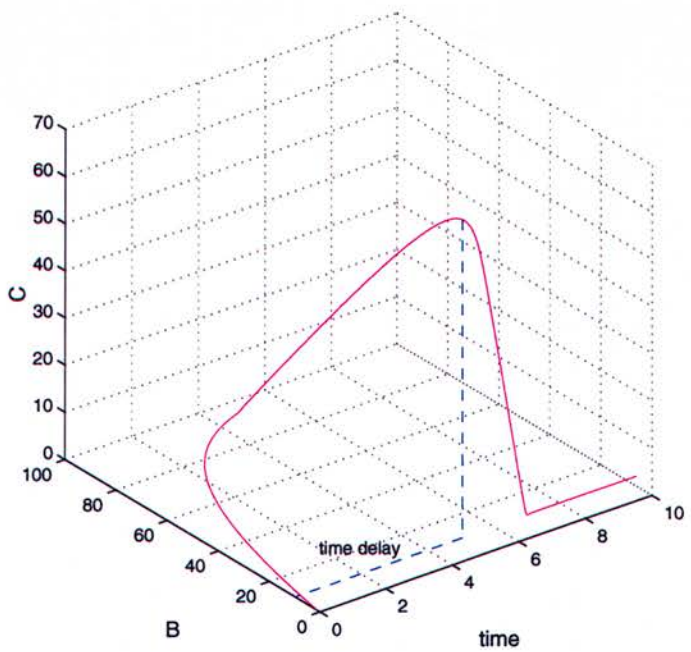

Figure 8.9: Behaviour of the minimal model in response to a glutamate step. B concentration of active mGluRs, C calcium concentration.

[2]Other excitable systems, like the FitzHugh-Nagumo model (FitzHugh, 1960), lack a sigmoidal $x - \dot{x}$ relation.

Chapter 9

Calcium Oscillations, Parameters and the Benefit of Multiple Models

9.1 Introduction

So far, the thesis has focussed on one particular computational function of the metabotropic glutamate receptor (mGluR) signalling network in a cerebellar Purkinje cell: the adaptation of the time delay between the stimulation of the mGluRs and the release of Ca^{2+} from intracellular stores.

It was shown how a *delayed* Ca^{2+} response can be generated by the combination of Ca^{2+} dependent negative feedback and autocatalysis, and it was demonstrated that an *adaptive* time delay can be implemented by two antagonistic phosphorylation reactions that adjust the concentration of available mGluRs. Three possible functions of the delay adjustment in Purkinje cells were suggested:

1. The adaptive timing of the classically conditioned eye-blink response by a single Purkinje cell.

2. A form of temporal radial basis function learning by a single Purkinje cell.

3. The clustering of temporal parallel fibre patterns by a group of Purkinje cells.

The adaptation of the time delay between receptor stimulation and Ca^{2+} response is not the only possible function of the mGluR signalling network in a Purkinje cell. In the following sections of this chapter, a different behaviour of the mGluR signalling cascade will be studied. It will be investigated if and when the interaction between mGluRs and Ca^{2+} can lead to *damped oscillations of the cytoplasmic Ca^{2+} concentration.*

Recently, Kawabata et al. (1996) have shown that the ability of the mGluR signalling network to generate damped Ca^{2+} oscillations depends on the subtype of mGluRs in the cell. In their experiments, cells were transfected with cDNA encoding the mGluR1α or the mGluR5a receptor subtype, and the temporal pattern of the cytoplasmic Ca^{2+} concentration in response to a glutamate pulse was determined. It was found that the glutamate pulse induced *damped Ca^{2+} oscillations* in mGluR5a transfected cells, but triggered a *single Ca^{2+} peak* in mGluR1α transfected cells (figure 9.1).

Using chimaeric receptors, Kawabata et al. managed to show that the Ca^{2+} response pattern is determined by the *i4 segment*, a sequence of 19 amino acids in the intracellular C-terminal tail of the receptor. In cells that were transfected with chimaeric receptors containing the *i4* segment of the mGluR5a subtype, the glutamate pulse resulted in an oscillatory Ca^{2+} response. In contrast, cells with chimaeric receptors which contained the mGluR1α instead of the mGluR5a *i4* segment responded with a single Ca^{2+} peak to glutamate stimulation.

The *i4* segments of the two receptor subtypes differ by only a single amino acid: instead of an aspartate in mGluR1α, mGluR5a contains a threonine. The presence of the threonine in mGluR5a generates of a protein kinase C (PKC) consensus sequence. As a consequence, PKC can phosphorylate the *i4* segment of mGluR5a, but *not* the *i4* segment of mGluR1α. Given that the *i4* segment is important for the interaction of the receptor with the G-protein complex, the following scenario might be responsible for the generation of the damped Ca^{2+} oscillations in mGluR5a transfected cells:

1. The increase in the glutamate concentration results in activation of mGluR5a.
2. The mGluR5a activation leads to activation of G-proteins and triggers a intracellular signalling cascade that results in the release of Ca^{2+} from the endoplasmic reticulum (ER) and an increase in the cytoplasmic Ca^{2+} concentration.
3. The increase in the Ca^{2+} concentration leads to the activation of PKC.
4. Active PKC phosphorylates the *i4* segment of mGluR5a.
5. As a result of the PKC phosphorylation, mGluR5a is transformed into an inactive form that is unable to activate G-proteins.
6. Thus, the rate of Ca^{2+} release from the ER is decreased, and the reuptake of Ca^{2+} back into the ER leads to a reduction in the cytoplasmic Ca^{2+} concentration.
7. The decrease of the Ca^{2+} concentration leads to a decrease in the concentration of active PKC.
8. As a consequence, the concentration of phosphorylated mGluR5a is reduced, and the concentration of dephosphorylated receptors which are able to activate G-proteins is increased.
9. This results in an increase of the cytoplasmic Ca^{2+} concentration, and the cycle starts again at stage 3.

That the oscillations are *damped*, and not sustained, might be due to a "leak" at some point of the cycle. A number of leaks could be possible, for example the reduction of the extracellular glutamate concentration through diffusion, the desensitisation of the mGluRs or the IP_3 receptors or the decrease of the endoplasmic Ca^{2+} concentration.

In the following sections of the chapter, the plausibility of the scenario will be studied using two different computational models of the mGluR signalling network. The following three questions will be addressed:

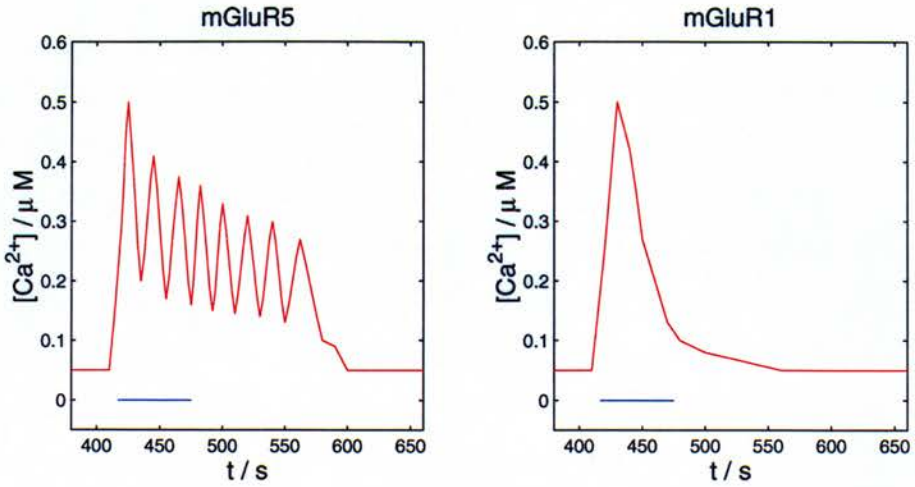

Figure 9.1: The results of Kawabata et al.'s experiments. The glutamate pulse (blue bar) leads to damped Ca^{2+} oscillations in mGluR5a tranfected cells (left), and to a single Ca^{2+} peak in mGluR1α transfected cells (right) (from Kawabata et al., 1996).

---

1. Can a model of the mGluR signalling network that contains a PKC mediated negative feedback connection between the Ca^{2+} concentration and the concentration of active mGluRs implement the damped oscillatory Ca^{2+} response to a glutamate pulse?

2. Is the Ca^{2+} dependent negative feedback necessary for the generation of the damped Ca^{2+} oscillations?

3. What other factors apart from the Ca^{2+} dependent negative feedback contribute to the oscillatory Ca^{2+} response?

The first question will be addressed with a *complex model* that uses 8 ordinary differential equations (ODEs) to represent the mGluR signalling network. To answer the second and third question, a *minimal model* of the mGluR evoked Ca^{2+} release will be analysed.

9.2 The Complex Model

9.2.1 The Eight Equations

Like all of the other mGluR signalling models that were discussed in the thesis, the complex Ca^{2+} oscillation model is a descendant of the 13 ODE Adaptive Timing Model. Out of all models in the thesis, it is the least simplified descendant, and six of the eight ODEs in the model are identical to the corresponding equations in the Adaptive Timing Model. The eight ODEs in the Ca^{2+} oscillation model describe the temporal evolution of the following eight variables:

1. Active mGluRs (B).
2. PKC-inactivated mGluRs (A).
3. IP_3 (I).
4. DAG (D).
5. Ca^{2+}-activated IP_3 receptors (R_a).
6. Ca^{2+}-inactivated IP_3 receptors (R_i).
7. Calcium ($[Ca^{2+}]$).
8. PKC (C).

As opposed to the Adaptive Timing Model, the complex Ca^{2+} oscillation model contains no explicit representation of active G-proteins $G_{PLC\alpha}$. The reason for the difference between the two models is the difference between the time scales of the two phenomena that are modelled. The Adaptive Timing Model generates a delayed Ca^{2+} peak with a width of approximately $100ms$. Thus, it has to be accurate in the *millisecond* range. The Ca^{2+} oscillation model investigates a much slower phenomenon. The period of the Ca^{2+} oscillations in Kawabata et al.'s experiments is in the order of ten *seconds*.

Compared to the Ca^{2+} oscillations, all of the reactions that involve G-proteins are fast. The concentrations of receptor-activated G-proteins and G-protein-activated phospholipase C (PLC*) reach their steady-state levels less than a second after the onset of the receptor stimulation (Wang et al., 1995; Vuong et al., 1984). Thus, in the Ca^{2+} oscillation model the concentrations of activated G-proteins $G_{PLC\alpha}$ and PLC* can be assumed to be in equilibrium and proportional to the concentration of activated mGluRs, and neither $G_{PLC\alpha}$ nor PLC* have to be represented as variables.

The concentration of active mGluRs B is *increased* by the binding of glutamate $[Glu]$ to the receptors, and *decreased* by the dissociation of glutamate and by the phosphorylation of the active receptors by PKC (C). The PKC phosphorylation transforms the active receptors into an inactive form A. Thus, the change in the concentrations of active and inactive mGluRs B and A is modelled by:

$$\frac{dB}{dt} = k_1 \left(B_a - B - A\right) [Glu] - k_{-1}\, B - k_2\, B\, C \tag{9.1}$$

$$\frac{dA}{dt} = k_2\, B\, C - k_3\, A \tag{9.2}$$

where B_a is the total concentration of available receptors.

As in the Adaptive Timing Model, the formation of IP_3 and DAG from PIP_2 is catalysed by the combined action of a Ca^{2+} activated form of PLC (Mignery et al., 1992) and a G-protein activated form of PLC. The activity of the Ca^{2+} dependent PLC is given by:

$$PLC([Ca^{2+}]) = \frac{[Ca^{2+}]^2}{[Ca^{2+}]^2 + K_{PLC}} \tag{9.3}$$

The activity of the G-protein-activated PLC is proportional to the concentration of active G-proteins which is proportional to the concentration of active mGluRs B (see above). As a consequence, the production and degradation of IP_3 (I) and DAG (D) can be represented by:

$$\frac{dI}{dt} = k_4\, B + k_5\, PLC([Ca^{2+}])) - k_6\, I \tag{9.4}$$

$$\frac{dD}{dt} = k_4\, B + k_5\, PLC([Ca^{2+}])) - k_7\, D \tag{9.5}$$

IP_3 binds to IP_3 receptor Ca^{2+} channels on the ER membrane. For the Ca^{2+} channels to open, the IP_3 receptors have to bind both IP_3 *and* a Ca^{2+} ion to an *activation* site. The binding of Ca^{2+} to an *inhibitory* site closes previously opened channels. The binding and dissociation of IP_3 is assumed to be in equilibrium with respect to the binding and dissociation of Ca^{2+}, and the concentration of open IP_3 receptors R_o depends on the concentration of Ca^{2+} activated IP_3 receptors R_a according to:

$$R_o = \frac{I}{I + K_I} R_a \tag{9.6}$$

The Ca^{2+} dependent activation and inactivation of the IP_3 receptors, the change of the cytoplasmic Ca^{2+} concentration, and the Ca^{2+} and DAG dependent activation of PKC are described by four ODEs which are identical to equations 4.8 - 4.15 in the Adaptive Timing Model.

9.2.2 Lost in Parameter Space

Like all other models in the thesis with more than two ODEs, the complex Ca^{2+} oscillation model was implemented in C++, and a fifth order Runge-Kutta algorithm with adaptive stepsize control was used to numerically integrate it. The numerical simulation of the model attempts to answer the question:

> *Can a model of the mGluR signalling network with a PKC mediated negative feedback connection between the cytoplasmic Ca^{2+} concentration and the concentration of active mGluRs implement damped Ca^{2+} oscillations in response to a glutamate pulse?*

The question can be rephrased as:

> *Is it possible to find a set of parameters that implement damped Ca^{2+} oscillations?*

The behaviour of the complex model depends on the values of 34 different parameters. Fourteen of the 34 parameters could be found in the literature; their values and the references are listed in appendix A.6. Two parameter values are constrained by their relation to other parameters. The rate constant for the dissociation of the mGluR-glutamate complex k_{-1} is given by the product of the rate constant for the binding of glutamate k_1 and the dissociation constant of the complex K_{mGluR}. Similarly, the rate constant for the PKC inactivation k_{11} is equal to the rate constant for the formation of the Ca^{2+}-DAG-PKC complex k_{10} times the dissociation constant of the complex K_{PKC}.

The remaining eighteen parameters are *free*. Thus, to determine if the model can generate damped Ca^{2+} oscillations, an *18-dimensional parameter space* has to be searched.

An 18-dimensional parameter space is too large for an exhaustive search. As a consequence, the answer to the question if the model can implement the damped oscillations must be positive to be conclusive.

An attempt was made to automate the parameter search by using a *Genetic Algorithm* (GA, Holland, 1975). The GA tries to find a set of 18 parameter values that implement the experimentally observed damped Ca^{2+} oscillations by applying the biologically inspired principles of mutation and selection. Sets of parameters are encoded as bit strings and called *chromosomes*.

Initially, a random population of chromosomes is chosen. For each of the chromosomes, a numerical simulation is performed and, depending on the similarity between the simulation results and the damped oscillatory Ca^{2+} response in Kawabata et al.'s experiments, the chromosome is assigned a *fitness* value. The *fittest* chromosomes are allowed to propagate to the next generation with a probability that increases with their fitness value. During each reproduction cycle, the parameter values of the chromosomes can be changed by *crossover* and *mutation*. As a result of the fitness dependent propagation and the mutation dependent variation, both the average fitness of the population and the fitness of the fittest chromosome are gradually increased. Given that the fitness is a measure of the similarity between the simulation and the experimental results, the GA should be able to find a set of parameters that implement the damped Ca^{2+} oscillations which were observed by Kawabata et al. (1996).

The performance of a GA depends on a number of factors, including the mutation probability, the crossover technique, the influence of the fitness on the reproduction probability and, most importantly, the *fitness function* that calculates the fitness value for a given parameter set. After a number of preliminary studies, the parameter space of the complex Ca^{2+} oscillation model was searched with a GA that had the following characteristics (explained in detail in Beasley et al., 1993a, 1993b):

- A population of 50 chromosomes.
- A constant mutation probability $P = 0.1$.

- *Uniform* crossover.
- *Fitness ranking* to calculate the reproduction probability for each chromosome.

When designing a GA, the most crucial decision is the choice of the fitness function. In the Ca^{2+} oscillation GA, the fitness of each chromosome was detemined by performing a numerical simulation of the model with the parameter values of the chromosome. The fitness of the chromosome was given by a negative error measure:

$$\begin{aligned} Fitness &= -Error \\ &= -\alpha \sum_{i=1}^{N} \left([Ca^{2+}]_{target,i} - [Ca^{2+}]_{actual,i} \right)^2 \\ &\quad -\beta \sum_{i=1}^{N-1} \left(\frac{\Delta [Ca^{2+}]_{target,i}}{\Delta_i t} - \frac{\Delta [Ca^{2+}]_{actual,i}}{\Delta_i t} \right)^2 \end{aligned} \tag{9.7}$$

where $[Ca^{2+}]_{actual,i}$ is the simulated calcium concentration at sample point $i, 1 \leq i \leq N$, $[Ca^{2+}]_{target,i}$ is the experimentally observed calcium concentration at the same sample point, $\Delta [Ca^{2+}]_{actual,i} / \Delta_i t$ is the ith simulated temporal gradient of the calcium concentration, $\Delta [Ca^{2+}]_{target,i} / \Delta_i t$ is the corresponding gradient in Kawabata eta al.'s experiments and $\alpha = 0.001$ and $\beta = 1.0$ are two constant weighting factors.

The reason for including the gradient error in the fitness measure was the consideration that a feature that distinguishes an oscillatory response from a plateau response or a single peak is a large proportion of sample points with large absolute gradient values. In spite of this attempt to design an oscillation-sensitive fitness function, even after 500 generations with a population size of 50 chromosomes, the GA had not managed to discover a set of parameters that implemented the desired damped oscillatory Ca^{2+} response.

To improve the performance of the GA, it might be necessary to use a fitness function that rewards the existence of an *oscillatory* reponse more explicitly, and the fitness

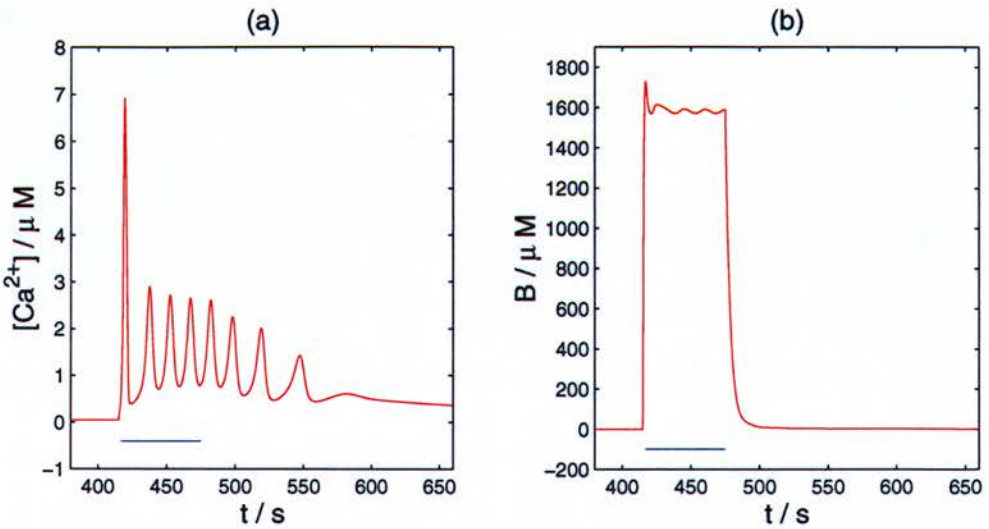

Figure 9.2: Behaviour of the complex model in response to a $10\mu M$ glutamate pulse from $t = 415s$ to $t = 475s$ (blue bar). (a) Cytoplasmic Ca^{2+} concentration, (b) concentration of active mGluRs B. The parameters are listed in appendix A.6.

function should probably be independent of the exact quantitative agreement at given sample points. Depending on the available computational resources, one could also increase the population size or experiment with time-varying mutation rates (Beasley et al., 1993b, J. Hallam, personal communication). Alternatively, a different optimisation strategy could be used, for example simulated annealing (Rutenbar, 1989). It has been shown that simulated annealing outperforms genetic algorithms as a parameter search strategy for small compartmental models of neurons (Vanier & Bower, 1996).

Compared to the difficulties with the *automated* parameter search, tuning the parameters *by hand* turned out to be surprisingly easy. After approximately 50 hours of manual parameter tuning, damped Ca^{2+} oscillations were found that agreed in their frequency and damping, but not in their amplitude, with Kawabata et al.'s experimental values (figure 9.2 (a), compare figure 9.1). The parameters that implement the damped Ca^{2+} oscillations are listed in appendix A.6.

Even though the complex model does not *exactly* reproduce Kawabata's data, it is able to generate a very similar pattern of damped Ca^{2+} oscillations in response to a glutamate pulse. Thus, it could be shown that a model of the mGluR signalling network

that contains a negative feedback connection between the Ca^{2+} concentration and the concentration of active mGluRs *can* generate damped Ca^{2+} oscillations in response to a glutamate pulse. However, the complex model does not show if the presence of the negative feedback connection *alone* leads to the damped oscillations, or if other interactions between the components of the mGluR signalling network are involved. To identify the intracellular processes that are responsible for the damped Ca^{2+} oscillations, a minimal model was developed that represents the mGluR dependent Ca^{2+} release with two ODEs. Three variations of the minimal model will be analysed in the following section.

9.3 The Minimal Model

9.3.1 Three Different Minimal Models

The aim of the minimal model is to determine which of the interactions between the components of the mGluR signalling network are essential for the generation of the damped Ca^{2+} oscillations that were observed by Kawabata et al. (1996). The model focusses on the effect of two Ca^{2+} dependent processes: *negative feedback* and *autocatalysis*. Three different variations of the 2 ODE model will be analysed in the following three sections:

1. A model with Ca^{2+} dependent negative feedback and autocatalysis.
2. A model without negative feedback, but with Ca^{2+} autocatalysis.
3. A model with negative feedback, but without Ca^{2+} autocatalysis.

9.3.2 Calcium Dependent Negative Feedback and Autocatalysis

In the model with negative feedback and autocatalysis, the dynamics of active mGluRs r and calcium c are described by the following two equations:

$$\frac{dr}{dt} = f_1(r, c) = k_1 - k_2\, r\, c \tag{9.8}$$

$$\frac{dc}{dt} = f_2(r, c) = k_3\, r\, c - k_4\, c \tag{9.9}$$

In equation 9.8, k_1 represents the activation of the receptors by glutamate, and $-k_2\, r\, c$ is the Ca^{2+} dependent inactivation of the mGluRs by PKC phosphorylation. In equation 9.9, $k_3\, r\, c$ is a simplified description of the mGluR and Ca^{2+} activated Ca^{2+} release into the cytoplasm, and $-k_4\, c$ models the reuptake of Ca^{2+} back into the endoplasmic reticulum.

The first step towards analysing the behaviour of the model is the calculation of the *nullclines* and the *fixed points* (described in detail in Edelstein-Keshet, 1987; Arrowsmith & Place, 1992). The model has a single r-nullcline representing the set of (r, c) loci which are given by $\dot{r} = 0$ (figure 9.4 (a)):

$$r = \frac{k_1}{k_2\, c} \tag{9.10}$$

There are two c-nullclines which describe the (r, c) loci that satisfy $\dot{c} = 0$. The first c-nullcline is identical to the r-axis ($c = 0$), and the second c-nullcline is given by:

$$r = \frac{k_4}{k_3} \tag{9.11}$$

At the intersection of the r-nullcline (equation 9.10) with the second c-nullcline (equation 9.11), the system has a single fixed point with the coordinates $\bar{r}$ and $\bar{c}$:

$$(\bar{r}, \bar{c}) = \left(\frac{k_4}{k_3}, \frac{k_1 k_3}{k_2 k_4} \right) \tag{9.12}$$

Close to the fixed point $(\bar{r}, \bar{c})$, the non-linear system (equations 9.8 and 9.9) behaves very similarly to the linear system:

$$\begin{pmatrix} \dot{r} \\ \dot{c} \end{pmatrix} = \mathbf{A} \begin{pmatrix} r \\ c \end{pmatrix} \tag{9.13}$$

where $\mathbf{A} = \mathbf{J}_{(\bar{r},\bar{c})}$ is the Jacobian matrix of the system at the fixed point $(\bar{r}, \bar{c})$. The Jacobian depends on the partial derivatives of $f_1(r, c)$ and $f_2(r, c)$ at $(\bar{r}, \bar{c})$ and is given by:

$$\mathbf{A} = \begin{pmatrix} a_{11} & a_{12} \\ a_{21} & a_{22} \end{pmatrix} = \mathbf{J}_{(\bar{r},\bar{c})} = \begin{pmatrix} \frac{\partial f_1}{\partial r} & \frac{\partial f_1}{\partial c} \\ \frac{\partial f_2}{\partial r} & \frac{\partial f_2}{\partial c} \end{pmatrix}_{(\bar{r},\bar{c})} = \begin{pmatrix} -k_2 \bar{c} & -k_2 \bar{r} \\ k_3 \bar{c} & k_3 \bar{r} - k_4 \end{pmatrix} \tag{9.14}$$

The behaviour of the system in the vicinity of the fixed point can be determined by calculating the eigenvalues of the Jacobian. For *complex* eigenvalues $\lambda_{1,2} = \alpha \pm \beta i$ with a *negative real part* $\alpha < 0$, the fixed point is the focus of a *stable spiral*. A stable spiral in the (r, c)-phase plane represents damped oscillations in the concentrations of active mGluRs and Ca^{2+}. Thus, determining the conditions for the generation of damped Ca^{2+} oscillations is equivalent to determining the conditions that lead to complex eigenvalues with a negative real part.

The eigenvalues of the Jacobian $\mathbf{A}$ are given by:

$$\lambda_{1,2} = \frac{1}{2}\left(Tr\,\mathbf{A} \pm \sqrt{disc\,\mathbf{A}}\right) \tag{9.15}$$

where $Tr\,\mathbf{A}$ and $disc\,\mathbf{A}$ are the *trace* and the *discriminant* of the Jacobian, respectively. The trace is defined as the sum of the diagonal terms:

$$Tr\,\mathbf{A} = a_{11} + a_{22} = -\frac{k_1\,k_3}{k_4} \tag{9.16}$$

As all parameters k_i are larger than zero, the trace of the Jacobian is always negative. Thus, if the eigenvalues are complex they must have a negative real part (equation 9.15), and the only type of oscillations that are possible in the system are *damped* oscillations.

Equation 9.15 shows that the Jacobian has a pair of complex conjugate eigenvalues if the discriminant $disc\,\mathbf{A}$ is negative. The discriminant is related to the trace and the determinant ($det\,\mathbf{A}$) by:

$$disc\,\mathbf{A} = (Tr\,\mathbf{A})^2 - 4\,det\,\mathbf{A} \tag{9.17}$$

where $det\,\mathbf{A}$ is given by:

$$det\,\mathbf{A} = a_{11}\,a_{22} - a_{12}\,a_{21} = k_1\,k_3 \tag{9.18}$$

Thus, the discriminant depends on the parameters $k_1 - k_4$ as follows:

$$disc\,\mathbf{A} = \frac{k_1^2\,k_3^2}{k_4^2} - 4\,k_1\,k_3 \tag{9.19}$$

The discriminant of the Jacobian is negative if the parameters k_1, k_3 and k_4 satisfy the following condition:

$$k_4 > \frac{\sqrt{k_1\,k_3}}{2} \tag{9.20}$$

The value of k_4 determines the rate of the Ca^{2+} reuptake from the cytoplasm back into the endoplasmic reticulum. Thus, if the Ca^{2+} reuptake is sufficiently fast compared to the mGluR activation and the Ca^{2+} release, the Jacobian has complex eigenvalues with a negative real part, and the system can exhibit damped Ca^{2+} oscillations.

For complex eigenvalues and eigenvectors, the linearised system (equation 9.13) has a general real-valued solution of the form:

$$\begin{pmatrix} r \\ c \end{pmatrix} = A_1\,\mathbf{u}(t) + A_2\,\mathbf{w}(t) \tag{9.21}$$

where A_1 and A_2 are constants, and $\mathbf{u}(t)$ and $\mathbf{w}(t)$ are the following real-valued solutions of equation 9.13:

$$\mathbf{u}(t) = e^{\alpha t}\,(\mathbf{a}\,\cos\,\beta t - \mathbf{b}\,\sin\,\beta t) \tag{9.22}$$

$$\mathbf{w}(t) = e^{\alpha t}\,(\mathbf{a}\,\sin\,\beta t - \mathbf{b}\,\cos\,\beta t) \tag{9.23}$$

In equations 9.22 and 9.23, **a** and **b** are the real and the imaginary part of the complex conjugate *eigenvector* pair:

$$\mathbf{v}_{1,2} = \mathbf{a} \pm i\,\mathbf{b} \tag{9.24}$$

and α and β are the real and imaginary part of the complex conjugate *eigenvalue* pair:

$$\lambda_{1,2} = \alpha \pm \beta\, i \tag{9.25}$$

Given that α and β are equal to $Tr\mathbf{A}/2$ and $\sqrt{-disc\mathbf{A}}/2$ (equation 9.15), the *frequency* and the *amplitude* of the oscillations are governed by the *discriminant* and the *trace* of the Jacobian, respectively. From equation 9.16, it can be seen that the amplitude of the oscillations decreases with a time course that is given by:

$$exp\,(\,-\frac{k_1 k_3}{2\,k_4}\,t\,) \tag{9.26}$$

Thus, the damping of the oscillations increases with k_1 and k_3, and decreases with k_4. In other words, the duration of the damped oscillatory response increases with the Ca^{2+} reuptake rate, and decreases with the Ca^{2+} release and the mGluR activation rates.

The region of the parameter space that leads to a negative discriminant, and the dependence of the discriminant and the trace on the Ca^{2+} reuptake rate constant k_4 are shown in figure 9.3. If the three other constants k_1, k_2 and k_3 are set to 1, k_4 has to be larger than 0.5 to generate a negative discriminant and enable the system to oscillate.

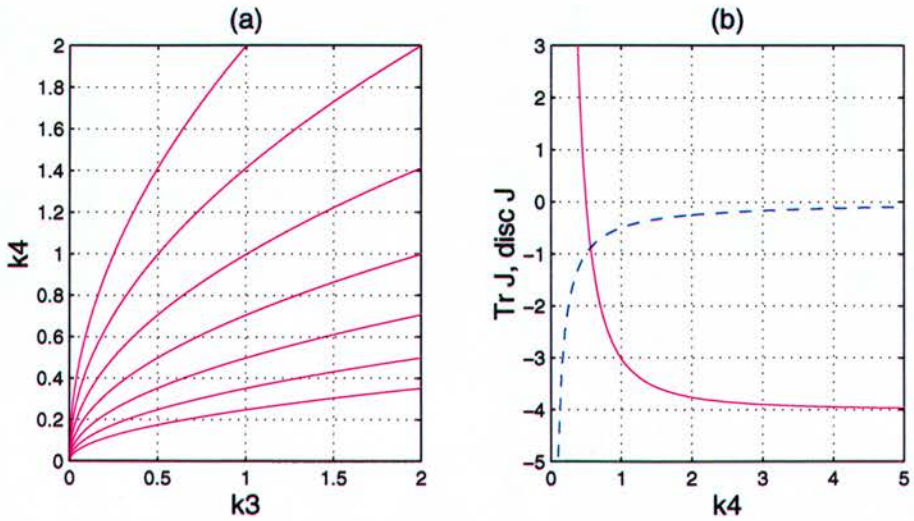

Figure 9.3: Parameter dependence of $Tr\mathbf{A}$ and $disc\mathbf{A}$ for the minimal model with Ca^{2+} dependent negative feedback and autocatalysis. (a) Graphs of $k_4 = \sqrt{k_1 k_3}/2$ for $k_1 = \{16, 8, 4, 2, 1, 0.5, 0.25\}$ (from top to bottom). For $k_4 > \sqrt{k_1 k_3}/2$, the discriminant of the Jacobian is negative and the system can exhibit damped Ca^{2+} oscillations. (b) Trace (dashed blue) and discriminant (solid magenta) of the Jacobian for $k_1 = k_2 = k_3 = 1$ and varying k_4. $k_4 > 0.5$ results in a negative $disc\mathbf{A}$. $Tr\mathbf{A}$, and therefore the damping, decreases with increasing k_4.

The GRIND numerical integrator (De Boer, 1983) was used to simulate the behaviour of the model with $k_2 = k_3 = 1$ and $k_4 = 3$ in response to a glutamate stimulus. Before the application of glutamate, the mGluRs are activated with a very low baseline rate $k_1 = k_1^0$, and the state of the system is given by the fixed point at the intersection of the r-nullcline and the second c-nullcline (indicated by (o) in figure 9.4 (a)):

$$\mathbf{S}^0 = (\bar{r}^0, \bar{c}^0) = \left(\frac{k_4}{k_3}, \frac{k_1^0 k_3}{k_2 k_4} \right) \tag{9.27}$$

The glutamate step results in an increase of the receptor activation rate to $k_1^* \gg k_1^0$. As a consequence, the r-nullcline (equation 9.10) is shifted from $r = k_1^0/(k_2 c)$ to $r = k_1^*/(k_2 c)$ in the phase plane, and the fixed point moves to a new location at:

$$\mathbf{S}^* = (\bar{r}^*, \bar{c}^*) = \left(\frac{k_4}{k_3}, \frac{k_1^* k_3}{k_2 k_4} \right) \tag{9.28}$$

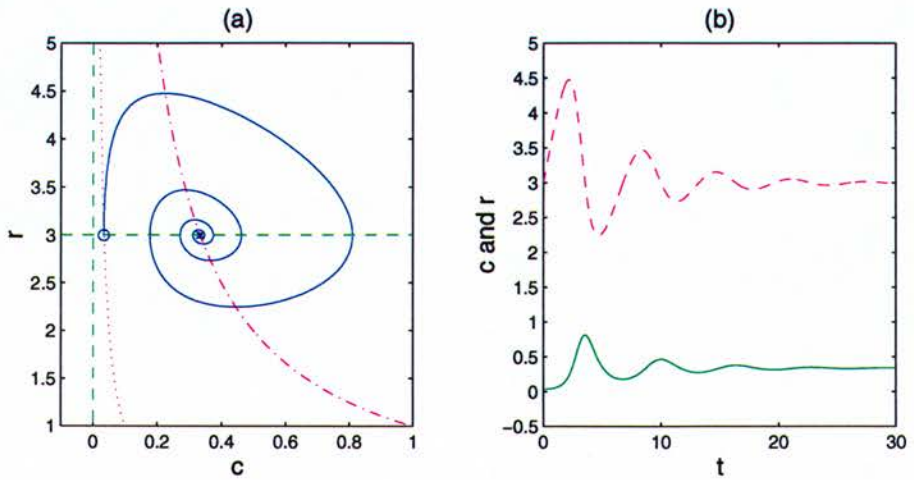

Figure 9.4: Behaviour of the minimal model with Ca^{2+} dependent negative feedback and autocatalysis in response to a glutamate pulse. The parameters are $k_2 = k_3 = 1$ and $k_4 = 3$, and the glutamate step is represented as an increase in k_1 from $k_1^0 = 0.1$ to $k_1^* = 1$. (a) The increase in k_1 leads to a shift of the r-nullcline from $r = k_1^0/(k_2 c)$ (dotted magenta) to $r = k_1^*/(k_2 c)$ (dashdot magenta) and to a shift of the fixed point from $\mathbf{S}^0$ (o) to $\mathbf{S}^*$ (x). The trajectory of the state vector (r, c) from $\mathbf{S}^0$ to $\mathbf{S}^*$ is a stable spiral (solid blue line). The two c-nullclines are shown as dashed green lines. (b) The spiral in the phase plane corresponds to damped oscillations of the concentrations of Ca^{2+} (c, green) and active mGluRs (r, dashed magenta).

Thus, the current state of the system $\mathbf{S}^0$ is destabilised, and the state vector $\mathbf{S} = (r, c)$ travels through the phase plane to the new fixed point $\mathbf{S}^*$ (indicated by (x) in figure 9.4 (a)). As the discriminant and the trace of the Jacobian $\mathbf{J}_{(\bar{r}^*, \bar{c}^*)}$ are negative, the trajectory from $\mathbf{S}^0$ to $\mathbf{S}^*$ is a spiral (solid blue line in figure 9.4 (a)), and the system responds with damped oscillations of the concentrations of Ca^{2+} and active mGluRs (figure 9.4 (b)).

To summarise, so far it has been shown that the combination of Ca^{2+} dependent negative feedback and autocatalytic Ca^{2+} release is *sufficient* to generate damped Ca^{2+} oscillations in response to a glutamate pulse, given that the removal of Ca^{2+} from the cytoplasm is fast enough compared to the Ca^{2+} release and the activation of the mGluRs. The remaining sections of the chapter will address the question if both processes are *necessary* for the generation of a damped oscillatory Ca^{2+} response. In the next section, a version of the minimal model without a negative feedback connection between the Ca^{2+} concentration and the concentration of active mGluRs will be analysed. Finally, a version of the model without Ca^{2+} autocatalysis will be studied.

9.3.3 The Model without Negative Feedback

In the version of the minimal model without Ca^{2+} dependent negative feedback, the term that describes the decrease in the concentration of active mGluRs has been changed from $-k_2\, r\, c$ to $-k_2\, r$, and the dynamics of Ca^{2+} (c) and active mGluRs (r) are described by:

$$\frac{dr}{dt} = f_3(r, c) = k_1 - k_2\, r \tag{9.29}$$

$$\frac{dc}{dt} = f_2(r, c) = k_3\, r\, c - k_4\, c \tag{9.30}$$

As in the model *with* the negative feedback, the other three terms represent the activation of the receptors by glutamate (k_1), the autocatalytic Ca^{2+} release from the endoplasmic reticulum ($k_3\, r\, c$), and theremoval of Ca^{2+} from the cytoplasm ($-k_4\, c$).

The model has a single r-nullcline (see figure 9.5 (a)):

$$r = \frac{k_1}{k_2} \tag{9.31}$$

The first of the two c-nullclines is identical to the r-axis ($c = 0$), and the second c-nullcline runs parallel to the c-axis and the r-nullcline:

$$r = \frac{k_4}{k_3} \tag{9.32}$$

At the intersection of the r-nullcline with the r-axis, the system has a fixed point with the following coordinates:

$$(\overline{r}, \overline{c}) = \left(\frac{k_1}{k_2}, 0 \right) \tag{9.33}$$

Again, the behaviour in the vicinity of the fixed point can be determined by linearising equations 9.29 and 9.30. The Jacobian of the system is given by:

$$\mathbf{A} = \mathbf{J}_{(\overline{r},\overline{c})} = \begin{pmatrix} \frac{\partial f_3}{\partial r} & \frac{\partial f_3}{\partial c} \\ \frac{\partial f_2}{\partial r} & \frac{\partial f_2}{\partial c} \end{pmatrix}_{(\overline{r},\overline{c})} = \begin{pmatrix} -k_2\,\overline{c} & -k_2\,\overline{r} \\ k_3 & -k_4 \end{pmatrix} \tag{9.34}$$

From equations 9.33 and 9.34, the trace and the determinant of the Jacobian can be calculated as:

$$Tr\,\mathbf{A} = -k_2 + \frac{k_1\,k_3}{k_2} - k_4 \tag{9.35}$$

and

$$det\,\mathbf{A} = -k_1\,k_3 + k_2\,k_4 \tag{9.36}$$

With $disc\mathbf{A} = (Tr\mathbf{A})^2 - 4det\mathbf{A}$, this gives us the following expression for the discriminant:

$$disc\,\mathbf{A} = \frac{k_1^2\,k_3^2}{k_2^2} + k_2^2 + k_4^2 - \frac{2\,k_1\,k_3\,k_4}{k_2} + 2\,k_1\,k_3 - 2\,k_2\,k_4 \tag{9.37}$$

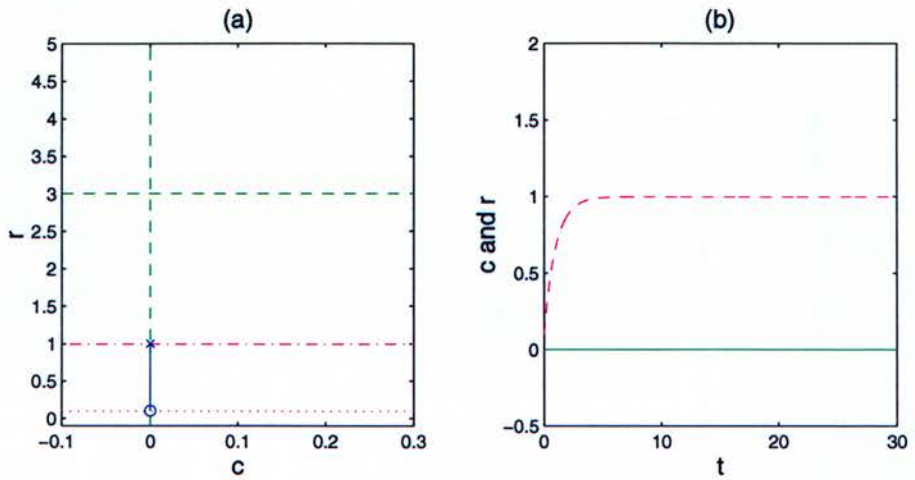

Figure 9.5: Behaviour of the minimal model without Ca^{2+} dependent negative feedback in response to a glutamate pulse. The parameters are $k_2 = k_3 = 1$ and $k_4 = 3$, and the glutamate step is represented as an increase in k_1 from $k_1^0 = 0.1$ to $k_1^* = 1$. (a) The increase in k_1 leads to a shift of the r-nullcline from $r = k_1^0/k_2$ (dotted magenta) to $r = k_1^*/k_2$ (dashdot magenta) and to a shift of the fixed point from $\mathbf{S}^0$ (o) to $\mathbf{S}^*$ (x). As a consequence, the state vector (r, c) travels along the r-axis from $\mathbf{S}^0$ to $\mathbf{S}^*$ (solid blue line). The two c-nullclines are shown as dashed green lines. (b) Temporal evolution of the concentrations of Ca^{2+} (c, green) and active mGluRs (r, dashed magenta).

This can be rewritten as:

$$disc\,\mathbf{A} = \left(-k_2 - \frac{k_1\,k_3}{k_2} + k_4\right)^2 \tag{9.38}$$

Thus, for any combination of parameter values, the Jacobian has a positive discriminant and real eigenvalues. From equation 9.15, it can be seen that the first eigenvalue is always negative:

$$\lambda_1 = -k_2 \tag{9.39}$$

The second eigenvalue is given by:

$$\lambda_2 = \frac{k_1\,k_3}{k_2} - k_4 \tag{9.40}$$

Depending on the values of $k_1 - k_4$, three cases can be distinguished:

1. If the product of the rate constants k_2 and k_4 for the *decrease* of r and c is larger than the product of the rate constants k_1 and k_3 for the *increase* of r and c, λ_2 is *negative* and the fixed point is *stable*.
2. For $k_2\,k_4 < k_1\,k_3$, λ_2 is *positive* and the fixed point is a *saddle point*.
3. For $k_2\,k_4 = k_1\,k_3$, the system is *non-simple*. The determinant and λ_2 are equal to zero, the r-nullcline and the second c-nullcline are identical and every point on the common nullcline is a fixed point.

Given that there is no combination of parameter values that results in complex eigenvalues, the system without feedback is unable to generate damped oscillations.

Figure 9.5 summarises the behaviour of the model with $k_2 = k_3 = 1$ and $k_4 = 3$ in response to a glutamate step, represented as an increase in k_1 from $k_1^0 = 0.1$ to $k_1^* = 1$. For both values of k_1, λ_2 is negative and the fixed point $(\bar{r}, \bar{c})$ is stable.

Before the application of glutamate, the r-nullcline is given by $r = k_1^0/k_2$, and the system is in the stable state $\mathbf{S}^0 = (k_1^0/k_2, 0)$. The glutamate stimulus shifts the r-nullcline to $r = k_1^*/k_2$ and the fixed point to $\mathbf{S}^* = (k_1^*/k_2, 0)$. As a consequence, the current state $\mathbf{S}^0$ ceases to be a fixed point, and the state vector travels along the r-axis to the new fixed point $\mathbf{S}^*$. Thus, the system responds to a glutamate step with an increase in the concentration of active mGluRs, while the Ca^{2+} concentration stays constantly at zero (figure 9.5 (b)).

To summarise, the existence of a *negative feedback* connection between the Ca^{2+} concentration and the concentration of active mGluRs is a *necessary* condition for the generation of a damped oscillatory Ca^{2+} response to a glutamate pulse. To determine if the existence of Ca^{2+} dependent *autocatalysis* is also necessary, a variation of the minimal model without autocatalytic Ca^{2+} release will be analysed in the next section.

9.3.4 The Model without Autocatalysis

In the variation of the minimal model without Ca^{2+} autocatalysis, the change in the concentrations of active mGluRs (r) and Ca^{2+} (c) is described by the following two equations:

$$\frac{dr}{dt} = f_1(r, c) = k_1 - k_2\, r\, c \tag{9.41}$$

$$\frac{dc}{dt} = f_4(r, c) = k_3\, r - k_4\, c \tag{9.42}$$

Compared to the model *with* Ca^{2+} autocatalysis, the Ca^{2+} increase term $k_3\, r\, c$ has been replaced by $k_3\, r$, and the release of Ca^{2+} from the endoplasmic reticulum is only dependent on the concentration of active mGluRs, but not on the Ca^{2+} concentration itself. The other three terms are the same as in the original model (equations 9.8 and 9.9).

As shown in figure 9.7, the model has a single r-nullcline:

$$r = \frac{k_1}{k_2\, c} \tag{9.43}$$

and a single c-nullcline:

$$r = \frac{k_4\, c}{k_3} \tag{9.44}$$

At the intersection of the two nullclines, there is a fixed point with the coordinates:

$$(\overline{r}, \overline{c}) = \left(\sqrt{\frac{k_1\, k_4}{k_2\, k_3}}, \sqrt{\frac{k_1\, k_3}{k_2\, k_4}} \right) \tag{9.45}$$

The linearisation of the system about the fixed point leads to the Jacobian matrix:

$$\mathbf{A} = \mathbf{J}_{(\overline{r},\overline{c})} = \begin{pmatrix} \frac{\partial f_1}{\partial r} & \frac{\partial f_1}{\partial c} \\ \frac{\partial f_4}{\partial r} & \frac{\partial f_4}{\partial c} \end{pmatrix}_{(\overline{r},\overline{c})} = \begin{pmatrix} -k_2 & 0 \\ k_3\, \overline{c} & k_3\, \overline{r} - k_4 \end{pmatrix} \tag{9.46}$$

The trace and the determinant of the Jacobian are given by:

$$Tr\, \mathbf{A} = -\sqrt{\frac{k_1\, k_2\, k_3}{k_4}} - k_4 \tag{9.47}$$

and:

$$det\, \mathbf{A} = 2\, \sqrt{k_1\, k_2\, k_3\, k_4} \tag{9.48}$$

Combining equations 9.47 and 9.48 with $disc\mathbf{A} = (Tr\mathbf{A})^2 - 4det\mathbf{A}$ gives us the following expression for the discriminant:

$$disc\, \mathbf{A} = \frac{k_1\, k_2\, k_3}{k_4} + k_4^2 - 6\, \sqrt{k_1\, k_2\, k_3\, k_4} \tag{9.49}$$

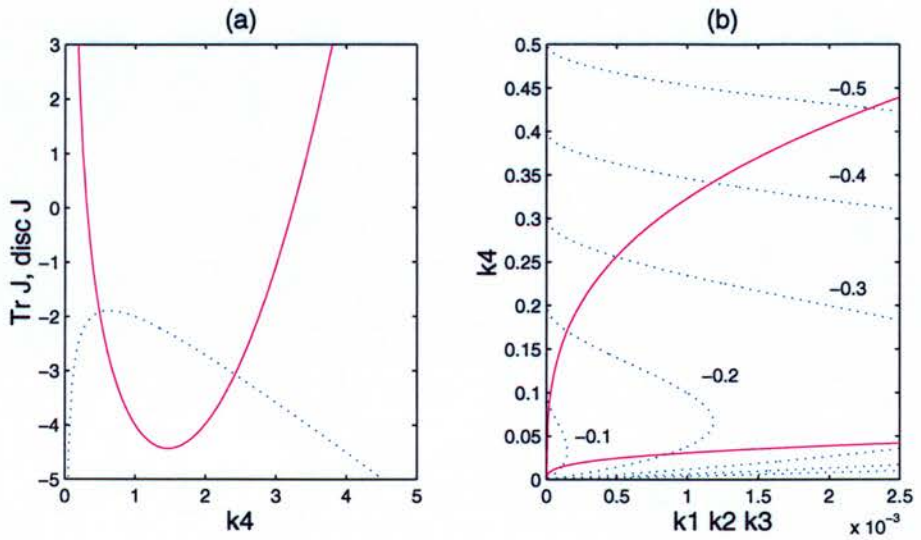

Figure 9.6: Parameter dependence of the discriminant and the trace of the Jacobian in the minimal model without autocatalysis. (a) $disc\mathbf{A}$ (solid magenta) and $Tr\mathbf{A}$ (dotted blue) for $k_1 = k_2 = k_3 = 1$ and varying values of k_4. (b) Area of the $(k_1 k_2 k_3) \times k_4$ space that can generate damped oscillations. The two solid magenta lines indicate the maximum and minimum values of k_4 that result in a negative discriminant (equation 9.50), and the dotted blue lines are a contour plot representing the parameter values that generate the indicated values of $Tr\mathbf{A} = \{-0.1, -0.2, -0.3, -0.4, -0.5\}$. Note that the product $k_1 k_2 k_3$ has to be very small to result in a small negative value of $Tr\mathbf{A}$.

The trace of the Jacobian is *always* negative, and the discriminant is negative for:

$$(3 + \sqrt{8})^{2/3} (k_1\, k_2\, k_3)^{1/3} < k_4 < (3 - \sqrt{8})^{2/3} (k_1\, k_2\, k_3)^{1/3} \tag{9.50}$$

Thus, if the Ca^{2+} reuptake rate constant k_4 is in a certain range, the Jacobian has complex eigenvalues with a negative real part, and the system *without* Ca^{2+} autocatalysis *can* exhibit damped Ca^{2+} oscillations. However, compared to the system *with* Ca^{2+} autocatalysis, the trace of the Jacobian has a much larger negative value, and the oscillations are much more strongly damped (compare equations 9.21 - 9.23). The Ca^{2+} removal rate constant k_4 that results in the smallest negative value of $Tr\mathbf{A}$ and therefore the weakest damping is:

$$k_{4,max} = 2^{-2/3} (k_1\, k_2\, k_3)^{1/3} \tag{9.51}$$

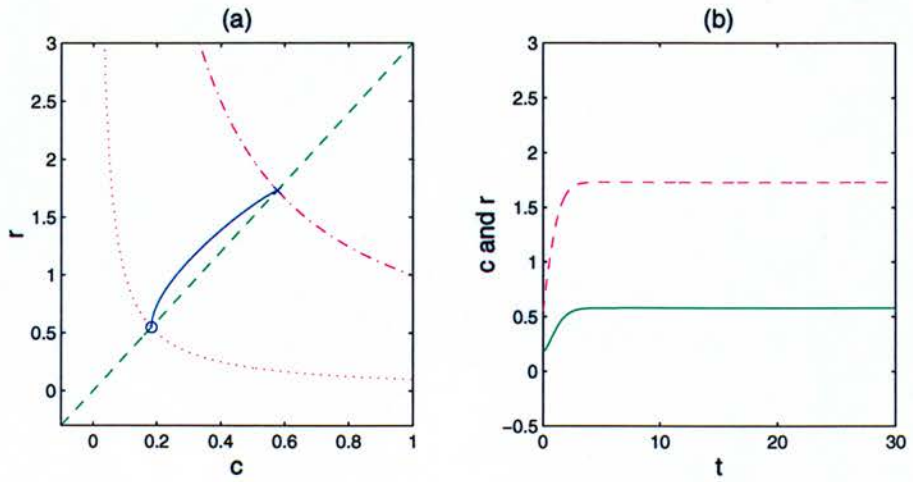

Figure 9.7: Behaviour of the minimal model without Ca^{2+} autocatalysis in response to a glutamate pulse. The parameters are $k_2 = k_3 = 1$ and $k_4 = 3$, and the glutamate step is represented by an increase in k_1 from $k_1^0 = 0.1$ to $k_1^* = 1$. (a) The increase in k_1 leads to a shift of the r-nullcline from $r = k_1^0/(k_2 c)$ (dotted magenta) to $r = k_1^*/(k_2 c)$ (dashdot magenta), and to a shift of the fixed point from $\mathbf{S}^0$ (o) to $\mathbf{S}^*$ (x). As a consequence, the state vector (r, c) travels from $\mathbf{S}^0$ to $\mathbf{S}^*$ through the phase plane (solid blue line). The green dashed line indicates the c-nullcline $r = (k_4 c)/k_3$. (b) Temporal evolution of the concentrations of Ca^{2+} (c, green) and active mGluRs (r, dashed magenta).

For $k_4 = k_{4,max}$, the trace of the Jacobian is given by:

$$Tr\,\mathbf{A}_{max} = -(k_1\,k_2\,k_3)^{1/3}\left(2^{1/3} + 2^{-2/3}\right) \tag{9.52}$$

The dependence of $Tr\mathbf{A}$ on the value of k_4 is shown in figure 9.6 (a). For the parameter combination $k_1^* = k_2 = k_3 = 1$ that was used in the other two versions of the minimal model, $Tr\mathbf{A}$ can never be less negative than $-2^{1/3} - 2^{-2/3} \approx -1.89$, and the strong damping prevents the generation of oscillations in the system. Only for very small values of k_1, k_2 and k_3, and for a very limited range of k_4 values, the absolute value of the trace can be small enough for the system to oscillate (figure 9.6 (b)).

Figure 9.7 summarises the behaviour of the model with $k_2 = k_3 = 1$ and $k_4 = 3$ in response to a glutamate stimulus. As in the other two versions of the model, the glutamate pulse is represented by an increase in k_1 from $k_1^0 = 0.1$ to $k_1^* = 1$, and results

in a shift of the r-nullcline and the fixed point. As a result, the state vector $\mathbf{S} = (r, c)$ travels from the old fixed point $\mathbf{S}^0$ to the new fixed point $\mathbf{S}^*$ through the phase plane. Because of the damping, the trajectory from $\mathbf{S}^0$ to $\mathbf{S}^*$ is fairly direct and *not* a spiral. The trajectory in the phase plane corresponds to an increase in the concentrations of active mGluRs and Ca^{2+} (figure 9.7 (b)).

To summarise, the existence of autocatalytic Ca^{2+} release is *not strictly necessary* for the generation of damped Ca^{2+} oscillations. However, without Ca^{2+} autocatalysis, most combinations of parameters lead to a very strong *damping effect*. For the vast majority of parameter combinations, the system without autocatalysis responds to a glutamate pulse by settling directly into the new steady state, *without* a phase of damped oscillations.

9.4 Chapter Conclusions

This chapter concludes the results section of the thesis. In the five chapters of the results section, two different functions of the metabotropic glutamate receptor (mGluR) signalling network in a cerebellar Purkinje cell were discussed:

1. The generation of an *adaptive time delay* between the activation of the mGluRs by glutamate and the release of Ca^{2+} from intracellular stores.
2. The generation of *damped Ca^{2+} oscillations* in response to the mGluR activation.

The adaptation of the time delay between the receptor activation and the Ca^{2+} release was the main subject of the thesis. In chapters 5 - 8, it was shown that the mGluR signalling network in a Purkinje cell *can* implement an adaptive time delay, and the *mechanism* and three possible computational *functions* of the delay adaptation were studied in detail.

In the present chapter, the conditions that lead to the generation of damped Ca^{2+} oscillations in the mGluR signalling network were investigated. Recently, Kawabata et al. (1996) have shown that the ability of the mGluR signalling network to implement Ca^{2+} oscillations depends on the metabotropic glutamate receptor subtype in the cell. In their experiments, different cells were transfected with the receptor subtypes mGluR1α and mGluR5a. It was found that a glutamate pulse triggered a brief stretch of damped Ca^{2+} oscillations in mGluR5a transfected cells, but only a single Ca^{2+} peak in mGluR1α transfected cells. Given that the G-protein binding region of mGluR5a, but not of mGluR1α, can be phosphorylated by protein kinase C (PKC), Kawabata et al. have suggested that the basis of the damped oscillatory response is the Ca^{2+} dependent inactivation of the receptors by PKC phosphorylation.

Here, two computational models of the mGluR signalling network were used to examine Kawabata et al.'s suggestion. The behaviour of a *complex model* with 8 ordinary differential equations (ODEs) was studied by numerically integrating it, and a *simplified model* with 2 ODEs was analysed using phase plane methods.

In both models, the ability to generate damped Ca^{2+} oscillations is *parameter dependent*. The behaviour of the complex model depends on the values of 34 different parameters. Fourteen of the 34 parameter values could be found in the literature. Two parameters are constrained by their relation with other parameter values. The remaining eighteen parameters are free. Thus, to determine if the complex model could implement damped Ca^{2+} oscillations, an 18-dimensional parameter space had to be searched.

For the search of the parameter space, two different strategies were used: a genetic algorithm (GA), and the tuning of the parameters by hand. Even after 500 generations and a total number of 25,000 simulations, the GA had not managed to find an oscillatory solution. In contrast, when tuning the parameters by hand, less than 250 simulations were necessary to find an area of the parameter space that resulted in damped Ca^{2+} oscillations.

Thus, with the right choice of parameters, a complex model of the mGluR signalling network that contains a PKC mediated negative feedback connection between the

Ca^{2+} concentration and the concentration of active mGluRs *can* implement damped Ca^{2+} oscillations in response to a glutamate pulse. However, the complexity of the model made it impossible to decide if the existence of the negative feedback loop was *sufficient* to generate the damped oscillations, or if other interactions between mGluR signalling components were involved. To identify the *minimal* set of interactions that are necessary for a damped oscillatory Ca^{2+} response, a simplified model was developed. In the simplified model, the dynamics of active mGluRs and cytoplasmic Ca^{2+} are represented by two ODEs.

The simplified model focussed on the effect of two Ca^{2+} dependent processes: *negative feedback* and *autocatalysis*. For three different versions of the two ODE model, a linear stability analysis was performed:

1. A model with Ca^{2+} dependent negative feedback and autocatalysis.
2. A model with autocatalysis, but without negative feedback.
3. A model with negative feedback, but without autocatalysis.

By analysing the three different versions of the model, it could be shown that the presence of the following four processes is *necessary* for the generation of a damped oscillatory Ca^{2+} response:

1. mGluR activation.
2. mGluR activated Ca^{2+} release.
3. *Negative feedback* by Ca^{2+} dependent mGluR inactivation.
4. Ca^{2+} dependent Ca^{2+} reuptake.

However, if *only* these four processes are present, the system is very strongly *damped* and settles immediately into the steady state, without a stretch of Ca^{2+} oscillations. There are two possible sets of conditions that result in decreased damping and enable the system to oscillate:

1. (a) The presence of *autocatalytic* Ca^{2+} *release* and
   (b) a Ca^{2+} reuptake rate that is at least as fast as the other three processes.

2. (a) Very slow mGluR activation, mGluR inactivation and Ca^{2+} release, and
   (b) a very limited range of Ca^{2+} reuptake rates.

Thus, the existence of a Ca^{2+} dependent negative feedback connection alone can implement damped Ca^{2+} oscillations, but only for a very limited range of parameter values. In contrast, a system with *negative feedback and autocatalysis* can generate a damped oscillatory Ca^{2+} response for a large range of parameter values.

Chapter 10

Conclusions

10.1 Aims of the Thesis

The aim of this thesis was to contribute to a better understanding of the network of intracellular signalling molecules in a cerebellar Purkinje cell. The focus of the thesis was the subset of the signalling network that is linked to the activation of *metabotropic glutamate receptors (mGluRs)* by parallel fibre input to the Purkinje cell. The following two questions were addressed:

1. *What can the mGluR signalling network compute?*
2. *How exactly does it perform the computations?*

To address the two questions, ten different computational models of the mGluR signalling network were constructed. Depending on their complexity, the ten models were either numerically integrated or mathematically analysed. The results of the computer simulations and mathematical analyses will be summarised in the following sections.

10.2 Adaptive Timing in the mGluR Network

The main result of the thesis is that the mGluR signalling network in a cerebellar Purkinje cell can implement an *adaptive time delay* between activation of the mGluRs by glutamate and release of Ca^{2+} from intracellular stores. The increase in the cytoplasmic Ca^{2+} concentration has a number of different effects. For example, it triggers an *inward current* through the Na^{+}/Ca^{2+} exchanger and an *outward current* through Ca^{2+} activated K^{+} (K_{Ca}) channels. Both of these currents affect the membrane potential of the cell and result in a change of the simple spike firing rate. As a consequence, a Purkinje cell can learn a time delay between the activation of the mGluRs by parallel fibre input and the increase or decrease of the simple spike firing rate. The adaptive time delay between the parallel fibre input and the Purkinje cell response can have at least three different computational functions:

1. It can enable a single Purkinje cell to learn the adaptive timing of the classically conditioned eye-blink response.
2. It can enable a single Purkinje cell to learn a radial basis function (RBF)-like response to temporal parallel fibre input patterns.
3. It can enable a group of Purkinje cells to discover different clusters in a temporal parallel fibre input space.

The adaptation of a *synaptic delay* as opposed to a *synaptic weight* represents a novel *non-Hebbian* learning mechanism. By systematically simplifying the original model, it was shown that the following processes are responsible for the generation of the adaptive time delay:

1. Two phosphorylations that adjust the concentration of available mGluRs.
2. mGluR and Ca^{2+} dependent (*autocatalytic*) Ca^{2+} release.
3. *Negative feedback* by Ca^{2+} dependent inhibition of the active mGluRs.
4. Ca^{2+} dependent Ca^{2+} reuptake.

Thus, a very limited set of intracellular signalling interactions can generate a complex set of behaviours in a Purkinje cell. Furthermore, the limited set of intracellular signalling interactions can provide the basis for a simple *behavioural phenomenon*: the adaptive timing of the classically conditioned eye-blink response.

10.3 Oscillations and Excitability in the mGluR Network

The adaptation of the time delay between mGluR stimulation and intracellular Ca^{2+} release is not the only possible behaviour of the mGluR signalling network. With a different set of biochemical rate constants, the network can respond to a glutamate pulse by damped oscillations of the cytoplasmic Ca^{2+} concentration. By analysing three simplified models of the mGluR induced Ca^{2+} release, it was shown that the crucial feature of the network that is responsible for the damped Ca^{2+} oscillations is the presence of a *negative feedback* connection between the Ca^{2+} concentration and the concentration of active mGluRs. Furthermore, the presence of Ca^{2+} *autocatalysis* reduces the damping and enables the system to oscillate for a larger range of parameter values.

Thus, the combination of Ca^{2+} dependent negative feedback and autocatalysis in the mGluR signalling network can generate *both damped Ca^{2+} oscillations and single Ca^{2+} peaks*. Another neuronal system that can produce both oscillations and single spikes are the voltage gated ion channels in the plasma membrane. The generation of spikes by the interaction of voltage gated channels has been studied extensively in the Hodgkin-Huxley, FitzHugh-Nagumo and Morris-Lecar models of neural excitation (Hodgkin & Huxley, 1952; FitzHugh, 1960; Morris & Lecar, 1981). Like these three models of neural excitation, the models of the mGluR signalling network belong to a general class of *excitable* systems that react to small deviations from the steady state by a *large excursion through the phase space*. Depending on the magnitude of the initial deviation from the steady state and the parameters of the system, the excursion through the phase space can result in oscillations or in a single spike.

To summarise, all neurons with mGluRs contain at least two types of *excitable and oscillatory systems*: the set of voltage dependent ion channels in the plasma membrane, and the mGluR signalling network that controls Ca^{2+} release from intracellular stores. These systems operate on very different time scales, and they differ in several other respects. The oscillations of the membrane voltage that are based on the interactions of ion channels can be *sustained*, and the time delay between current stimulus and voltage spike is in the range of a few milliseconds. In contrast, the Ca^{2+} oscillations in the mGluR signalling models are *damped*, and the time delay between mGluR stimulation and Ca^{2+} peak can range between 200 milliseconds and one second.

The thesis has studied three possible computational functions of the *adaptation* of the time delay between mGluR stimulation and intracellular Ca^{2+} release. Even *without* the adaptation of the time delay, a neuron might benefit from the existence of two excitable systems. Excitable systems are the only systems that can generate *spikes*. The generation of Ca^{2+} spikes by the mGluR signalling network has at least two advantages. A system that uses Ca^{2+} spikes is insensitive to small fluctuations in the Ca^{2+} concentration and is therefore *noise resistant*. Furthermore, a spike based system is more versatile and can use two different encoding schemes: a *temporal code* where the information is represented by the time of the Ca^{2+} peaks, or a *rate code* where the input is encoded by the frequency of Ca^{2+} peaks in a sampling interval. Recently, it has been suggested that frequency encoded Ca^{2+} signals can be decoded by calmodulin (CaM) dependent kinase II (Putney, 1998; De Koninck & Schulman, 1998).

10.4 Future Work

In the previous section, it was argued that the mGluR signalling network is an *excitable system* that can perform different kinds of computations, and that it operates as a *neuron within a neuron*. The computational capabilities of the mGluR signalling network and other intracellular signalling networks are a promising subject for future

research. One of the aspects of intracellular signalling in neurons that should be studied in more detail are the interactions between the network of intracellular signalling molecules and the Ca^{2+}, voltage and neurotransmitter gated channels that generate the short-term variations of the membrane potential.

In the Purkinje cell models that were investigated in the thesis, the K_{Ca} channels are the only ion channels that are represented explicitly. In the different versions of the Adaptive Timing Model, the phosphorylations of K_{Ca} channels and mGluRs implement the long-term changes of the Purkinje cell responsiveness that are the basis of the eye-blink learning and the temporal pattern recognition.

An important link between intracellular signalling and neural excitability that is *not* represented in the models is the Ca^{2+} dependent *phosphorylation of AMPA receptors* at the synapses between parallel fibres and Purkinje cells. The AMPA receptor phosphorylation results in long-term depression (LTD) of the parallel fibre synapses, and potentially in a decrease of the simple spike firing rate in response to parallel fibre input. Given that the Adaptive Timing Model investigates the temporal evolution of the simple spike firing rate, it should be modified to take the effects of AMPA receptor mediated EPSPs and AMPA receptor LTD into account.

AMPA receptors are Na^{+} channels with opening and closing time constants in the millisecond range (Holmes & Levy, 1990; De Schutter & Bower, 1994b). To study the effect of AMPA receptor mediated EPSPs on the Purkinje cell firing pattern, the conduction delays along the dendritic tree have to be modelled. Previous modelling studies have shown that the spatial and temporal integration of the EPSPs is under the control of voltage gated channels in the Purkinje cell dendrites (De Schutter & Bower, 1994c). Thus, a more realistic version of the Adaptive Timing Model should also include a representation of voltage gated channels.

An *advantage* of a more realistic Purkinje cell model with a representation of voltage dependent channels is that it can be more easily tuned to fit electrophysiological data, and that it can be used to make quantitative predictions. Two issues that could be

addressed with a realistic model are the mechanism and the temporal properties of the induction of parallel fibre LTD. The temporal properties of LTD induction have implications for the involvement of LTD in motor learning.

A *disadvantage* of the realistic model is that it becomes very complicated, and difficult to understand in detail. The next step after the development of the realistic model should be its simplification, similar to the different simplifications of the mGluR signalling models that were developed in this thesis.

Bibliography

Albus, J. S. (1971). A theory of cerebellar function. *Math. Biosci., 10*, 25–61.

Arkin, A., & Ross, J. (1994). Computational functions in biochemical reaction networks. *Biophys. J., 67*, 560–578.

Armstrong, D. M., & Rawson, J. A. (1979). Activity patterns of cerebellar cortical neurones and climbing fibre afferents in the awake cat. *J. Physiol., 289*, 425–448.

Arrowsmith, D. K., & Place, C. M. (1992). *Dynamical Systems: Differential Equations, Maps and Chaotic Behaviour*. Chapman & Hall, London.

Artola, A., & Singer, W. (1993). Long-term depression of excitatory synaptic transmission and its relationship to long-term potentiation. *Trends Neurosci., 16*, 480–487.

Atkins, P. (1998). *Physical Chemistry* (sixth edition). W. H. Freeman, New York.

Barik, S., & deBeaurepaire, R. (1996). Evidence for a functional role of the dopamine D3 receptors in the cerebellum. *Brain Res., 737*, 347–350.

Batchelor, A. M., & Garthwaite, J. (1993). Novel synaptic potentials in cerebellar Purkinje cells: probable mediation by metabotropic glutamate receptors. *Neuropharmacology, 32*, 11–20.

Batchelor, A. M., Madge, D. J., & Garthwaite, J. (1994). Synaptic activation of metabotropic glutamate receptors in the parallel fibre–Purkinje cell pathway in rat cerebellar slices. *Neuroscience, 63*, 911–915.

Batini, C., Buisseret-Demas, C., Compoint, C., & Daniel, H. (1989). The GABAergic neurones of the cerebellar nuclei in the rat: projections to the cerebellar cortex. *Neurosci. Lett., 99*, 251–256.

Baumann, O., Walz, B., Somlyo, A. V., & Somlyo, A. P. (1991). Electron probe microanalysis of calcium release and magnesium uptake by endoplasmic reticulum in bee photoreceptors. *Proc. Natl. Acad. Sci. USA, 88*, 741–744.

Bear, M. F., Cooper, L. N., & Ebner, F. F. (1987). A physiological basis for a theory of synapse modification. *Science, 237*, 42–48.

Beasley, D., Bull, D. R., & Martin, R. R. (1993a). An overview of genetic algorithms: Part 1, fundamentals. *University Computing, 15*, 58–69.

Beasley, D., Bull, D. R., & Martin, R. R. (1993b). An overview of genetic algorithms: Part 2, research topics. *University Computing, 15*, 170–181.

Berthier, N. E., & Moore, J. W. (1986). Cerebellar Purkinje cell activity related to the classically conditioned nictitating membrane response. *Exp. Brain Res., 63*, 341–350.

Berthier, N. E., & Moore, J. W. (1990). Activity of deep cerebellar nuclear cells during classical conditioning of nictitating membrane extension in rabbits. *Exp. Brain Res., 83*, 44–54.

Bezprozvanny, I., Watras, J., & Ehrlich, B. E. (1991). Bell-shaped calcium-dependent curves of Ins(1,4,5)-P3 gated and calcium gated channels from endoplasmic reticulum of cerebellum. *Nature, 351*, 751–754.

Bialek, W., Rieke, F., de Ruyter van Steveninck, R., & Warland, D. (1991). Reading a neural code. *Science, 252*, 1854–1857.

Bickford, P. (1995). Aging and motor learning: a possible role for norepinephrine in cerebellar plasticity. *Reviews Neurosci., 6*, 35–46.

Bloedel, J. R. (1992). Functional heterogeneity with structural homogeneity: how does the cerebellum operate?. *Behav. Brain Sci., 15*, 666–678.

Bloedel, J. R., Bracha, V., Milak, M., & Shimansky, Y. (1997). Cerebellar contributions to the acquisition and execution of learned reflex and volitional movements. *Prog. Brain Res., 114*, 499–509.

Bower, J. M. (1994). Constructing new models. In Bower, J. M., & Beeman, D. (Eds.), *The book of GENESIS: exploring realistic neural models with the GEneral NEural SImulation System*, pp. 183–190. Springer Verlag, New York.

Bracha, V., Stewart, S. L., & Bloedel, J. R. (1993). The temporary inactivation of the red nucleus affects performance of both conditioned and unconditioned nictitating membrane responses in the rabbit. *Exp. Brain Res., 94*, 225–236.

Bracha, V., Webster, M. L., Stachowiak, M. K., & Bloedel, J. R. (1995). Injection of anisomycin into the interposed nuclear regions affect consolidation of the conditioned eyeblink response. *Soc. Neurosci. Abs., 21*, 1222.

Bracha, V., Webster, M. L., Winters, N. K., Irwin, K. B., & Bloedel, J. R. (1994). Effects of muscimol inactivation of the cerebellar interposed-dentate nuclear complex on the performance of the nictitating membrane response in the rabbit. *Exp. Brain Res., 100*, 453–468.

Braitenberg, V., & Atwood, R. P. (1958). Morphological observations on the cerebellar cortex. *J. Comp. Neurol., 109*, 1–33.

Bray, D. (1990). Intracellular signalling as a parallel distributed process. *J. Theor. Biol., 143*, 215–231.

Bray, D. (1995). Protein molecules as computational elements in living cells. *Nature, 376*, 307–312.

Brown, T. H., Kairiss, E. W., & Keenan, C. L. (1990). Hebbian synapses: biophysical mechanisms and algorithms. *Annu. Rev. Neurosci., 13*, 475–511.

Butt, E., Abel, K., Krieger, M., Palm, D., Hoppe, V., Hoppe, J., & Walter, U. (1994). cAMP-dependent and cGMP-dependent protein kinase phosphorylation sites of the focal adhesion vasodilator-stimulated phosphoprotein (VASP) *in vitro* and in intact human platelets. *Biochemistry, 269*, 14509–14517.

Carafoli, E. (1987). Intracellular calcium homeostasis. *Ann. Rev. Biochem., 56*, 395–433.

Chapman, P. F., Steinmetz, J. E., Sears, L. L., & Thompson, R. F. (1990). Effects of lidocaine injection in the interpositus nucleus and red nucleus on conditioned behavioral and neuronal responses. *Brain Res., 537*, 149–156.

Chapman, P. F., Steinmetz, J. E., & Thompson, R. F. (1988). Classical conditioning does not occur when direct stimulation of the red nucleus or cerebellar nuclei is the unconditioned stimulus. *Brain Res., 442*, 97–104.

Chen, C., & Thompson, R. F. (1992). Associative long-term depression revealed by field potential recording in rat cerebellar slice. *Soc. Neurosci. Abs., 18*, 1215.

Chen, C., & Thompson, R. F. (1995). Temporal specificity of long-term depression in parallel fibre-Purkinje synapses in rat cerebellar slice. *Learning & Memory, 2*, 185–198.

Chen, L., Bao, S. W., Lockard, J. M., Kim, J. J., & Thompson, R. F. (1996). Impaired classical eyeblink conditioning in cerebellar-lesioned and Purkinje-cell degeneration (pcd) mutant mice. *J. Neurosci., 16*, 2829–2838.

Cheun, J. E., & Yeh, H. H. (1996). Noradrenergic potentiation of cerebellar Purkinje cell responses to GABA: cyclic AMP as intracellular intermediary. *Neuroscience, 74*, 835–844.

Clark, R. E., & Lavond, D. G. (1993). Reversible lesions of the red nucleus during acquisition and retention of a classically conditioned behavior in rabbit. *Behav. Neurosci., 107*, 264–270.

Clark, R. E., Zhang, A. A., & Lavond, D. G. (1992). Reversible lesions of the cerebellar interpositus nucleus during acquisition and retention of a classically conditioned behavior. *Behav. Neurosci., 106*, 879–888.

Coleman, S. R., & Gormezano, I. (1971). Classical conditioning of the rabbit's (*Oryctolagus cuniculus*) nictitating membrane response under symmetrical CS-US interval shifts. *J. Comp. Physiol. Psychol., 77*, 447–455.

Crépel, F., & Jaillard, D. (1990). Protein kinases, nitric oxide, and long-term depression of synspses in the cerebellum. *Neuroreport, 1*, 133–136.

Crépel, F., & Jaillard, D. (1991). Pairing of pre- and postsynaptic activities in cerebellar Purkinje cells induces long-term changes in synaptic efficacy *in vitro*. *J. Physiol., 432*, 123–141.

Crépel, F., & Krupa, M. (1988). Activation of protein kinase C induces a long-term depression of glutamate sensitivity of cerebellar Purkinje cells. An *in vitro* study. *Brain Res., 458*, 397–401.

Daniel, H., Hemart, N., Jaillard, D., & Crépel, F. (1993). Long-term depression requires nitric oxide and guanosine 3':5' cyclic monophosphate production in cerebellar Purkinje cells. *Eur. J. Neurosci., 5*, 1079–1082.

Daniel, H., Levenes, C., & Crépel, F. (1998). Cellular mechanisms of cerebellar LTD. *Trends Neurosci., 21*, 401–407.

De Boer, R. J. (1983). GRIND. GReat INtegrator Differential equations User Manual. Theoretical Biology, Utrecht University, The Netherlands.

De Koninck, P., & Schulman, H. (1998). Sensitivity of CaM kinase II to the frequency of Ca2+ oscillations. *Science, 279*, 227–230.

De Meis, L., & Inesi, G. (1982). The transport of calcium by sarcoplasmic reticulum and various microsomal preparations. In Carafoli, E. (Ed.), *Membrane Transport of Calcium*, pp. 141–186. Academic Press, London.

De Schutter, E. (1995). Cerebellar long-term depression might normalize excitation of Purkinje cells: a hypothesis. *Trends Neurosci., 18*, 291–295.

De Schutter, E. (1996). One cannot build theories of cerebellar function on shaky foundations: Induction properties of long-term depression have to be taken into account. *Behav. Brain Sci., 19*, 440–441.

De Schutter, E. (1997). A new functional role for cerebellar long term depression. *Prog. Brain Res., 114*, 531–544.

De Schutter, E., & Bower, J. M. (1994a). An active membrane model of the cerebellar Purkinje cell. I. Simulation of current clamps in slice. *J. Neurophysiol., 71*, 375–400.

De Schutter, E., & Bower, J. M. (1994b). An active membrane model of the cerebellar Purkinje cell. II. Simulation of synaptic responses. *J. Neurophysiol., 71*, 401–419.

De Schutter, E., & Bower, J. M. (1994c). Simulated responses of cerebellar Purkinje cells are independent of the dendritic location of granule cell synaptic inputs. *Proc. Natl. Acad. Sci. USA, 91*, 4736–4740.

De Schutter, E., & Smolen, P. (1998). Calcium dynamics in large neuronal models. In Koch, C., & Segev, I. (Eds.), *Methods in neuronal modeling: from synapses to networks*. MIT Press, Cambridge MA.

Eccles, J. C., Ito, M., & Szentagothai, J. (1967). *The cerebellum as a neuronal machine.* Springer Verlag, Berlin.

Edelstein-Keshet, L. (1987). *Mathematical Models in Biology.* McGraw-Hill Inc., New York.

Eilers, J., Augustine, G. J., & Konnerth, A. (1995). Subthreshold synaptic calcium signalling in fine dendrites and spines of cerebellar Purkinje neurons. *Nature, 373,* 155–158.

Eilers, J., Plant, T., & Konnerth, A. (1996). Localized calcium signalling and neuronal integration in cerebellar Purkinje neurones. *Cell Calcium, 20,* 215–226.

Ekerot, C. F., & Kano, M. (1985). Long-term depression of parallel fibre synapses following stimulation of climbing fibres. *Brain Res., 342,* 357–360.

Ekerot, C. F., & Kano, M. (1989). Stimulation parameters influencing climbing fibre induced long-term depression of parallel fibre synapses. *Neurosci. Res., 6,* 264–268.

Ekerot, C. F., & Oscarsson, O. (1981). Prolonged depolarization elicited in Purkinje cell dendrites by climbing fibre impulses in the cat. *J. Physiol., 318,* 207–221.

Fiala, J. C., Grossberg, S., & Bullock, D. (1996). Metabotropic glutamate receptor activation in cerebellar Purkinje cells as substrate for adaptive timing of the classically conditioned eye-blink response. *J. Neurosci., 16,* 3760–3774.

FitzHugh, R. (1960). Thresholds and plateaus in the Hodgkin-Huxley nerve equations. *J. Gen. Physiol., 43,* 867–896.

Foy, M. R., Krupa, D. J., Tracy, J., & Thompson, R. F. (1992). Analysis of single unit recordings from cerebellar cortex of classically conditioned rabbits. *Soc. Neurosci. Abs., 18,* 1215.

Foy, M. R., & Thompson, R. F. (1986). Single unit analysis of Purkinje cell discharge in classically conditioned and untrained rabbits. *Soc. Neurosci. Abs., 12,* 518.

Freeman, J. H., Shi, T., & Schreurs, B. G. (1998). Pairing-specific long-term depression prevented by blockade of PKC or intracellular Ca2+. *Neuroreport, 9,* 2237–2241.

Freund, R. K., & Palmer, M. R. (1997). Ethanol depression of cerebellar Purkinje neuron firing involves nicotinic acetylcholine receptors. *Exp. Neurology, 143,* 319–322.

Gerstner, W., Kempter, R., van Hemmen, J., & Wagner, H. (1996). A neuronal learning rule for sub-millisecond temporal coding. *Nature, 383,* 76–78.

Gilbert, P. F. C. (1974). A theory of memory that explains the structure and function of the cerebellum. *Brain Res., 128,* 1–18.

Gilbert, P. F. C. (1975). How the cerebellum could memorise movements. *Nature, 254,* 688–689.

Glauber, R. J. (1963). Time-dependent statistics of the Ising model. *J. Math. Physics, 4,* 294–307.

Goldbeter, A. (1995). A model for circadian oscillations in the *Drosophila* period protein (PER). *Proc. R. Soc. Lond. B, 261,* 319–324.

Gormezano, I. (1966). Classical conditioning. In Sidowski, J. B. (Ed.), *Experimental methods and instrumentation in psychology,* pp. 385–420. McGraw–Hill, New York.

Gormezano, I., Schneiderman, N., Deaux, E. G., & Fuentes, J. (1962). Nictitating membrane classical conditioning and extinction in the albino rabbit. *Science, 138,* 33–34.

Grossberg, S. (1976). Adaptive pattern classification and universal recording: Ii. feedback, expectation, olfaction, illusions. *Biol. Cybernetics, 23,* 187–202.

Hartell, N. A. (1996). Strong activation of parallel fibres produces localized calcium transients and a form of LTD that spreads to distant synapses. *Neuron, 16,* 601–610.

Hawkins, R. D., Carew, T. J., & Kandel, E. R. (1986). Effects of interstimulus and contingency on classical conditioning of the *Aplysia* siphon withdrawal reflex. *J. Neurosci., 6,* 1695–1701.

Hebb, D. O. (1949). *The Organization of Behavior.* Wiley Press, New York.

Herrero, I., Miras-Portugal, M. T., & Sánchez-Prieto, J. (1994). Rapid desensitization of the metabotropic glutamate receptor that facilitates glutamate release in rat cerebrocortical nerve terminals. *Eur. J. Neurosci., 6,* 115–120.

Hertz, J. A., Krogh, A. S., & Palmer, R. G. (1991). *Introduction to the theory of neural computation.* Addison-Wesley Publishing, Redwood City, CA.

Hille, B. (1992). *Ionic Channels of Excitable Membranes* (second edition). Sinauer Associates, Sunderland, Massachusetts.

Hirano, T. (1990). Depression and potentiation of the synaptic transmission between a granule cell and a Purkinje cell in rat cerebellar culture. *Neurosci. Lett., 119,* 141–144.

Hodgkin, A. L., & Huxley, A. F. (1952). A quantitative description of membrane current and its application to conduction and excitation in nerve. *J. Physiol., 117,* 500–544.

Hodgkin, A. L., & Nunn, B. J. (1987). The effect of ions on sodium-calcium exchange in salamander rods. *J. Physiol., 391,* 371–398.

Holland, J. H. (1975). *Adaptation in Natural and Artificial Systems.* MIT Press, Cambridge, MA.

Holmes, W. R., & Levy, W. B. (1990). Insights into associative long-term potentiation from computational models of NMDA receptor mediated calcium influx and intracellular calcium conentrtaion changes. *J. Neurophysiol., 63,* 1148–1168.

Hopfield, J. (1995). Pattern recognition computation using action potential timing for stimulus representation. *Nature, 376,* 33–36.

Huang, K.-P., Huang, F. L., Mahoney, C. W., & Chen, K.-H. (1991). Protein kinase C subtypes and their respective roles. *Prog. Brain Res., 89,* 143–155.

Huganir, R. L., & Greengard, P. (1990). Regulation of neurotransmitter receptor desensitization by protein phosphorylation. *Neuron, 5,* 555–567.

Ito, M. (1984). *The cerebellum and neural control.* Raven Press, New York.

Ito, M. (1989). Long-term depression. *Annu. Rev. Neurosci., 12,* 85–102.

Ito, M. (1996). The new hypothesis does not detract from the MAIT theory. *Trends Neurosci., 19,* 11.

Ito, M. (1998). Book review of: The cerebellum: from structure to control. *Trends Neurosci., 21,* 419.

Ito, M., & Karachot, L. (1990). Messengers mediating long-term desensitization in cerebellar Purkinje cells. *Neuroreport, 1,* 129–132.

Ito, M., Sakurai, M., & Tongroach, P. (1982). Climbing fibre induced depression of both mossy fibre responsiveness and glutamate sensitivity of cerebellar Purkinje cells. *J. Physiol., 324,* 133–134.

Jacobson, M. (1991). *Developmental Neurobiology.* Plenum Press, New York.

Kandel, E. R., Schwartz, J. H., & Jessell, T. M. (1991). *Principles of Neural Science* (third edition). Elsevier Science Publishing, New York.

Kano, M., Rexhausen, J., Dreessen, J., & Konnerth, A. (1992). Synaptic excitation produces a long-lasting rebound potentiation of inhibitory synaptic signals in cerebellar Purkinje cells. *Nature, 356,* 601–604.

Karachot, L., Kado, R. T., & Ito, M. (1994). Stimulus parameters for induction of long-term depression in in vitro rat Purkinje cells. *Neurosci. Res., 21,* 161–168.

Kawabata, S., Tsutsumi, R., Kohara, A., Yamaguchi, T., Nakanishi, S., & Okada, M. (1996). Control of calcium oscillations by phosphorylation of metabotropic glutamate receptors. *Nature, 383,* 89–92.

Kelly, T. M., Zuo, C., & Bloedel, J. R. (1990). Classical conditioning of the eyeblink reflex in the decerebrate-decerebellate rabbit. *Behav. Brain Res., 38,* 7–18.

Kim, J. J., & Thompson, R. F. (1997). Cerebellar circuits and synaptic mechanisms involved in classical eyeblink conditioning. *Trends Neurosci., 20,* 177–181.

Knöpfel, T., Audinat, E., & Gähwiler, B. H. (1991). Climbing fibre responses in olivocerebellar slice culture. II. Dynamics of cytosolic calcium in Purkinje cells. *Eur. J. Neurosci., 3,* 343–348.

Konnerth, A., Dreessen, J., & Augustine, G. J. (1992). Brief dendritic calcium signals initiate long-lasting synaptic depression in cerebellar Purkinje cells. *Proc. Natl. Acad. Sci. USA, 89*, 7051–7055.

Krupa, D. J., Thompson, J. K., & Thompson, R. F. (1993). Localization of a memory trace in the mammalian brain. *Science, 260*, 989–991.

Krupa, D. J., & Thompson, R. F. (1995). Inactivation of the superior cerebellar peduncle blocks expression but not acquisition of the rabbit's classically conditioned eyeblink response. *Proc. Natl. Acad. Sci. USA, 92*, 5097–5101.

Laurent, G. (1996). Dynamical representation of odors by oscillating and evolving neural assemblies. *TINS, 19*, 489–496.

Lefkowitz, R. J., & Caron, M. G. (1988). Adrenergic receptors. Models for the study of receptors coupled to guanine nucleotide regulatory proteins. *J. Biol. Chem., 263*, 4993–4996.

Lev-Ram, V., Makings, L. R., Keitz, P. F., Kao, J. P. Y., & Tsien, R. Y. (1995). Long-term depression in cerebellar Purkinje neurons results from coincidence of nitric oxide and depolarization-induced Ca2+ transients. *Neuron, 15*, 407–415.

Lewis, J. L., LoTurco, J. J., & Solomon, P. R. (1987). Lesions of the middle cerebellar peduncle disrupt acquisition and retention of the rabbit's classically conditioned nictitating membrane response. *Behav. Neurosci., 101*, 151–157.

Lincoln, J. S., McCormick, D. A., & Thompson, R. F. (1982). Ipsilateral cerebellar lesions prevent learning of the classically conditioned nictitating memebrane/eyelid response of the rabbit. *Brain Res., 242*, 190–193.

Linden, D. J. (1994). Long-term synaptic depression in the mammalian brain. *Neuron, 12*, 457–472.

Linden, D. J., & Connor, J. A. (1992). Participation of postsynaptic PKC in cerebellar long-term depression in culture. *Science, 254*, 1656–1659.

Linden, D. J., Dickinson, M. H., Smeyne, M., & Connor, J. A. (1991). A long-term depression of AMPA currents in cultured cerebellar Purkinje neurons. *Neuron, 7*, 81–89.

Llano, I., Leresche, N., & Marty, A. (1991). Calcium entry increases the sensitivity of cerebellar Purkinje cells to applied GABA and decreases inhibitory synaptic currents. *Neuron, 6*, 565–574.

Llinas, R. (1982). General discussion: radial connectivity in the cerebellr cortex: a novel view regarding the functional organization of the molecular layer. In Palay, S. L., & Chan-Palay, V. (Eds.), *The Cerebellum: New Vistas*, pp. 189–192. Springer Verlag, Berlin.

Llinas, R., & Sugimori, M. (1980). Electrophysiological properties of *in vitro* Purkinje cell dendrites in mammalian cerebellar slices. *J. Physiol., 305*, 197–213.

Lytton, J., Westlin, M., Burk, S. E., Shull, G. E., & MacLennan, D. H. (1992). Functional comparisons between isoforms of the sarcoplasmic or endoplasmic reticulum family of calcium pumps. *J. Biol. Chem., 267,* 14483–14489.

Maass, W. (1996). Lower bounds for the computational power of networks of spiking neurons. *Neural Computation, 8,* 1–40.

Maex, R., & De Schutter, E. (1998). Synchronization of Golgi and granule cell firing in a detailed network model of the cerebellar granule cell layer. *J. Neurophysiol., 80,* 2521–2537.

Marais, R. M., Nguyen, O., Woodgett, J. R., & Parker, P. J. (1990). Studies of the primary sequence requirements for PKC-α, -β_1 and -γ peptide substrates. *FEBS letters, 277,* 151–155.

Marr, D. A. (1969). A theory of cerebellar cortex. *J. Physiol., 202,* 437–470.

Masu, M., Tanabe, Y., Tsuchida, K., Shigemoto, R., & Nakanishi, S. (1991). Sequence and expression of a metabotropic glutamate receptor. *Nature, 349,* 760–765.

Mauk, M. D., Steinmetz, J. E., & Thompson, R. F. (1986). Classical conditioning using stimulation of the inferior olive as the unconditioned stimulus. *Proc. Natl. Acad. Sci. USA, 83,* 5349–5353.

Maura, G., Guadagnin, A., & Raiteri, M. (1995). Low nanomolar serotonin inhibits the glutamate-receptor nitric-oxide cyclic-GMP pathway in slices from adult-rat cerebellum. *Neuroscience, 68,* 255–263.

McCormick, D. A., Guyer, P. E., & Thompson, R. F. (1982). Superior cerebellar peduncle lesions selectively abolish the ipsilateral classically conditioned nictitating membrane/eyelid response of the rabbit. *Brain Res., 244,* 347–350.

McCormick, D. A., Lavond, D. G., Clark, G. A., Kettner, R. E., Rising, C. E., & Thompson, R. F. (1981). The engram found? Role of the cerebellum in classical conditioning of nictitating membrane and eyelid responses. *Bull. Psychon. Soc., 18,* 103–105.

McCormick, D. A., Lavond, D. G., & Thompson, R. F. (1982). Concomitant classical conditioning of the rabbit nictitating membrane and eyelid responses: correlations and implications. *Physiol. Behav., 28,* 769–775.

McCormick, D. A., Steinmetz, J. E., & Thompson, R. F. (1985). Lesions of the inferior olivary complex cause extinction of the classically conditioned eyeblink response. *Brain Res., 359,* 120–130.

McCormick, D. A., & Thompson, R. F. (1984a). Cerebellum: essential involvement in the classically conditioned eyelid response. *Science, 223,* 296–299.

McCormick, D. A., & Thompson, R. F. (1984b). Neuronal responses of the rabbit cerebellum during aquisition and performance of a classically conditioned nictitating membrane-eyelid response. *J. Neurosci., 4,* 2811–2822.

Meissner, G., Darling, E., & Eveleth, J. (1986). Kinetics of rapid Ca^{2+} release by sarcoplasmic reticulum. Effects of Ca^{2+} : Mg^{2+} and adenine nucleotides. *Biochemistry, 25,* 236–244.

Mignery, G. A., Johnston, P. A., & Südhof, T. C. (1992). Mechanism of Ca^{2+} inhibition of inositol 1,4,5-trisphosphate ($InsP_3$) binding to the cerebellar $InsP_3$ receptor. *J. Biol. Chem., 267,* 7450–7455.

Millenson, J. R., Kehoe, E. J., & Gormezano, I. (1977). Classical conditioning of the rabbit's nictitating membrane response under fixed and mixed CS-US intervals. *Learn. Motiv., 8,* 351–366.

Missiaen, L., Parys, J. B., De Smedt, H., Oike, M., & Casteels, R. (1994). Partial calcium release in response to submaximal inositol 1,4,5-trisphosphate receptor activation. *Mol. Cell. Endocrinology, 98,* 147–156.

Morris, C., & Lecar, H. (1981). Voltage oscillations in the barnacle giant muscle fiber. *Biophys. J., 35,* 193–231.

Murphy, J. T., & Sabah, N. H. (1970). Spontaneous firing of cerebellar Purkinje cells in decerebrate and barbiturate anesthesized cats. *Brain Res., 17,* 515–519.

Natschläger, T., & Ruf, B. (1998). Spatial and temporal pattern analysis via spiking neurons. *Network, 9,* 319–332.

Nauta, W., & Feirtag, M. (1986). *Fundamental Neuroanatomy.* W. H. Freeman, New York.

Nishizuka, Y. (1988). The molecular heterogeneity of protein kinase C and its implications for cellular regulation. *Nature, 334,* 661–665.

Nishizuka, Y., Shearman, M. S., Oda, T., Berry, N., & Tanaka, C. (1991). Protein kinase C family and nervous function. *Prog. Brain Res., 89,* 125–141.

Nordholm, A. F., Lavond, D. G., & Thompson, R. F. (1991). Are eyeblink responses to tone in the decerebrate, decerebellate rabbit conditioned responses?. *Behav. Brain Res., 44,* 27–34.

Nordholm, A. F., Thompson, J. K., Dersarkissian, C., & Thompson, R. F. (1993). Lidocaine infusion in a critical region of cerebellum completely prevents learning of the conditioned eyeblink response. *Behav. Neurosci., 107,* 882–886.

Nusser, Z., Mulvihill, E., Streit, P., & Somogyi, P. (1994). Subsynaptic segregation of metabotropic and ionotropic glutamate receptors as revealed by immunogold localization. *Neuroscience, 61,* 421–427.

Palay, S. L., & Chan-Palay, V. (1982). *The Cerebellum: New Vistas.* Springer Verlag, Berlin.

Pavlov, I. P. (1927). *Conditioned Reflexes: An Investigation of the Physiological Activity of the Cerebral Cortex.* Oxford University Press, London.

Perrett, S. P., Ruiz, B. P., & Mauk, M. D. (1993). Cerebellar cortex lesions disrupt the timing of classically conditioned eyelid responses. *J. Neurosci., 13*, 1708–1718.

Plant, T., Eilers, J., & Konnerth, A. (1996). Ca2+ signals underlying synaptic plasticity in cerebellar Purkinje neurones. *Sem. Neurosci., 8*, 271–279.

Putney, J. W. (1998). Calcium signaling: Up, down, up, down... What's the point?. *Science, 279*, 191–192.

Racine, R. J., Wilson, D. A., Gingell, R., & Sutherland, D. (1986). Long-term potentiation in the interpositus and vestibular nuclei in the rat. *Exp. Brain Res., 63*, 158–162.

Rescorla, R. A. (1988). Behavioral studies of Pavlovian conditioning. *Ann. Rev. Neurosci., 11*, 329–352.

Rosenfield, M. E., & Moore, J. W. (1983). Red nucleud lesions disrupt the classically conditioned nictitating membrane response in rabbits. *Behav. Brain Res., 10*, 393–398.

Rutenbar, R. A. (1989). Simulated annealing algorithms: an overview. *IEEE Circuits and Devices Magazine, 89*, 19–26.

Sakurai, M. (1987). Synaptic modification of parallel fibre-Purkinje cell transmission in *in vitro* guinea pig cerebellar slices. *Proc. Natl. Acad. Sci. USA, 87*, 3383–3385.

Schreurs, B. G., & Alkon, D. L. (1993). Rabbit cerebellar slice analysis of long-term depression and its role in classical conditioning. *Brain Res., 631*, 235–240.

Schumann, E. M., & Madison, D. V. (1994). Nitric oxide and synaptic function. *Annu. Rev. Neurosci., 17*, 153–183.

Sears, L. L., & Steinmetz, J. E. (1991). Dorsal accessory inferior olive activity diminishes during acquisition of the rabbit classically conditioned eyelid response. *Brain Res., 545*, 114–122.

Smith, M. C., Coleman, S. R., & Gormezano, I. (1969). Classical conditioning of the rabbit's nictitating membrane response at backward, simulataneous, and forward CS–US intervals. *J. Comp. Physiol. Psychol., 69*, 226–231.

Solomon, P. R., Van der Schaaf, E. R., Thompson, R. F., & Weisz, D. J. (1986). Hippocampus and trace conditioning of the rabbit's classically conditioned nictitating membrane response.. *Behav. Neurosci., 100*, 729–744.

Steinmetz, J. E. (1990a). Classical nictitating membrane conditioning in rabbits with varying interstimulus intervals and direct activation of cerebellar mossy fibres as the CS.. *Behav. Brain Res., 38*, 97–108.

Steinmetz, J. E. (1990b). Neuronal activity in the rabbit interpositus nucleus during classical NM conditioning with a pontine-nucleus-stimulation CS.. *Psychol. Sci., 1*, 378–382.

Steinmetz, J. E., Lavond, D. G., Ivkovich, D., Logan, C. G., & Thompson, R. F. (1992). Disruption of classical eyelid conditioning after cerebellar lesions: damage to a memory trace system or a simple performance deficit?. *J. Neurosci., 12,* 4403–4426.

Steinmetz, J. E., Lavond, D. G., & Thompson, R. F. (1989). Classical conditioning in rabbits using pontine nucleus stimulation as a conditioned stimulus and inferior olive stimulation as an unconditioned stimulus. *Synapse, 3,* 225–232.

Steinmetz, J. E., Logan, C. G., Rosen, D. J., Thompson, J. K., Lavond, D. G., & Thompson, R. F. (1987). Initial localization of the acoustic conditioned stimulus projection system to the cerebellum essential for classical eyelid conditioning. *Proc. Natl. Acad. Sci. USA, 84,* 3531–3535.

Steinmetz, J. E., Rosen, D. J., Chapman, P. F., Lavond, D. G., & Thompson, R. F. (1986). Classical conditioning of the rabbit eyelid response with a mossy fibre stimulation CS. I. Pontine nuclei and middle cerebellar peduncle stimulation. *Behav. Neurosci., 100,* 871–880.

Stemmer, P. M., & Klee, C. B. (1994). Dual calcium ion regulation of calcineurin by calmodulin and calcineurin B. *Biochemistry, 33,* 6859–6866.

Tegge, W., Frank, R., Hofmann, F., & Dostmann, W. R. G. (1995). Determination of cyclic nucleotide-dependent protein kinase substrate specificity by the use of peptide libraries on cellulose paper. *Biochemistry, 34,* 10569–10577.

Thompson, J. K., Krupa, D. J., Weng, J., & Thompson, R. F. (1993). Inactivation of motor nuclei blocks expression but not acquisition of rabbit's clssically conditioned eyeblink response. *Soc. Neurosci. Abs., 19,* 999.

Thompson, R. F. (1989). Role of inferior olive in classical conditioning. In Strata, P. (Ed.), *The Olivocerebellar System in Motor Control,* pp. 347–362. Springer Verlag, New York.

Thompson, R. F., & Krupa, D. J. (1994). Organization of memory traces in the mammalian brain. *Ann. Rev. Neurosci., 17,* 519–549.

Thomsen, C., Mulvihill, E. R., Haldeman, B., Pickering, D. S., R., H. D., & Suzdak, P. D. (1993). A pharmacological characterization of the mGluR1α subtype of the metabotropic glutamate receptor expressed in a cloned baby hamster kidney cell line. *Brain Res., 619,* 22–28.

Thorpe, S., Fize, F., & Marlot, C. (1996). Speed of processing in the human visual system. *Nature, 381,* 520–522.

Tyrrell, T., & Willshaw, D. J. (1992). Cerebellar cortex: its simulation and the relevance of Marr's theory. *Phil. Trans. R. Soc. Lond. B, 336,* 239–257.

Vanier, M. C., & Bower, J. M. (1996). A comparison of automated parameter searching methods for neural models. In Bower, J. M. (Ed.), *Computational Neurscience: Trends in Research 1995.* Academic Press, San Diego.

Vincent, P., Armstrong, C. M., & Marty, A. (1992). Inhibitory synaptic currents in rat cerebellar Purkinje cells: modulation by postsynaptic depolarization. *J. Physiol., 456*, 453–471.

Voogd, J., & Glickstein, M. (1998). The anatomy of the cerebellum. *Trends Neurosci., 21*, 370–375.

Vuong, T. M., Chabre, M., & Stryer, L. (1984). Millisecond activation of transducin in the cyclic nucleotide cascade of vision. *Nature, 311*, 659–661.

Wang, S. S.-H., Alousi, A. A., & Thompson, S. H. (1995). The lifetime of inositol 1,4,5-trisphosphate in single cells. *J. Gen. Physiol., 105*, 149–171.

Wang, X., & Robinson, P. J. (1995). Cyclic cGMP dependent protein kinase substrates in rat brain. *J. Neurochem., 65*, 595–603.

Wehr, M., & Laurent, G. (1996). Odour encoding by temporal sequences of firing in oscillating neural assemblies. *Nature, 384*, 162–166.

Welsh, J. P., & Harvey, J. A. (1989). Cerebellar lesions and the nictitating membrane reflex: performance deficits of the conditioned and unconditioned response. *J. Neurosci., 9*, 299–311.

Welsh, J. P., & Harvey, J. A. (1991). Pavlovian conditioning in the rabbit during inactivation of the interpositus nucleus. *J. Physiol., 444*, 459–480.

Willshaw, D. J., Buneman, O. P., & Longuet-Higgins, H. C. (1969). Non-holographic associative memory. *Nature, 222*, 960–962.

Yeo, C. H., Hardiman, M. J., & Glickstein, M. (1985a). Classical conditioning of the nictitating membrane response of the rabbit: I.Lesions of the cerebellar nuclei. *Exp. Brain Res., 60*, 87–89.

Yeo, C. H., Hardiman, M. J., & Glickstein, M. (1985b). Classical conditioning of the nictitating membrane response of the rabbit: II.Lesions of the cerebellar cortex. *Exp. Brain Res., 60*, 99–113.

Zhang, A. A., & Lavond, D. G. (1991). Effects of reversible lesions of reticular or facial neurons during eyeblink conditioning. *Soc. Neurosci. Abstr., 17*, 869.

Appendix A

Parameters

A.1 Spectral Timing Parameters

A.1.1 Original Parameters of the Spectral Timing Model

Parameter	Description	Value
B_a	total concentration of available mGluRs	variable
G_{max}	total G-protein concentration	$1.0\mu M$
I_{max}	total (bound and unbound) IP_3 concentration	$1.0\mu M$
D_{max}	total (bound and unbound) DAG concentration	$1.0\mu M$
C_{max}	total PKC concentration	$6.0\mu M$
N_{max}	total calcineurin concentration	$2.0\mu M$
$\bar{g}_{KCa,max}$	maximum KCa channel conductance	$600.0S$
$[cGMP]_{max}$	maximum cGMP concentration	$1.0\mu M$
$[Ca^{2+}]_{ER}$	reticular Ca^{2+} concentration	$1mM$
$[Ca^{2+}]_{ext}$	extracellular Ca^{2+} concentration	$2mM$
$[Na^{+}]_{ext}$	extracellular Na^{+} concentration	$125mM$
$[Na^{+}]_{cyt}$	cytoplasmic Na^{+} concentration	$8mM$
T	thermodynamic temperature	$293K$
R	gas constant	$8.3145JK^{-1}mol^{-1}$
F	Faraday constant	$96.494JmV^{-1}mol^{-1}$

Parameter	Description	Value
k_1	rate constant for glutamate binding to mGluRs	$50.0\mu M^{-1}s^{-1}$
k_{-1}	rate constant for glutamate dissociation from mGluRs	$k_1\, K_{mGluR}$
k_2	rate constant for PKC phosphorylation of mGluRs	$80.0\mu M^{-1}s^{-1}$
k_3	rate constant for dephosphorylation of mGluRs	0
k_4	rate constant for mGluR activation of G-proteins	$0.1\mu M^{-1}s^{-1}$
k_5	rate constant for spontaneous inactivation of G-proteins	$1.0s^{-1}$
k_6	rate constant for PKC phosphorylation of G-proteins	$20.0\mu M^{-1}s^{-1}$
k_7	rate constant for G-protein activated formation of IP_3/DAG	$4.0\mu M^{-1}s^{-1}$
k_8	rate constant for Ca^{2+} activated formation of IP_3/DAG	$40.0s^{-1}$
k_9	rate constant for IP_3/DAG degradation	$8.0s^{-1}$
k_{10}	rate constant for Ca^{2+} and DAG activation of PKC	$5.0\mu M^{-2}s^{-1}$
k_{11}	rate constant for PKC inactivation	$k_{10}\, K_{PKC}$
k_{12}	rate constant for Ca^{2+} activation of IP_3Rs	$60.0\mu M^{-1}s^{-1}$
k_{13}	rate constant for dissociation of Ca^{2+} from activated IP_3Rs	$48.6s^{-1}$
k_{14}	rate constant for Ca^{2+} inactivation of IP_3Rs	$7.55\mu M^{-1.65}s^{-1}$
k_{15}	rate constant for dissociation of Ca^{2+} from inactivated IP_3Rs	$0.42s^{-1}$
k_{16}	rate constant for release of Ca^{2+} from ER	$2.0\mu M^{-1}s^{-1}$
k_{17}	rate constant for removal of Ca^{2+} by the ATPase	$8.0\mu Ms^{-1}$
k_{18}	rate constant for removal of Ca^{2+} by the exchanger	$25.0\mu Ms^{-1}$
k_{19}	converts Ca^{2+} flux through exchanger to electric current	$4.0mV\mu M^{-1}$
k_{20}	leakage conductance divided by membrane capacitance	$10.0s^{-1}$
k_{21}	rate constant for Ca^{2+} activation of calcineurin	$1.0\mu M^{-3}s^{-1}$
k_{22}	rate constant for inactivation of calcineurin	$12.0s^{-1}$
k_{23}	rate constant for PKC phosphorylation of KCa channels	$2.0\mu M^{-2}s^{-1}$
k_{24}	rate constant for dephosphorylation of KCa channels	$0.4\mu M^{-1}s^{-1}$
K_{mGluR}	dissociation constant for glutamate binding to mGluRs	$0.296\mu M$
K_{PKC}	dissociation constant for Ca^{2+} and DAG binding to PKC	$6.0\mu M^2$
K_{PLC}	activation constant for Ca^{2+} activation of PLC	$20.0\mu M^2$
K_I	activation constant for IP_3 activation of IP_3Rs	$0.2\mu M$
K_{ATPase}	binding constant for Ca^{2+} binding to the ATPase	$0.2\mu M^2$
K_{NaCa}	binding constant for Ca^{2+} binding to the exchanger	$2.0\mu M$
τ_1	cGMP decay time constant	$25.0ms$
τ_2	cGMP rise time constant	$5.0ms$

Although the definition of k_{19} has been changed compared to the original model (compare Fiala et al., 1996, and equation 4.16), the value has been readjusted ($k_{19,new} = k_{19,old}/k_{18}$ with $k_{19,old} = 100.0mVs^{-1}$) and is equivalent to the value in Fiala et al.'s original simulations.

A.1.2 Changes to the Spectral Timing Parameters

Parameter	Description	Value
R_{max}	total concentration of available IP_3Rs	$1.105\mu M$
k_3	rate constant for dephosphorylation of mGluRs	$0.5\mu Ms^{-1}$
k_{23}	rate constant for PKC phosphorylation of KCa channels	$0.5\mu M^{-2}s^{-1}$
k_{24}	rate constant for dephosphorylation of KCa channels	$0.1\mu M^{-1}s^{-1}$

A.1.3 Initial Values

Variable	Description	Value
$B(0)$	initial concentration of active mGluRs	$0.01\mu M$
$A(0)$	initial concentration of phosphorylated mGluRs	$0.01\mu M$
$G(0)$	initial concentration of active G-protein $G_{s\alpha}$	$0.01\mu M$
$I(0)$	initial concentration of active = unbound IP_3	$0.01\mu M$
$D(0)$	initial concentration of active = unbound DAG	$0.01\mu M$
$R_a(0)$	initial concentration of Ca^{2+} activated IP_3Rs	$0.01\mu M$
$R_i(0)$	initial concentration of Ca^{2+} inactivated IP_3Rs	$0.01\mu M$
$[Ca^{2+}](0)$	initial calcium concentration	$0.06\mu M$
$C(0)$	initial concentration of active PKC	$0.01\mu M$
$V(0)$	initial Purkinje cell membrane potential	$-50mV$
$N(0)$	initial concentration of active calcineurin	$0.01\mu M$
$cGMP(0)$	initial = baseline cGMP	0
$\bar{g}_{KCa}(0)$	initial K_{Ca} channel conductance	0

A.2 Adaptive Timing Parameters

The parameter values of the Adaptive Timing Model are identical to the original Spectral Timing parameter values (section A.1.1), with the following exceptions:

Parameter	Description	Value
k_3	rate constant for dephosphorylation of mGluRs	$0.5\mu M s^{-1}$
k_9	rate constant for IP_3/DAG degradation	$80.0 s^{-1}$
k_{17}	rate constant for removal of Ca^{2+} by the ATPase	$16.0\mu M s^{-1}$
k_{18}	rate constant for removal of Ca^{2+} by the exchanger	$80.0\mu M s^{-1}$
k_{23}	rate constant for PKC phosphorylation of KCa channels	$0.2\mu M^{-2} s^{-1}$
k_f	rate constant for PKC phosphorylation of inhibited mGluRs	$0.08\mu M^{-2} s^{-1}$
k_b	rate constant for PKG phosphorylation of available mGluRs	$1.0\mu M^{-1} s^{-1}$
$[cGMP]_{max}$	maximum cGMP concentration	$5.0\mu M$

A.3 Leaky Integrator Parameters

Parameter	Description	Value
τ_m	apparent membrane time constant	$200ms$
τ_s	apparent synaptic time constant	$75ms$
δ	effective time window for delay updates	$500ms$
ITI	intertrial interval	$2s$
η	learning rate	0.1
α	adaptation factor of the mGluR evoked current	0.995

A.4 Parameters of the 5 ODE Delayed Response Model

Parameter	Description	Value
k_1	rate constant for glutamate binding to mGluRs	$0.1\mu M^{-1}s^{-1}$
k_{-1}	rate constant for glutamate dissociation from mGluRs	$0.01s^{-1}$
k_2	rate constant for PKC phosphorylation of mGluRs	$4.0\mu M^{-1}s^{-1}$
k_7	rate constant for G-protein activated formation of IP_3/DAG	$0.2\mu M^{-1}s^{-1}$
k_8	rate constant for Ca^{2+} activated formation of IP_3/DAG	$40.0s^{-1}$
k_9	rate constant for IP_3/DAG degradation	$80.0s^{-1}$
k_{12}	rate constant for Ca^{2+} activation of IP_3Rs	$60.0\mu M^{-1}s^{-1}$
k_{13}	rate constant for dissociation of Ca^{2+} from activated IP_3Rs	$48.6s^{-1}$
k_{14}	rate constant for Ca^{2+} inactivation of IP_3Rs	$7.55\mu M^{-1.65}s^{-1}$
k_{15}	rate constant for dissociation of Ca^{2+} from inactivated IP_3Rs	0.0
k_{16}	rate constant for release of Ca^{2+} from ER	$2.0\mu M^{-1}s^{-1}$
k_{17}	rate constant for removal of Ca^{2+} by the ATPase	$50.0\mu Ms^{-1}$
K_I	activation constant for IP_3 activation of IP_3Rs	$0.2\mu M$
K_{ATPase}	binding constant for Ca^{2+} binding to the ATPase	$0.2\mu M^2$
K_C	activation constant for Ca^{2+} activation of PLC	$20.0\mu M^2$
B_a	total concentration of available mGluRs	$20.0\mu M$
I_{max}	total (bound and unbound) IP_3 concentration	$1.0\mu M$
R_{max}	total concentration of available IP_3Rs	$1.0\mu M$
C_{ER}	reticular Ca^{2+} concentration	$1mM$
$B(0)$	initial concentration of active mGluRs	$0.01\mu M$
$I(0)$	initial concentration of active = unbound IP_3	$0.01\mu M$
$R_a(0)$	initial concentration of Ca^{2+} activated IP_3Rs	$0.01\mu M$
$R_i(0)$	initial concentration of Ca^{2+} inactivated IP_3Rs	$0.01\mu M$
$C(0)$	initial calcium concentration	$0.06\mu M$

A.5 Parameters of the 2 ODE Delayed Response Model

Parameter	Description	Value
k_1	rate constant for glutamate activation of the mGluRs	0.05
k_2	rate constant for dissociation of glutamate from the mGluRs	0.1
k_3	rate constant for Ca^{2+} dependent inactivation of the mGluRs	10.0
k_4	rate constant for Ca^{2+} release from intracellular stores	10.0
K_1	Hill constant for Ca^{2+} dependent incativation of the mGluRs	1.2
K_2	Hill constant for Ca^{2+} release from intracellular stores	1.2
K_3	Hill constant for Ca^{2+} uptake into intracellular stores	2.0
B_a	total concentration of available mGluRs	120.0
n	Hill coefficient for Ca^{2+} dependent processes	4.0

A.6 Parameters of the Complex Calcium Oscillation Model

A.6.1 Initial Values

Variable	Description	Value
$B(0)$	initial concentration of active mGluRs	0
$A(0)$	initial concentration of phosphorylated mGluRs	0
$I(0)$	initial concentration of IP_3	0
$D(0)$	initial concentration of DAG	0
$R_a(0)$	initial concentration of Ca^{2+} activated IP_3Rs	0
$R_i(0)$	initial concentration of Ca^{2+} inactivated IP_3Rs	0
$[Ca^{2+}](0)$	initial calcium concentration	$0.05\mu M$
$C(0)$	initial concentration of active PKC	0

A.6.2 Parameters from the Literature

Parameter	Description	Reference	Value
$[Ca^{2+}]_{ER}$	reticular Ca^{2+} conc.	Baumann et al. (1991)	$1mM$
$[Ca^{2+}]_{ext}$	extracellular Ca^{2+} conc.	Eilers et al. (1995)	$2mM$
$[Na^{+}]_{ext}$	extracellular Na^{+} conc.	Eilers et al. (1995)	$125mM$
$[Na^{+}]_{cyt}$	cytoplasmic Na^{+} conc.	Eilers et al. (1995)	$8mM$
T	thermodyn. temperature	Eilers et al. (1995)	$293K$
R	gas constant	Atkins (1998)	$8.3145JK^{-1}mol^{-1}$
F	Faraday constant	Atkins (1998)	$96.494JmV^{-1}mol^{-1}$
V	membrane voltage	Fiala et al. (1996)	$-50mV$
K_{mGluR}	mGluR dissociation const.	Thomsen et al. (1993)	$0.296\mu M$
K_{PKC}	PKC dissociation const.	Nishizuka (1988)	$6.0\mu M^2$
K_{PLC}	PLC activation const.	Mignery et al. (1992)	$20.0\mu M^2$
K_I	IP_3R activation const.	Missiaen et al. (1994)	$0.2\mu M$
K_{ATPase}	ATPase binding const.	De Meis and Inesi (1982)	$0.2\mu M^2$
K_{NaCa}	exchanger binding const.	Hodgkin and Nunn (1987)	$2.0\mu M$

A.6.3 Constrained Parameters

Parameter	Description	Value
k_{-1}	rate constant for glutamate dissociation from mGluRs	$k_1\, K_{mGluR}$
k_{11}	rate constant for PKC inactivation	$k_{10}\, K_{PKC}$

A.6.4 Free Parameters

Parameter	Description	Value
B_a	total concentration of available mGluRs	$2.5mM$
R_{max}	total concentration of available IP_3Rs	$0.1\mu M$
C_{max}	total PKC concentration	$0.3\mu M$
k_1	rate constant for glutamate binding to mGluRs	$0.001\mu M^{-1}s^{-1}$
k_2	rate constant for PKC phosphorylation of mGluRs	$1.0\mu M^{-1}s^{-1}$
k_3	rate constant for dephosphorylation of mGluRs	$1.0s^{-1}$
k_4	rate constant for G-protein activated formation of IP_3/DAG	$0.05s^{-1}$
k_5	rate constant for Ca^{2+} activated formation of IP_3/DAG	0
k_6	rate constant for IP_3 degradation	$0.5s^{-1}$
k_7	rate constant for DAG degradation	$0.5s^{-1}$
k_{10}	rate constant for Ca^{2+} and DAG activation of PKC	$2.0\mu M^{-2}s^{-1}$
k_{12}	rate constant for Ca^{2+} activation of IP_3Rs	$0.4\mu M^{-1}s^{-1}$
k_{13}	rate constant for dissociation of Ca^{2+} from activated IP_3Rs	$1.0s^{-1}$
k_{14}	rate constant for Ca^{2+} inactivation of IP_3Rs	$0.1\mu M^{-1.65}s^{-1}$
k_{15}	rate constant for dissociation of Ca^{2+} from inactivated IP_3Rs	$0.05s^{-1}$
k_{16}	rate constant for release of Ca^{2+} from ER	$0.25\mu M^{-1}s^{-1}$
k_{17}	rate constant for removal of Ca^{2+} by the ATPase	$2.5\mu Ms^{-1}$
k_{18}	rate constant for removal of Ca^{2+} by the exchanger	$3.0\mu Ms^{-1}$